Evaluation of Liquefaction Behavior of Sandy Soils Using Critical State Soil Mechanics and Instability Concept

Dissertation

as a requirement of the degree of
Doktor-Ingenieur (Dr.-Ing.)

at the Faculty of
Civil and Environmental Engineering
Ruhr-Universität Bochum

submitted by
Negar Rahemi

Reviewers
Prof. Dr.-Ing. habil. Achim Hettler
Prof. Dr.-Ing. habil. Torsten Wichtmann
Prof. Maria Datcheva

Bochum, December 2017

Abstract

The goal of this research is to explore the influence of high fines content (non plastic) on the large strain properties of granular materials, and to determine the shape and position of their Steady State Lines (SSL). In the first part of the study, the influence of fines content is examined; in the second part, the application of the steady state concept in the field is assessed.

- Compression triaxial tests were conducted on clean Hostun Sand to find the influence of mean effective stress, p', and void ratio, e, on the mechanical behavior of clean sand. Then, the effect of fines on the maximum shear strength, q_{max}, and the shape and location of the SSLs, was investigated with a systematic increase in fines content, f_c, up to 50% and, 100%. The experimental results revealed that q_{max} decreased with an increase in e and f_c. Furthermore, they showed that the void ratio of the mixtures decreased with an increase in fines content up to a certain amount of fines, f_{cth} (around 30% in this study), and it then increased with further increase in fines content beyond the f_{cth}. Moreover, SSLs of the mixtures followed the SSL shape of clean sand, which was almost curved shaped in e-log p', moving downward with an increase in f_c up to f_{cth} . Thereafter, with further increase in fines content SSLs followed the behavior of silt and changed to a linear shape in e-log p' diagram. From a microscopic investigation mixtures of sand with fines can develop two different micro-structures: "fines-in-sand" and "sand-in-fines". For "fines-in-sand", fine particles are partially active in the sand force structure and for "sand-in-fines", sand particles float in fine particles. The void ratio, e, does not represent the force structure or fabric of the sample, and only represents the density of the sample. In contrast, the equivalent granular void ratio, e^*, is the parameter for both the density and the fabric of the sample in case of mixtures.
  Analyses conducted in this study revealed that e^* in comparison with e provides a unique relationship for the SSL, where the SSLs for lower amounts of fines content ($f_c < f_{cth}$) are the same as for clean sand. For higher amount of fines content ($f_c > f_{cth}$), the SSLs are the same as for pure silt. This relationship can be used to predict the steady state and instability properties of granular materials containing fines based on test results for clean sand and pure fines (silt).

- A series of monotonic and cyclic triaxial tests have been conducted on sandy soils from the dump site of a brown coal open pit mine in Germany. These tests formed a case study to investigate the effect of mean effective stress, p', and void ratio, e, on static liquefaction behavior of the soil. Moreover, these tests allowed an evaluation of the effect of different cyclic stress ratios on the liquefaction resistance of the soils under cyclic loading.
  To determine the effect of lateral earth pressure (K_0), a number of samples was anisotropically consolidated and tested under cyclic loading. The results revealed that the initiation of liquefaction occurred at a lower number of cycles for samples under higher cyclic stress ratio. Furthermore, at the anisotropic consolidation state, the initiation of liquefaction occurred at a lower number of cycles for samples consolidated at lower K_0 value (initial state was closer to the related flow liquefaction surface, FLS).

- The application of the steady state concept in the field was investigated. A conceptual approach was proposed using critical state soil mechanics and instability concept to derive criteria which can be used for predicting the liquefaction susceptibility of a soil in-situ. Considering the initial state of the soil in the field and the obtained instability state of the material from triaxial tests results, the excess pore water pressure initiating of the liquefaction can be estimated. The suggested conceptual approach can be useful in the design and monitoring of a compaction campaign or important infrastructure.

Zusammenfassung

Verflüssigungserscheinungen von Böden wurden bisher meistens im Zusammenhang mit zyklischen, undrainierten Beanspruchungen infolge von Erdbeben untersucht. Allerdings sind in jüngerer Vergangenheit größere Verflüssigungsereignisse in Kippengeländen ehemaliger Braunkohlentagebaue aufgetreten, welche nicht durch Erdbeben ausgelöst wurden. Im Allgemeinen sind die Eigenschaften und der Zustand des anstehenden Bodens, die Größe und Art der zyklischen oder statischen Einwirkung sowie die hydraulischen Verhältnisse Einflussparameter, welche das undrainierte Scherverhalten, und somit die Verflüssigung, kontrollieren.
Das steady state-Konzept (auch: critical state) stellt eine Möglichkeit zur Modellierung des Spannungsdehnungs-Verhaltens dar. In dieser Arbeit wird im ersten Teil der Einfluss des Feinkorngehaltes auf die Lage und Funktion der steady state-Linie (SSL) experimentell untersucht. Im zweiten Teil wird das steady state-Konzept angewendet, um das Verflüssigungspotenzial von Lausitzer Kippensanden zu untersuchen und quantitativ einzuschätzen.
Im ersten Teil der Arbeit wurden statische, triaxiale Kompressionsversuche an reinem Hostun Sand (Grobkorn), reinem Schluff (Feinkorn) sowie Mischungen mit Feinkorngehalten von 10%, 20%, 30%, 40% und 50% durchgeführt. Eine Erhöhung der Porenzahl und des Feinkorngehaltes führte zu einer verringerten maximalen Deviatorspannung. Weiterhin zeigte sich, dass die maximale und minimale Porenzahl zunächst bis zu einem Grenzfeinkorngehalt f_{cth} abnahmen und mit darüberhinausgehendem Feinkorngehalt wieder zunahmen. Hinsichtlich der Funktion und der Lage der SSL mit variierendem Feinkorngehalt wurde festgestellt, dass diese für den Bereich unterhalb des Grenzfeinkorngehaltes im Porenzahleffektive Spannungen-Diagramm parallel und gekrümmt verlaufen, während für Feinkorngehalte oberhalb des Grenzfeinkorngehaltes die SSL linear mit unterschiedlicher Steigung verlaufen. Die sogenannte equivalente Porenzahl e^* ist ein Parameter, welcher die konventionelle Porenzahl e und den Feinkorngehalt beinhaltet und somit eine einheitliche funktionale Beschreibung der SSL für verschiedene Feinkorngehalte darstellt. Die Ergebnisse aus dieser Arbeit zeigen, dass jeweils für den Bereich unterhalb und oberhalb des Grenzfeinkorngehaltes eine separate Funktion für die equivalente SSL gefunden werden kann. Eine einheitliche Beschreibung über den gesamten Feinkornbereich zwischen null und 100% war nicht möglich.
Im zweiten Teil der Arbeit wurde eine weitere Versuchsreihe von statischen und zyk-

lischen triaxialen Kompressionsversuchen an zwei Lausitzer Kippensanden durchgeführt. Die relevanten Grenzlienen (SSL und Instabilitätslinie) des steady state-Konzeptes wurden bestimmt, wobei die initiale Porenzahl und der Spannungszustand, das zyklische Spannungsverhältnis und das Seitendruckverhältnis K_0 variiert wurden. Zur Verfügung stehende in-situ Messdaten von Drucksondierungen und Porenwasserdruckmessungen im Rahmen eines Testfeldes zur Sprengverdichtung wurden ausgewertet und in Bezug zu den ermittelten Grenzlinien des steady state-Konzeptes quantitativ interpretiert.

Vorwort des Herausgebers

Die vorliegende Arbeit von Frau Negar Rahemi entstand im Rahmen verschiedener Forschungsarbeiten zur Verflüssigung bzw. dem undrainierten Verhalten von sandigen Böden mit unterschiedlichem Feinkornanteil infolge statischer und zyklischer Belastung. Die Arbeit von Frau Rahemi wurde von Prof. Tom Schanz initiiert und geleitet. Prof. Tom Schanz verstarb am 12. Oktober 2017 völlig unerwartet kurz vor Fertigstellung der Arbeit.
Es sind verschiedene schwere Schadensfälle seit Anfang des 20. Jahrhunderts in der Literatur dokumentiert, welche auf das Phänomen der Verflüssigung zurückzuführen sind. Bodenmechanisch gesehen kann die Verflüssigung als ein Versagen infolge Reduzierung der Scherfestigkeit eines Bödens infolge Porenwasserdruckanstieg definiert werden. Allerdings können die Randbedingungen, welche in-situ zu einer Verflüssigung führen, sehr verschieden sein. So können sowohl zyklische Belastungen infolge Erdbeben oder anderer externer Belastungsquellen, als auch statische Belastungen zur Entstehung von verflüssigungsinduzierenden Porenwasserüberdrücken führen. Besondere hydrologische Verhältnisse, zum Beispiel Sickerwasser, können ebenfalls zur Reduzierung der effektiven Spannungen in einem Maß beitragen, dass Verflüssigung induziert werden kann. Neben den mechanischen und hydraulischen Randbedingungen und Einwirkungen sind in erster Linie auch die Eigenschaften des Bodenmaterials selbst (Korngröße, Kornform, Feinkorngehalt) sowie dessen Zustand (z.B. Lagerungsdichte) Einflussparameter, welche das Verflüssigungspotenzial des Bodens bestimmen. In Deutschland waren in der jüngeren Vergangenheit insbesondere Kippengelände ehemaliger Braunkohletage von Verflüssigungserscheinungen betroffen.
Vor diesem Anwendungshintergrund lässt sich die Arbeit von Frau Rahemi einordnen. Im ersten Teil hat sie mit einem umfangreichen Laborprogramm an Triaxialversuchen den Einfluss des Feinkorngehaltes auf das undrainierte Scherverhalten und insbesondere auf die resultierende Lage und Form der Steady State-Linie einer Schluff-Sand-Mischung untersucht. Der von ihr gewonnene Datensatz ist vollumfänglich, da der Feinkorngehalt in der kompletten Bandbreite zwischen null und 100% betrachtet wird. Basierend auf diesem Datensatz konnte Frau Rahemi Schlussfolgerungen hinsichtlich der Anwendungsgrenzen von äquivalenten Zustandsparametern ziehen, welche die Vorhersage des bodenmechanischen Verhaltens von Böden verschiedenen Feinkorngehaltes erlauben.
Der zweite Teil von Frau Rahemis Arbeit beschäftigt sich mit der Übertragbarkeit des steady state-Konzeptes zur Beurteilung des Verflüssigungspotenzials von Kippensanden

in-situ. Dazu wurden an zwei Kippensanden ein Triaxialversuchsprogramm durchgeführt und die relevanten Grenzlinien steady state-Linie sowie Instabilitätslinie als Funktion des Zustandsparameters ermittelt. Für ein Testfeld einer Sprengverdichtungsmaßnahme hat Frau Rahemi erstmals Feldversuchsdaten (Drucksondierungen und Porenwasserdruckmessungen) in Bezug zu den zuvor ermittelten Grenzlinien quantitativ ausgewertet und interpretiert.
Mit ihrer Dissertation hat Frau Rahemi einen wesentlichen Beitrag zum Verständnis des Scherverhaltens von Sand-Schluff-Mischungen geleistet, als auch innovative Möglichkeiten aufgezeigt, wie das klassische bodenmechanische steady state-Konzept zur ingenieurpraktischen Beurteilung des Verflüssigungspotenzials von konkreten Standorten unter Einbeziehung von in-situ Messungen verwendet werden kann.

Bochum, Dezember 2017

Acknowledgements

This research was carried out in the Chair of Foundation Engineering, Soil and Rock Mechanics, Ruhr-Universität Bochum. The work presented in this thesis would not have been possible without my close association with many people. I take this opportunity to extend my sincere gratitude and appreciation to all those who made this PhD thesis possible.

First and foremost, I would like to express my sincere gratitude to my supervisor Prof. Tom Schanz for the continuous support and encouragement during my pursuit for completion of my study, for his special personality, motivation, and immense knowledge. His guidance helped me in all the time of research and writing of this thesis. Unfortunately, he passed away a few months before the final defense. He will be forever missed and never forgotten, he will always be in my heart and memory.

I also express my sincere thanks to Dr. Wiebke Baille for her continuous help and lots of constructive suggestions during my research work. She taught me about research problems and ways to solve in different manner, and always provided me constant moral support to overcome many crisis situation and finish the dissertation.

I am very much grateful to my advisory committee members, Prof. Achim Hettler, Prof. Torsten Wichtmann, and Prof. Maria Datcheva, for their insightful comments and supports. I would give my warm gratitude to my colleagues in RUB who provide me so much help in my work and life. Especially Dr. Meisam Goudarzy who helped me during my research and for his comments and suggestions throughout these years. My gratitude should also be extended to Dr. Diethard König, our secretary Mrs. Traas and our laboratory staffs Mr. Skubisch, Mr. Müller, Mr. Mosinski and Mr. Blazytko, and to all parties who indirectly assisted me during my period of stay in Bochum.

A special mention of thanks to my friends for their constant support and cooperation during my research. Their timely help and friendship will always be remembered.

Last but not least, I sincerely thank my parents in law for their affection and amazing support during these years. I express my heartfelt gratitude to my family in Germany, Karin and Gerhard, Fereshteh and Mohammad, who supported me emotionally through this entire process, for their encouragement, moral support, personal attention and care. I feel a deep sense of gratitude for my parents and brother, who formed part of my vision and taught me good things that really matter in life. I must thank them for their endless love and encouraging me in all of my pursuits and inspiring me to follow my dreams. I

must thank them for teaching me that my job in life was to learn, to be kind, and to know and understand myself; only then could I know and understand others. I owe my deepest gratitude towards my better half for his eternal support and understanding of my goals and aspirations. His infallible love and support has always been my strength. His patience and sacrifice will remain my inspiration throughout my life. Without his help, I would not have been able to complete much of what I have done and become who I am. This journey would not have been possible without the support of my beloved Nariman, thank you for being always by my side.

Bochum, December 2017 Negar Rahemi

Contents

List of Figures

List of Tables

Nomenclature

B Skempton's value

b Fraction of active fines in sand force structure

C_u Uniformity coefficient

C_c Coefficient of curvature

C_{uc}, C_{uf} Uniformity coefficient of coarse and fine mixture

CSR Cyclic stress ratio

D, d Size of coarse and fine particles

D_{10} The grain (coarse grains) diameter at 10% passing

D_{30} The grain (coarse grains) diameter at 30% passing

D_{50} The grain (coarse grains) diameter at 50% passing

D_{60} The grain (coarse grains) diameter at 60% passing

d_{50} The grain (fine grains) diameter at 50% passing

D_r Relative density

e Void ratio

e_0 Initial void ratio after consolidation

e_{ss} Steady state void ratio

$e_{skeleton}$, e_s Skeleton void ratio

e_{max}, e_{min} Maximum and minimum void ratio

e^* Equivalent granular void ratio

e_{lim} Empirical parameter to get fitting steady state void ratio

f_c Fines content

f_r Frequency of cyclic loading

f_{cth} Threshold fines content

G_s Specific gravity

k_0 Coefficient of lateral earth pressure

m Fitting parameter to calculate the equivalent granular void ratio of mixture

N Number of cycles to initiation of liquefaction

n Fitting parameter to calculate b value

p' Mean effective stress

p'_{ss} Mean effective stress at steady state

p_a Atmospheric pressure

q_{ampl} Amplitude of cyclic loading

q_{max} Maximum shear strength

R_c Contractiveness value

R Roundness of the particles

r_u Excess pore water pressure ratio

S Sphericity of particles

u Pore pressure

w Water contents

z The depth from ground level

α Fitting coefficient in f_{cth} function

β Fitting coefficient in f_{cth} function

Δu Excess pore water pressure

Δu_{allow} Allowable excess pore water pressure

ϵ_1 Axial strain

ϵ_{vol} Volumetric strain

η_{IS} Instability stress ratio

λ, n_b Fitting parameters of b function

μ Fitting parameter in b function

ρ Density of sample

ρ_{dmin} and ρ_{dmax} Minimum and maximum dry density

$\sigma_1, \sigma_2, \sigma_3$ Stress components

$\sigma'_1, \sigma'_2, \sigma'_3$ Effective tress components

τ Shear strength

ϕ Friction angle

1. Introduction

1.1. Motivation and Background

Occurrences of liquefaction phenomena have been recognized over the past six decades. Terzaghi & Peck (1948) referred to the term "spontaneous liquefaction" to explain the sudden loss of strength in loose saturated sand that caused landslides. Later, it was considered as the main cause of drastic damage during the earthquakes in Niigata (1964), Alaska (1964), Loma Prieta (1989), Kobe (1995) and the Chi-Chi (1999) earthquakes and for the San Fernando Dam failure (1971). It is important to note that liquefaction may not only occur due to earthquake loading. In Germany, an increased number of liquefaction events have occurred during the last decade within the loosely deposited sand dumps in former open pit mines. The general reason for the liquefaction events is the re-increase of water table since the stop of the ground water pumping at the end of active mining in the 1990ies together with the loose state of the sandy dumps. The observed liquefaction events were not earthquake-induced but the trigger were found to be earth construction or dynamic compaction works, or even specific weather conditions like winter storm combined with frost. For some liquefaction events, the precise trigger could not be identified. Due to the observed destructive potential of liquefaction and its related phenomena, extensive research work has been conducted to understand the undrained behavior of soils under static and cyclic loading, and to establish prediction and design methods. Substantial research work has been conducted to identify soils being prone to liquefaction based on correlations established from field tests such as SPT or CPT tests (Youd & Idriss 2001; Robertson et al. 1994; Robertson 2015). The present study targets an investigation based on laboratory triaxial testing using critical state soil mechanics. Therefore, the aforementioned methods will not be further considered in the present work. Historically, liquefaction induced damages caused by earthquake occur mostly in sandy soil containing a fraction of fines (Baziar & Dobry 1995; Yamamuro & Lade 1999; Yamamuro & Covert 2001). Fines including silts are typically classified as soil grains with diameters ranging from 0.075 mm to 0.002 mm. Silty soils are commonly found at all

places where glaciation or alluviation have occurred in their history but also in mine tailings (Yang 2004). However, while numerous experimental laboratory studies have been carried out on clean sands and clays to understand their undrained response and liquefaction potential, systematic studies on the undrained behaviour of sand-silt mixtures can be found from the 1980's (Rahman 2009).

Based on laboratory tests, there are three different theories on the effect of fines on the liquefaction potential of sand-fines mixtures. The first theory, suggested by Troncoso (1986), was that liquefaction susceptibility increases with increasing fines content. Later, Cubrinovski & Ishihara (2000) proved this idea by conducting triaxial shear tests on sand-fines mixtures. The second point of view came from Kuerbis et al. (1988); Pitman et al. (1994) and Amini & Qi (2000), who stated that liquefaction susceptibility decreases with increasing fines content. The third and relatively recent theory by Zlatovic & Ishihara (1995); Thevanayagam (1998); Xenaki & Athanasopoulos (2003) and Yang et al. (2005) reveals that liquefaction susceptibility increases with an increase in fines content up to a threshold fines content, f_{cth}, and then decreases with increasing fines content beyond the threshold value. Some researchers (e.g. Polito & Martin 2001; Xenaki & Athanasopoulos 2003; Rahman 2009) believe that these contradictory results are because of differing interpretation bases. Considering that liquefaction often occurs in sand-fines mixtures, it is important to understand thoroughly how fines influence the undrained behavior of sand (Rees 2010). It should be noted that Lacasse & Nadim (1994) suggested developing a database regarding the static and cyclic behavior of sand-silt mixtures with high amount of silt (silty sands) and pure silt. They mentioned this issue as one of the most relevant and urgent issues in geotechnical engineering (Yang 2004). In the last few decades, numerous static and cyclic triaxial tests have been conducted to determine the stress-strain behavior of sandy soils. However, it can be concluded from the literature that systematic studies on the effect of high fines content on the liquefaction behavior in the context of steady state of soils, are rare.

There are many studies on the behavior of different clean sands interpreted using the steady state framework, e.g. Castro (1969); Been et al. (1991); Verdugo & Ishihara (1996); Yamamuro & Lade (1997); Vaid & Sivathayalan (2007); Fuentes & Triantafyllidis (2015); Wichtmann (2015). There has also been much work on sand-fines mixtures with low amounts of fines content, e.g. Been & Jefferies (1985); Yamamuro & Lade (1998); Rahman et al. (2008); Carrera et al. (2011); Rahman, Cubrinovski & Cameron (2012); Belkhatir et al. (2014); Lashkari (2015). To date, however there are only few studies available considering sand-fines mixtures with high fines content. Most of the previous studies has been restricted to the effect of limited fines content on the undrained behavior of the

host sands. Studies of the effect of high fines content on the shape and position of steady state lines of mixtures in e-log p' space at different initial conditions are rare (Zlatovic & Ishihara 1995; Thevanayagam 1998; Thevanayagam & Mohan 2000; Yamamuro & Covert 2001; Yang et al. 2006a).

Therefore, the goal of this study is to find the effect of high fines contents on the location and shape of the steady state lines in e-log p' space of various sand-fines mixtures at different conditions, such as relative density and initial effective stress and the resulting state parameter ψ. Based on the studies at lower fines contents, concepts for the normalization of the steady-state lines with respect to fines content have been proposed. These concepts consisted in the transformation of the global void ratio e to an equivalent void ratio e^*, which takes the fines content into account. The possible unification of the steady-state lines from low to high fines content will be investigated based on the data obtained from this study.

The steady state line in void ratio-effective stress space represents one of the criteria dividing intitial states leading to contractive behavior, thus potentially liquefying at undrained conditions, from those leading to dilative behavior. However, in literature another criterion was used known as instability line or flow liquefaction surface (Hill 1958; Rahman & Lo 2012; Liu et al. 2013) to separate stable from unstable stress states. The instability criterion applies to both static and cyclic loading.

The engineering background of the liquefaction events observed in former open pit mines provides the motivation for the second part of the current study, where an approach for the evaluation of the liquefaction susceptibility of a soil will be suggested and verified by available in-situ data. The approach is based on the critical state concept and the instability concept combined with the knowledge of the in-situ state of soil.

1.2. Objective and Scope of Study

From the motivation and background explained in the above section, the general scope of the study is to investigate the effect of fines on the shear behavior and on the steady state of sand-silt mixtures considering the wide range of fines content below and above the threshold fines content. In this context, the applicability of concepts for normalization of steady-state lines with respect to fines content in the high fines content range will be discussed. The second general scope consists in the suggestion and verification of an approach for evaluation of liquefaction susceptibility. The specific objectives are to answer the following questions:

- What is the effect of non-plastic fines on the stress-strain behavior and on the shape and location of the steady state lines for sand silt mixtures with fines content below and above threshold fines content?
- Are concepts for the normalization of steady state lines with respect to fines content by transforming the global void ratio and respective state parameter ψ into equivalent void ratio and equivalent state parameter applicable at higher fines contents? In other words, can the behavior of a mixture of any fines content be predicted based on data of pure sand?
- How can the steady state concept together with the instability concept be used for the prediction of liquefaction susceptibility of soils in-situ?
- What is the potential of the suggested approach with respect to engineering tasks such as monitoring of susceptible sites and important infrastructure or the design of necessary soil improvement based on quantitative criteria?

1.3. Organization of the Thesis

This study comprises six chapters. The oncoming chapters are summarized below:
Chapter 2: presents the background of relevant topics. The definition of liquefaction phenomena, and different research results for the static and cyclic behavior of clean sand and the packing of sand and silt are illustrated. This chapter will highlight the performed research on the steady state concept.
Chapter 3: presents the characteristics of sand, silt and sand-silt mixtures, and relevant test equipment used in the laboratory. The procedures adopted and their limitations are described. The test programs are also presented in this chapter.
Chapter 4: contains methods used for data interpretation based on triaxial test results. The experimental results on the influence of fine particles on the undrained behavior of Hostun sand, sand-silt mixtures, and pure silt are presented and interpreted. The steady state concept will be used to interpret the observed experimental results.
Chapter 5: presents the response of sands from open pit mining dumps in Lusatian region in Germany. Furthermore, it interprets the laboratory test data, as well as proposing a new concept for combining in-situ test results with laboratory test results to design the appropriate compaction measures.
Chapter 6: draws conclusions from this study. It highlights the main contribution of this study to the knowledge of the undrained behavior of sand mixed with high fines

content along with the liquefaction susceptibility of mixtures and steady state line concept. Finally, recommendations are suggested for further research.
All individual test results are available in detail in the appendices.

2. Literature Review

2.1. Terminology and Definitions

2.1.1. General Aspects of Liquefaction

This chapter presents a review of the literature on liquefaction phenomena of cohesionless soils under static and cyclic loading.
In 1920, Hazen used the term "liquefies" to describe the liquefaction related phenomenon, which occurred in Calaveras Dam in California (Castro 1969). Castro & Poulos (1977) presented a more general definition of liquefaction as: "A phenomenon wherein a saturated sand loses a large percentage of its shear resistance (due to static or to cyclic loading) and flows in a manner resembling a liquid until the shear stress acting on the mass is as low as its reduced shear resistance." Sladen et al. (1985) improved the Castro and Poulos definition, stating that: "Liquefaction is a phenomenon wherein a mass of soil loses a large percentage of its shear resistance, when subjected to static, cyclic, or shock loading, and flows in a manner resembling a liquid until the shear stresses acting on the mass are as low as the reduced shear resistance". A comparison of different definitions of liquefaction indicates that liquefaction is the occurance of rapid deformation when a mass of saturated/partially saturated cohesionless soil loses strength due to the generation of excess pore water pressure and reduction in effective stress. Some examples of soil liquefaction related phenomena include landslides, lateral movements of bridge supports, settling and tilting of buildings, and failure of waterfront retaining structures.
Due to pore water pressure generation in samples under undrained conditions, undrained triaxial tests are commonly used to investigate liquefaction susceptibility. However, liquefaction events have been recorded as a cause of natural disasters around the world for a long time. Some examples include Niigata and Alaska (1964), San Fernando Dam failure (1971), and the Loma Prieta (1989), Kobe (1995) and Chi-Chi (1999) Kocaeli (1999) earthquakes. All these hazards attracted the attention of engineers and seismologists (Baziar & Jafarian 2007). Over the years, considerable efforts have been made to

develop understanding of the liquefaction hazards and related phenomena. In the past few decades, a large number of experimental studies have been conducted to determine the stress-strain properties of granular packings and natural sands at large strains. The following literature review is organized in four different parts. Part one presents the liquefaction phenomenon of clean sand and sand-fines mixtures and the corresponding terms used in previous studies, especially for undrained behavior. Part two focuses on the effect of fines content on soil behavior. Part three discusses the relationship between void ratio and mean effective stress at steady state (Steady State Line, SSL). Part four presents the effect of fines content on the shape and position of SSLs.

Hazen 1918; Casagrande 1936; Roscoe et al. 1958; Castro 1969; Castro & Poulos 1977; Casagrande 1975; Ishihara et al. 1975; Poulos 1981; Castro et al. 1982; Been & Jefferies 1985; Sladen et al. 1985; Ishihara 1993; Robertson 1992; Lade 1993; Thevanayagam 1998; Chu & Leong 2002; Cubrinovski & Ishihara 2000; Ni et al. 2004; Yang et al. 2006a; Rahman 2009; Belkhatir et al. 2010a; Lade & Yamamuro 2011; Bayat et al. 2013; Sze & Yang 2014 presented valuable experimental results with respect to the evaluation of liquefaction phenomena. The published data indicate that the constitutive behavior of sands is affected by various parameters, including stress conditions, void ratio, fines content, overconsolidation ratio (OCR), soil gradation, soil structure (sample preparation), and degree of saturation. Among these parameters, the fines content, void ratio and soil structure are predominant. During soil investigations fine sand, silt and sand-silt mixtures were found in different field, due to these finding recently, the behavior of silty soils has been taken into account more than before. The effects of some important parameters, including particle characteristics, void ratio, confining pressure, and fines content, on the constitutive behavior of sand-silt mixtures are presented in this chapter. The effects of wide range of fines content and void ratio on the steady state and instability state will be highlighted in this chapter.

It is worth mentioning that previous studies have represented two different types of liquefaction mechanisms. These are flow liquefaction/cyclic instability (Li & Ming 2000; Lo et al. 2010; Mohamad & Dobry 1986; Yamamuro & Covert 2001; Baki 2011): and cyclic mobility (Castro & Poulos 1977; Vaid & Chern 1985; Ishihara 1993; Li & Ming 2000; Baki 2011). Depending on the nature and characteristics of the loading, soil liquefaction phenomenon can be divided into two main categories: flow liquefaction and cyclic mobility (Kramer 1996). As Baki (2011) stated, static liquefaction, also referred to as static instability, is in fact undrained deviatoric strain softening behavior. Furthermore, cyclic liquefaction can occur in the form of either cyclic instability or cyclic mobility. In cyclic instability conditions, the soil shows deviatoric strain softening response due to a

series of cyclic stress pulses and rapid generation of excess pore water pressure. As this type of failure results in catastrophic and/or flow-like deformation, it is the most drastic type of liquefaction failure. Cyclic instability is also sometimes known as flow liquefaction (Ishihara et al. 1991; Li and Ming 2000) or simply cyclic liquefaction (Yamamuro & Covert 2001). However, failure under cyclic loading can be categorized as a state where the effective stress path temporarily almost reaches zero effective stress in a load cycle. In general, flow liquefaction induces flow failure and large deformations, and cyclic mobility induces deformations that develop incrementally during cyclic loading.

2.1.2. Behavior of Sands under Monotonic Loading

A review of the literature indicates that the undrained behavior of loose, saturated sands has been the main object of many recent research studies. Previous studies have mostly considered loose saturated cohesionless soils and revealed that these types of soils can show strain-softening behavior during undrained static loading resulting in liquefaction, however the presence of fines in natural soils is not uncommon.

The most devastating structural failures caused by liquefaction were the result of flow liquefaction phenomena. Flow liquefaction occurs when the shear strength of soil at steady state is less than the shear stress needed for static equilibrium (Casagrande 1975; Castro et al. 1982; Robertson 1992). In that case, flow liquefaction produces a large deformation under the effect of static shear.

Liquefaction phenomena happen due to pore water pressure generation under undrained conditions in the soil. Therefore, as mentioned before, undrained triaxial tests are widely used in liquefaction studies. However, some literature claims that liquefaction instability is also observed in the case of drained conditions (Chu & Leong 2002; Bobei & Lo 2005; Lo et al. 2010). This chapter focuses on the undrained behavior of clean sand and sand-fines mixtures under static loading.

Figure 2.1 shows the typical undrained behavior of clean sands under undrained monotonic loading. This figure illustrates three different types of stress-strain behavior of soil samples. These three types of behavior are dependent on the initial state of the sample, such as initial void ratio, e_0 / initial density, D_r and initial mean effective stress, p'_0.

The samples show high contractive tendency at initial loose state and under high initial mean effective stress. The stress path of loose samples under monotonic loading gradually approaches the Steady State (SS) after passing a peak undrained shear strength at a small shear strain. The increase in the pore water pressure results in the decrease of effective confining pressure without any tendency for dilation (see curve number 3 in Fig-

ure 2.1). The loose sample shows strain softening behavior, i.e. a decrease of deviatoric stress under continued shearing, which is also called "flow liquefaction". Synonyms are "flow deformation"(Guzman et al. 1988), "unstable state" (Yamamuro & Lade 1997), and "instability state" (Rahman 2009). Ishihara (1993) reported that the steady state is a state where the soil deforms continuously at constant volume, constant shear stress and constant effective stress. Castro et al. (1992) indicated that the steady state of soil deformation is achieved only after the orientations of all particles have reached a steady state condition, and after all particle breakage, if any, is complete.
The strength of the soil at the steady state is termed the undrained steady state strength or undrained shear strength (S_{su}), see Figure 2.1. The S_{su} value highly depends on the particle characteristics and initial void ratio of the sample (Casagrande 1975; Castro 1969; Castro & Poulos 1977; Poulos 1981).
At the dense state, when the sample is subjected to monotonic loading, the soil initially shows contractive tendency at small strains. This results in the generation of small excess pore water pressure. At larger strains, the volume change behavior changes from contractive to dilative. Consequently, negative increments of pore water pressure start to develop, leading to an increase in mean effective stress. In that phase the specimen shows strain hardening behavior (see curve number 1 in Figure 2.1). The third type of behavior is typical for medium-dense soil (curve number 2 in Figure 2.1), where the sample initially exhibits strain-softening behavior, which then changes to a dilative tendency at intermediate strain. The medium dense sample shows a temporary drop of shear stress followed by strain hardening until the steady state is reached. The point where this reversal from contractive to dilative or softening to hardening behavior occurs, is called the phase transformation point (PT) (Ishihara et al. 1975). This type of behavior is sometimes also recognized as "limited flow liquefaction". Since this is a type of unstable behavior, many researchers (Lade 1993; Chu & Leong 2002; Lade & Yamamuro 2011) have investigated the strain-softening behavior of soil in terms of its instability. All stress paths in Figure 2.1 ultimately reach the SSL as a unique locus of the steady state point of samples in p′-q diagram.

While, these three types of behavior are illustrated schematically in Figure 2.1, the effect of different parameters on the soil behavior under undrained monotonic loading has been investigated by many researchers in the laboratory. Ishihara (1993) illustrated the effect of initial mean effective stress and initial density on liquefaction behavior of Toyoura sand. He found that in case of samples having the same initial density, the contractive tendency increased with increasing initial mean effective stress. Moreover, he showed that, the sample behavior changes from contractive to dilative with increasing

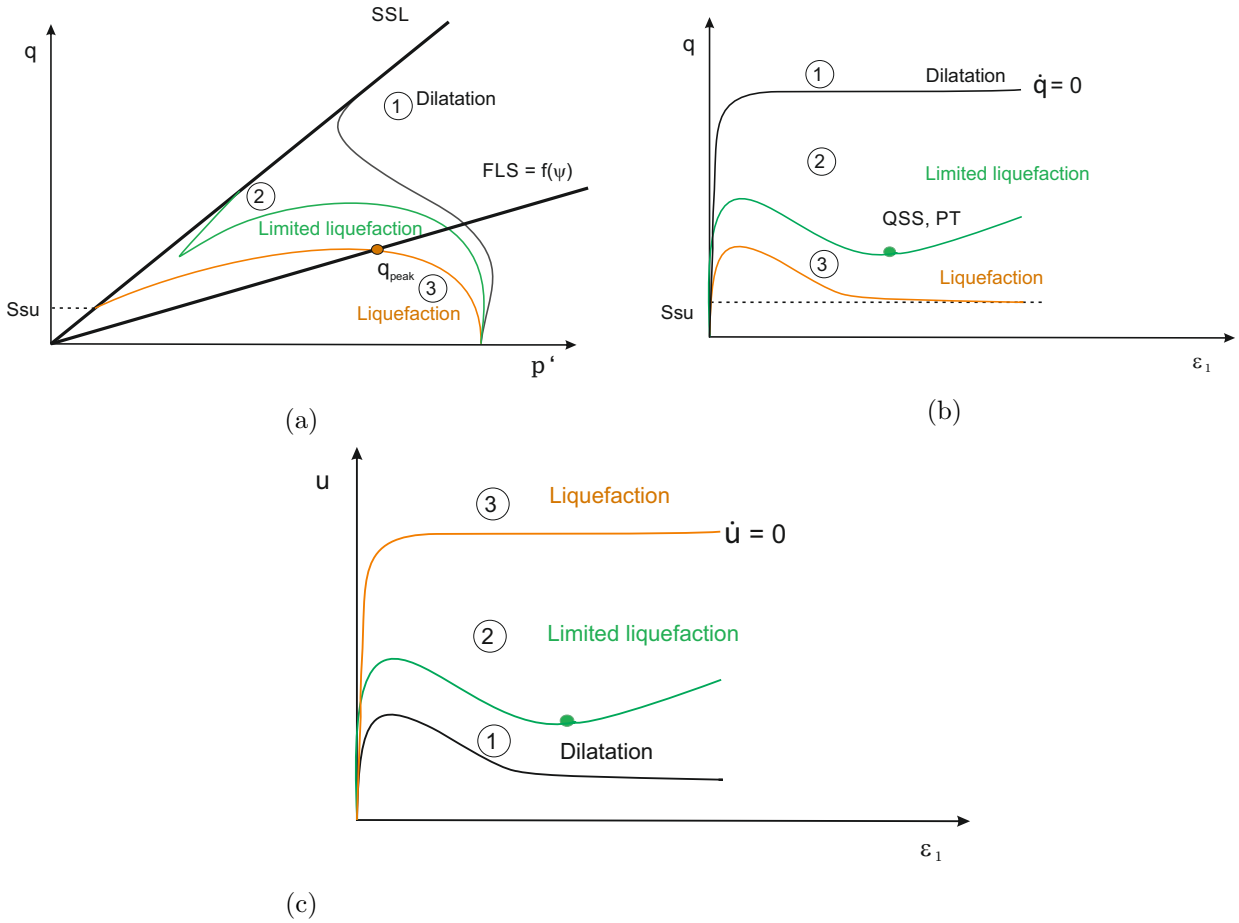

Figure 2.1.: Schematic undrained behavior of sands under monotonic loading, modified after Kramer (1996) (a) stress path; (b) stress-strain behavior; (c) pore pressure variation vs. axial strain

initial density at the same initial mean effective stress p'_0, see Figure 2.2. Yamamuro & Lade (1999) stated that complete static liquefaction occurs at low confining pressures. As confining pressures increase, the liquefaction potential decreases resulting in increased stability. Furthermore, several investigators (e.g. Thevanayagam & Mohan 2000; Murthy et al. 2007; Lade & Yamamuro 2011, Belkhatir et al. 2014) have performed experimental studies to identify the parameters influencing the behaviour under undrained monotonic loading as shown in Figure 2.1.

2.2. Steady State Concept

As Olson (2001) stated, almost all liquefaction phenomena can be reasonably explained in terms of the critical void ratio concept developed 80 years ago by Casagrande (1936). The critical state was first mentioned by Casagrande (1936), and then defined by Roscoe et al. (1958) as a state in where soil is continuously deformed at constant stress and constant void ratio. This state is the ultimate state that will be reached when a soil is sheared. This concept can be expressed mathematically as follows:

$$dq = 0, dp' = 0, d\varepsilon_v = 0 \; while \; |d\varepsilon_q| \neq 0 \tag{2.1}$$

where, $p' = (\sigma_1'+2\sigma_3')/3$ is the mean effective stress, $q = \sigma_1'$-σ_3' is the deviatoric stress, ε_v is volumetric strain, and ε_q is the deviatoric strain. σ_1' and σ_3' are vertical and horizontal effective stress, respectively, in the triaxial test.

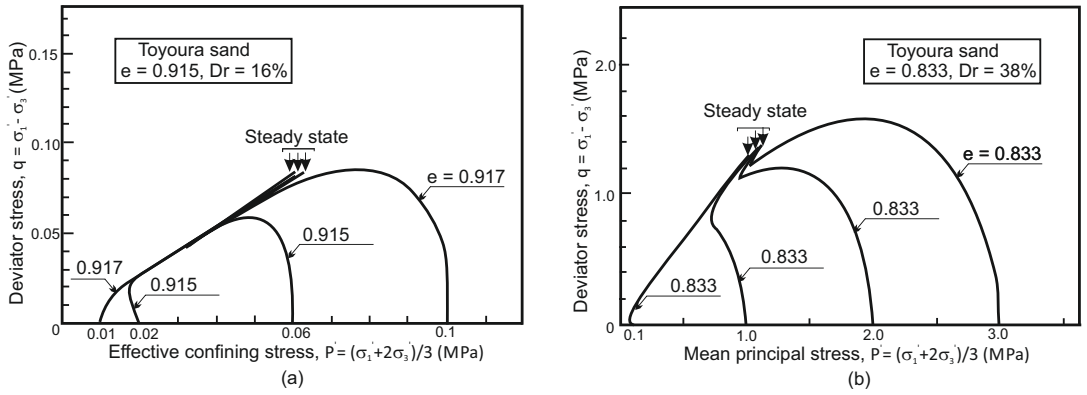

Figure 2.2.: Undrained monotonic behavior of Toyoura sand: (a) loose samples, (b) medium dense samples; (Ishihara 1993)

Castro (1969) proposed the concept of steady state, as *the state at which the mass is continuously deforming at constant volume, constant normal effective stress, constant shear stress and constant velocity.* Equation 2.2 describes this concept mathematically:

$$dq = 0, dp' = 0, d\varepsilon_v = 0 \; while \, |d\varepsilon_q| \neq 0 \tag{2.2}$$

Some literature has postulated that Critical State (CS) and Steady State (SS) are not the same (Guzman et al. 1988; Konrad 1990). On the other hand, a lot of researchers have reported the similarity of critical state and steady state (Casagrande 1975; Poulos 1981; Been & Jefferies 1985; Sladen et al. 1985; Verdugo & Ishihara 1996; Yamamuro & Lade 1998; Thevanayagam 1998). Casagrande (1975) separated these two definitions by applying the critical state concept only for drained tests, and the steady state concept for undrained tests. In contrast to Casagrande's theory, Been et al. (1991), Ishihara (1993) and Yang (2002) believed these two concepts to be almost identical. It should be noted that following the arguments of Lo and his co-workers (Chu et al. 1992; Bobei & Lo 2001, 2005; Rahman & Lo 2012), CS and SS are considered as equivalent in this thesis. Therefore, solely term Steady State (SS) is used in this study.

2.2.1. Steady State Line (SSL)

The steady state is an important concept in the modeling of soil behavior within the Critical State Soil Mechanics (CSSM) framework (Rahman 2009). The steady state includes two aspects. The first one is a locus or line in the deviatoric shear stress - mean effective stress plane (q-p'). The second is a curve in the void ratio - mean effective stress space (e-p'). The SSL in q-p' plane is a straight line passing through the origin and the stress point at steady state. The slope of this line is constant (M_{ss}). Figure 2.6 represent the steady state schematically in a e-log p' space. In the e-log p' space, the SSL is treated conventionally as a straight line in terms of Equation 2.3:

$$e_{ss} = \Gamma - \lambda \log p'_{ss} \tag{2.3}$$

where e_{ss} and p'_{ss} are the void ratio and mean effective stress at steady state, and Γ and λ are intrinsic soil properties commonly determined by test data. However, several triaxial test results on sands show a certain curvature of the steady state line. This implies that the straight steady state line in the e-log p' plane is not applicable for all soils (Verdugo & Ishihara 1996; Thevanayagam et al. 2002; Rahman 2009). Therefore, Wang et al. (2002) proposed that the steady state in the e-log p' plane can also be represented by the following

power function:

$$e_{ss} = e_{lim} - \lambda \left(\frac{{p_{ss}}'}{p_{atm}} \right)^{\zeta} \tag{2.4}$$

where p_{atm} is atmospheric pressure, and e_{lim}, λ and ζ are empirical parameters. Furthermore, in case of triaxial compression tests, the steady state friction angle (φ_{ss}) can be obtained from the inclination M_{ss} of the steady state line in the q-p' plane using Equation 2.5:

$$\sin \varphi_{ss} = \frac{3M_{ss}}{6 + M_{ss}} \tag{2.5}$$

2.2.2. Flow Liquefaction Surface (FLS)

Figure 2.3 shows schematically typical stress paths in case of flow liquefaction and limited liquefaction of sand samples with different initial confining pressure. Flow liquefaction surface (FLS) is defined for stress paths showing flow liquefaction of limited flow liquefaction. The FLS goes through the peak point of each stress path and the origin of the q-p' space. This surface has been given different names by different researchers. Sladen et al. (1985) defined a Collapse Line (CL) as a line connecting the steady state point and the maximum shear stress in the q-p' diagram, where the collapse is initiated. Chu & Leong (2002) demonstrated multiple instability lines for different stress paths with different void ratios but the same initial mean effective stress, see Figure 2.4. Guzman et al. (1988) termed the line passing through the peak shear stress point and the quasi steady state point as Critical State Ratio (CSR) line. Figure 2.5b shows that Ishihara (1993) follows the same concept as Guzman et al. (1988), except he called it the "collapse line". A number of researchers (Yamamuro & Lade 1997; Chu & Leong 2002; Rahman 2009) named this line as Instability Line (IL). In the present thesis, the term FLS is used to define this line.

Figure 2.4 shows, that the flow liquefaction surface is not unique. It should be noted that this line is known as a boundary to the initiation of the strain softening behavior. The peak point of the effective stress path is identical to the starting point of static instability (Murthy et al. 2007; Lade et al. 2009; Lade & Yamamuro 2011; Baki 2011). Therefore, it is an important point that can be obtained from the stress path of samples that show liquefaction or limited liquefaction behavior. This point is illustrated in Figure 2.3. The ratio of deviatoric shear stress to mean effective stress at the peak point of the stress path is known as the instability stress ratio, $\eta_{IS} = q_{max}$ / $\mathrm{p}'_{related-to-qmax}$.

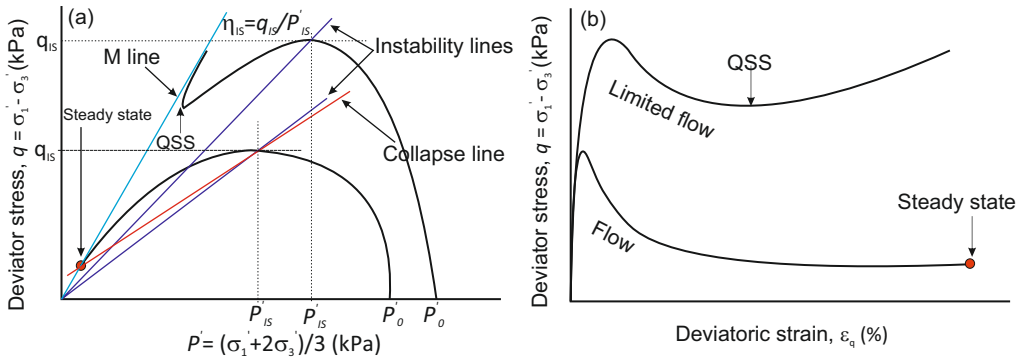

Figure 2.3.: Typical static instability behavior under undrained loading with related terms, (a) effective stress paths and (b) deviatoric stress-strain response, Baki (2011)

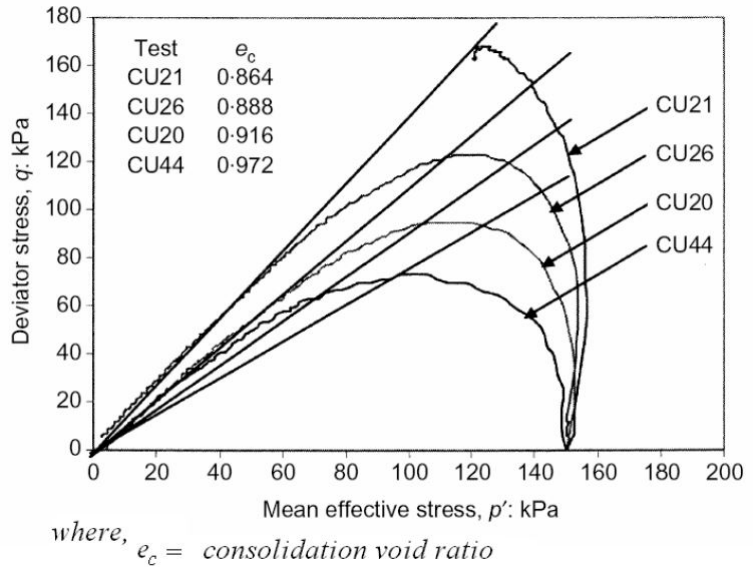

Figure 2.4.: Multiple instability lines for different void ratios but same initial mean effective stress, after Chu & Leong (2002)

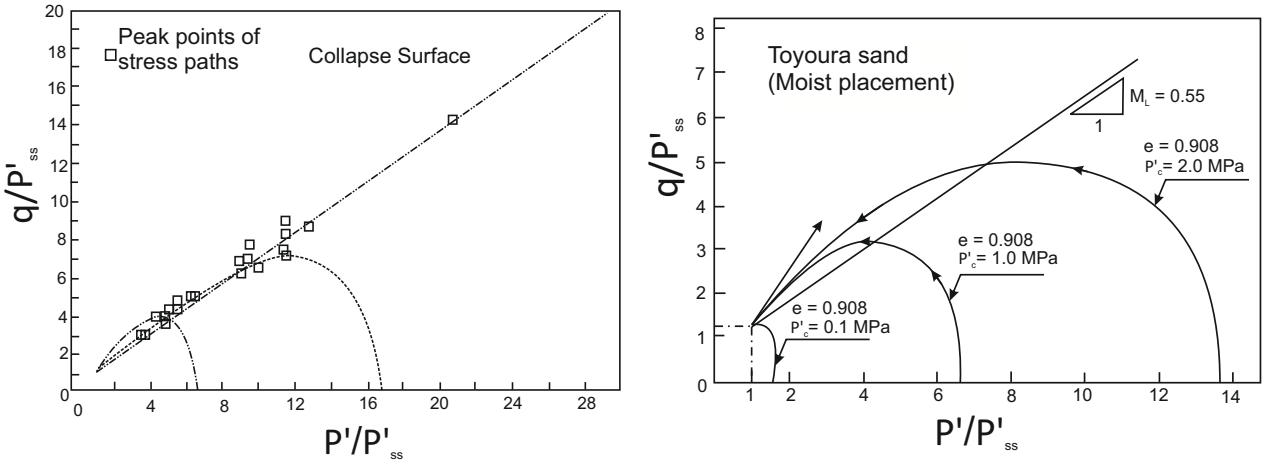

(a) (b)

Figure 2.5.: Collapse line in normalized q-p' stress space; (a) for Banding No. 6 sand after Sladen et al. (1985), (b) for Toyoura sand, after Ishihara (1993) where p'_s or p'_{ss} are the mean effective stress at quasi steady state and q_s or q_{ss} are the corresponding values of deviatoric stress

2.2.3. State Parameter

It has been recognized that soil behavior is strongly affected by the initial state, which is usually expressed in terms of initial void ratio, e_0, and mean effective stress, p_0'. Schofield & Wroth 1968 reported that the undrained response of a saturated, cohesionless soil depends on its void ratio and effective stress at the beginning of shear. The contactive and dilative tendency of a soil sample during shear is a function of its initial state (e_0, p_0'). There are many state variables describing density that have been proposed in previous studies. These variables were used to represent the concurrent effect of stress state and density state on a tested sample. These variables are defined as follows: 1) "state parameter, ψ" proposed by Been & Jefferies (1985), 2) "state pressure index, I_p" proposed by Wang et al. (2002), 3) "inter-granular state parameter" proposed by Thevanayagam & Mohan (2000), 4) "modified state parameter, ψ_m" proposed by Bobei & Lo (2001). Among all of these suggested parameters, the state parameter ψ is most frequently applied. It is defined as the difference between the current void ratio and the void ratio at the same mean effective stress on the steady state line, see Equation 2.6:

$$\psi = e - e_{ss} \tag{2.6}$$

According to the definition of the state parameter ψ, soils that have an initial state above the SSL (initially loose) with $\psi > 0$, show contractive behavior, and soils with the initial

state below the SSL (initially dense) with $\psi < 0$, show a dilative response. Castro (1969) and Ishihara (1993) stated that, when the initial state of the soil sample locates near the SSL, the sample shows a moderately contractive behavior up to intermediate strains, followed by a moderately dilative behavior at larger strains.

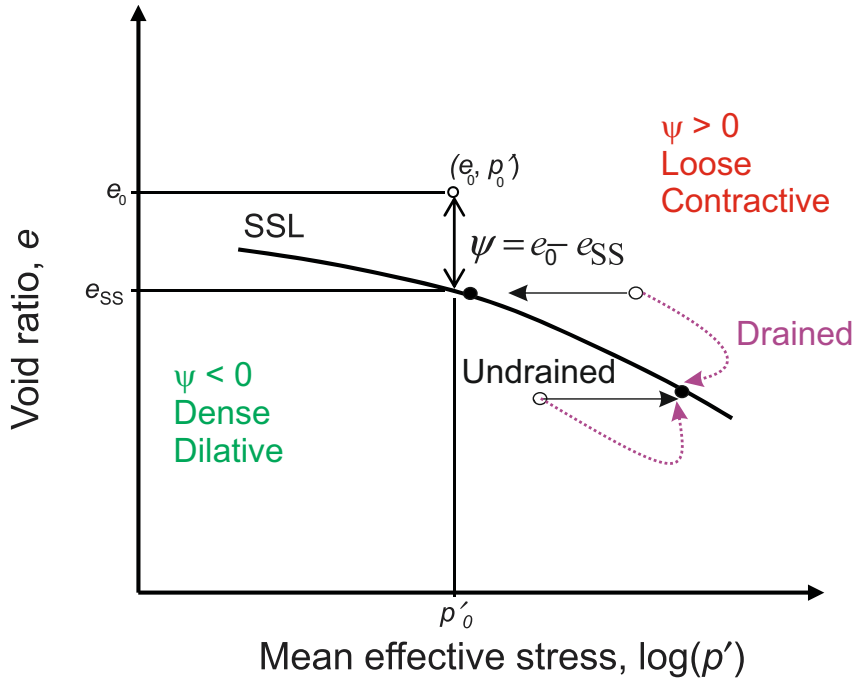

Figure 2.6.: Definition of the state parameter ψ, after Been & Jefferies (1985)

2.3. Effect of Fines

2.3.1. Effect of Fines on Undrained Monotonic Behavior of Sand-Fines Mixtures

The effect of fines content on liquefaction behavior of sands is also investigated in their study. Figure 2.7 shows that increasing the fines content increases the liquefaction potential, even though the density increases. The effect of fines content is discussed in detail in the current section. A review of previous work shows that early studies on liquefaction were mainly focused on the undrained monotonic behavior of clean sand. However, the presence of fines in natural soils is not uncommon. It is well known that the presence of fines in sand changes soil behavior significantly (Lade & Yamamuro 1997; Thevanayagam

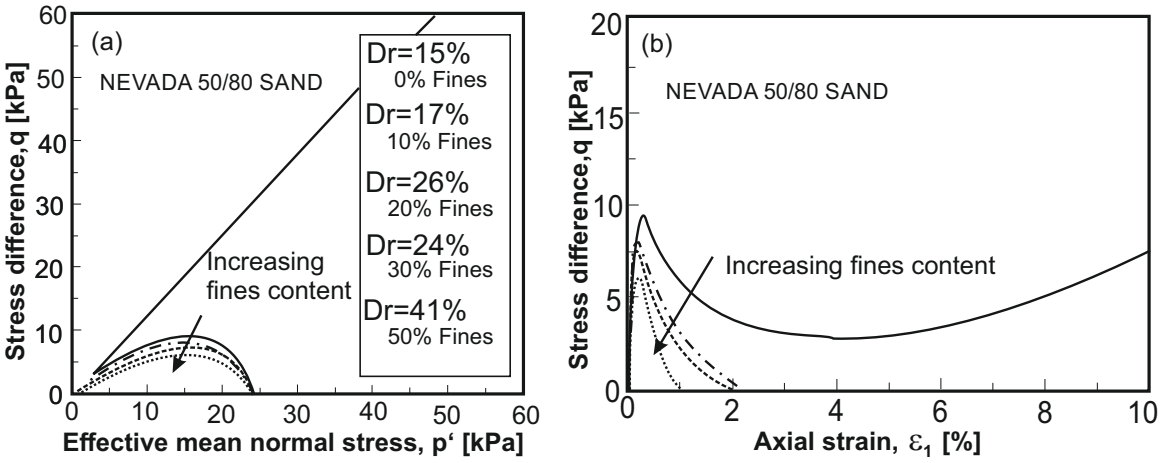

Figure 2.7.: Undrained behavior of Nevada sand with variation of fines content: (a) stress paths; (b) stress-strain relationships, after Lade & Yamamuro (1997)

1998; Chu & Leong 2002; Georgiannou 2006; Rahman 2009; Baki 2011). For instance, Lade & Yamamuro (1997) demonstrated that with increasing in fines content, flow liquefaction susceptibility increases. They have tested samples with two different gradations for both Nevada sand and Ottawa sand mixed with 0% to 50% of non-plastic fines. All samples were prepared by dry funnel deposition method, consolidated isotropically and tested under 25 kPa mean effective stress, p_0'. Figure 2.7 in Section 2.1.2 illustrates one of their test results for Nevada 50/80 sand with $F_c = 0$ to 50% at the loosest possible density state.

The test results of Lade & Yamamuro (1997) are contrasted by those of Georgiannou (2006), who performed two undrained static triaxial tests on anisotropically consolidated samples of loose Jumana sand (JS) mixed with 0 and 2.5% non-plastic fines (HPF4). The samples were prepared by the air pluviation method. Both tests were conducted with an initial effective stress $p_0' = 66$ kPa and an initial deviatoric shear stress of $q_0 = 52$ kPa. It was reported that liquefaction resistance increases considerably due to the addition of just 2.5% fines, see Figure 2.8. Another opinion on the effect of fines on the behavior of sand-fines mixture was reported by Das & Sitharam (2011). In their work, undrained triaxial tests were conducted on Ahmedabad sand with a non-plastic fines (I_p=1.57%). It was reported that liquefaction resistance decreases with increasing fines content up to a certain amount of fines (20%). By adding more fines, liquefaction resistance increases. Figure 2.9 shows one of their presented test results. Similar results were also found by other researchers (Pitman et al. 1994; Zlatovic & Ishihara 1995). So, the above discussions show that fines play an important role in undrained soil behavior, but also that there exists some uncertainty regarding its influence.

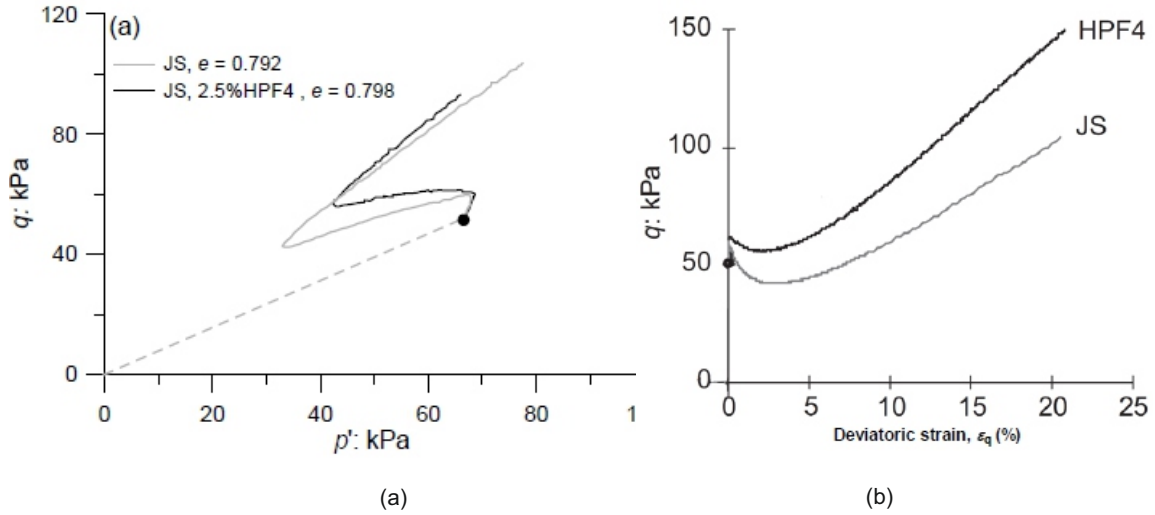

Figure 2.8.: Undrained monotonic behavior of Jumuna sand with fines (0% - 2.5%), (a) effective stress path and (b) stress-strain response, replotted by Baki (2011) using original data reported in Georgiannou (2006)

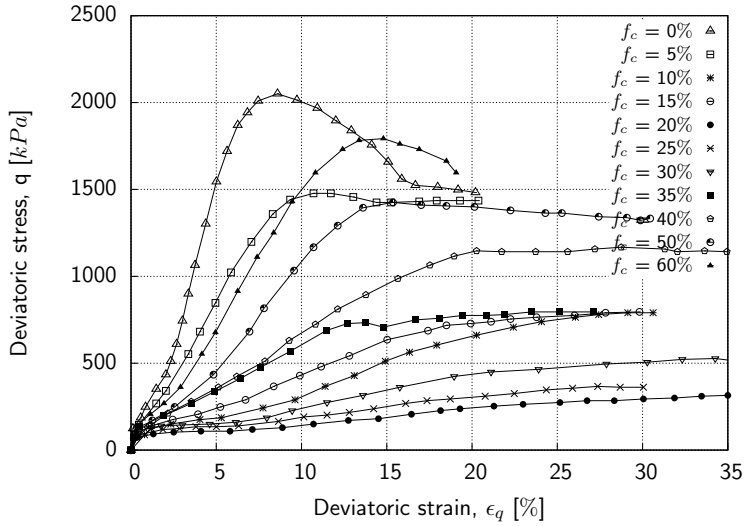

Figure 2.9.: Stress-strain response of Ahmedabad sand mixed with non-plastic fines (0%-60%) in undrained monotonic triaxial tests, $e_c = 0.44$ under $\sigma'_3 = 100$ kPa, after Das & Sitharam (2011)

2.3.2. Effect of Fines on Instability State of Sand-fines Mixtures

The peak shear strength of each sample can be determined from the effective stress path during undrained monotonic loading when the specimen shows liquefaction or limited-liquefaction behavior. As explained above, many researchers have reported that instability was initiated after the effective stress path had crossed the instability point. Therefore, peak shear stress is an important state. This section presents a few examples from previous studies on the instability state of sand-fines mixtures. Chu & Leong (2002) demonstrated the relationship between instability stress ratio and void ratio after consolidation (Figure 2.10). They reported that, by increasing the void ratio, the instability stress ratio decreases. Furthermore, Murthy et al. (2007) performed undrained triaxial tests on Ottawa sand mixed with 0 to 15% non-plastic fines using two different sample preparation methods, the moist tamping and the slurry deposition methods. They showed that, for a given sample preparation method, (in case of small amounts of fines content, $f_c < f_{cth}$) an increase in soil density caused an increase in the instability stress ratio. Furthermore, Murthy et al. (2007) stated that the undrained instability state has a practical importance because this point is the starting point for flow liquefaction. The same outcomes were also reported by Yang et al. (2006a) based on a test series on Hokksund sand with Chengbei fines. Figure 2.11a illustrates this relationship for various values of fines content. Yang et al. (2006a) introduced a new term a in the definition of the instability stress ratio as shown in Equation 2.7:

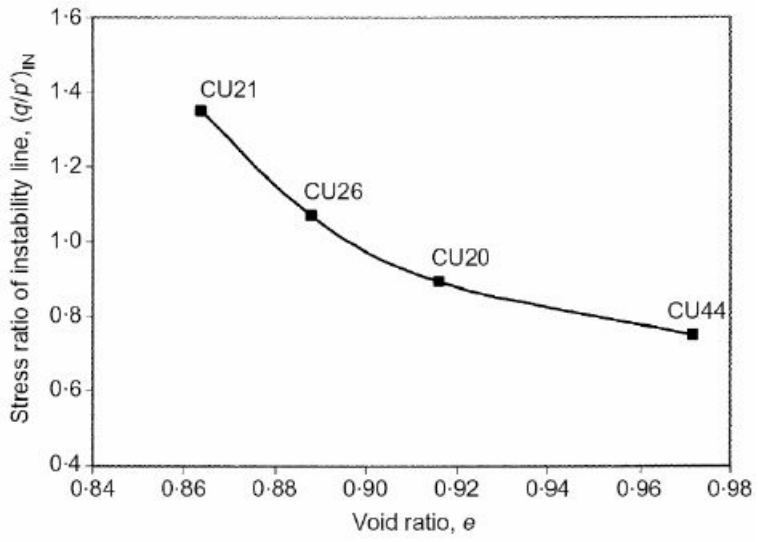

Figure 2.10.: Relation between void ratio and instability stress ratio, after Chu & Leong (2002)

$$\eta_{IS} = q_{IS}/(p'_{IS} + a) \tag{2.7}$$

where $a = \mathrm{c}/\tan\varphi$ and c and φ are the cohesion and friction angle of the soil, respectively. The value of a is very small and close to zero in their results. They showed that with increasing fines content (for $f_c < f_{cth}$), the location of instability curve in $\eta_{IS} - e$ space moved to the left (Figure 2.11a). Furthermore, they reported that an analysis of the experimental data with the equivalent granular void ratio e_{cor} (also termed e^*), leads to a single instability curve in the η_{IS}-e_{cor} diagram (Figure 2.11b).

Abedi & Yasrobi (2010) conducted four test series on poorly graded sand mixed with 0

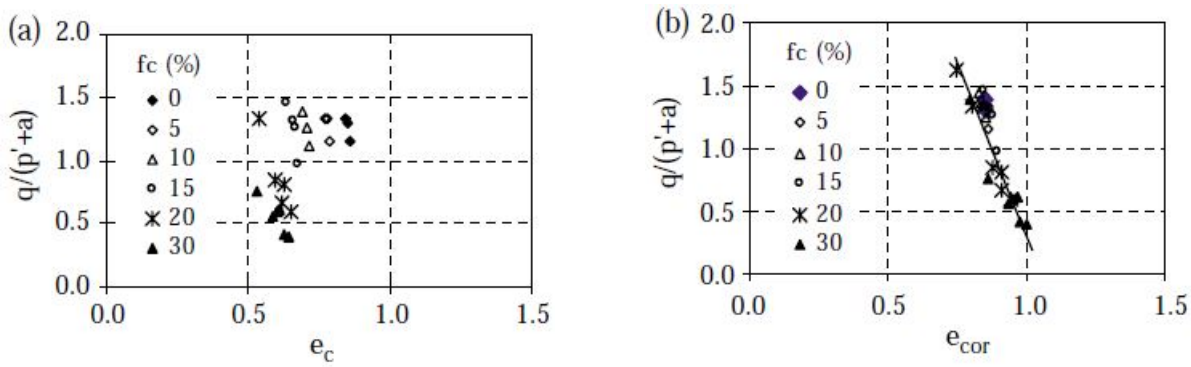

(a) (b)

Figure 2.11.: Relation between instability stress ratio for different sand-fines mixtures with (a) global void ratio (b) equivalent granular void ratio, after Yang et al. (2006a)

to 30% of fines with $I_p = 30\%$. The samples were tested with two different initial densities (1.45, 1.5 g/cm^3) and under two different initial values of mean effective stress (100, 400 kPa). As can be seen in Figure 2.12, the peak undrained shear strength (corresponding to η_{IS}) decreased with increasing fines content. Furthermore, the results indicated that the instability state is not just a function of density state, but also depends on initial mean effective stress.

However, uncertainty still exists regarding the effect of fines content f_c and other variables like shape and size of the fines affect the undrained behavior of sand-fines mixtures (transition soils). Many contradictory results have been reported from previous studies, with respect to the influence of fines on the undrained monotonic behavior of sand-fines mixtures. Furthrmore, early investigations into the behavior of sand with fines did not always vary the fines content systematically (Rees 2010). Therefore, there is still some need for systematic studies on sand with fines.

The incompatible interpretation basis is reported as a reason for the contradictory outcomes on the effect of fines on the behavior of the sand-fines mixtures (Polito & Martin

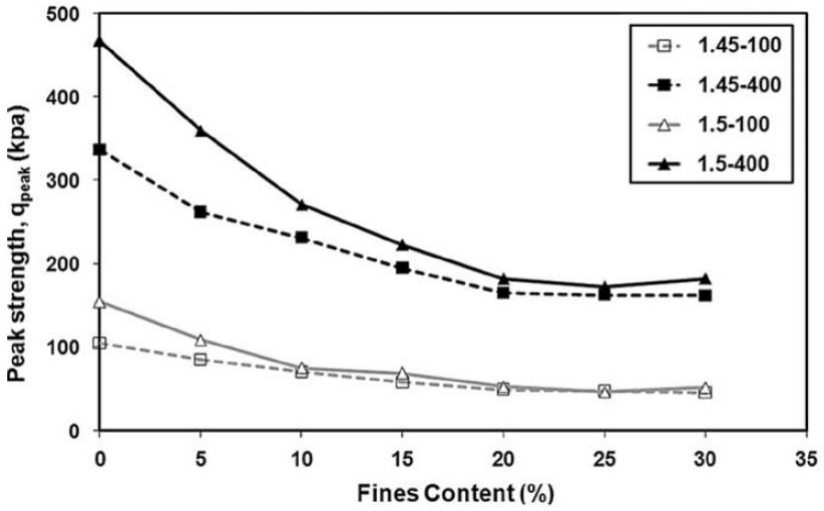

Figure 2.12.: Variation of undrained peak shear strength with fines content, after Abedi & Yasrobi (2010)

2001; Xenaki & Athanasopoulos 2003; Sadek & Saleh 2007).
Four different outcomes have been reported in the literature.

- increasing fines content led to a decrease in liquefaction susceptibility (Seed & Idriss 1971; Kuerbis 1985; Pitman et al. 1994; Amini & Qi 2000)

- increasing fines content up to significant amounts of fines (threshold fines content, f_{cth}), led to increases in liquefaction susceptibility. An increase in fines beyond the threshold causes liquefaction susceptibility to decrease (Koester 1994; Polito 1999; Das & Sitharam 2011)

- increasing fines content up to threshold fines content led to a decrease in liquefaction susceptibility. An increase in fines beyond the threshold fines content causes the liquefaction susceptibility to increase again (Zlatovic & Ishihara 1995; Thevanayagam 1998; Xenaki & Athanasopoulos 2003; Rahman 2009)

- increasing fines content led to an increase in liquefaction susceptibility (Shen et al. 1977; Troncoso 1986; Georgiannou et al. 1990; Lade & Yamamuro 1997; Salgado et al. 2000; Naeini & Baziar 2004; Yang et al. 2006a; Baziar & Sharafi 2011; Belkhatir et al. 2013)

Many researchers considered the void ratio as a comparison basis of the outcomes (third and fourth group of above mentioned researchers). Following, they reported that the void ratio may be not a good parameter to interpret sand-fines mixture behavior.

2.3.3. Effect of Fines on the Shape and Position of Steady State Lines

Theoretically, steady state data points in the e-log p' plane should follow a single trend that is called the steady state line, (SSL). Recently, the change of the shape and the position of the SSL in the e-log p' space of sands with increasing fines content has received increasing attention. However, there is still much debate over the trend of SSLs with fines content. There is few data on the steady state lines for sand-silt mixtures covering a wide range of fines content. The research results of different authors seem contradictory. Interpretations of the shape and position of SSLs can be divided into two groups. The first group reported that SSLs are linear and the slope of SSL changes with changing fines content (Been & Jefferies 1985; Fear & Robertson 1995; Bouckovalas et al. 2003), whereas the second group showed that SSLs are curved and more or less parallel for different fines content (Zlatovic & Ishihara 1995; Thevanayagam et al. 2002; Rahman et al. 2008). It has been also reported that an increase in fines content within the range $f_c < f_{cth}$ gradually leads to a downward movement of the SSL in the e-log p' space, while beyond the threshold value with increasing fines content it moves upward again (Pitman et al. 1994; Zlatovic & Ishihara 1995; Thevanayagam & Mohan 2000; Thevanayagam et al. 2002; Yang et al. 2006b; Murthy et al. 2007; Papadopoulou & Tika 2008; Rahman et al. 2008; Bobei et al. 2009; Carrera et al. 2011; Wei & Yang 2014). In the following paragraphs, the effect of fines content on the location of SSL is discussed in more detail.

Been & Jefferies (1985) realized that the slope of the SSLs increases with increasing fines content in e-log p' space, see Figure 2.13a. As can be seen in Figure 2.13b, the same trend was reported by Fear & Robertson (1995). Both test series were restricted to mixtures with low fines content of 0 to 10%.

By performing 42 tests Bouckovalas et al. (2003), observed that, the SSL rotates clockwise around a pivot point in e-log p' space with increasing fines content, see Figure 2.14.

Poulos et al. (1985); Cho et al. (2006) indicated that a small change in soil gradation and grain angularity resulted in significant changes in the location and the slope of the SSLs. They also showed that increasing grain angularity results in steeper SSLs. Castro & Poulos (1977) demonstrated results from tests on four sands, where the steepest SSL belongs to the sand with the most angular grains. Similar results were reported by Olson (2001), who showed that grain angularity may affect the slope of the SSL more significantly than the fines content. He postulated a relationship between fines content and slope of the steady state line. As can be seen in Figure 2.15, there is no clear trend of the slope of the steady state line with increasing fines content.

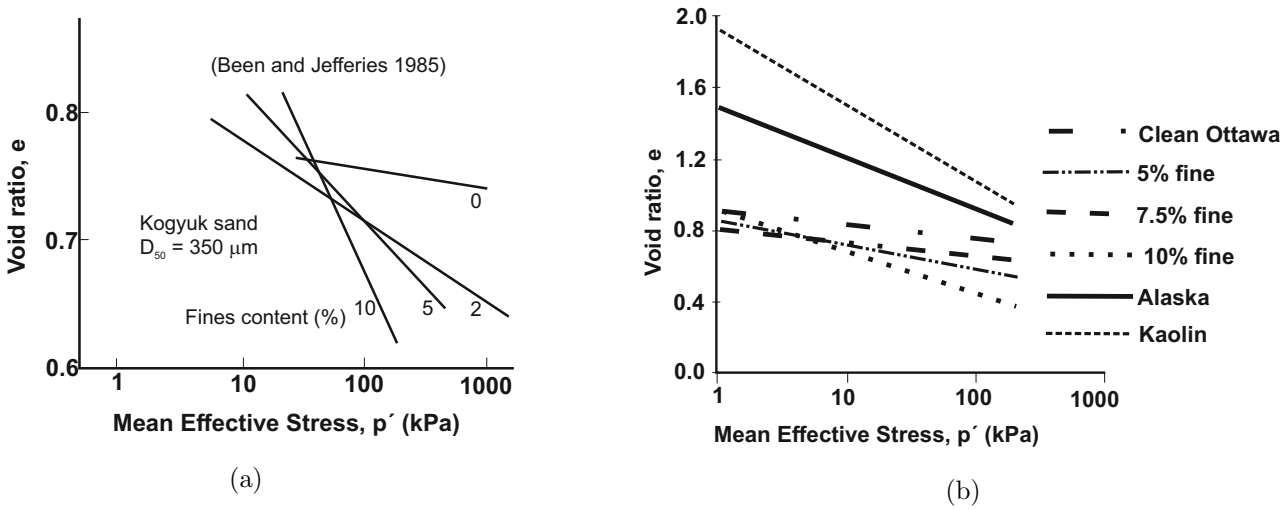

(a) (b)

Figure 2.13.: Steady state lines of sand with different fines content: after (a) Been & Jefferies (1985); (b) Fear & Robertson (1995)

Yamamuro & Lade (1998) performed drained and undrained triaxial tests on Nevada

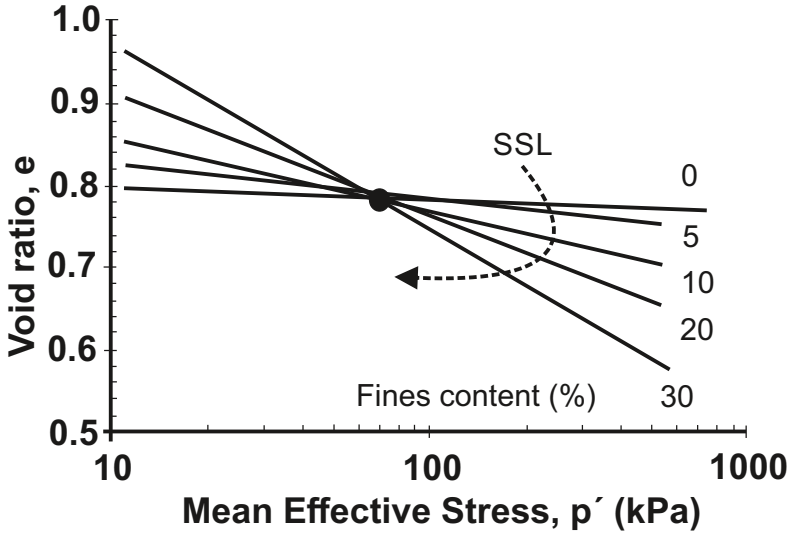

Figure 2.14.: Effect of fines content on SSL, after Bouckovalas et al. (2003)

sand containing 7% non-plastic silt. They showed that the SSLs of clean sand and sand with fines from drained tests met each other at confining pressures higher than 200 kPa, but the two lines diverge at low pressures. Murthy et al. (2007) conducted several drained and undrained triaxial tests with different sample preparation methods (moist tamping (MT), water pluviation (WP), slurry deposition (SD)) on Ottawa sand mixed with non-plastic fines from 0 to 15%. They stated that the location of the SSL moves downwards in e-log p' space with increasing fines content, see Figure 2.16a. Rahman (2009) reported

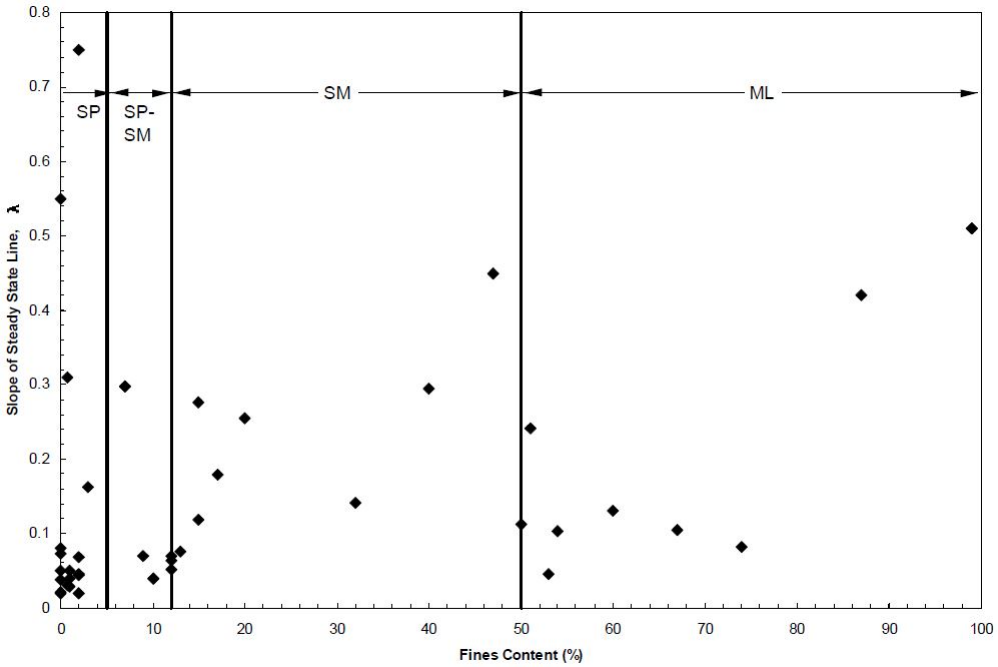

Figure 2.15.: Effect of fines content on slope of SSL, Olson (2001)

a similar tendency for Sydney sand mixed with different percentages of non-plastic fines from 0 to 30%. The results of his study are presented in Figure 2.16b.

Chiu & Fu (2008) performed tests on poorly graded sand mixed with 0 to 30% fines with low plasticity ($I_p = 9\%$). The samples were prepade by the moist tamping method. They reported downward movement of SSLs in the e-log p' space with increasing fines content from 0 to 20%. At higher fines content, the shifting direction was reversed. Furthermore, Papadopoulou & Tika (2008) tested Quartz sand with non-plastic fines of 0 to 100%. Their results are depicted in Figure 2.17, showing that SSLs shift downwards with increasing fines content up to 35% (known as threshold fine content, f_{cth}) and thereafter the trend is reversed up to $f_c = 100\%$. Thevanayagam & Martin (2002) obtained similar results for the location of the SSLs of sand-silt mixtures with fines content of 0 to 100%. Their results indicated that the SSL moved downwards from pure sand to sand with 40% fines content (f_{cth}) and then, moved upwards with increasing amounts of fines content right up to pure silt, see Figure 2.18. Naeini & Baziar (2004) observed the same SSL tendency for Ardebil sand mixed with non-plastic fines, where the samples were prepared using moist tamping with the under-compaction method. In their work, the f_{cth} was around 35%. Thereafter, as can be seen in Figure 2.19, Yang et al. (2006a) performed several drained and undrained triaxial tests on mixtures of sand with 0 to 94% of silt. The results showed the downward shifting of SSLs from 0 to 30% fines content (threshold), and then

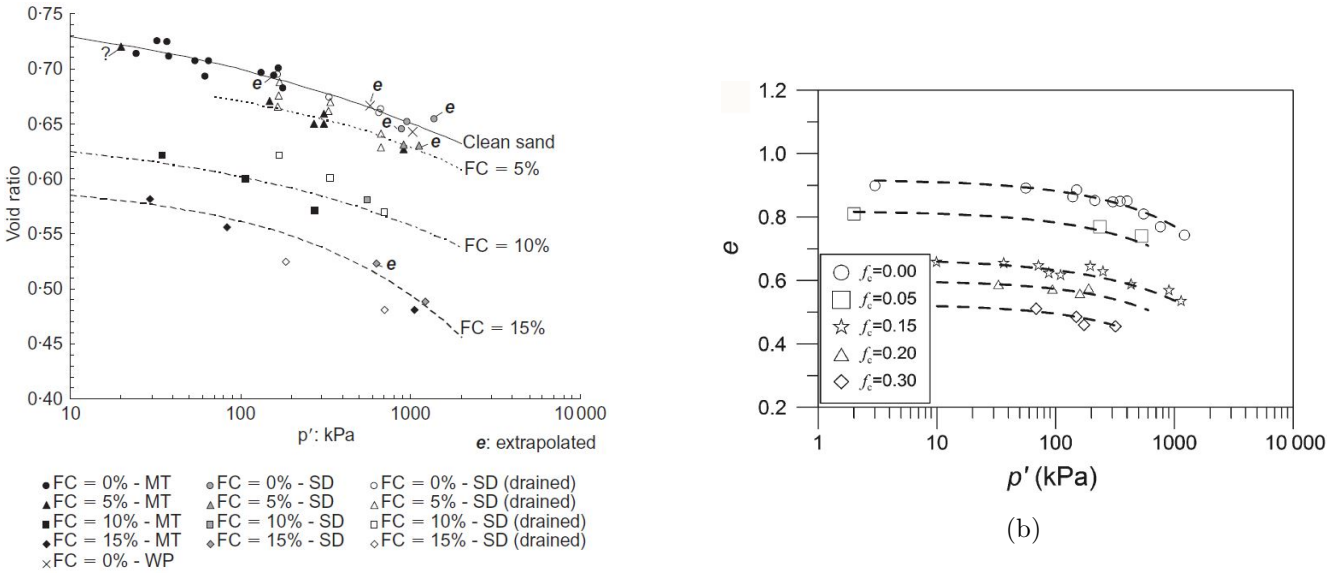

(a) (b)

Figure 2.16.: (a) SSLs of Ottawa sand with fines content of 0 to 15%, Murthy et al. (2007); (b) SSLs of Sydney sand with fines content of 0 to 30%, Rahman (2009)

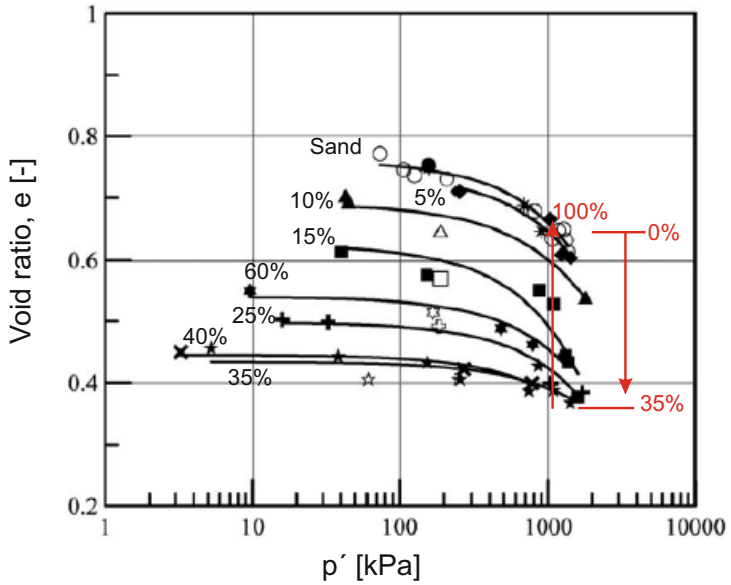

Figure 2.17.: SSLs of Quartz sand with fines content of 0 to 100%, after Papadopoulou & Tika (2008)

an upward movement of SSLs (beyond 30%) by increasing fines content to 94%.

In summary, the importance of fines content in shifting the location of SSLs in e-log p'

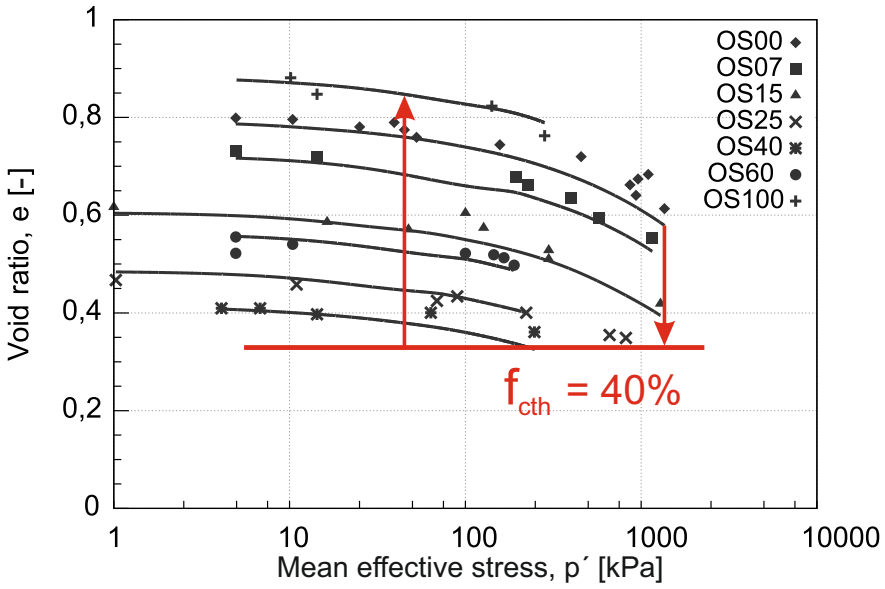

Figure 2.18.: SSLs of sand with non-plastic fines content from 0 to 100%, after Thevanayagam & Martin (2002)

framework is indicated. This resulted in difficulties in applying the framework of CSSM to analyze the mechanical behavior of sand-fines mixtures, as a single independent SSL is needed for each fines content. Due to this reason, the equivalent void ratio, e^* concept has been developed. The equivalent granular void ratio replaced the conventional void ratio, considering the effect of fines content not only on the position of SSLs, but also on the overall undrained behavior of the mixtures.

2.4. Equivalent Granular Void Ratio, e^*

2.4.1. Effect of Fines on Sand Structure

It has been recognized that the internal structure of sandy soil is affected by additional fines (Rees 2010). In 1956, Terzaghi (Terzaghi 1956) proposed that an addition of silt grains to the sand could create a metastable soil structure that could help to explain the flow liquefaction behavior of sand-fines mixtures (Yamamuro & Covert 2001). This type of structure is also reported by Yamamuro & Lade 1997, based on their investigation on the compressibility of Nevada and Ottawa sands mixed with fines. They concluded that

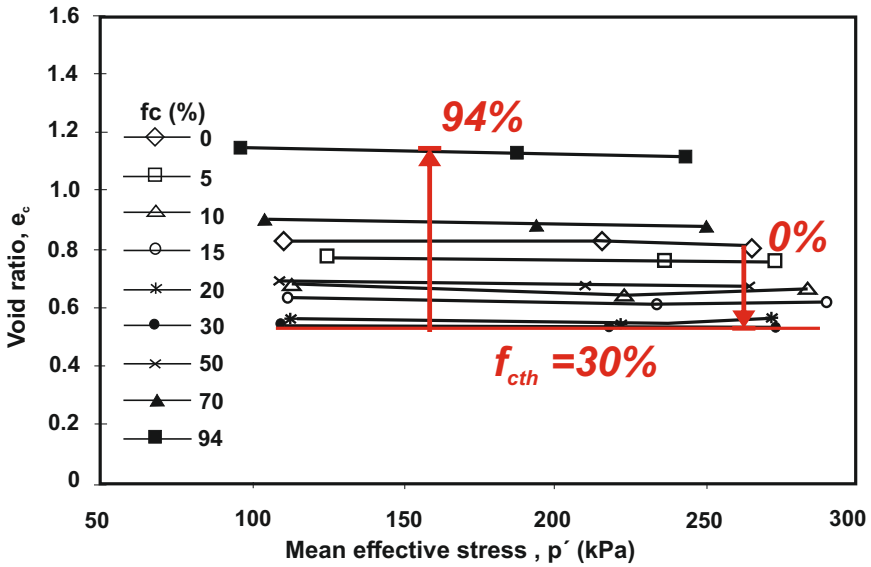

Figure 2.19.: SSLs of sand-silt mixtures with 0 to 94% fines, after Yang et al. (2006a)

sand with small amounts of fines at loose state was much more compressible, particularly at low confining pressures, than clean sand. They suggested that the metastable soil structure could be the reason for the observed increase in compressibility. Figure 2.20 shows the development of the metastable structure of a sand-fines mixture under shearing schematically.

Later on, the relationship between the fines content and the minimum and maximum void

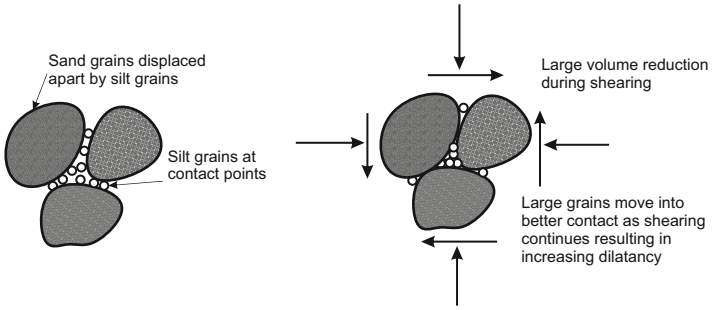

Figure 2.20.: Scheme of loose sand with fines particle arrangement. The left-hand side shows the particle arrangement before shearing; the right-hand side shows the particle arrangement at after shearing, Yamamuro & Lade (1997)

ratio, e_{min} and e_{max}, of sand-fines mixtures was investigated. The results of these studies (Lade et al. 1998; Cubrinovski & Ishihara 2000) indicated that initially the minimum and maximum void ratios of Cambria sand mixtures tends to decrease with increasing Nevada fines, up to a fines content of between 20% to 40%. Above 40%, as can be seen in

Figure 2.21, the effect reversed and the minimum and maximum void ratios continuously increased until they finally reached the highest values at 100% fines content. It should be noted that fines are not the only effective parameter on the variation of minimum and maximum void ratio. Others are the grain size distribution and the fabric (Cubrinovski & Ishihara 2000). Cubrinovski & Ishihara (2000) also reported that, unlike the composite soil (gap graded sand-fines mixtures), natural sands do not show any notable drop in e_{max} or e_{min} as fines content increases from 0 to 30%.

It is worth to mentioned that due to the segregation of particles during pluviation, there is no applicable ASTM procedure to determine the maximum and minimum void ratios of soils with fines content of 15% or more. However, despite that the ASTM standard has been used to determine the maximum and minimum void ratios for coarse materials containing high fines content (more than 15%) in previous works (e.g. Tao et al. 2004; Yang 2004; Goudarzy 2015).

Moreover, the inter-granular structure of the sand is also affected by the addition of fines

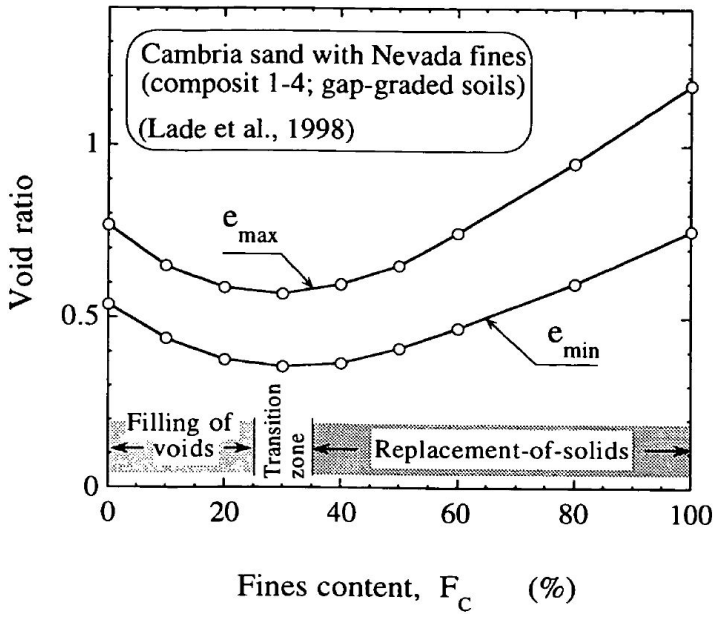

Figure 2.21.: Maximum and minimum void ratios of Cambria sand mixed with Nevada fines, Cubrinovski & Ishihara (2000)

to sand (Rees 2010). The soil force-chains and their activity in load transfer were discussed by Thevanayagam (1998). He reported that the inter-particle force-chains transfer the load applied to the soil. However, it is possible that the smaller particles such as fines do not participate in the load transferring force-chains, because they may be located in the void space that is created by the coarser particles. A number of studies have used this concept of inter-particle structure of sand with fines to assess its undrained behavior.

Shen et al. (1977) conducted cyclic triaxial tests on Ottawa sand and used the void ratio of the sand structure as a state for the test specimens. The fines were assumed to have no contribution in resistance against shear stress. This concept uses only the void ratio of the sand structure, which is known as a "skeleton void ratio, e_s" or "inter-granular void ratio, e_g". This concept of assuming the fines as inactive particles located in the voids formed by the sand matrix is depicted on the left-hand side of Figure 2.22.

The concept of inter-granular void ratio has been widely used to interpret sand-fines mix-

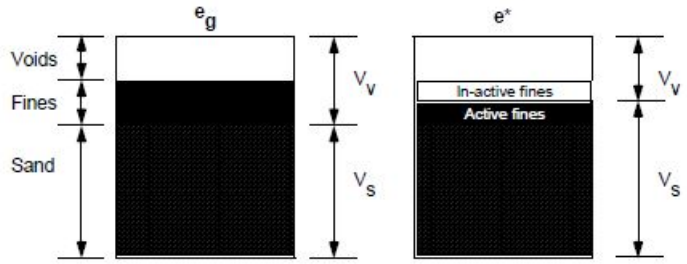

Figure 2.22.: Phase diagrams showing the concept of the inter-granular void ratio, e_g and equivalent void ratio, e^*, Rees (2010). The volume V_v is assumed not to contribute to force transmission within the grain skeleton.

ture behavior under different types of loading. It was first proposed by Mitchell (1976). It can be seen in previous studies that researchers used different names and different definitions to introduce the inter-granular void ratio term. Table 2.1 summarizes some of these terms and expressions.

The inter-granular void ratio (skeleton void ratio) is not applicable to mixtures with a fines content being larger than the threshold fines content. However, it has been taken into account as a suitable density state variable for mixtures with lower fines content relative to the threshold fines content (Pitman et al. 1994; Zlatovic & Ishihara 1995; Thevanayagam 2000; Thevanayagam et al. 2002; Naeini & Baziar 2004; Yang et al. 2006a).
Later, comprehensive studies revealed that not all fines are inactive in the force-chain structure of sand-fines mixtures. Therefore, Thevanayagam et al. (2002) introduced the equivalent granular void ratio e^*, and proposed five different ranges with different contribution of fines in transferring load through the force chains of sand-fines mixtures (see Figure 2.23).
It seems more appropriate to use the equivalent granular void ratio instead of void ratio to investigate the behavior of sand-fines mixtures. It is important to recognize which case is appropriate to evaluate the behavior of the given sand-fines mixture. Case 1 is related to clean sand without fines content.

Table 2.1.: Different terms and definitions used in the literature to introduce the inter-granular void ratio, after Baki (2011)

References	Used term	Used expressions
Mitchell (1976)	Void ratio at granular phase	(w/100)+(C/100 G_{SC}) = (1-(C/100))(e_G/G_{SC})
Kuerbis & Vaid (1988)	Skeleton void ratio $e_{skeleton}$	$e_{skeleton}$= ($V_T G_S \rho_W$-(M_T-M_{silt}))/(M_T-M_{silt})
Georgiannou et al. (1990)	Granular void ratio e_{gr}	e_{gr}=(Volume of voids+Volume of clay)/(Volume of granular phase)
Thevanayagam (1998)	Inter-granular void ratio e_g	e_g=(e+f_c)/(1-f_c)
Monkul & Yamamuro (2011); Belkhatir et al. (2014)	Inter-granular void ratio e_s	e_s=(e+(G/G_f)(f_c))/(1-(G/G_f)(f_c))

where w= water content, C= percent clay by weight, G_{SC},G_f= specific gravity of clay particles and fines respectively, G_{SG}=specific gravity of granular particles, e_G= void ratio of granular phase, V_T = total volume of specimen, G_S,G= specific gravity of sand, ρ_w= density of water, M_T= total mass of specimen and M_{silt}= mass of silt in specimen, e= global void ratio and f_c= fines content (in decimal) with respect to total weight of solid

.

Case 2 is related to sand-fines mixtures where all of the fines in this binary packing can be considered as void space and their contribution to the force structure can be neglected. Case 3 is related to sand-fines mixtures with higher amounts of fines content (relative to Case 2). In this case, the fines begin to contribute to the force structure. However, the sand grains dominate the behavior of sand-fines mixtures. Therefore, Thevanayagam et al. (2002) proposed the use of equivalent granular void ratio e^* instead of conventional void ratio. The b parameter in the related equation represents the fraction of fines that is active in the force structure.
Case 4 is related to sand-fines mixtures with higher amounts of fines content (relative to Case 3). The small contribution of sand grains to the force structure is observed in this binary packing. Therefore, the behavior of the mixtures is dominated by the fines.
Case 5 is related to pure fines material.

It is worth noting that the equivalent void ratio e^* is used as a unique measure of state that represents the soil state for different levels of fines participation in a soil force network (Rees 2010). Figure 2.22 illustrates that if the inter-granular void ratio used, then all fines assume to be inactive, i.e. they act as voids. If the global void ratio is used, then all fines are assumed to be active. Both parameters are inappropriate to describe the role

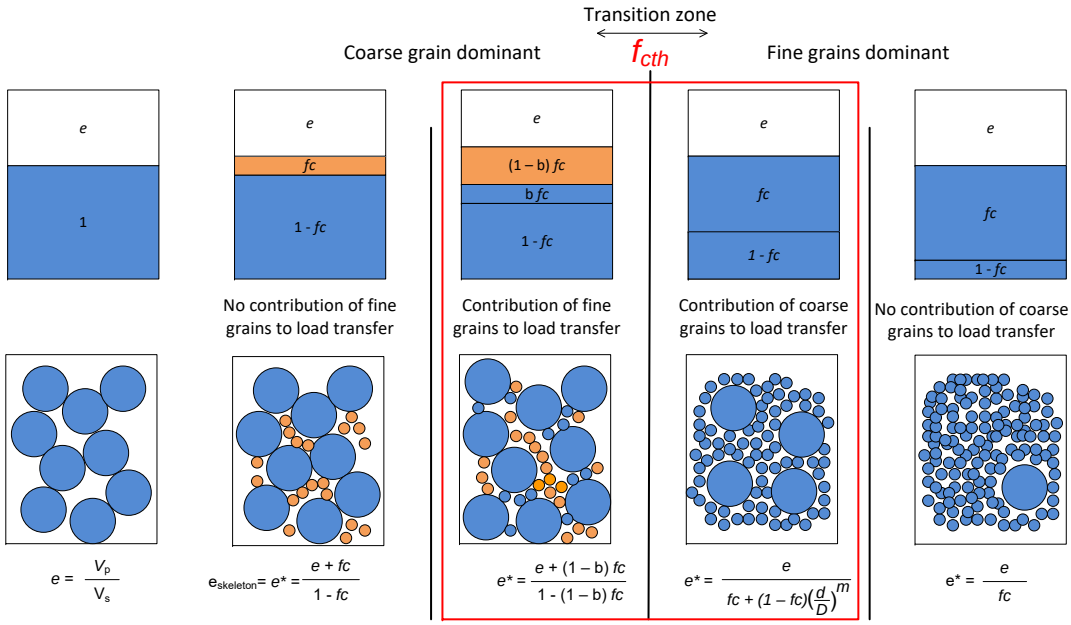

Figure 2.23.: Classification of inter-granular sand and fines mixtures, after Thevanayagam et al. (2002)

of fines in soil force-chain structure. The use of the equivalent granular void ratio e^* offers a better understanding of the participation of fines in transferring and sustaining stress during undrained loading. Fines can be described as particles that have partial contact with coarse grains by forming a bridge between two coarse grains. This contribution is described by using parameter b in equation e^*. The determination of b value will be discussed in one of the following sections.

To further define the effects of fines in a load transferring network, a determination of the threshold fines content f_{cth} is needed. As Figure 2.23 shows, the boundary between two different levels of contribution of fines in load transferring matrices of sand-fines mixtures is indicated by f_{cth}. It can be understood from Figure 2.23, that the most important parameter to get the appropriate equivalent void ratio, is the threshold fines content f_{cth}. Thevanayagam & Mohan (2000) stated that the value of f_{cth} is mostly observed between 20% to 40%. At the threshold fines content, the mixtures are dominated by coarse grains (fines-in-sand) or fine grains (sand-in-fines). Various methods exist to obtain the value of f_{cth} for a given sand-fines mixture (Lade et al. 1998; Yang et al. 2005; Rahman 2009). These methods are discussed in upcoming sections.

According to the amount of fines the sand-fines mixtures can be divided into two different skeleton structures: fines-in-sand and sand-in-fines. The following section introduces equations for e^* for both fines-dominant and coarse-dominant structures. These equations

were proposed by Thevanayagam et al. (2002).

2.4.2. e^* for f_c less than f_{cth} (fines-in-sand)

The concept of e^* is based on the skeleton void ratio concept first raised by Mitchell (1976) regarding inactive fines as void in force chains of sand-fines mixtures. After Mitchell (1976), many researchers used different formulations based on his concept, to determine the large strain behavior of soil (e.g. Kuerbis & Vaid, 1988; Thevanayagam, 1998; Georgiannou, 2006; Chu & Leong, 2002; Moayerian et al., 2011). The skeleton void ratio, $e_{skeleton}$, is defined by Eq. 2.8.

$$e_s = \frac{e + f_c}{1 - f_c} \tag{2.8}$$

where e is the conventional void ratio and f_c is the fines content (in decimal). When the volume of fines content is small enough compared to that of the sand grains, then the fines are regarded as void and the force structure of the soil is dominated by the sand skeleton (fines-in-sand). The experimental data (e.g. Pitman et al., 1994; Zlatovic & Ishihara, 1995) revealed that the assumption of inactive fines irrespective of their relative amount in sand is not appropriate. Therefore, Thevanayagam et al. (2002) adopted the b parameter to obtain e^* value (see Equation 2.9) for sand-fines mixtures with $f_c < f_{cth}$ to consider the fraction of fines being active in the transmission of inter-particle forces.

$$e^* = \frac{e + (1 - b)f_c}{1 - (1 - b)f_c} \tag{2.9}$$

2.4.3. e^* for f_c more than f_{cth} (sand-in-fines)

By increasing fines content beyond the threshold, fine grains can intrude between the coarser grains till the sand grains are floating in the fines, leading to a reduction in intergranular contact. Then the force structure of the soil is dominated by the fines skeleton (sand-in-fine). For that case, Thevanayagam et al. (2002) suggested Equation 2.10 for the determination of the e^* value.

$$e^* = \frac{e}{f_c + (1 - f_c)/(R_d)^m} \tag{2.10}$$

where, $R_d = D_{50}/d_{50}$ and m is a fitting parameter obtained by back analysis in the current study. D_{50} and d_{50} are size of sand at 50% finer, size of fines at 50% finer, respectively.

2.4.4. Determination of b and m Parameter

The steady state line for the sand-fines mixture with fines content less than f_{cth} should follow a unique trend in the e^*-log p' space (Thevanayagam 1998). This unique relationship is achieve by choosing an appropriate b value for mixtures fines content $f_c < f_{cth}$. Thevanayagam et al. (2002) used the back analysis method to obtain the b value for their results. They assumed b to be constant with a value $b = 0.25$ for a whole range of fines content below the threshold as 0.25. Later, other researchers reported the same value for the soil whichThevanayagam 1998 used, using back analysis (Yang et al. 2006a; Baki 2011). Note, that Yang et al. (2006a) used a constant b value of 0.25 for mixtures with fines contents less than the threshold, $b = 0.4$ for $f_c = f_{cth}$, and $m = 0.65$ for mixtures with fines contents higher than the threshold, to achieve a good fit for their own data. Thereafter, Rees (2010) found a b value of 0.35 for Toyoura sand, while Ni et al. (2004) considered a b value of 0.25 for the same soil. Carrera et al. (2011) found $b = 0.8$ to be the optimum value for the Stava tailings soils with $f_c < f_{cth}$.

Moreover, previous researchers stated that the b value may vary between 0 to 1 and m is also an empirical parameter (Thevanayagam 1998; Chu & Leong 2002; Thevanayagam et al. 2002; Rahman & Lo 2008; Rahman 2009; Rahman et al. 2011; Lashkari 2014). A b value of 0 means that fines are not contributing to force transmission in the soil structure. This assumption leads to an e^* value being equal to the skeleton void ratio e_s. Kanagalingam & Thevanayagam (2005) reported that the b value, which they obtained from back analysis, may depend on soil grading parameters. These grading parameters are: (1) particle size ratio, defined as R_d=(D_{50}/d_{50}), (2) uniformity coefficient of sand, defined as C_{uc}=(D_{60}/D_{10}), and (3) uniformity coefficient of fines, defined as C_{uf}=(d_{60}/d_{10}), where D and d are the grain sizes of sand and fines respectively. They proposed a correlation between b and $C_{uc}{C_{uf}}^2/\mathrm{R}_d$ for R_d>6, which is shown in Figure 2.24.

Furthermore, Ni et al. (2004) suggested a linear relationship between m and $C_{uc}{C_{uf}}^2/\mathrm{R}_d$ for mixtures with high fines content. Recently, Goudarzy et al. (2016) performed a series of resonant column tests on Hostun sand mixed with quartz powder, and their results were in agreement with the function as suggested by Ni et al. (2004), see Figure 2.25. It should be noted that the data of aforementioned studies were not sufficient to take a final decision regarding suitable functions for b and m parameters considering grain

characteristics of the fine and coarse particles. Thevanayagam et al. (2002) and Rahman

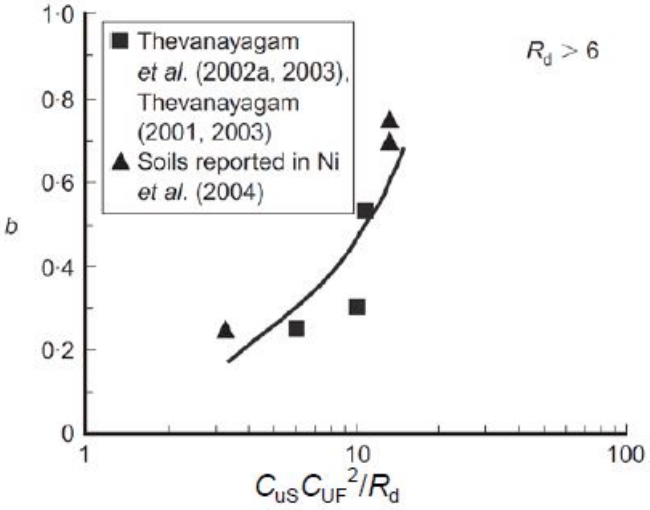

Figure 2.24.: Correlation of b with soil grading parameters, Kanagalingam & Thevanayagam (2005)

& Lo (2012) discussed the effect of fines content on the b value. Rees (2010) suggested different correlations to obtain the b value as a function of particle size ratio, χ=D_{10}/d_{50} and maximum void ratio of the sand.

Recently, the so-called prediction method has been suggested to obtain the b value by Rahman and his co-workers (Rahman & Lo 2008; Rahman 2009; Rahman et al. 2011; Rahman & Lo 2012). It is used in many recent studies. They suggested an empirical equation based on re-analysis of the McGeary (1961) study on the void ratio of binary packings. They indicated that the b value can be represented by a functional relationship of particle diameter ratio, χ and fines content, i.e. $b = F(\chi, f_c)$. A number of empirical constants are also used in this equation, which are defined according to the soil characteristics. This semi-empirical equation is used to get the b value for sand-fines mixtures with $f_c < f_{cth}$, see Equation 2.11.

$$b = \left\{1 - \exp\left[-\mu \frac{(f_c/f_{cth})^n}{k}\right]\right\} \left(\frac{r f_c}{f_{cth}}\right)^r \tag{2.11}$$

where, $r = \chi^{-1} = d_{50}/D_{10}$, $k = (1 - r^{0.25})$, and μ is a fitting parameter. Rahman and his co-workers used eight different published data sets to develop Equation 2.11. Figure 2.26 illustrates these data sets, in terms of the threshold fines content f_{cth} in dependence of particle size ratio χ.

Recently, Lashkari (2014) recommended a new definition of the b parameter, renamed as β and formulated as a function of fines content and grain shape. The empirical rela-

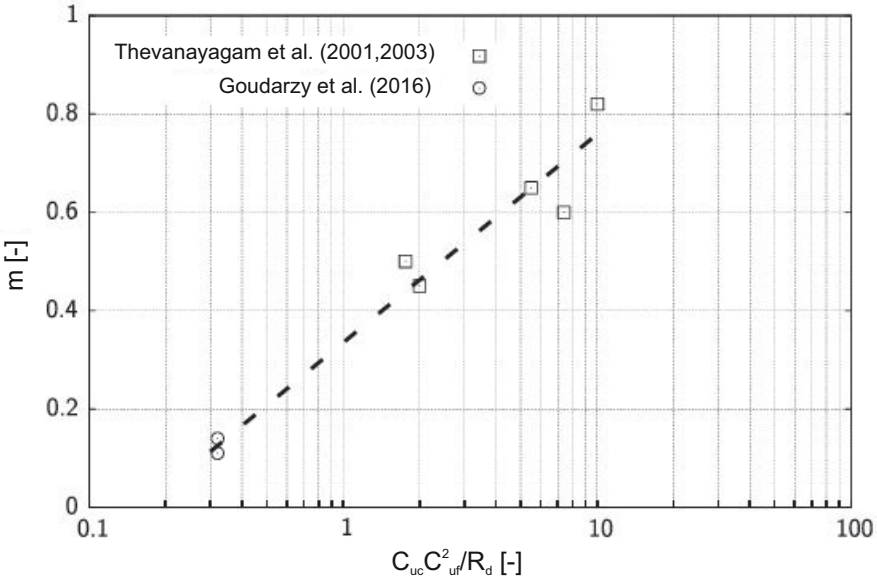

Figure 2.25.: Correlation of m with soil grading parameters, Goudarzy et al. (2016)

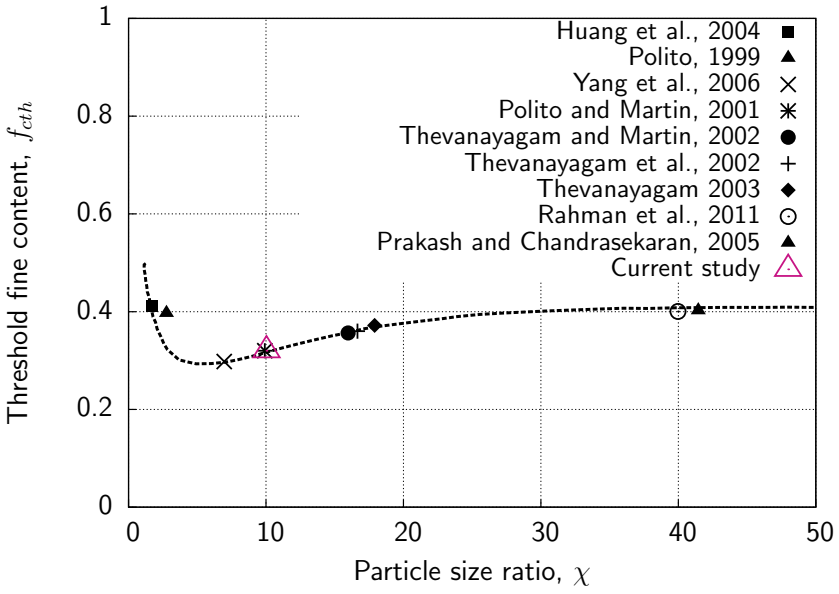

Figure 2.26.: Relation between threshold fine content, f_{cth}, and particle diameter ratio, χ after Rahman & Lo (2012)

tionship in Equation 2.12 is proposed to obtain the β parameter.

$$\beta = \beta_0(r, F_c) F_c \chi^a \tag{2.12}$$

where the term $\beta_0(r,F_c)$ considers the combined influence of the roundness of coarse and fine constituents. a is a material parameter, with $a\approx$-0.2 being a reasonable estimate for various silty sands and χ is the particle diameter ratio, D_{10}/d_{50}. Based on available data in the literature, the parameter $\beta_0(r,f_c)$ is formulated, according to Equation 2.13.

$$\beta_0(r, f_c) = (1.93 + 0.04(r-1)^2).(1 + 3.2(r-1)^2 \exp(-22 f_c)) \tag{2.13}$$

where, $r = R_c/R_f$ is the roundness ratio in which R_c and R_f are the average roundness of the coarse and the fine fraction, respectively. Lashkari (2014) stated that, when the mixtures have well-rounded to sub-rounded coarse particles, then the divergence between calculated b and calculated β parameter will be significant, see Figure 2.27. The gray linear curve is the equation for b, while the black solid curve with data points shows β. It can be implied that when the roundness ratio of coarse grains and the roundness ratio of fine grains are almost the same then the value of b and β would be the same.

A simple procedure for the calibration of the parameters μ and n in Equation 2.11 is as follows:

1. determination of threshold fines content, f_{cth} (see next section)
2. assuming the empirical parameters (μ and n) based on literature and calculation of the corresponding b from Equation 2.11
3. calculating the equivalent granular void ratio, e^* using this b value
4. checking whether, by using e^*, irrespective of the amount of fines content, a unique SSL in the e^*-log p' plane is obtained
5. repeating steps 2 to 4 until the best fit SSL is reached, with minimal observed scatter of the data points

Rahman et al. (2008) found an effect of fines content on the b value as shown in Figure 2.28. At lower fines content the influence of the fines content, or the ratio f_c/f_{cth} respectively on parameter b is very small, but at higher fines content this influence begins to be more significant. This means that chosing a suitable b value depends on reliable values of f_c and f_{cth}.

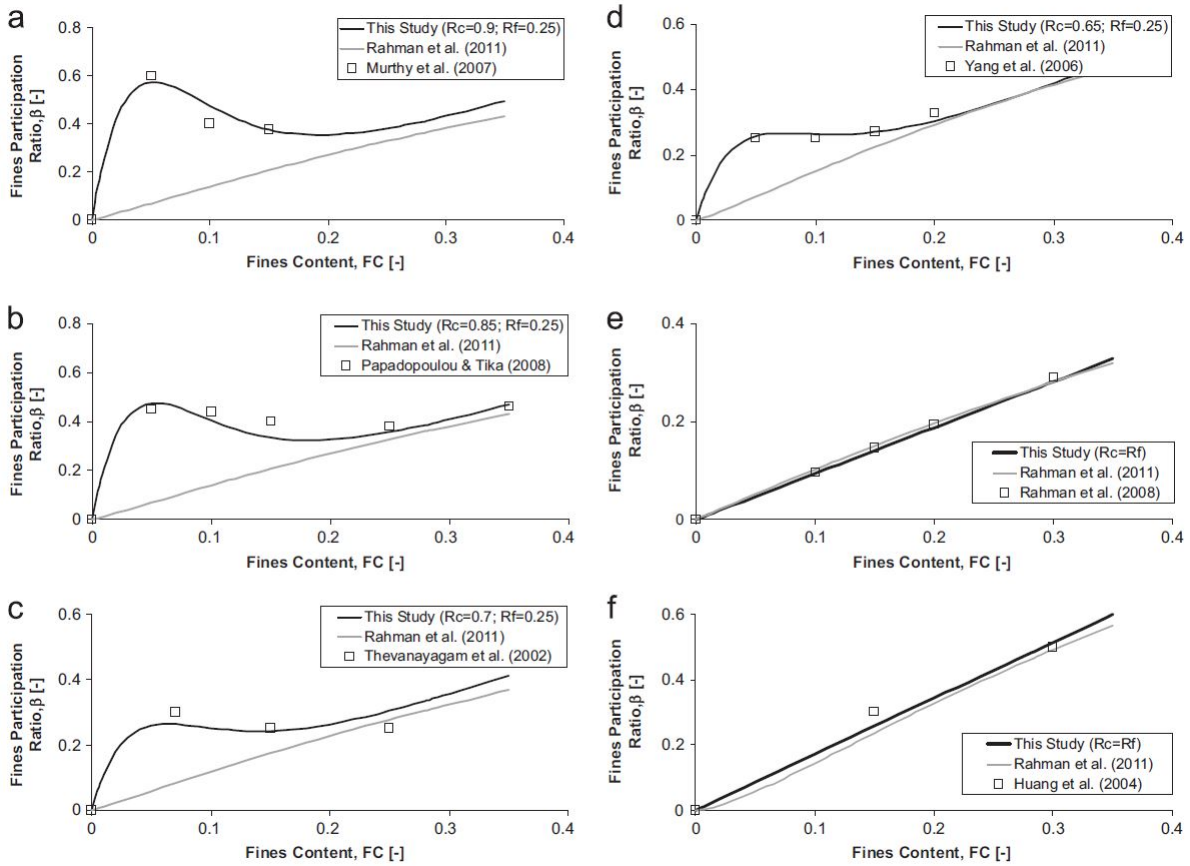

Figure 2.27.: Effect of angularity on the β parameter, Lashkari (2014)

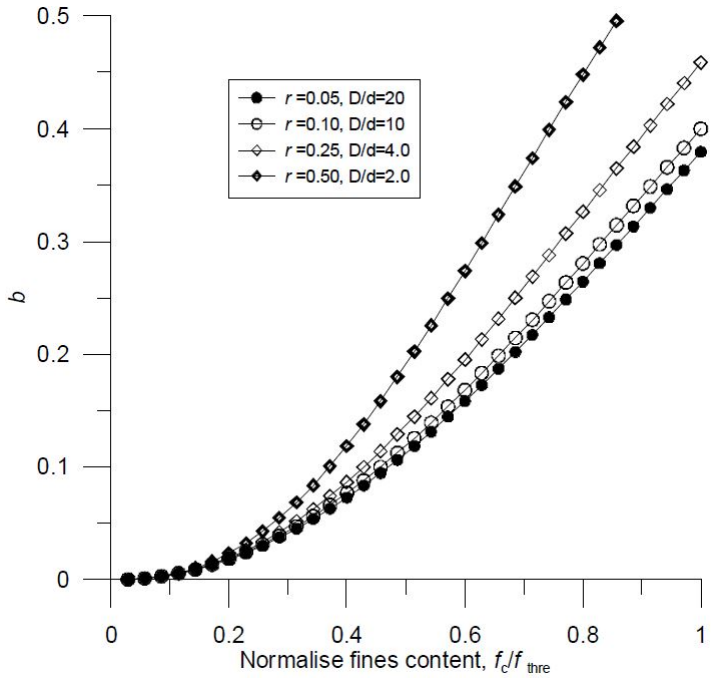

Figure 2.28.: Influence of fines content on b for f_{cth}=0.35, Rahman & Lo (2008)

2.4.5. Prediction of Threshold Fine Content, f_{cth}

As noted before, an initial approximation of threshold fines content is needed to predict the b value. As can be seen in Figure 2.29, based on experimental results showing the minimum void ratio versus the fines content, the minimum point of the V-shape e-f_c-relationship is defined as the threshold fines content, f_{cth}. This point is also considered as point marking the transition from the fines-in-sand regime to the sand-in-fines regime.

Equation 2.14 was developed by Rahman and his co-workers (Rahman & Lo 2008;

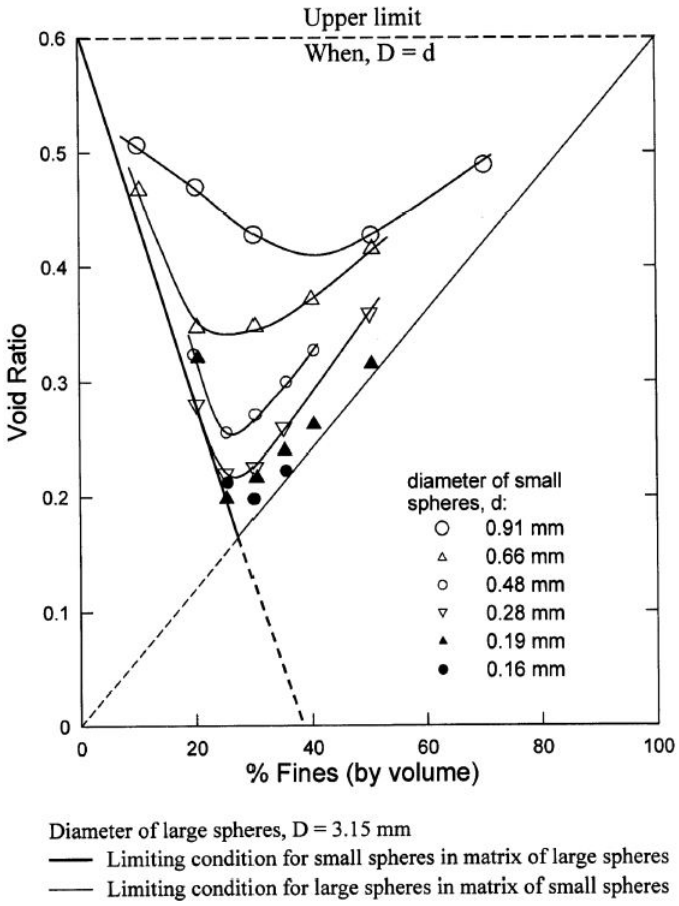

Figure 2.29.: Effect of fines content on minimum void ratio of binary packing, Rahman & Lo (2008) (after Lade et al. 1998)

Rahman 2009; Rahman et al. 2011; Rahman & Lo 2012) to estimate f_{cth} for different types of sand-fines mixtures.

$$f_{cth} = A\Big(\frac{1}{1+e^{\alpha-\beta\chi}} + \frac{1}{\chi}\Big) \tag{2.14}$$

where the coefficient A has an approximate value of 0.4, and α and β are determined by curve fitting for different ranges of χ.

To demonstrate the application of Equations 2.11 and 2.14, Table 2.2 summarized some previous studies on sand-fines mixtures and gives calculated f_{cth} and b values using the empirical parameters of Rahman & Lo (2012).

The b value for all previous studies is calculated using Equation 2.11, and the threshold

Table 2.2.: Summary of some previous work on sand-fines mixture, after Rahman & Lo (2012)

Reference	D_{10} [mm]	d_{50} [mm]	f_c [%]	f_{cth} [%]	χ [-]	b value [-]
Vaid (1994)	0.07	0.007	0-21	32	10	0-0.276
Zlatovic & Ishihara (1995)	0.116	0.01	0-30	33	11.6	0-0.360
Polito (1999)	0.089	0.031	0-37	30	2.87	0-0.389
Polito & Martin (2001)	0.311	0.031	0-25	32	10.03	0-0.321
Thevanayagam et al. (2002)	0.160	0.010	0-25	36	2.87	0-0.280
Huang et al. (2004)	0.08	0.044	0-30	41	1.82	0-0.481
Bobei & Lo (2005)	0.225	0.006	0-20	40	40	0-0.195
Yang et al. (2006a)	0.225	0.032	0-30	7.03	30	0-0.410
Present(own) study	0.265	0.0264	0-100	32	10.038	0-0.495

value is calculated using Equation 2.14 based on source data. However, in some cases, Equation 2.14 is used to find the threshold fine content.

It should be noted that in the current thesis, $\mu = 0.46$ is estimated to provide the best fit of steady state data points. However, for the data collected from the literature, the value of $\mu = 0.3$ was used to obtain the b parameter.

The steady state line in e^*-log p' space is known as the Equivalent Granular Steady State Line (EG-SSL). The applicability of EG-SSL has been clearly demonstrated by Rahman & Lo (2008) for a bunch of published data for f_c<f_{cth}, see Figure 2.30. The hatched area indicates the location of the SSLs of the individual sand-fines mixtures. The discrepancy in location of SSLs of the mixtures from the SSL of clean sand manifested the dependency of position of the SSLs on fines content in e-log p'. However, the SS data points based on e^* are almost located within a narrow band. The SSL at a given f_c can be converted into the EG-SSL by using e^* instead of e. The EG-SSL for Sydney sand derived from experiments by Rahman et al. (2011) with fines f_c<f_{cth} is shown in Figure 2.31. Furthermore, Rahman et al. (2014) indicated that using the concept of a EG-SSL helps to infer the SSLs for a particular f_c, see Figure 2.32.

It can be seen in Table 2.3 that only a small number of previous studies have been focused on SSLs for mixtures with high amounts of fines content at different ranges of

initial density. It is important to keep in mind that previous researchers have observed the same curved or linear trends for mixtures with $f_c < f_{cth}$ and $f_c > f_{cth}$, which were tested in the same range of initial density.

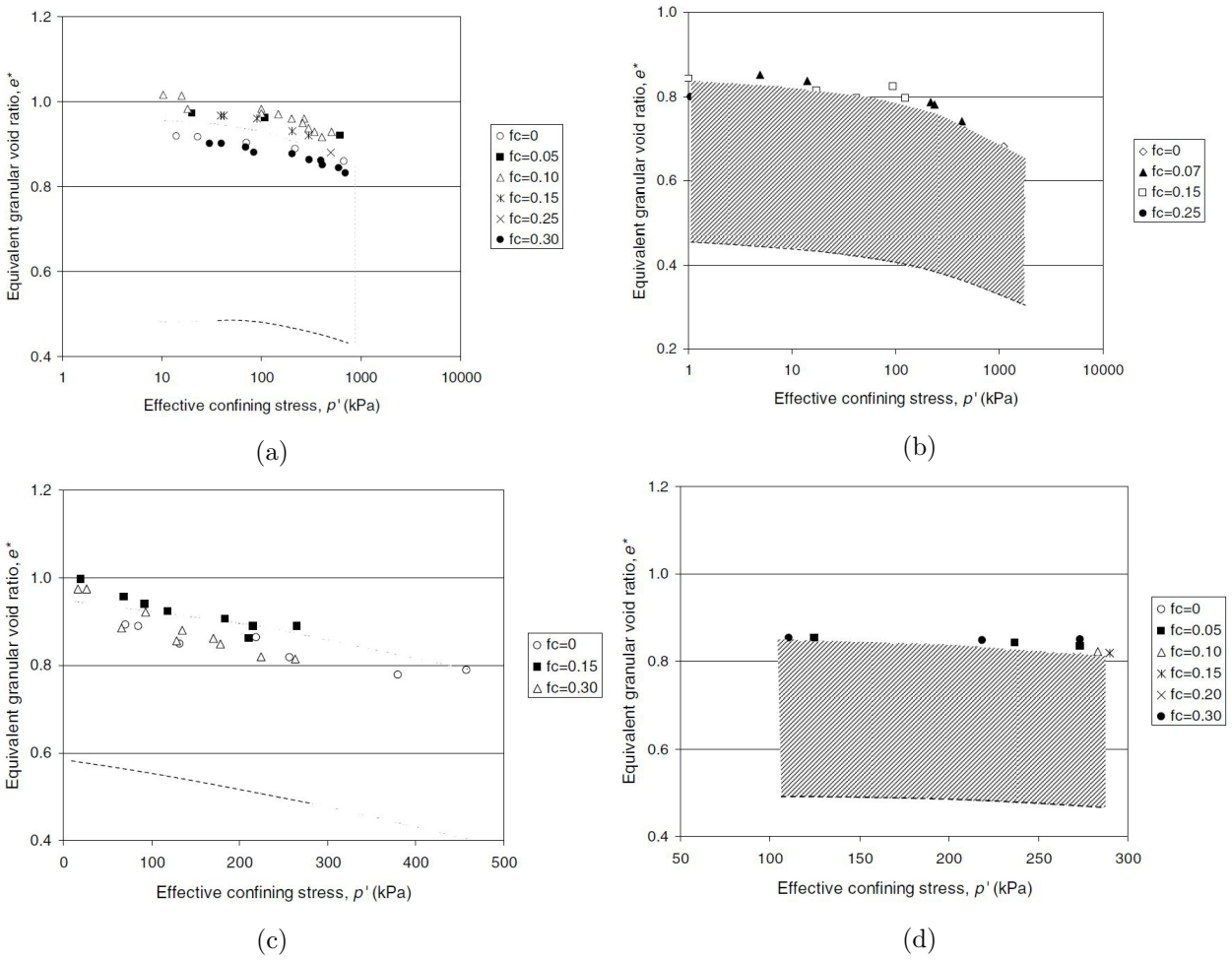

Figure 2.30.: Steady state lines of: (a) Toyuora sand with fines; (b) Foundry sand with non-plastic fines; (c) Mai Liao sand with fines; (d) Hokksund sand with Chengbei non-plastic fines, Rahman & Lo (2008)

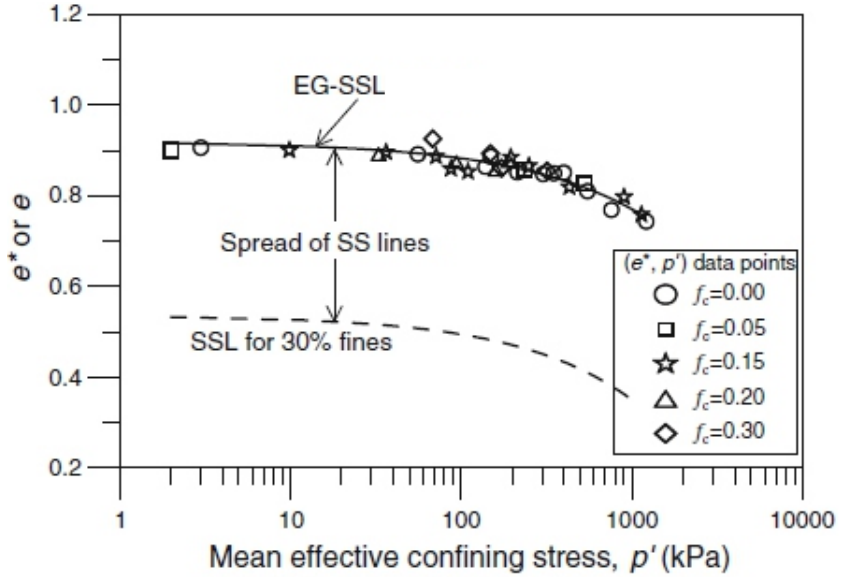

Figure 2.31.: Equivalent granular steady state line of Sydney sand, after Rahman et al. (2011)

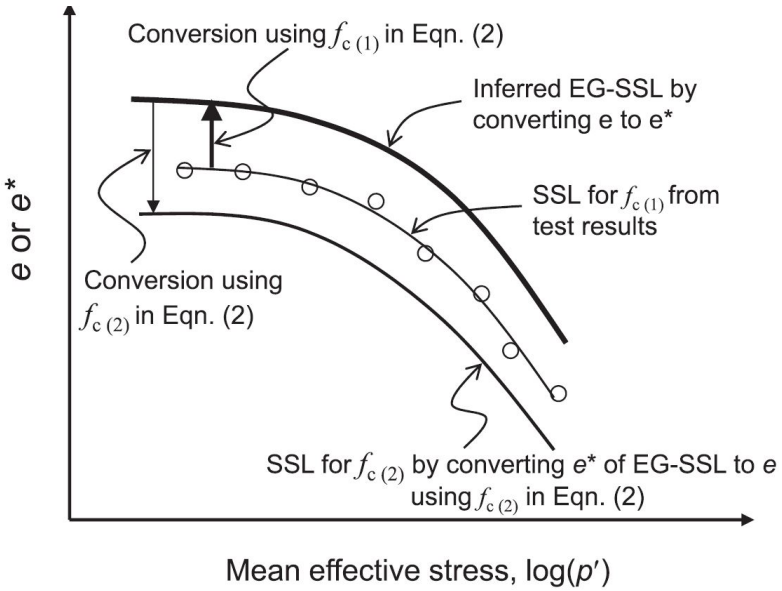

Figure 2.32.: SSL for a certain fines content $f_{c(2)}$ using a known SSL for another fines content $f_{c(2)}$, Rahman et al. (2014)

Table 2.3.: Summary of related researches on sand-silt mixtures

Study	Tested fines content	Fines type	Grains shape	GSD	SSLs Shape and position	Note
Been & Jefferies (1985)	$f_c < f_{cth}$ 0,2,5,10 %	non-plastic silt	no information	no information	increasing the slope of SSL with increasing f_c/linear shape	e^* concept was not discussed
Zlatovic & Ishihara (1995)	$f_c > f_{cth}$ 0,5,10,15,25, 30,40,100 [%]	non-plastic silt milled host sand used as f_c	no information	gap-graded	SSLs move downward up to f_{cth} then move upward to pure silt	e^* concept was not discussed
Bouckovalas et al. (2003)	$f_c < f_{cth}$ 0,5,10,20,30 [%]	non-plastic silt	no information	no information	increasing the slope of SSL with increasing f_c, rotate clockwise around the pivot point/linear shape	e^* concept was not discussed
Thevanayagam et al. (2002)	$f_c > f_{cth}$ 0,7,15,25,40 60,100 [%]	non-plastic silt	crushed silt	gap-graded	SSLs move downward up to f_{cth} then move upward to pure silt /almost curved	e^* concept was discussed, b=0.25 m=0.65 used to get e^* /two separate EGSSL for $f_c < f_{cth}$ and $f_c > f_{cth}$ but same tendency
Yang (2004)	$f_c > f_{cth}$ 0,5,10,15,20,30 50,70,94 [%]	non-plastic silt	sharp edges, cubical sand / angular silt	gap-graded	SSLs move downward up to f_{cth} then move upward to 94% silt /almost linear	e^* concept was discussed, b=0.25,0.34 m=0.65 used to get e^* /two separate EGSSL for $f_c < f_{cth}$ and $f_c > f_{cth}$ but same tendency
Rahman et al. (2010)	$f_c < f_{cth}$ 0,5,15,20,30 [%]	low-plastic silt	no information	poor-graded sand well-graded silt	SSLs move downward up to f_{cth}	e^* concept was discussed, b calculated to get e^* / single EGSSL with same tendency like sand
Carrera et al. (2011)	$f_c < f_{cth}$ 0,30,50,100 [%]	low-plastic silt	sub-angular to sub-rounded silt	gap-graded	SSLs move downward up to f_{cth} then move upward to 100% silt	e^* concept was discussed, b=0.8 used to get e^* / single EGSSL with same tendency like sand

2.5. Cyclic Response of Soils

Many researchers worked on the liquefaction behavior of soils under cyclic loading and their results revealed other mechanisms of liquefaction known as cyclic mobility. As Castro et al. (1982), Chung (1985) and Vaid & Chern (1985) reported, there exist many resemblances between cyclic and monotonic behavior. Most of the previous studies with cyclic loading were conducted on clean sand (Hyodo et al. 1998; Hyodo et al. 1994; Ishihara et al. 1975; De Gennaro et al. 2004; Vaid & Sivathayalan 2007; Yang & Sze 2010). In order to determine the liquefaction potential of soils three major laboratory methods are usually used to simulate the stress conditions in the field: cyclic simple shear test, cyclic triaxial test and cyclic torsional shear test. In the study described in this thesis, cyclic triaxial tests are performed on isotropically and anisotropically consolidated clean sand.

Previous work demonstrated that a soil that shows dilation behavior or only limited strain under monotonic loading, may develop large strains when subjected to cyclic loading (Kuerbis 1985). This is a result of the development of cyclic mobility. When the soil is subjected to cyclic loading under undrained conditions, a gradual softening response is observed in the soil sample as the pore pressure and shear strain increase. Seed (1979) indicated that small shear strain occurs until the excess pore water pressure increases to almost 60% of the initial effective stress. In general, during cyclic loading, deformations become large when effective stresses approach zero. However, deformations will usually stabilize when the cyclic loading stops.

Castro & Poulos (1977) stated that "cyclic mobility is the progressive softening response of a saturated sand specimen when subjected to cyclic loading at constant void ratio. The softening is accompanied by high pore water pressure, increasing cyclic deformation and in some cases permanent deformations. However, it does not lead to loss in shear strength, nor to continuous deformation". Cyclic mobility is the result of excess pore water pressure generation and simultaneous degradation of shear stiffness due to seismic or cyclic loading (Vaid & Chern 1985). Furthermore, Ishihara (1993) proposed a definition of initial liquefaction related to cyclic mobility, as the occurrence of zero effective stress, and a definition of full liquefaction as the state where a certain value of the double amplitude of axial strain, DA, (e. g. 5%) is reached. After initial liquefaction, a state of zero effective stress may be temporary reached during a load cycle, and the cyclic stresses can still be sustained for a few further cycles, until the criterion of full liquefaction (or failure) is fulfilled. This form of cyclic liquefaction is recognized as cyclic mobility and this terminology is used to identify this type of behavior in the current study. Typical

cyclic mobility behavior is depicted in Figure 2.33.
During cyclic loading (e.g. caused by an earthquake), an element of soil is subjected to a series of cyclic shear strains that reverse directions many times during loading, as shown in Figure 2.34. Figure 2.35 illustrates the stress conditions of soil elements in the cyclic triaxial test. This figure shows three stress conditions at different stages of cyclic loading tests. In the case of Figure 2.35(a), the specimen is subjected to all-around pressure (isotropic condition). The Mohr-stress circle for this stress condition is a point and the stress on the 45°-plane is equal to σ_3. In Figure 2.35(b), the vertical stress is increased by an amount of $(q/2)$ and the horizontal stress is reduced by an equal amount of $(q/2)$. The Mohr-stress circle is presented in the second column. It can be seen that the normal stress on a 45°-plane is still equal to σ_3, but a shear stress equal to $(q/2)$ has also been induced. In Figure 2.35(c), the vertical stress is reduced by $(q/2)$ with respect to the isotropic state and the horizontal stress is increased by an equal amount. The normal stress on a 45°-plane is still equal to σ_3, and a shear stress of $(q/2)$ has also been induced but in the opposite direction to case (b). The effects of the intermediate stress are neglected as is common in triaxial tests (Seed & Lee 1966).

To quantify the applied stress during cyclic triaxial testing, the Cyclic Stress Ratio (CSR) is defined as the ratio of cyclic shear stress (τ_{cyc}) to the initial mean effective stress (p'_0). Another quantity that is used to indicate the cyclic strength of a soil sample is termed Cyclic Resistance Ratio (CRR). The CRR can be defined as the CSR needed to cause (initial liquefaction or a certain failure criterion (a certain value of the double axial strain amplitude) in a specified number of loading cycles, which is usually lying between 10 and 20 (Baki 2011).
Silver et al. (1976) and Mulilis et al. (1978) found that the shape of the loading pattern has a strong effect on the cyclic strength of a soil. In previous studies, several waveforms were tested such as, rectangular, degraded rectangular, or triangle, and sinusoidal waves. The effects of various wave shapes on the relationship between cyclic stress for Monterey #0 sand are depicted in Figure 2.36 (after Silver et al. 1976). Polito 1999 reported that sinusoidal waves can produce cyclic strengths, 15 to 30 percent higher than those produced under rectangular waves of the same maximum amplitude. This increase in strength is presumably the result of the drastic velocity changes that happen during the application of the rectangular shape of loading. It should be noted that, all other waveforms (e.g. triangle, sinusoidal, degraded square) lead to the same liquefaction resistance. A sinusoidal shaped function is used in this thesis.

Previous researchers worked on the effect of the presence of fines on the cyclic resistance

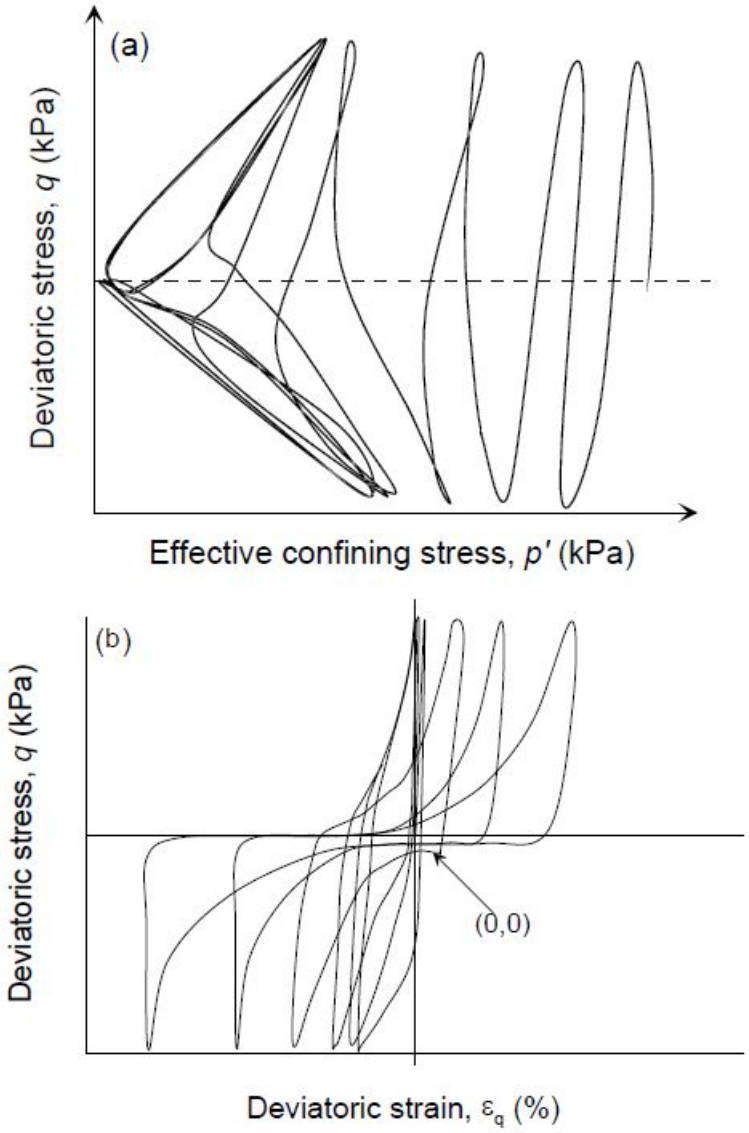

Figure 2.33.: Typical cyclic mobility behavior of a sand under two way symmetrical cyclic loading in the triaxial test, Baki (2011)

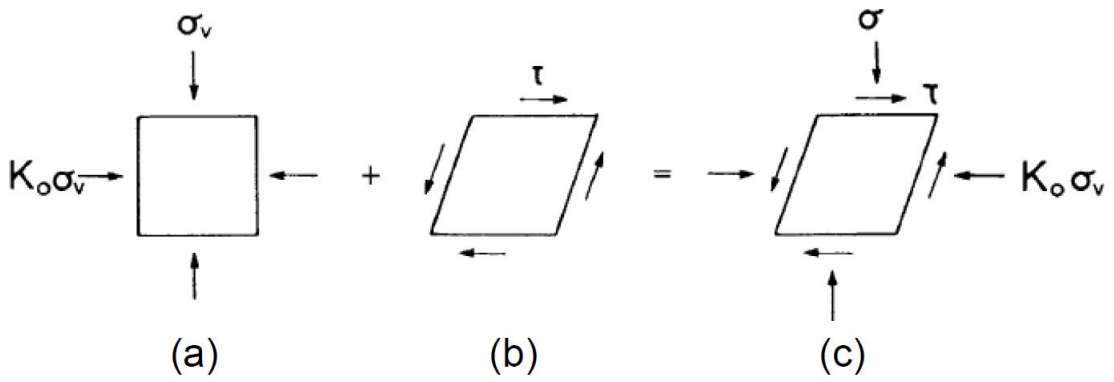

Figure 2.34.: Idealized stress conditions of a soil element below ground surface under cyclic loading, after Seed & Lee (1966)

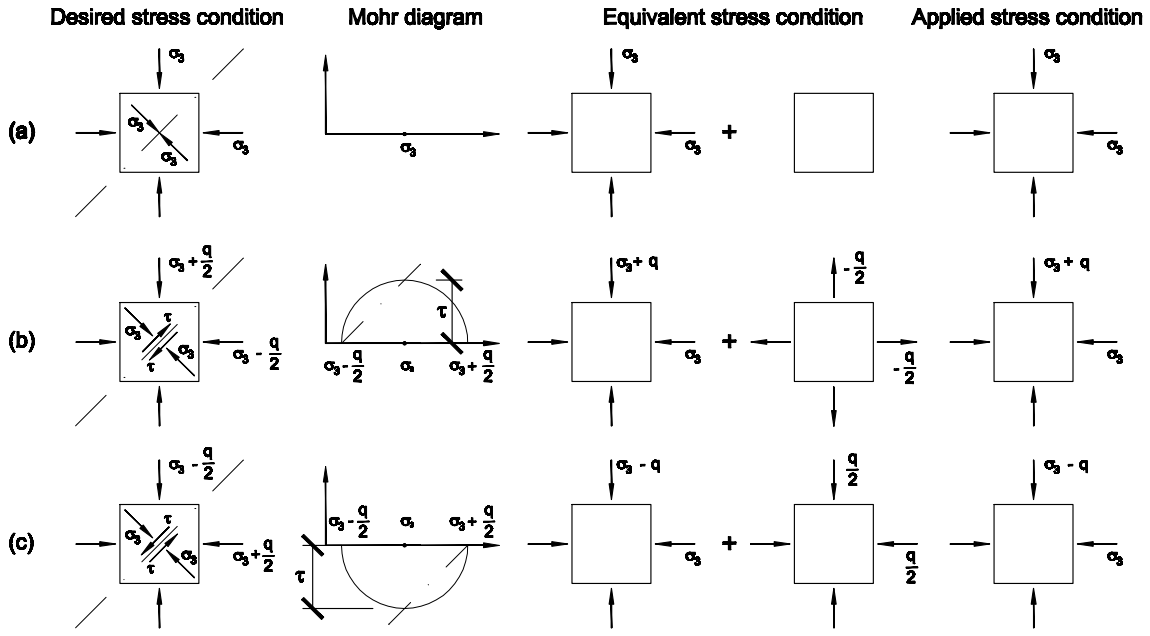

Figure 2.35.: Stress conditions in cyclic triaxial tests on saturated sand, after Seed & Lee (1966)

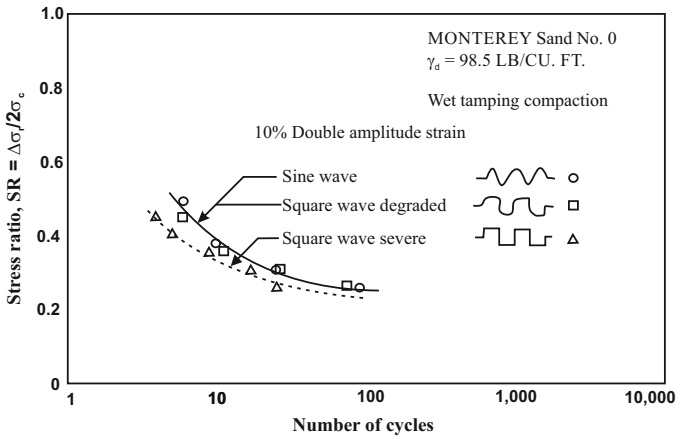

Figure 2.36.: The effect of wave shape on liquefaction resistance after Silver et al. (1976)

of the soil at a constant void ratio. There are many uncertainties in the literature regarding this effect. Some researchers (Troncoso & Verdugo 1985; Kuerbis et al. 1988; Koester 1994; Vaid 1994; Finn et al. 1994; Chien et al. 2002; Belkhatir et al. 2010a,b; Stamatopoulos 2010) reported that cyclic resistance decreased with increase in fines content. On the other hand, some studies (Amini & Qi 2000; Chang et al. 1982) indicated opposite results. Other researchers (Polito & Martin 2001; Xenaki & Athanasopoulos 2003; Ghahremani et al. 2006; Sadek & Saleh 2007; Athanasopoulos & Xenaki 2008; Papadopoulou & Tika 2008) reported that cyclic strength increases with an increase in fines content up to a significant amount of f_c, and beyond this point, the trend reversed with an increase in f_c. As stated in the previous works, two methods exist to assess the excess pore water pressure response of soils. The first method was proposed by Lee & Albaisa (1974). It predicts the pore pressure response as a function of the ratio of the number of loading cycles to the cycles needed for an initiation of liquefaction. The second method was suggested by Dobry et al. (1982), where the excess pore water pressure is predicted based on acting strain amplitudes.

2.5.1. Frequency of cyclic Loading

The effect of the frequency of loading on cyclic strength in sand has been studied by several researchers, including Mulilis et al. (1975); Grozic et al. (2000); Polito (1999); De Gennaro et al. (2004). Mulilis et al. (1975) reported that lower loading frequencies produced slightly higher cyclic strengths, while Lee & Fitton (1968) found the contrary effect. Later, Polito (1999) performed cyclic triaxial tests on Monterey No. 0/30 sand

with two different frequencies of 1 Hz and 0.5 Hz. It can be seen that small changes in frequency of loading do not have any measurable effect on the cyclic strength of the adopted sand, see Figure 2.37.
In the entire test program of the present study, a frequency of 0.1 Hz with sinusoidal wave pattern was maintained.

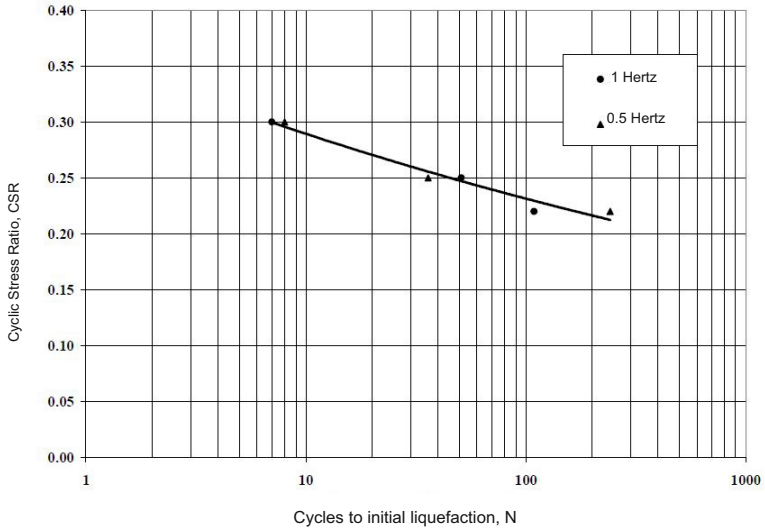

Figure 2.37.: Effect of different frequency of loading on number of cycles to initial liquefaction of sand, after Polito (1999)

2.5.2. Linkage Between Static and Cyclic Instability

In previous studies, the linkage between cyclic and static instability of sand and sand with fines has been examined by performing replicate test pairs where a test-pair comprised an undrained monotonic and an undrained cyclic loading test (Baki 2011; Rahman, Baki, Lo & Gnanendran 2012). However, due to different characteristics lines proposed for the linkage of static and cyclic instability, some contradictions were discovered in their outcomes. Ishihara et al. (1975) reported that the cyclic instability of Fuji river sand, in a loose state and under non-symmetrical cyclic loading, happened very close to the triggering point of the phase transformation of the undrained monotonic test. Sladen et al. (1985) demonstrated that instability of samples under cyclic loading is triggered in the instability zone when the FLS is crossed. The FLS can be determined from the corresponding undrained monotonic test. The instability stress ratio, η_{IS} is introduced as the slope of FLS (q_{max} / p'_{IS}), where the q_{max} and p'_{IS} are the deviatoric stress and

the mean effective stress at the onset of static instability, respectively. According to the other researchers (Yamamuro & Covert 2001; Lo et al. 2010; Yang & Sze 2010; Baki 2011; Rahman, Cubrinovski & Cameron 2012), the instability under cyclic loading is triggered shortly after the cyclic stress path crosses the flow liquefaction surface. An investigation of cyclic behavior of clean sand and its linkage to the undrained monotonic response is presented in Chapter 5 of this study.

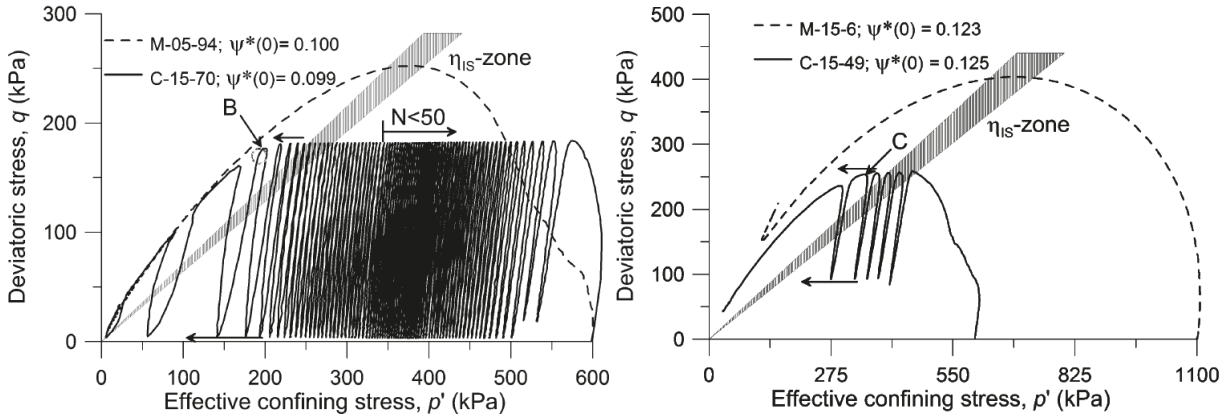

(a) (b)

Figure 2.38.: Comparison between a monotonic and a one-way cyclic loading test with the same initial state parameter, Rahman, Baki, Lo & Gnanendran (2012)

2.6. Summary

The above review reveals that it can be conducted that, the behavior of sand-fines mixtures under undrained monotonic and cyclic loading is complicated. According to the results presented, for undrained triaxial tests, the liquefaction resistance of mixtures may increase or decrease with increasing fines content. Soils with fines content showed higher volumetric strain and compressibility in drained tests, while the cyclic stress ratio may increase or decrease. It is difficult to draw a conclusion on the reason for these different observations. Several factors may play a role in that context on the cyclic behavior of mixtures e.g., initial mean effective stress, type of coarse and fine soil involved in the mixture, soil grain shape and so on. It is desirable to find appropriate equations and parameters to describe the mechanical behavior of mixtures in a unified way. For example, the relative density is not an appropriate parameter to characterize the behavior of sand-silt mixtures. As can be seen in Figure 2.7, despite the fact that the relative density

of the samples increased slightly with an increase in the fines content, the liquefaction resistance of the mixtures decreased. The equivalent granular void ratio, e^* was proposed for characterizing the behavior of mixtures, but due to the lack of research on the behavior of sand-silt mixtures with high fines content, further experimental investigations are required to confirmed the e^* concept. For many years the steady state concept has been widely investigated. The reported results were focused mainly on the uniqueness of the steady state line of a pure sand and sand-fines mixtures with small amounts of fines content.

More experimental research is still needed on a application of the combination of laboratory test results (SSL concept) with in-situ test results (CPT) to estimate liquefaction susceptibility, and to find a link between laboratory results and engineering estimation. So, based on the review of literature presented in this chapter a respective experimental investigation has been carried out. It is documented in the next chapters. The following tasks have been undertaken in this study:

- Evaluation of the effect of high fines content at different initial state (relative density and initial mean effective stress) on liquefaction behavior of sands. Only non-plastic fines were used and aging and cementation effects were not considered.
- Investigating the effect of high fines content on the uniqueness, shape and position of the steady state line.
- Application of laboratory test (triaxial test) results in combination with in-situ test data (CPT) to provide a new concept for a proper design of compaction measures (by working on a case study).

3. Material and Experimental Program

3.1. General

A systematic experimental program was undertaken to assess the undrained behavior of (1) artificial sand-silt-mixtures with varying content of non-plastic fines and (2) sandy soils sampled from the dump site of former open-pit mines in Lusatian area in Germany. The first section of the chapter is dedicated to the physical and geotechnical properties of the materials used in particular the grain shape characteristics. The test materials are Hostun sand, Querenburg silt and binary mixtures of these two constituents on one hand, and Seese sand sampled from two different locations in the dumps of the former open-pit mining site in Lusatia on the other hand. In the second and third section, the triaxial testing program performed on the above sets of material as well as the triaxial apparatus used are presented.

3.2. Material Characterization

Two types of materials were used in this research: 1) Hostun sand; and 2) Querenburg non-plastic silt (local soil), which were adopted as host material and fines content, respectively. They were used for studying the effect of fines on the position of the steady state line and liquefaction behavior of the mixtures. The physical properties of these materials are presented in the following sections. Two different types of microscopes were used for the grain shape analysis due to the different size of the sand and the fines particles. They were: Environmental Scanning Electron Microscope (ESEM), and light microscope. The ESEM images show the shape and size of the fines, while the light microscope images help to get a visual overview of the particle arrangement in sand-silt mixtures with changing fines content. The findings from the pictures taken with the microscopes are discussed in detail in the following subsections.

3.2.1. Hostun Sand

Hostun sand has been used in many previous studies (Schanz & Vermeer 1996; De Gennaro et al. 2004; Sadek et al. 2006; Lins 2009; Guo & Zhao 2013) and has become a standard sand in soil mechanics research. Hostun sand originates from a place called Hostun in the Drome department in France. It is a quartz sand with grain sizes ranging from 0.075 mm to 1.0 mm. According to the unified soil classification system (USCS), the material is a poorly-graded medium sand SP. The color of Hostun sand may vary between gray-white and rosy-beige, while its chemical components consist of high siliceous amount ($SiO2 > 98\%$) (Amat 2007; Goudarzy 2015). The grain size distribution (DIN 18123) is shown in Figure 3.1b. A microscopic image of Hostun sand particles is presented in Figure 3.1a. The grain shape varies from angular to sub-angular. The values of the minimum and maximum void ratios, e_{min} and e_{max}, of Hostun sand were determined according to DIN 18126 standard. The physical properties of Hostun sand are summarized in Table 3.3.
To get a first impression on the volume change behavior of Hostun sand drained monotonic triaxial tests were conducted at an effective confining pressure of $\sigma'_3 = 100$ kPa, on dense and loose samples. The stress-strain curves and volume change of dense and loose Hostun sand are shown in Figure 3.1.

Figure 3.2a shows that the samples reach the steady state zone at a vertical strain of

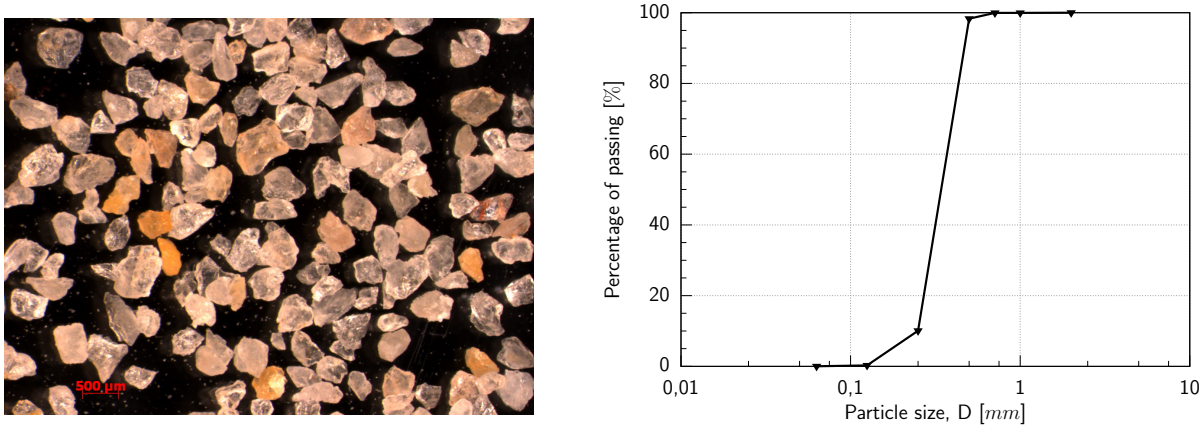

(a) (b)

Figure 3.1.: Particle characteristics of Hostun Sand: (a) shape of particles (light microscope picture); (b) grain size distribution

almost 15%. Furthermore, the results in Figure 3.2 show that a dense sample starts to dilate at a vertical strain less than 2%.

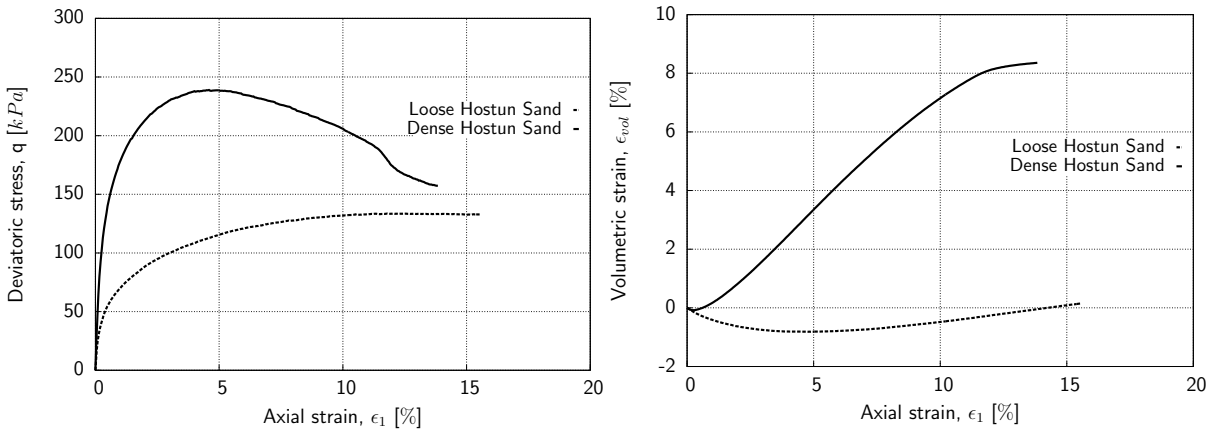

(a) (b)

Figure 3.2.: Behaviour of loose and dense samples of Hostun Sand in drained monotonic triaxial tests with an effective confining pressure of 100 kPa: (a) stress strain behavior; (b) volumetric strain versus axial strain

3.2.2. Fines (Querenburg silt)

The Querenburg silt used for this study was collected from an area in the city of Bochum, Germany. Querenburg silt is a brown colored non-plastic silt. The grain size distribution curve for Querenburg silt obtained using the Hydrometer test (DIN 18123) is shown in Figure 3.3b. The physical properties of Querenburg silt are presented in Table 3.3, and a microscopic image is shown in Figure 3.3a. The shape of the silt grains was found to be angular. The chemical composition of tested fines as determined by X-Ray Fluorescence (XRF) analysis is listed in Table 3.1. The Atterberg limits of the used silt were determined according to the German standard DIN 18122. The liquid and plastic limits of the silt are $w_L = 26.2\%$, $w_P = 20.6\%$, respectively, which results in the plasticity index PI = 5.7%.

Table 3.1.: Chemical compositions of Querenburg silt

Oxides name	SiO_2	Al_2O_3	Fe_2O_3	K_2O	Na_2O	TiO_2	MgO	CaO	P_2O_5	MnO
%	81.37	9.18	3.40	2.42	1.10	0.76	0.75	0.68	0.11	0.08

Previous studies (e.g. Bowman et al. 2001; Fernlund 2005; Rodriguez et al. 2013) have used different methods and techniques to determine the geometrical shape of grains, and detailed measurements of roundness are rarely reported in the literature. Powers (1953) introduced a qualitative classification to describe particle shape by means of roundness. Powers' classification procedure is presented in Figure 3.4 along with Table 3.2. A visual comparison of the grains of Hostun sand with the pictures in Figure 3.4 according to

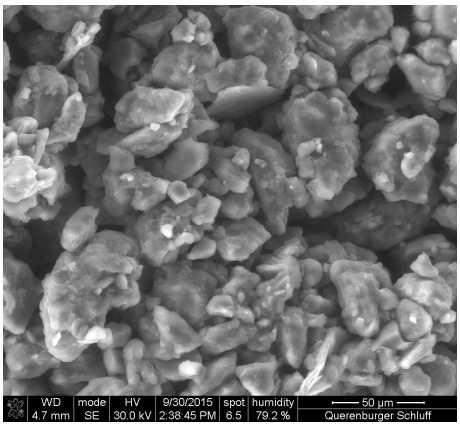

(a)

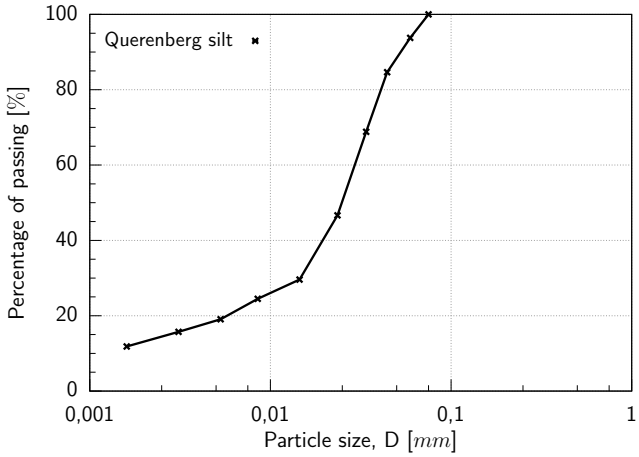

(b)

Figure 3.3.: Particle characteristics of Querenburg silt: (a) grain size distribution; (b) shape of particles (ESEM picture)

Powers' classification system (Powers 1953) is used in this study. Moreover, the sphericity of the grains are calculated based on Wadell (1933), see Equation 3.1. Roundness of the grains is calculated based on Cho et al. (2006) and Powers (1953), using Equation 3.2 and Figure 3.5. The Sphericity, S is defined as the ratio of the radius of a circle having an area equal to the largest projected area to the radius of the smallest circle that will circumscribe the grain projection, Wadell (1933).

$$S = \frac{r_{max-in}}{r_{min-cir}} \tag{3.1}$$

where r_{max-in} and $r_{min-cir}$ are the radius of the largest inscribed and smallest circumscribed spheres, respectively, see Figure 3.5. Roundness, R measures the degree of sharpness or curvature of the particle corners. Roundness is calculated by Equation 3.2.

$$R = \frac{\sum(r_i/N)}{r_{max-in}} \tag{3.2}$$

where r_i is the radius of the largest sphere inscribed in the i^{th} corner of the particle surface, see Figure 3.5. The roundness and sphericity of the Hostun sand is determined as 0.34 and 0.78, respectively. The roundness and sphericity of adopted silt is determined as 0.24 and 0.65, respectively. It can be concluded from Table 3.2 and Figures powerfig and 3.5 that Hostun sand grains have subangular shape and the silt grains have an angular shape.

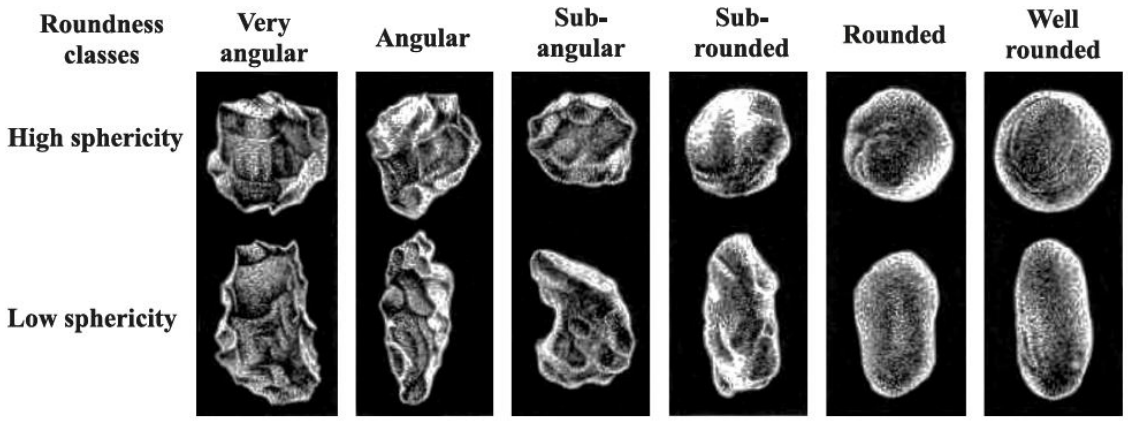

Figure 3.4.: Visual shape classification of grains, Powers (1953)

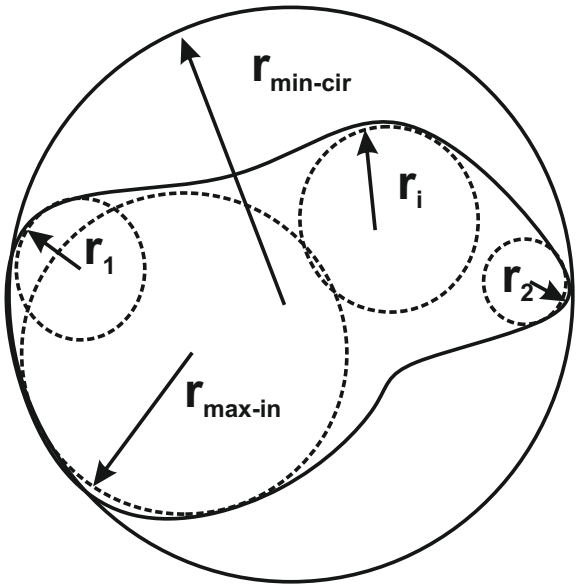

Figure 3.5.: Sphericity of the grains, after Wadell (1933) in Cho et al. (2006)

Table 3.2.: Description of grains shape and the associated roundness intervals, Powers (1953)

Description	Very angular	Angular	Sub-angular	Sub-rounded	Rounded	Well rounded
R	0.12≤R<0.17	0.17≤R<0.25	0.25≤R<0.35	0.35≤R<0.49	0.49≤R<0.70	0.70≤R<1.0

*R = Roundness

3.2.3. Sand-silt Mixtures

Various amounts of Querenburg silt were mixed with clean Hostun sand to obtain a target fines content from 10 to 100% by dry weight of solids. The resulting grain size distribution curves are shown in Figure 3.6 together with those of the pure Hostun sand and the pure Querenburg silt.

In order to assure that the results could be compared with the international literature,

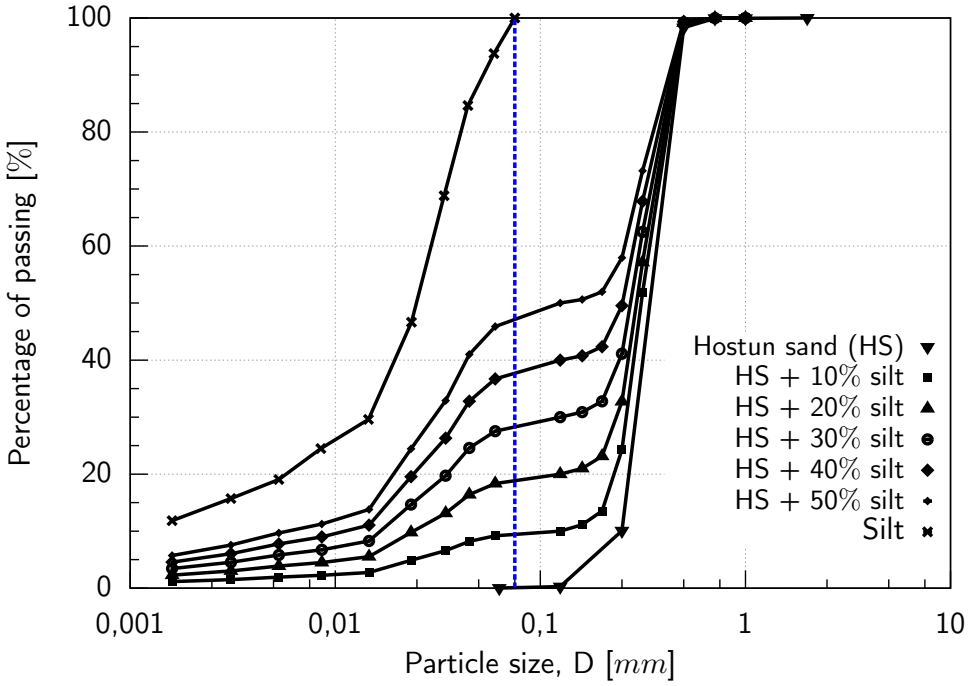

Figure 3.6.: Grain size distribution of Hostun sand-silt mixtures

the relevant diameter separating fine grains from coarse grains was chosen to be 0.075 mm according to ASTM standard. Thus, any fines content in the present study has a diameter $\leq$ 0.075 mm. Hostun sand was washed to separate any particles with a diameter of less than 0.075 mm.

The maximum and minimum void ratios of the mixtures have been determined according to DIN 18126. It should be noted that the standard procedure for the determination of e_{max} and e_{min} is usually only applicable for sand with fines content up to 15%, because at higher fines content segregation during pouring of the mixed soil may occur. However, for lack of other methods available, and in agreement with other literature (e.g. Tao et al. 2004) the e_{min} and e_{max} values of the mixtures with 20%, 30%, 40% and 50% fines content were also determined by the standard procedure. According to the DIN 18126 standard, the value of e_{max} was determined by placing the standard funnel at the bottom

of a standard mold. Then, the funnel was raised slowly so that the sand-silt mixture could flow out and from a cone. This procedure was carried out without any drop height of the soil, in order to reduce particle segregation. To determine the value of minimum void ratio of the mixtures with a fines content of 0%, 10% and 20%, the soil sample was divided into five equal masses. After placing each of these masses as an individual layer inside the mold, the mold was tapped uniformly with a standard hammer. The variation of e_{max} and e_{min} for Hostun sand with different percentages of f_c and the other physical properties of the mixtures are summarized in Table 3.3.

The graphical presentation of the test results for e_{min} and e_{max} in Figure 3.7 show that

Table 3.3.: The physical properties of Hostun Sand-Querenburg silt mixtures

Soil	D_{50} [mm]	D_{30} [mm]	D_{10} [mm]	G_s [-]	C_u [-]	e_{max} [-]	e_{min} [-]	Shape of grains
Hostun Sand	0.365	0.30	0.265	2.65	1.45	1.023	0.671	Subangular
HS+10% fc	0.320	0.285	0.135	2.652	2.59	0.984	0.496	
HS+20% fc	0.298	0.225	0.0235	2.654	13.83	0.896	0.378	
HS+30% fc	0.280	0.135	0.0185	2.655	16.22	0.851	0.331	
HS+40% fc	0.265	0.04	0.013	2.656	22.69	0.892	0.369	
HS+50% fc	0.135	0.03	0.006	2.658	45.83	0.967	0.383	
Querenburg Silt	0.0264	0.017	0.0016	2.665	18.750	1.676	0.479	Angular

e_{min} decreased up to a fines content of around 30% and then increased with further increase of f_c. The fines content at which the minimum void ratio changes from decreasing to increasing tendency is defined as the threshold fines content, f_{cth} (Naeini & Baziar 2004; Zuo & Baudet 2015). Based on Figure 3.7, the threshold fines content for the given mixtures was found to be 32%. This value is in accordance with that calculated by Equation 3.3 (Rahman & Lo, 2012).

$$f_{cth} = 0.4\left(\frac{1}{1+e^{0.5-0.13\chi}} + \frac{1}{\chi}\right) \tag{3.3}$$

Table 3.3 presents the coefficients of uniformity of the sand-silt mixtures. An abrupt jump from 2.59 to 13.83 can be observed as silt content increases from 10 to 20%. It increases further up to about 46 for the mixture with 50% fines and decreases to about 19% for pure silt. This shows that the coefficient of uniformity gives a rather poor basis for the classification of silty sand gradation or its behavior (Kuerbis 1985).

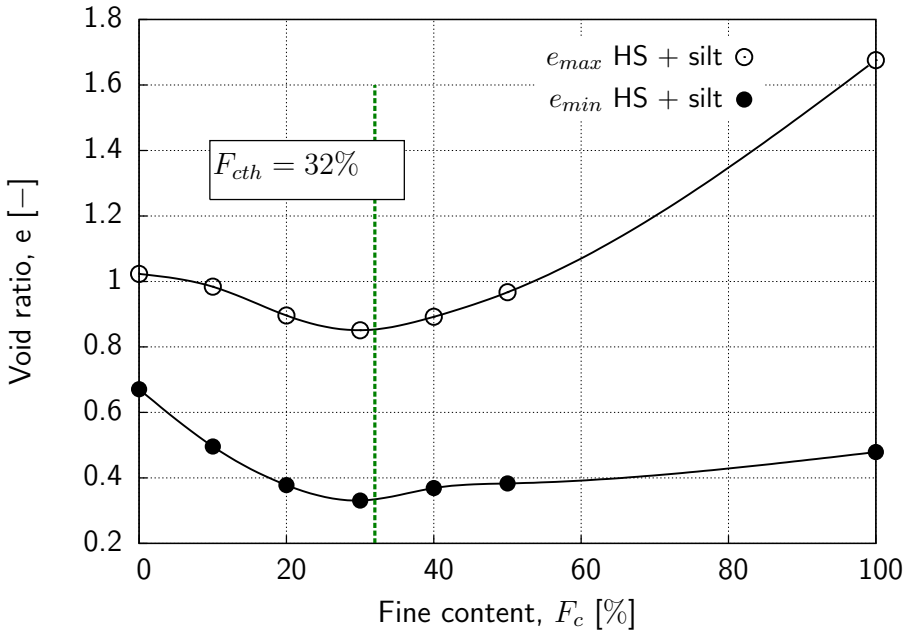

Figure 3.7.: Variation of maximum and minimum void ratio of Hostun sand-silt mixtures with fines content

3.2.4. Seese Sand

Disturbed samples of Seese sand were used in the present study. They originate from two different deposit areas of former open-pit mines, namely Schlabendorf-Süd (RL13) and Seese-West (HWW) (Figure 3.8). These material are natural sands. However, the original fluvial sand deposits were dug up and re-deposited during the technological process of open-pit brown coal mining. Since active mining in these areas ceased in the early nineties of the last century, the age of the deposits varies between 25 years and more.

Figure 3.9 shows the grain size distribution curves (DIN 18123) of the two sands. The grading parameters deduced are given in Table 3.4. The measured density of the grains (DIN 18124) and the values of minimum and maximum density and void ratios are presented in Table 3.5. For determination of particle shape, microscopic pictures were taken of both samples, see Figure 3.10.

Both materials are classified as poorly-graded sand (SP), containing very small amounts of fines ($< 1\%$). With respect to the grain shape, both sands have a similar shape. Roundness determined according to Power (1953) is 0.44 (corresponds to sub-rounded) for the sample Seese-West and 0.35 (corresponds to sub-rounded, being close to sub-angular) for the sample Schlabendorf-Süd.

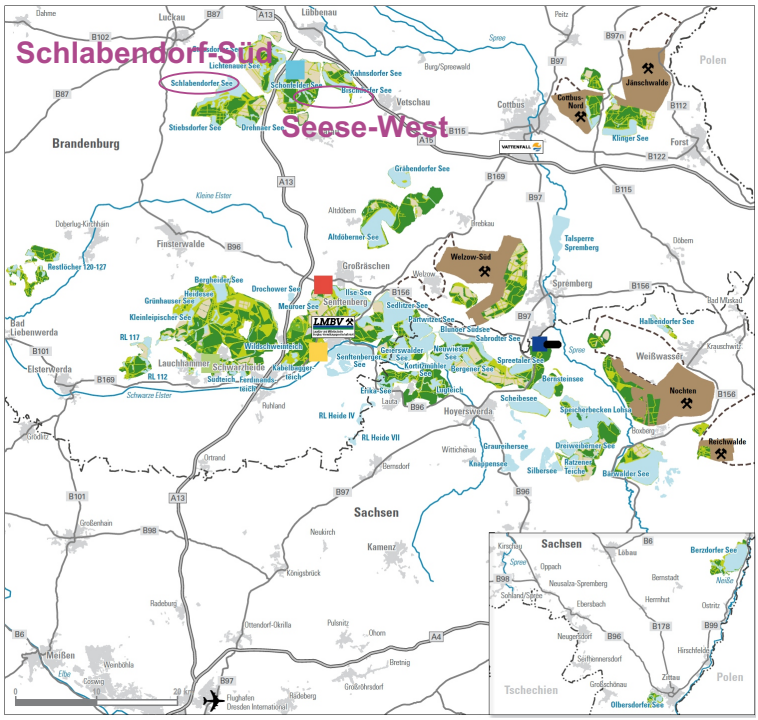

Figure 3.8.: Overview of Lusatian region with zones of former and active mining and the approximate location of sampling positions Schlabendorf-Süd and Seese-West (LMBV 2012)

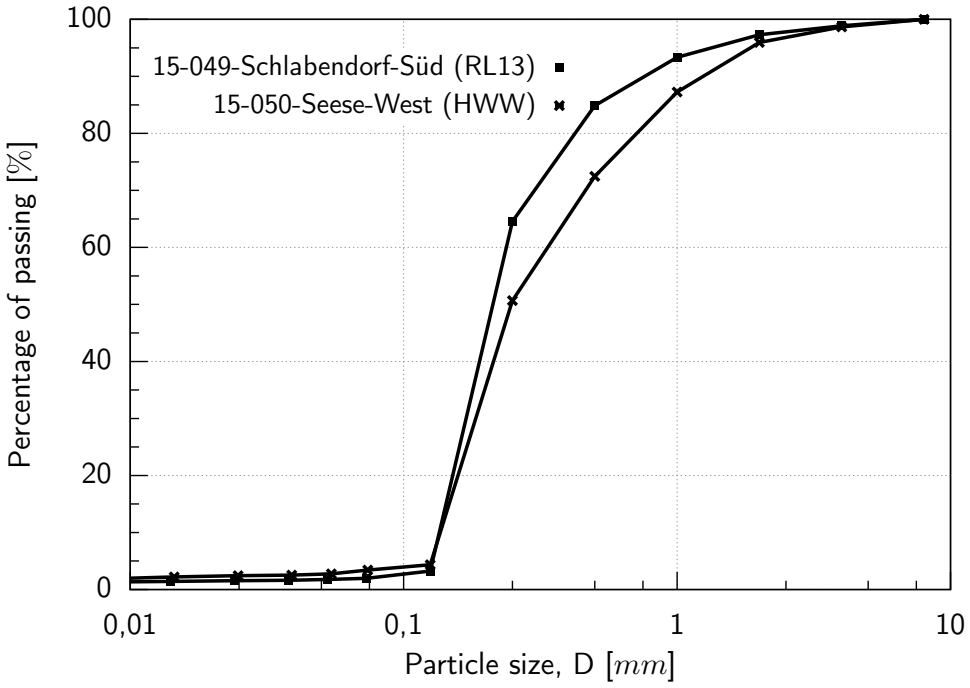

Figure 3.9.: Grain size distribution curves of samples Schlabendorf-Süd and Seese-West

Table 3.4.: Parameters of Seese sand

Sample No.	Location	D_{10} [mm]	D_{30} [mm]	D_{50} [mm]	D_{60} [mm]	C_u [-]	C_c [-]
15-049	Schlabendorf-Süd	0.145	0.185	0.215	0.230	1.58	1.02
15-050	Seese-West	0.150	0.191	0.260	0.315	2.10	0.77

Table 3.5.: Density of the grain, minimum and maximum densities and maximum and minimum void ratios of Seese sand

Sample No.	area	ρ_s $[\frac{g}{cm^3}]$	$\rho_{d,min}$ $[\frac{g}{cm^3}]$	$\rho_{d,max}$ $[\frac{g}{cm^3}]$	e_{max} [-]	e_{min} [-]
15-049	Schlabendorf-Süd	2.626	1.347	1.740	0.950	0.509
15-050	Seese-West	2.631	1.385	1.802	0.896	0.460

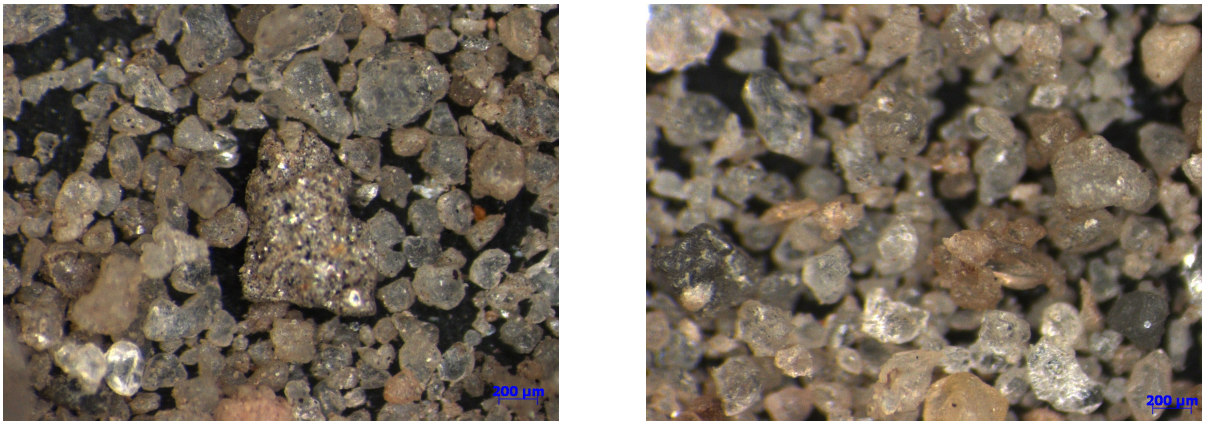

Figure 3.10.: Microscopic pictures of Seese sand (a) 15-049-Schlabendorf-Süd ; (b) 15-050-Seese-West

3.3. Triaxial Testing Program

3.3.1. Effect of Fines Content of Hostun Sand-Silt Mixtures

A series of 61 triaxial compression tests were conducted on Hostun sand-silt mixtures. The experimental program (Table 3.6) was designed in order to investigate the effect of fines on the undrained shear behavior and the locus of the steady-state line in the e-log p' plane. For the latter purpose, drained triaxial tests were included in the testing program. Samples were isotropically consolidated at a mean effective stress of between 50 and 500 kPa, and then subjected to an undrained monotonic loading in the axial direction with a constant rate of displacement of 0.1 mm/min. The initial mean effective stress range for the specimens was purposely chosen as it reflects the range of confining pressures at which soils are generally most susceptible to liquefaction in the field. Previous researchers (Stark & Olson 1995; Baki 2011) also reported that this range was selected based on field case histories of recognized level-ground liquefaction and the depths at which the liquefaction happened. More details about the testing program are given in Table 3.6. The following parameters are given in this table: the name of each test, fines content f_c, initial void ratio of samples after consolidation e_0, void ratio of the sample at steady state e_{ss}, relative density of the sample after consolidation D_r=e_{max}-e e$_{max}$-e_{min}, initial mean effective stress p'_0, state parameter ψ, the b and m parameters used to calculate the equivalent granular void ratio, and equivalent granular void ratio e^*.

Table 3.6.: Triaxial testing program on the effect of fines content (Hostun-sand-silt mixtures)

Test	f_c [%]	e_0 [-]	e_{ss} [-]	D_r [%]	p'_0 [kPa]	ψ [-]	b or m [-]	e^* [-]	Behavior
CU01-00-300	0	0.739	0.739	76	300	-0.122	0	0.739	Dilation
CU02-00-300	0	0.839	0.839	53	300	-0.022	0	0.839	Limited liquefaction
CU03-00-500	0	0.744	0.744	80	500	0.080	0	0.744	Dilation
CU04-00-50	0	0.719	0.719	86	50	-0.203	0	0.719	Dilation
CU05-00-100	0	0.719	0.719	86	100	-0.188	0	0.719	Dilation
CU06-00-300	0	0.715	0.715	87	300	-0.146	0	0.715	Dilation
CU07-00-500	0	0.713	0.713	87	500	-0.111	0	0.713	Dilation
CU08-00-300	0	0.874	0.874	38	300	0.013	0	0.874	Limited liquefaction
CU09-00-50	0	0.937	0.937	24	50	0.015	0	0.937	Limited liquefaction
CU10-00-100	0	0.855	0.855	47	100	-0.052	0	0.855	Dilation
CU11-00-120	0	0.890	0.890	38	120	-0.012	0	0.890	Limited liquefaction
CU12-00-120	0	0.920	0.920	29	120	0.018	0	0.920	Limited liquefaction
CU13-00-300	0	0.821	0.821	57	300	-0.04	0	0.821	Limited liquefaction
CU14-00-300	0	0.930	0.930	26	300	0.069	0	0.930	Liquefied

Continued on next page

Table 3.6 – *Continued from previous page*

Test	f_c [%]	e_0 [-]	e_{ss} [-]	D_r [%]	p'_0 [kPa]	ψ [-]	b or m [-]	e^* [-]	Behavior
CU15-00-500	0	0.855	0.855	47	500	0.031	0	0.813	Limited-liquefaction
CD16-00-50	0	0.672	0.794	100	50	-0.266	0	0.794	Dilation
CD17-00-100	0	0.672	0.784	100	100	-0.261	0	0.784	Dilation
CD18-00-150	0	0.673	0.781	100	150	-0.221	0	0.781	Dilation
CD19-00-200	0	0.672	0.783	100	200	-0.214	0	0.783	Dilation
CD20-00-200	0	0.787	0.850	66	200	-0.095	0	0.850	Dilation
CD21-00-500	0	0.691	0.728	94	500	-0.133	0	0.728	Dilation
CD22-00-500	0	0.705	0.750	100	500	-0.119	0	0.750	Dilation
CU23-10-300	10	0.559	0.559	87	300	-0.210	0.198	0.695	Dilation
CU24-10-120	10	0.585	0.585	81	120	-0.152	0.198	0.723	Dilation
CU25-10-300	10	0.796	0.796	38	300	0.100	0.198	0.953	Liquefied
CU26-10-120	10	0.801	0.801	37	120	0.064	0.198	0.958	Liquefied
CU27-10-300	10	0.711	0.711	55	300	0.015	0.219	0.860	Limited liquefaction
CU28-20-300	20	0.448	0.448	86	300	-0.180	0.365	0.659	Dilation
CU29-20-120	20	0.529	0.529	70	120	-0.140	0.365	0.751	Dilation
CU30-20-300	20	0.740	0.740	30	281	0.108	0.365	0.993	Liquefied
CU31-20-300	20	0.690	0.690	40	300	0.062	0.365	0.936	Liquefied
CU32-20-120	20	0.740	0.740	30	120	0.071	0.365	0.993	Liquefied
CD33-20-50	20	0.671	0.701	43	50	-0.018	0.365	0.949	Dilation
CU34-30-120	30	0.569	0.569	53	120	0.012	0.495	0.849	Liquefied
CU35-30-300	30	0.480	0.480	70	300	-0.036	0.495	0.745	Liquefied
CU36-30-300	30	0.601	0.601	47	300	0.085	0.495	0.887	Liquefied
CU37-30-300	30	0.414	0.414	83	300	-0.102	0.495	0.667	Dilation
CU38-30-120	30	0.610	0.610	46	120	0.053	0.495	0.898	Liquefied
CU39-30-300	30	0.636	0.636	40	300	0.120	0.495	0.928	Liquefied
CU40-30-300	30	0.436	0.436	79	300	-0.080	0.495	0.693	Liquefied
CD41-30-300	30	0.521	0.475	63	300	0.005	0.495	0.739	Contractive
CD42-30-50	30	0.661	0.597	36	50	0.084	0.495	0.882	Contractive
CU43-40-120	40	0.548	0.548	63	120	0.234	0.65	1.077	Liquefied
CU44-40-120	40	0.610	0.610	51	120	0.296	0.65	1.199	Liquefied
CU45-40-120	40	0.507	0.507	71	120	0.193	0.65	0.996	Liquefied
CU46-40-300	40	0.479	0.479	75	300	0.244	0.65	0.941	Liquefied
CU47-40-300	40	0.401	0.401	90	300	0.166	0.65	0.788	Liquefied
CU48-40-120	40	0.638	0.638	55	120	0.324	0.65	1.254	Liquefied
CD49-40-120	40	0.566	0.484	61	120	0.252	0.65	0.951	Contractive
CD50-40-300	40	0.434	0.377	87	300	0.199	0.65	0.741	Contractive
CU51-50-300	50	0.618	0.618	59	300	0.261	0.2	0.777	Liquefied
CU52-50-300	50	0.533	0.533	73	300	0.176	0.2	0.670	Liquefied
CU53-50-300	50	0.685	0.685	47	300	0.328	0.2	0.861	Liquefied
CU54-50-300	50	0.444	0.444	89	300	0.087	0.2	0.558	Liquefied
CU55-50-300	50	0.605	0.605	61	300	0.248	0.2	0.760	Liquefied
CU56-50-120	50	0.834	0.834	22	120	0.358	0.2	1.048	Liquefied
CD57-50-100	50	0.635	0.533	56	100	0.135	0.2	0.670	Contractive
CU58-100-300	100	0.644	0.644	86	300	0.504	-	0.644	Liquefied
CU59-100-120	100	0.838	0.838	70	120	0.439	-	0.838	Liquefied
CU60-100-120	100	0.910	0.910	64	120	0.511	-	0.908	Liquefied
CU61-100-300	100	0.532	0.532	95	300	0.532	-	0.532	Liquefied

*CU: consolidated Udrained *CD: consolidated drained

3.3.2. Seese Sand (Lusatian material)

A series of undrained monotonic and cyclic triaxial tests were conducted on disturbed samples of Seeses sand, to investigate the mechanical behavior and liquefaction potential of the soils. Main purpose was to determine the characteristic parameters for the steady-state line concept combined with the instability concept (steady-state line, flow-liquefaction surface, instability ratio η_{IS} as a function of state parameter ψ) for the evaluation of liquefaction susceptibility in-situ. Further, cyclic triaxial tests were included in the testing program. The boundary conditions and initial states of the performed monotonic triaxial tests are summarized in Tables 3.7 and 3.8. These two tables include initial void ratio, state parameter ψ, initial relative density and initial mean effective stress. Moreover, void ratio at steady state and equivalent granular void ratio are also presented in Tables 3.7 and 3.8. Overall, 20 monotonic tests with different initial mean effective stress and different initial relative density have been conducted on Seese sand samples. Furthermore, 12 isotropically consolidated cyclic tests with different initial mean effective stress and different amplitude of loading have been carried out on the samples. Moreover, 6 anisotropically consolidated samples were tested under cyclic loading conditions. Tables 3.9, 3.10, 3.11 and 3.12 represent the initial states of the performed cyclic tests.

Table 3.7.: Undrained monotonic triaxial tests on Schlabendorf-Süd sand

Test	Initial state						Notes
	Void ratio after cons. e_0 [-]	State Parameter ψ [-]	Relative density after cons. D_r [%]	Mean effective stress p'_0 $[kPa]$	Steady state void ratio e_{ss} [-]	e^* [-]	Behavior
15-049-1/CU	0.804	0.037	33	50	0.804	0.804	Liquefaction
15-049-2/CU	0.643	-0.11	70	100	0.643	0.643	Dilation
15-049-3/CU	0.804	0.056	33	100	0.804	0.804	Liquefaction
15-049-4/CU	0.807	0.105	32	300	0.807	0.807	Liquefaction
15-049-5/CU	0.710	0.039	54	500	0.710	0.710	Limited Liquefaction
15-049-6/CU	0.785	0.114	37	500	0.785	0.785	Liquefaction
15-049-7/CU	0.743	0.072	47	500	0.743	0.743	Liquefaction
15-049-8/CD	0.792	0.044	36	100	0.750	0.750	Contraction
15-049-9/CU	0.567	-0.135	87	300	0.567	0.567	Dilation
15-049-10/CU	0.814	0.112	31	300	0.814	0.814	Liquefaction

Table 3.8.: Undrained monotonic triaxial tests on Seese-West sand

Test	Initial state						Notes
	Void ratio after cons. e_0 [-]	State Parameter ψ [-]	Relative density after cons. D_r [%]	Mean effective stress p'_0 $[kPa]$	Steady state void ratio e_{ss} [-]	e^* [-]	Behavior
15-050-1/CU	0.736	0.04	37	50	0.736	0.736	Liquefaction
15-050-2/CU	0.736	0.061	37	100	0.736	0.736	Liquefaction
15-050-3/CU	0.739	0.116	37	300	0.739	0.739	Liquefaction
15-050-4/CU	0.705	0.117	44	500	0.705	0.705	Liquefaction
15-050-5/CD	0.618	-0.078	64	50	0.618	0.618	Dilation
15-050-6/CD	0.736	0.061	37	100	0.691	0.691	Contraction
15-050-7/CU	0.598	-0.098	69	50	0.598	0.598	Dilation
15-050-8/CU	0.523	-0.100	86	300	0.523	0.523	Dilation
15-050-9/CU	0.752	0.129	34	300	0.752	0.752	Liquefaction
15-050-10/CU	0.775	0.152	28	300	0.775	0.775	Liquefaction
15-050-11/CU	0.786	0.090	26	50	0.786	0.786	Liquefaction
15-050-12/CU	0.772	0.113	29	150	0.772	0.772	Liquefaction

Table 3.9.: Cyclic undrained triaxial tests on Schlabendorf-Süd sand, isotropically consolidated

Tests	Initial state				Steady state	Cyclic loading f_r=0.1 [Hz]		Notes
	Mean effective stress p'_0 $[kPa]$	Void ratio after cons. e_0 [-]	State Parameter ψ [-]	Relative density after cons. D_r [%]	Steady state void ratio e_{ss} [-]	q_{ampl} $[kPa]$	CSR [-]	Number of cycles to liquefaction N
15-049-11	100	0.643	-0.110	70	0.643	10	0.05	8504
15-049-12	100	0.793	0.05	35	0.793	10	0.05	443
15-049-13	100	0.810	0.06	32	0.810	30	0.15	2
15-049-14	100	0.812	0.06	31	0.812	15	0.075	64

Table 3.10.: Cyclic undrained triaxial tests on Schlabendorf-Süd sand, anisotropically consolidated

Tests	Initial state					Cyclic loading f_r=0.1 [Hz]		Notes
	Initial mean effective stress p'_0 $[kPa]$	Lateral stress coefficient K_0 [-]	Initial void ratio after cons. e_0 [-]	Initial relative density after cons. D_r [%]	State parameter ψ [-]	q_{ampl} $[kPa]$	CSR [-]	Number of cycle to liquefaction N
15-049-15	136	0.7	0.787	37	0.05	10	0.037	41
15-049-16	135	0.6	0.802	34	0.06	10	0.037	35
15-050-17	135	0.5	0.788	37	0.05	10	0.037	22

Table 3.11.: Cyclic undrained triaxial tests on Seese-West sand, isotropically consolidated

Tests	Initial state				Steady state	Cyclic loading f_r=0.1 [Hz]		Notes
	Mean effective stress p'_0 $[kPa]$	Void ratio after cons. e_0 [-]	State Parameter ψ [-]	Relative density after cons. D_r [%]	Steady state void ratio e_{ss} [-]	q_{ampl} $[kPa]$	CSR [-]	Number of cycle to liquefaction N
15-050-13	100	0.731	0.04	38	0.731	15	0.075	40
15-050-14	100	0.710	0.02	43	0.710	15	0.075	43
15-050-15	100	0.738	0.06	36	0.738	10	0.05	123
15-050-16	100	0.746	0.05	34	0.746	30	0.15	1
15-050-17	100	0.591	-0.1	70	0.591	10	0.05	3228
15-050-18 (a)	300	0.759	0.116	32	0.759	10	0.017	11000
15-050-18 (b)	250	0.759	0.105	32	0.759	15	0.03	5900
15-050-19	300	0.777	0.134	28	0.777	30	0.05	128
15-050-20	300	0.710	0.020	43	0.710	10	0.017	20000

Table 3.12.: Cyclic undrained triaxial tests on Seese-West sand, anisotropically consolidated

Tests	Initial state					Cyclic loading f_r=0.1 [Hz]		Notes
	Initial mean effective stress p'_0 $[kPa]$	Lateral stress coefficient K_0 [-]	Initial void ratio after cons. e_0 [-]	Initial relative density after cons. D_r [%]	State parameter ψ [-]	q_{ampl} $[kPa]$	CSR [-]	Number of cycle to liquefaction N
15-050-21	136	0.6	0.787	26	0.124	10	0.036	17
15-050-22	138	0.7	0.801	22	0.139	10	0.036	73
15-050-23	138	0.8	0.778	25	0.115	10	0.036	86

3.4. Triaxial Test Procedures

Details of the triaxial test apparatus, sample preparation, monotonic and cyclic triaxial testing procedures and adopted methods to interpret the data are described in the following sections.

3.4.1. Triaxial Test Apparatus

The triaxial device is a common laboratory device for measuring the intermediate and large strain properties of geo-materials. All monotonic triaxial tests were done using a Wykeham Farrance Eng. Ltd. (England) strain-controlled loading machine. The apparatus hardware is presented in Figure 3.11a. This photo shows the triaxial cell in the loading frame. In case of cyclic loading conditions the vertical loading is applied by means of a pneumatic loading system. HP-VEE software was installed on the PC to allow testing control. The principal construction of the triaxial cell is illustrated in the scheme in Figure 3.11b.

3.4.2. Sample Preparation

The engineering characteristics of granular soils are influenced by soil structure. In the laboratory the sample preparation procedure generates a certain soil structure, also called fabric. This fabric can be anisotropic. The term fabric to describe the arrangement of particles, particle groups and pore spaces in a given soil Mitchell & Soga (2005). During deposition of soil samples, the soil particles tend to be oriented in some preferred directions, which is known as initial or inherent anisotropy. Therefore, it is appropriate to assume that different sample preparation methods lead to different soil fabrics. The macroscopic behavior of granular material is affected by the initial fabric (Goudarzy 2015).

Several methods for preparing reconstituted specimens in the laboratory have been reported in the literature. Table 3.13 illustrates five available sample preparation methods which have been used by previous researchers. Different preparation methods lead to different initial fabrics of the grain skeleton. In case of undrained cyclic tests, different sample preparation methods resulted in different accumulation rates of excess pore pressure and therefore in different liquefaction resistances (Wichtmann 2005). To show the

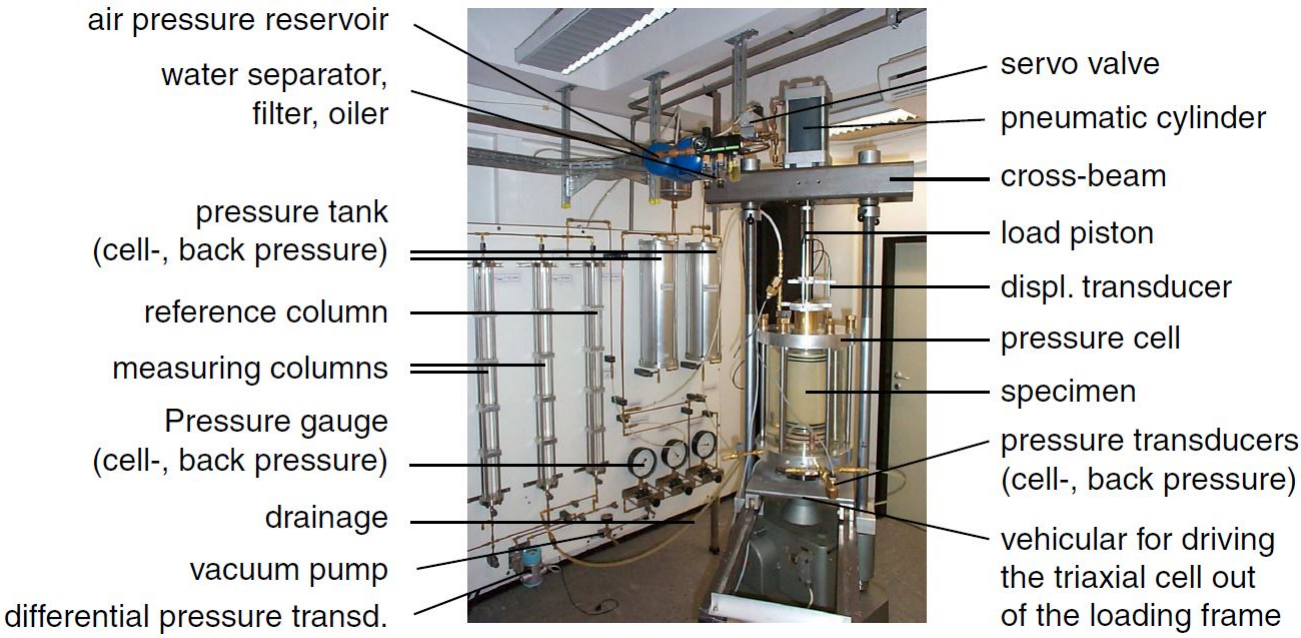

(a)

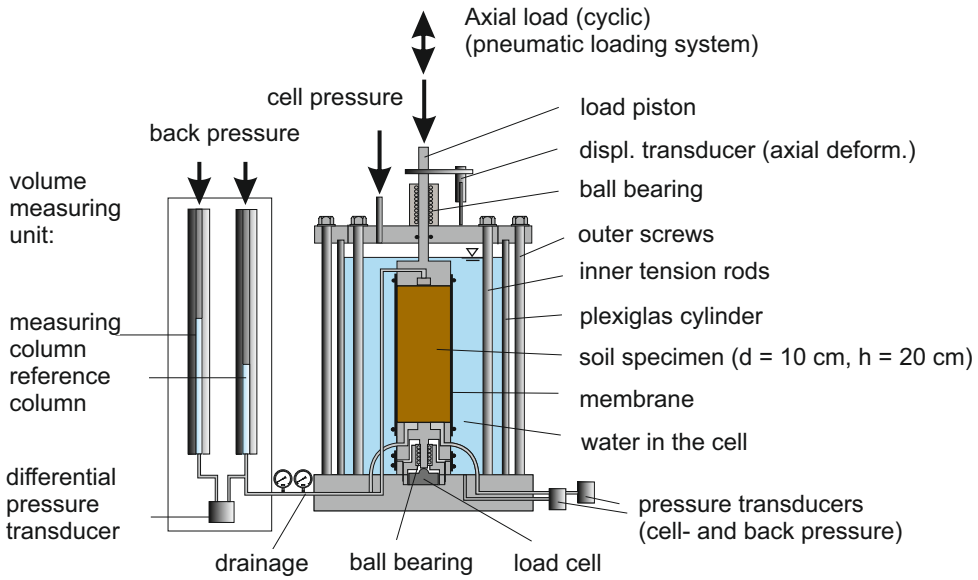

(b)

Figure 3.11.: (a) Triaxial device at Ruhr Universität Bochum; (b) Schematic details of Triaxial test device, after Wichtmann (2005)

effect of different sample preparation techniques, Ladd (1974) performed undrained cyclic triaxial tests on samples of the same sand prepared by three different techniques. The results demonstrated that the specimens prepared by moist tamping liquefied at four times higher numbers of cycles than specimens which were prepared by dry pluviation and compacted by vibration. It was also reported by Porcino et al. (2004) that samples prepared by air pluviation technique show significantly higher liquefaction potential than samples prepared by pluviation through water. Therefore, the choice of the sample preparation method depends on the aim of the study (Rahman 2009). As Kuerbis (1985) stated, the method for reconstituting soil samples must fulfill the following criteria: 1) the method must produce a wide range of density as expected within in-situ soil deposition from loose to dense; 2) the void ratio must be uniform through the sample; 3) the samples must be fully saturated; and 4) the samples must be well mixed to provide a homogeneous structure without segregation, particularly for transition soils (sand-fines mixture).
Air pluviation and the moist tamping method are two common methods for sample preparation. In the air pluviation method, dry sands are pluviated through a funnel from a constant height. The method may not be suitable for sand with more than 15% f_c, due to particle segregation. Moist tamping method is used for preparing reconstituted sand samples by compacting the soil with a certain water content in layers (Lambe 1951). Due to the water tension forces between particles, samples prepared by the moist tamping method may be prepared at much larger void ratios than possible in a dry state (Kuerbis 1985). Moreover, Casagrande (1975) stated that the honeycomb structure of very loose sands deposited in a moist state resulted in a high susceptibility to liquefaction. The honeycomb structure results from the capillary forces between moist particles during preparation. This technique is capable of producing specimens with different void ratios over a fairly wide range of densities, and offers the advantage of preventing a segregation of the constituents of the material (Ishihara 1993; Zhang 1997; Fourie & Papageorgiou 2001; Yamamuro et al. 2008). Additionally, a very high degree of specimen homogeneity is achievable with the moist tamping method (Fourie & Papageorgiou 2001). Therefore, in this study, the moist tamping in multiple layers was employed to prepare all the sand and sand-silt mixed samples.

Sand-fines mixtures were obtained by mixing pure Hostun sand with non-plastic silt in a dry state. A predetermined amount of water was added to control the water content (5% by weight). A membrane and a split mold were then installed on the platen. The predetermined amount of sand-silt mixture was placed in each of the 10 layers each having a height of $\approx 20\ mm$. Specimens were then prepared by placing and lightly tamping the predetermined quantity of material in ten layers of 20 mm thickness. The soil for the first

Table 3.13.: Available sample preparation methods, modified from Yang (2004)

Method	Moist tamping	Air pluviation	Water sedimentation	Slurry deposition	Under compaction
Procedure	Successively tamping of the moist layers to desired density	Sedimentation of the soil sample through the air	Sedimentation of the soil sample through water	Deposition of a slurry	Compacting successive dry/moist layers to desired density
Advantage	Easy, wide range of density	Easy	High degree of saturation	High degree of saturation, Uniformity	Homogeneous specimen
Disadvantage	Non-uniformity of density	Segregation, Unstable structure during saturation	Segregation	Segregation, Limited range of density	Non-uniformity of density
Reference	Koester (1994), Pitman et al. (1994), Amini & Qi (2000), Yang et al. (2006a), Chien et al. (2002), Sze & Yang (2014), Wichtmann (2015)	Lade et al. (1998), Thevanayagam (1998), Belkhatir et sl. (2014), Wichtmann (2015)	Amini & Qi (2000)	Vaid (1994)	Belkhatir et al. (2010b), Salgado et al. (2000), Ladd (1978)

layer was spooned into the mold and leveled approximately with the spoon. Once the layer was compacted to its target height, and the surface of each layer was leveled, the tamper was removed and the soil surface was scarified to a depth of approximately 2 mm. The soil for the next layer was then spooned into the mold and the process was repeated until the soil of the uppermost layer had been spooned into the mold and compacted. Figures 3.12 and 3.13 contain a schematic and photos of the sample preparation process, respectively. After preparing the specimen as described above, a small vacuum (25 kPa) was applied to the grain skeleton to maintain the stability of the sample before seating the top platen on the surface of the sample. Then the membrane was scrolled from the split mold and placed on the top platen. It was then sealed with two O-rings which had previously been placed around the top platen. At this stage the external vacuum applied to the membrane during specimen preparation was removed. Afterwards 50 kPa vacuum was applied to the drainage line to confine the soil specimen. Next, the split mold was carefully removed from the specimen. Then the diameter of the sample was measured in three different height and across three different axes using a caliper. These values were then averaged and corrected for the membrane thickness. The height of the specimen was also measured at three positions and an average value was set into approach. Once the specimen's dimensions were known, the initial dry density, void ratio and relative density of specimen could be calculated. If these values were within acceptable ranges as

desired, then the plexiglass cylinder of the triaxial cell was assembled carefully preventing a disturbance of the sample.
Then the cell was filled slowly with water. A small air cussion was let at the top of the water fill, on which the cell pressure was applied pneumatically. A cell pressure line was attached to the cell via a valve at its top, and the displacement transducer (LVDT) was mounted at the load piston to record the changes in specimen height. The cell pressure was increased gradually to 50 kPa while the vacuum inside the sample was reduced to 0 kPa. Transducers for the determination of pore pressure, cell pressure and axial deformation were then set to their initial zero levels.

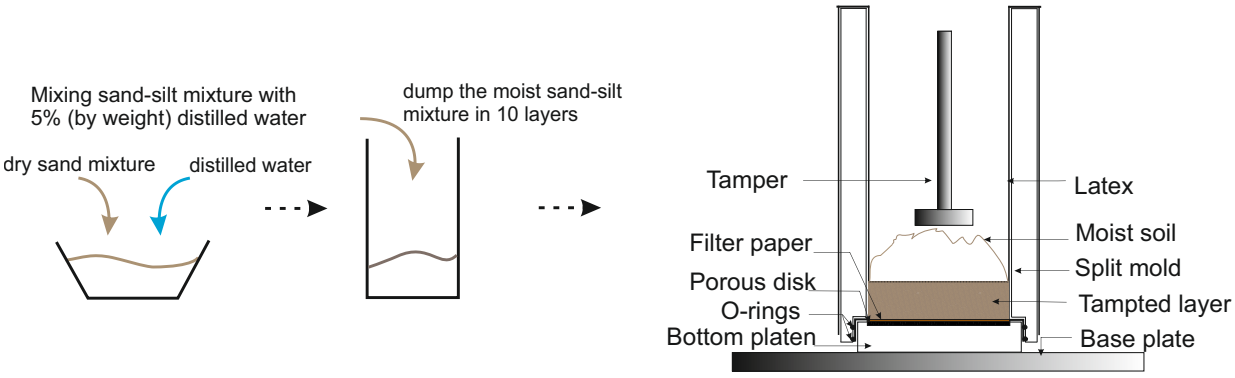

Figure 3.12.: Schematic steps for sample preparation

3.4.3. Membrane Controlling

Before each sample preparation the membrane had to be checked. A membrane controller was used to check possible leakage of the rubber membrane. It consists of a two cylinder platen, an air pressure tube, and two O-ring seals. The procedure was as follows: (1) a rubber membrane was installed on the two cylinder platen and secured with the two O-ring seals; (2) a low air pressure was applied inside the membrane; (3) the membrane was immersed in the water. The membrane has no leakage if no continuous air bubbles appear.
It should be noted, that all tested soils were classified as fine sand (Azeiteiro et al. 2017). Because of this classification, the potential error in void ratio stemming from membrane penetration effects was considered to be negligible (Sladen & Handford 1987).

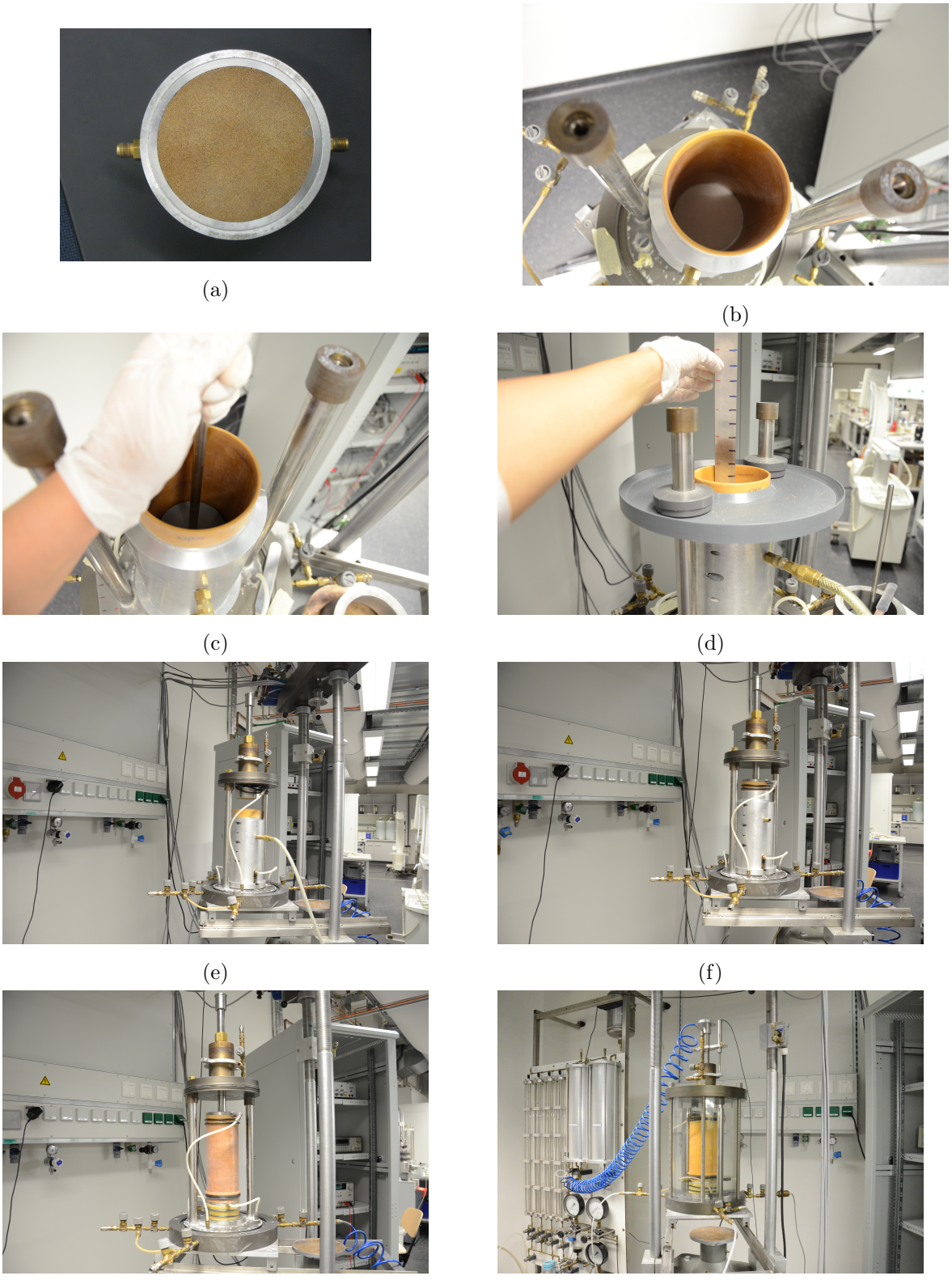

(a) (b) (c) (d) (e) (f) (g) (h)

Figure 3.13.: Sample preparation procedure at Ruhr-Universität Bochum laboratory

3.4.4. Saturation

Saturation of the specimen was done in three steps: carbon dioxide percolation, CO_2, de-aired water percolation and back-pressure saturation.
First, right after sample preparation, Carbon dioxide CO_2 was percolated through the sample under a cell pressure of 50 kPa from the bottom platen for about 30 to 60 minutes, for loose to dense samples, respectively. The flow rate was kept to 1 to 2 bubbles per second. Flow rate was easily verified by placing the outlet drainage tube into the water. The main purpose of CO_2 percolation was to replace the air in the specimen pores by CO_2. This process was carried out because CO_2 has much higher solubility in water than air under pressure. Therefore, this process facilitated obtaining a fully saturated soil specimen.
In the second step, the de-aired water flowed from a storage tank through the bottom platen of the specimen and then through the sample, replacing CO_2 bubbles inside the specimen and coming out at the drainage line connected to the top platen. Once the desired volume of de-aired water (approximately 2 liters) had flown through the sample, the second step ended. Note that the velocity of water flow within the sample should be kept low, so that the percolating water does not wash out the fines particles.
Before performing the third step, the valves were closed to stop water percolation. Then the drainage was connected to one pipe of the volume measuring unit. A typical back pressure of 200 kPa was applied via this pipe (in some cases the back pressure was 300 kPa). The cell pressure was always kept slightly higher than the back pressure. An isotropic mean effective stress, p' of 50 kPa was chosen during the saturation procedure, to guarantee minimum disturbance of the specimen. After a period of approximately 24 hours, the saturation of the specimen was checked by means of Skempton's B-value, (criterion to ensure a high degree of saturation: $B \geq 0.95$).
The axial deformation during saturation was recorded to evaluate the geometry of the specimen after saturation in order to obtain the correct value of void ratio before consolidation.

3.4.5. Consolidation

Once an acceptable B value was obtained, all of the specimens for monotonic and most of the samples for cyclic triaxial tests were isotropically consolidated under a target mean effective stress. Only a few specimens were anisotropically consolidated for cyclic triaxial

tests. For anisotropic consolidation, the targeted initial static shear stress was achieved by increasing the vertical stress under drained condition after having applied the targeted confining pressure. During the consolidation phase, the drainage valves were open. Specimens were allowed to consolidate for approximately one or two hours under these initial effective stresses. For the materials with low fines contents, this time was approximately 60 minutes, while for the pure silt a consolidation time of 90 to 120 minutes was chosen. During consolidation, volume and height changes were recorded. Consolidation of specimens was considered complete when specimen volume remained unchanged over a given period of time.
The triaxial apparatus was controlled by a personal computer through a data acquisition and control system. The data acquisition system (PEEKEL multi-channel compact amplifier system) was capable of reading about seventeen analog to digital channels. The volume and height changes during consolidation used to calculate dimensions and the void ratio of the specimen after consolidation. This void ratio was identical to the initial void ratio of the undrained shear phase.
The accuracy of the void ratio measurement is very important as it was used to indicate density state of a soil specimen and has a significant effect on interpreting soil behavior.

3.4.6. Monotonic Loading System

The axial load can be applied in stress-controlled or strain-controlled mode. The strain-controlled mode was used for the monotonic loading in this study, while the stress-controlled mode was applied for the cyclic tests. Pore water pressure in the sample and cell pressure were measured with pressure transducers. To record the deformation of the sample, a displacement transducer (LVDT) was used, which was connected directly to the axial load piston. The gauge had a maximum elongation of 50 mm. Volume changes were measured via the burette system using a differential pressure transducers. All data were recorded with a data acquisition system at a personal computer.
The confining pressure was applied to the specimen through the water inside the cell chamber. The axial deformation was applied with the predefined rate (0.1 mm/min) and the resulting change of axial stress was measured. The axial stress was measured by a pressure transducer installed at the top of the load piston, outside the pressure cell. Transducers with maximum capacities of 2 and 5 MPa were used in this test program. The changing in axial load was automatically calculated based on the measured axial stress.

The strain-controlled tests were chosen because they provide a better record of stress strain behavior and pore water pressure response than stress-controlled tests. The advantage of using strain-controlled tests becomes clear when the tested soil sample undergoes limited liquefaction or flow liquefaction (Kuerbis 1985). All tests were performed at an axial strain rate of 0.1 mm/min. This rate was selected so that pore water pressure response inside the specimen developed uniformly during undrained shearing. This rate proved to be sufficient to achieve reliable test data for liquefaction analysis (Verdugo & Ishihara 1996; Rahman 2009; Baki 2011). Several researchers (Chang et al. 1982; Castro et al. 1982; Chern 1985) reported that the rate of loading does not have a significant effect on the undrained shear behavior of sands.
The target strain of the specimens was 25% axial strain, as the objective of the undrained monotonic tests was to reach the steady state of deformation. Some specimens did not reach this strain level due to a number of factors. These include the maximum apparatus axial load being reached before steady state, irregular specimen deformations rendering the data unreliable, or the specimens undergoing complete flow liquefaction and reaching zero residual strength, particularly in the case of Seese sand samples (Lusatian material).

3.4.7. Cyclic Loading System

The cyclic tests were carried out in the same apparatus. The sinusoidal pattern of cyclic loading was applied to the specimens in a stress-controlled manner at different loading amplitudes and constant frequency, f_r of 0.1 Hz. The selected frequency was found to be adequate for uniform development of pore water pressure inside the sample.
Once consolidation was completed, the parameters of the cyclic loading were entered into the software, the drainage lines were closed, and the specimen was loaded cyclically. The pneumatic actuator applied the cyclic load according to the chosen sinusoidal wave shape with defined amplitude. The parameters entered into the computer included the maximum number of loading cycles (limited to 20000 cycles by the software), loading amplitude and frequency of loading. Once the necessary information had been entered, any necessary adjustments to the LVDT or pressure were made, and drainage valves were closed. The test was then started and the specimen was cyclically loaded until failure. This process was continued until an effective stress of zero was achieved. The number of cycles required to achieve liquefaction N were recorded by the computer.
After sample dismantling, when the specimen was pure sand, the soil was placed in a bowl and dried in an oven for reuse. However, when the specimen contained fines, it was dried at room temperature for reuse, in order to prevent any change in the fines properties

which could occur in case of oven drying. It was also possible to remove the fines material by washing the soil over a No. 200 sieve, and then reuse only the sand.
To verify the uniformity of the sand-fines mixture during the test, fines distribution was randomly controlled. When the test was completed, the sample was cut into five equal horizontal slices, and the fines content of each layer was measured. The results showed that the samples were remarkably homogeneous with respect to fines distribution, even though they have previously been consolidated and monotonically loaded to initial liquefaction.

4. Effect of Fines on the Shear Behavior of Mixtures

4.1. General

The results of the static triaxial tests performed on Hostun sand-silt mixtures with different fines content and different initial states are presented in this chapter. These results include the stress-strain behavior of specimens under static loading. The steady state concept is used to analyze the results and interpret the liquefaction potential of samples. To investigate the steady states of the different mixtures, it was intended to achieve the maximum axial strain that was possible in the apparatus, generally around 20-25%. Based on the test results it can be concluded that this strain level was sufficient to reach the steady state of deformation. The steady state lines were determined by plotting the mean effective stress at steady state (logarithmic) against the void ratio. Furthermore, the mean effective stress at steady state (logarithmic) was plotted against the equivalent granular void ratio of the mixtures, and also against the skeleton void ratio.

4.2. Stress-strain response of Hostun Sand-Silt Mixtures

4.2.1. Triaxial Test Results

The effect of a variation of density on the undrained monotonic response of soils is well-documented in the literature. For the present study, Hostun sand-silt mixtures the effect of density was investigated by evaluating the stress-strain relationships, the effective stress paths, and excess pore water pressure responses. The density ranges achieved for the test specimens are presented in Table 3.6. Test results for samples having the minimum and maximum achieved densities, along with results for a medium density, are used to discuss

the effects of density on the undrained response of Hostun sand with different fines contents.

Effective stress-paths of the clean Hostun sand and the sand-silt mixtures are presented in Appendix Figure A.1a to Figure A.26a. These plots clearly reveal that, for clean sand and mixtures with $f_c < f_{cth}$, increasing soil density resulted in more dilative responses, whilst mixtures with $f_c > f_{cth}$ show a contractive behavior, even with high relative density values. The mixtures with high range of fines content always showed contractancy in all range of density. This behavior can be explained in terms of the Lade & Yamamuro (1997) hypothesis, which is that the fines appear to create a particle structure in the soil that is highly compressible. This enhances the potential for liquefaction, even though the density of the soil increases. Figure 4.1 demonstrates the results of the current study, which are in a good agreement with the tendency published by Lade & Yamamuro (1997). Note, that as the fines content of the mixtures increase, the specimens with the same relative density tend to become more contractive, showing contraction even in denser states. It can be concluded from the results that the effect of fines content on the undrained behavior of sand-fines mixtures with high fines content ($f_c > f_{cth}$) is greater than the effect of density.

An unstable soil matrix structure is created when the sand is mixed with fine. In this

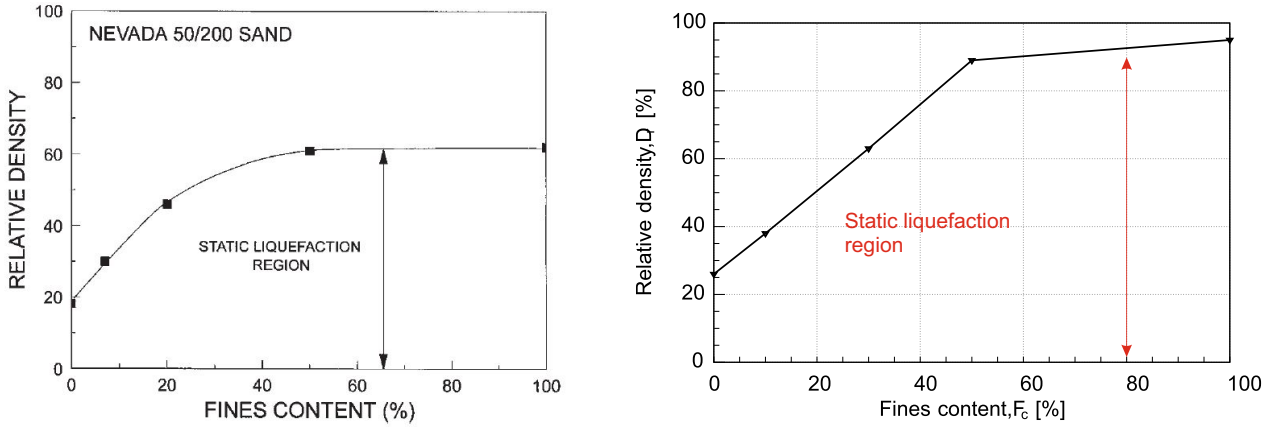

(a) (b)

Figure 4.1.: Effect of density on liquefaction behavior of sand-fines mixtures: (a) after Lade & Yamamuro (1997); (b) current study

condition, it is assumed that the fines grains try to separate the coarse grains leading to metastable inter-granular contacts (Thevanayagam 1998; Thevanayagam et al. 2002). This bridge can be easily broken by the application of a small shear strain. The Environmental Scanning Electron Microscope (ESEM) picture of Hostun sand with 20% fines content in Figure 4.2 demonstrates this metastable contact between two sand grains. In

some cases, with further strain, the coarser grain recaptures the contacts, which leads to limited liquefaction behavior, this behavior can be seen in the undrained response of Hostun sand mixture with 10 and 20% fines content.

Appendix, Figures A.1b to Figure A.26b collect the stress-strain response measured for

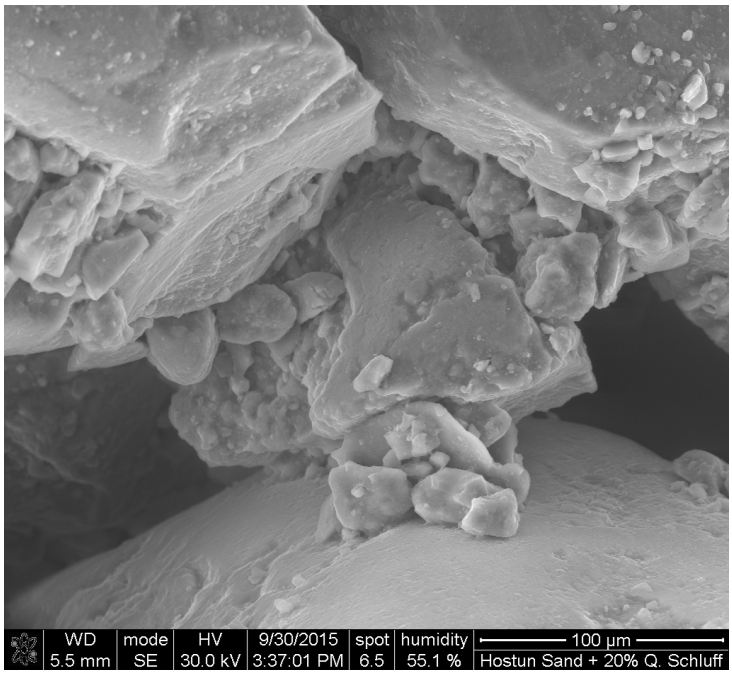

Figure 4.2.: Example of metastable inter-granular contact between Hostun sand and silt grains in the sand-silt mixture

Hostun sand, the pure silt and the sand-silt mixtures. The diagrams show the typical undrained response in which the peak and steady state (in the case of dilation) strengths increase with the initial density of the sample (for each mixture). As an example, tests on clean Hostun sand are compared. Test CU14-00-300 with $e = 0.930$ ($D_r = 26\%$) reaches a $q_{peak} \approx 180$ kPa in Figure 4.3b, while Test CU06-00-300 with $e = 0.715$ ($D_r = 86\%$) shows strain hardening behavior (dilative), and subsequently reaches a peak (steady state) strength of $q_{peak} \approx 2000$ kPa, see Figure 4.4b. It can be found from the obtained results, that the majority of specimens of mixtures tended to show strain-softening (contractive) behavior.

The excess pore pressure responses are directly related to the effective stress path. In the present work the excess pore water pressure is normalized by the initial mean effective stress p'_0 at the start of axial compression. This means that $\Delta u/p'_0 = 1.0$ corresponds to 100% excess pore water pressure or a mean effective stress of $p' = 0$ kPa. Figures A.1d to Figure A.26d display the excess pore water pressure responses.

The effects of increasing density on the undrained monotonic response of clean Hostun sand and sand-silt mixtures with $f_c < f_{cth}$ are as expected, and are summarized below. Increasing density results in:

- increase in the peak and steady state strength
- more pronounced strain-hardening behavior (dilative response)
- increasing contractancy with the increasing in f_c in sand-silt mixtures

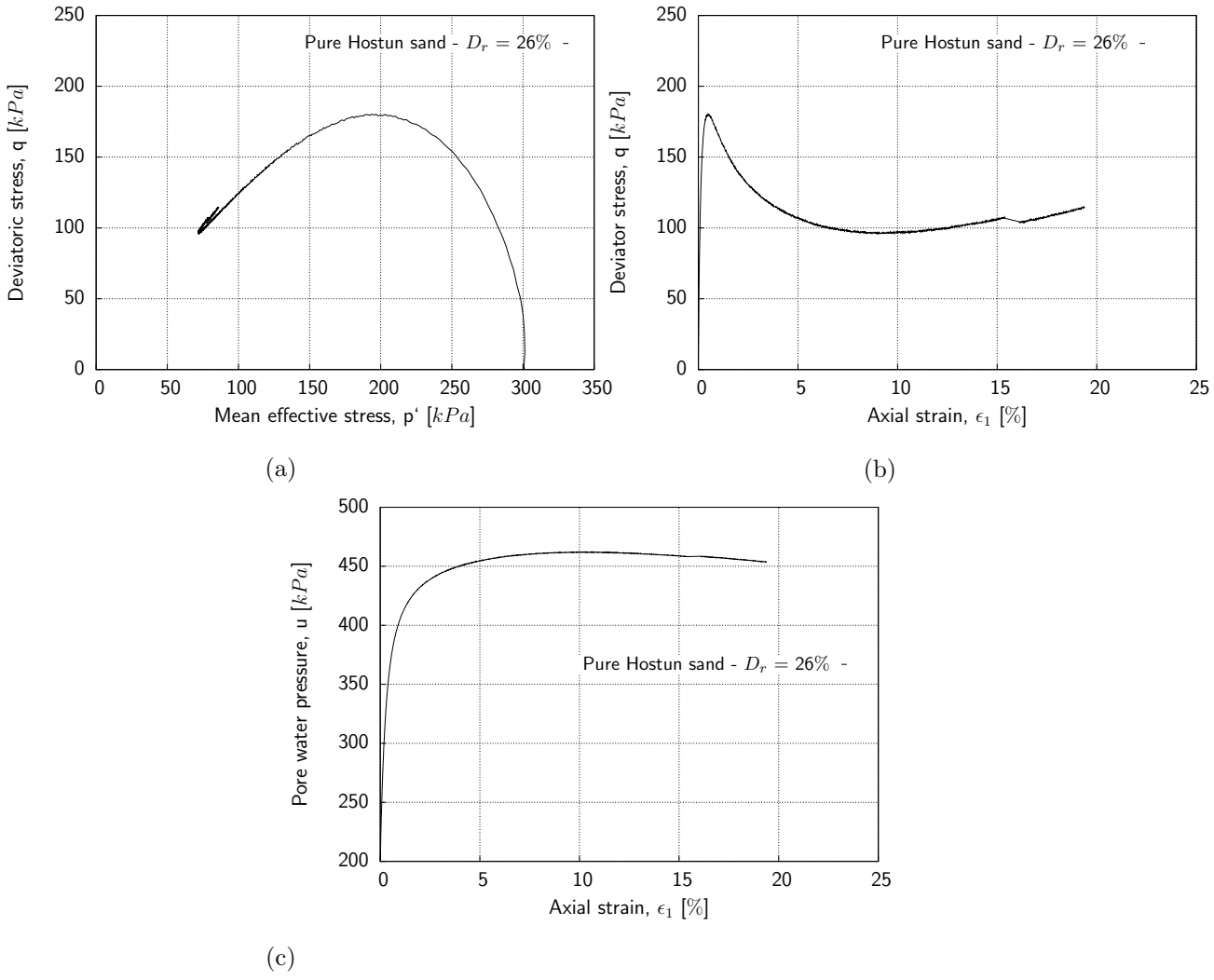

Figure 4.3.: Undrained response of loose Hostun sand: (a) stress path; (b) stress-strain behavior; (c) pore pressure variation vs. axial strain

Figure 4.5 depicts the undrained response of sand-silt mixtures with different fines content from 0 to 100%, but with almost the same relative density. The comparison of the

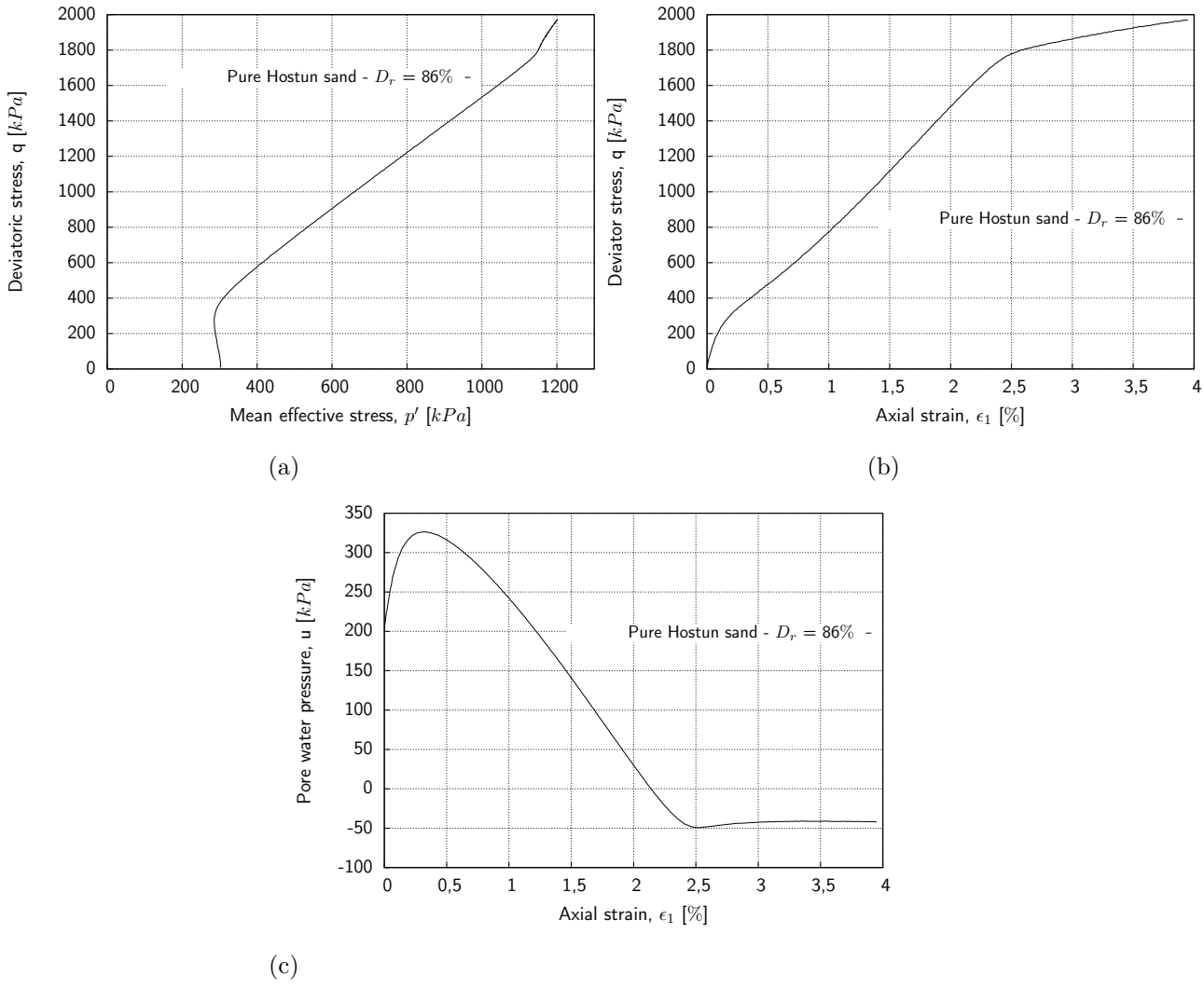

Figure 4.4.: Undrained response of dense Hostun sand: (a) stress path; (b) stress-strain behavior; (c) pore pressure variation vs. axial strain

stress paths and stress-strain curves of seven specimens reveals that static liquefaction occurred for all samples with a fines content beyond 20% initial relative density . It can be observed that the mixtures with 10% and 20% f_c showed a more dilative response and higher strength than the clean sand. This unexpected behavior of the mixtures with small amounts of fines content has been also observed by Carraro et al. (2003). Furthermore, a similar response is reported by Yang (2004) in her study on sand-silt mixtures. This behavior can be explained by noting that in mixtures with smaller amounts of fines, the fine grains will adjust to the pores of the clean sand during densification and consolidation. Therefore, the fines can generate a larger contact area between sand grains, so the mixture with 10% and 20% may have a higher undrained shear strength than clean sand at the same dense state, see Figure 4.6a and 4.6b. By further increasing the fines content, the sand grains will be moved apart by the fines particles, see Figure 4.6c and 4.6d. Due to this reason, the mixtures with a higher fines content behave in a contractive manner during the shearing, and consequently the peak undrained shear strength will be smaller.

Figure 4.7 displays the variation of peak shear strength of sand-silt mixtures with fines content for the same initial state $\approx 30\%$. It can be seen that the peak undrained shear strength q_{peak} decreases as the fines content of the sand increases. These results suggest that an increase in fines content reduces the strength of the sand, and results in a more pronounced strain-softening response in undrained triaxial compression tests. Similar stress-strain response for sand-silt mixtures has also been observed by many other researchers as discussed in Chapter 2 (e.g. Lade & Yamamuro 1997; Yang 2004; Baki 2011).

4.3. Steady State of Hostun Sand-Silt Mixtures

As discussed in Chapter 2, the steady state concept is a useful framework for interpreting and comparing the static and cyclic response of soil samples. Sand and sand-silt mixtures with $f_c < f_{cth}$ and densities greater than those at the steady state line ($\psi < 0$) show dilative response under monotonic loading, while samples with lower densities ($\psi > 0$) show contractive response. This implies that the steady state line provides a reference that can be used to estimate the soil response based on the initial state of the soil in terms of initial void ratio and stress. It should be noted that all sand-silt mixtures in this study with $f_c > f_{cth}$ at both low and high relative density, demonstrate contractive behavior. For a reliable interpretation of data for sands containing fines based on the steady state

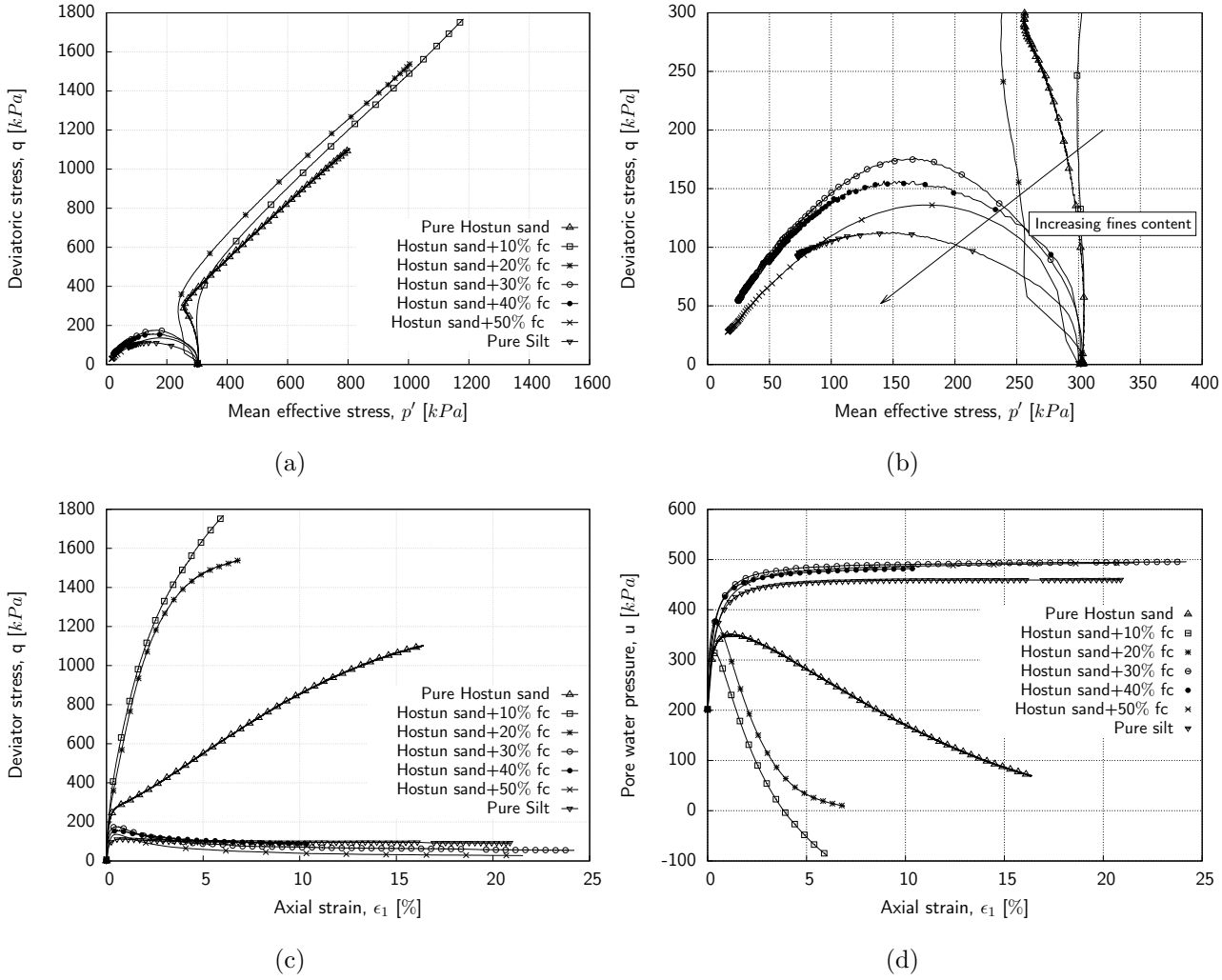

Figure 4.5.: Undrained behavior of sand-fines mixtures with the same range of density (dense): (a) stress path; (b) zoom in stress path; (c) stress-strain behavior; (d) pore pressure variation vs. axial strain

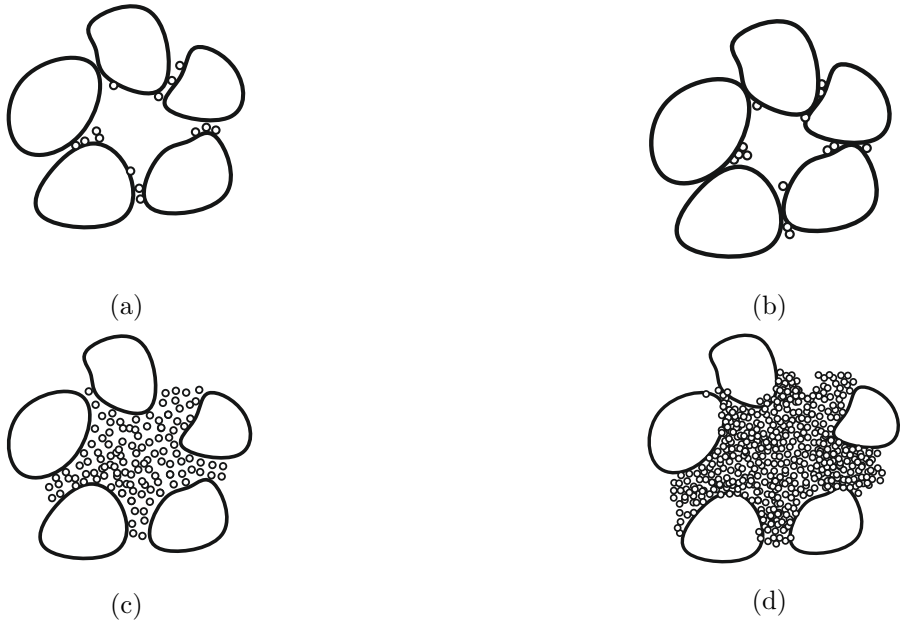

Figure 4.6.: Particle arrangement for sand with low fines content: (a) before consolidation; (b) after consolidation and with high fines content: (c) before consolidation; (d) after consolidation ,after Yang (2004)

concept, it is essential to recognize how the location of the steady state line alters in the e-log p' diagram with changes in fines content.

For this purpose, the steady state lines of the Hostun sand-silt mixtures with fines content of 0 to 100% are depicted in Figure 4.8a to Figure 4.9c. In these figures, the initial states of the samples are also included with the paths during the test indicated by the arrows. Note that filled symbols are used to show the steady state, and open symbols are used to present the initial state of the specimens. The maximum and minimum void ratios, e_{max} and e_{min}, are also displayed in the diagrams to show the potential range of sample's densities and the proximity of the respective steady state lines to these density states (Verdugo & Ishihara 1996; Baki 2011). The proximity of the samples SSLs to their respective maximum and minimum void ratio demonstrates the potential range of soil response with regards to the initial states. In order to recognize the intrinsic potential of liquefaction of a soil sample, Verdugo & Ishihara (1996) introduced the relative contractiveness value, R_c, which can be evaluated in a simplified manner based on Equation 4.1. As they reported, R_c is not a parameter to specify the state of the soil, but is rather an index to define an intrinsic material property that is highly dependent on the particle composition of a soil.

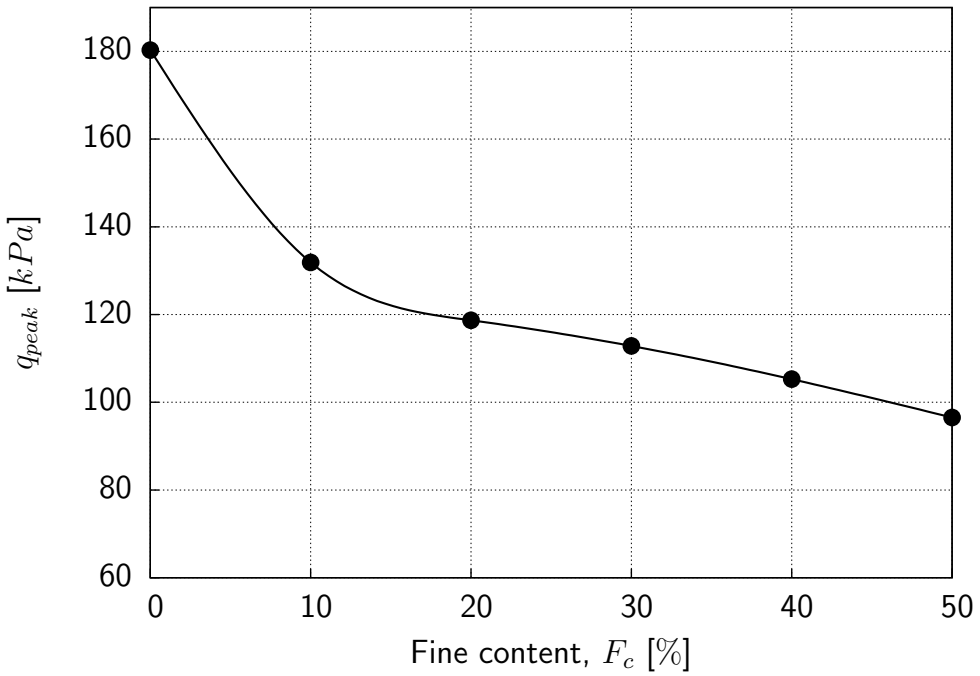

Figure 4.7.: Variation of peak shear strength vs. fines content for mixtures with same initial relative density ≈ 30%

$$R_c = \frac{(e_{max})_1 - (e_{ss})_1}{(e_{max})_1 - (e_{min})_1} \tag{4.1}$$

where $(e_{max})_1$, $(e_{min})_1$ and $(e_{ss})_1$ are the maximum, minimum and steady state void ratios for an effective mean stress of 0.1 MPa. R_c can take values between 0 and 1, where the zero value represents a soil that always shows dilative behavior whereas $R_c = 1$ represents a soil that always exhibits a contractive response for any initial state. Figure 4.10 shows the definition of R_c parameter schematically, and Figure 4.11 represents the data of Hostun sand-silt mixtures with respect to p'=50 kPa. It can be observed, that with increasing the fines content the R_c value tends to increase and gets closer to the value of 1. The larger the value of R_c, the higher is the intrinsic liquefaction potential.

The steady state lines of all mixtures based on the global void ratios are displayed in two diagrams in Figure 4.13. This figure includes two diagrams, one for $f_c < 30\%$ and the other one for $f_c \geq 40\%$. This figure indicates that the position of the steady state line moves downwards from clean sand till the fines content of the mixture reaches 30%. The SSLs of the Hostun sand and the sand-silt mixtures with low fines content are parallel and their shapes are similar, with all lines being relatively flat at low confining pressure and curved at higher confining pressures in the e-log p' space. This is typical for the steady state

lines of sandy soils with small amounts of fines, as has been reported by many researchers (Verdugo 1992; Zlatovic & Ishihara 1995; Thevanayagam et al. 2002; Baki 2011; Rahman et al. 2011; Carrera et al. 2011; Rahman et al. 2014). As Baki (2011) stated, the flat nature of the steady state line means that when the initial soil state is located close to the steady state line, small changes in soil density can result in soil response changing from being mainly contractive to mainly dilative. The shape of the steady state lines changed to linear with a further increase of the fines content beyond 30% (f_{cth}). It can be observed that for $f_c > f_{cth}$ the slope of SSLs increases with increasing fines content. This type of behavior has also been reported in previous studies (Been & Jefferies 1985; Fear & Robertson 1995; Bouckovalas et al. 2003). The data in Figure 4.13 reveal that fines content has a significant influence on the location and slope of the SSLs, especially for mixtures with $f_c > f_{cth}$. It should be noted that the arrows in Figures 4.8 and 4.9 show the void ratio path to reach its steady state, by changing the initial pressure in undrained tests (marked by horizontal arrows) and by changing the initial pressure and initial void ratio in drained tests (diagonal arrows). The samples with different initial state under drained and undrained condition lead to the same steady state line.

The maximum and minimum void ratio and the initial void ratio (after consolidation) of all performed tests are illustrated Figure 4.12. It can be seen that the threshold fines content is around 30%.

In the previous section, it is observed that at a given relative density, the soil samples with higher fines content tend to be contractive, whereas soil samples with lower fines content tend to show a dilative response. The observed trends explains the movement of the steady state lines in the e-log p' diagram. The contractive behavior at higher fines contents results in increased excess pore water pressure generation, which reduces the mean effective stresses and leads to reduced soil strength.

Rahman (2009) has compared five data sets extracted from published work on sand-fines mixtures to demonstrate a smaller scatter data when using the equivalent void ratio e^* instead of void ratio e or skeleton void ratio e_s. The data of the current study shows a similar tendency. Figure 4.14 illustrates the current data set in terms of skeleton void ratio. As can be seen, due to neglecting the effect of fines content, the data scattering is significant.

All steady state data points were re-plotted in Figure 4.15 using the equivalent granular void ratio e^*, with a b value calculated using the proposed Equation 2.11 and an m value by best fitting the test data. All the data points can be described by a single trend curve or line for the sand-silt mixtures with $f_c < f_{cth}$ and $f_c > f_{cth}$, respectively. Therefore, by using the equivalent granular void ratio as the state variable, a single EG-SSL for each

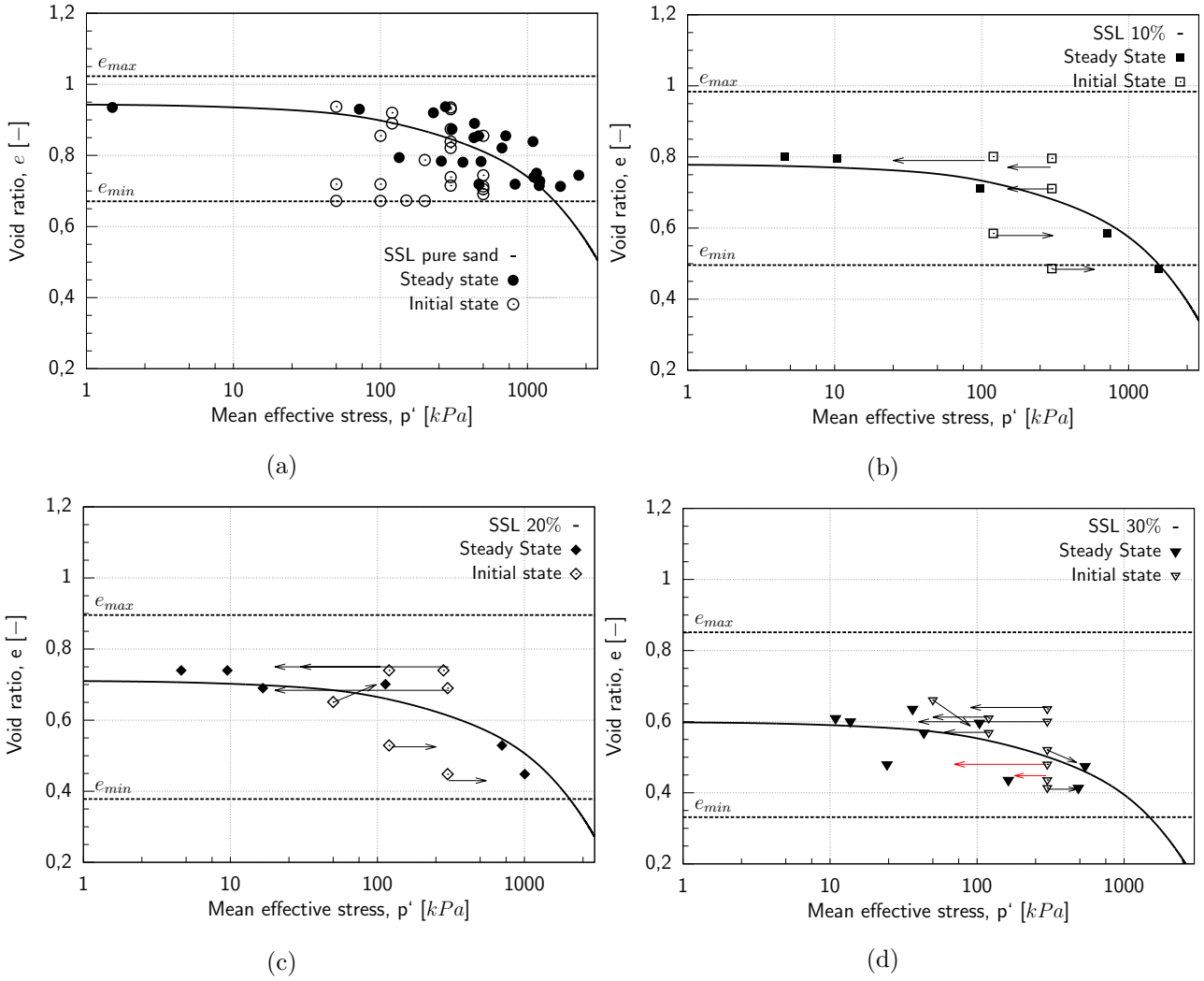

Figure 4.8.: Steady state line of: (a) clean Hostun sand; (b) Hostun sand mixed with 10% silt; (c) Hostun sand mixed with 20% silt; (d) Hostun sand mixed with 30% silt

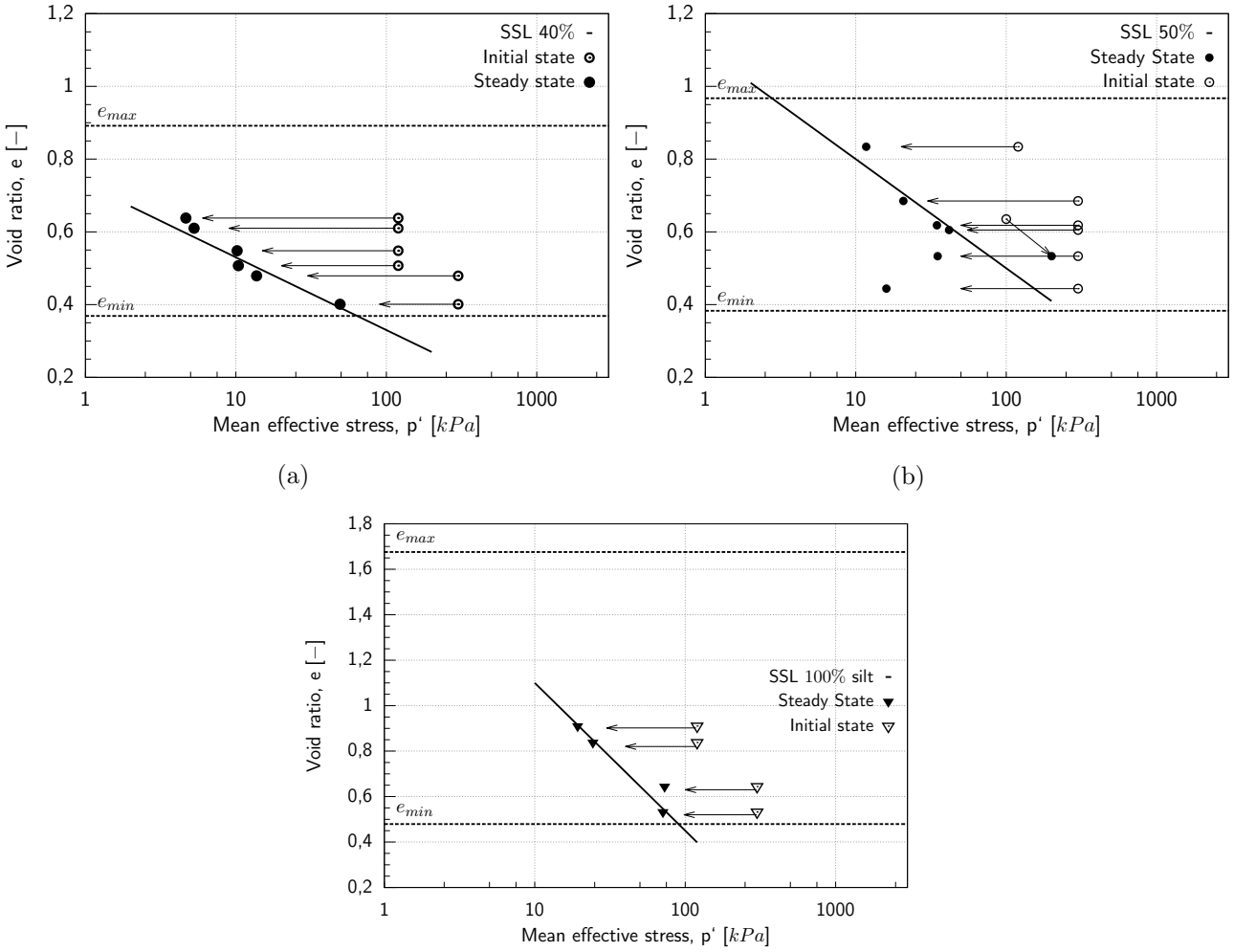

Figure 4.9.: Steady state line of: (a) Hostun sand mixed with 40% silt; (b) Hostun sand mixed with 50% silt; (c) pure silt (100% silt)

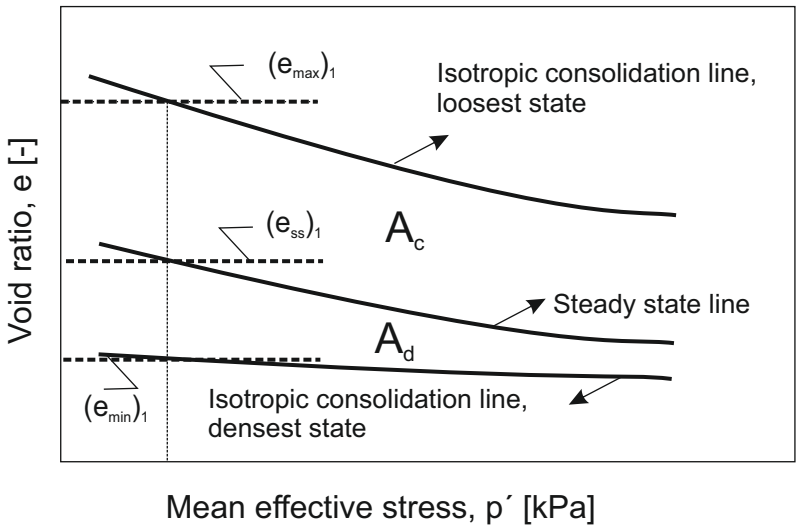

Figure 4.10.: Schematic definition of relative contractiveness, after Verdugo & Ishihara (1996)

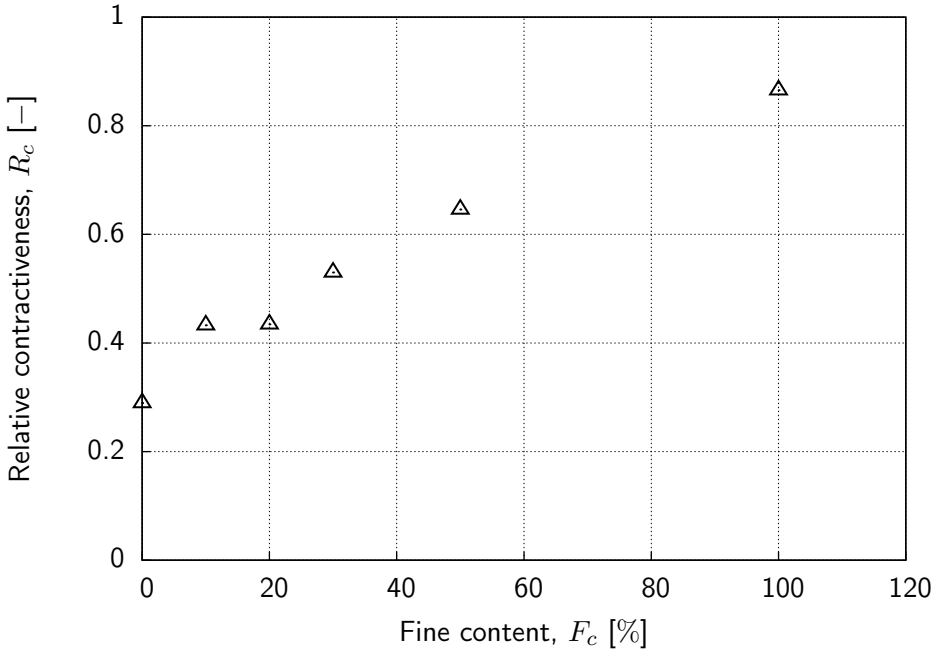

Figure 4.11.: Effect of fines content on the relative contractiveness of Hostun sand-silt mixtures

range of fines content $f_c < f_{cth}$ and $f_c > f_{cth}$ is obtained, separately. The equations used to get the best fit of EG-SSL are also shown in these diagrams.

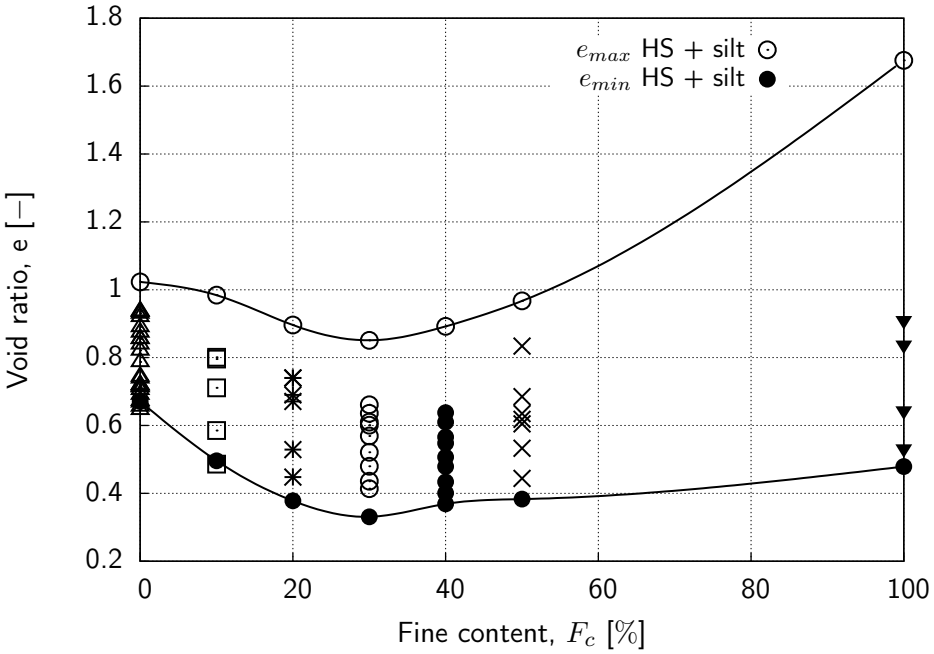

Figure 4.12.: Initial void ratios of performed tests vs. fines content with minimum and maximum void ratio of mixtures

4.3.1. Qualitative Verification of Volume Change During Shear of the Coarse and Fine Components

To understand the nature of shearing resistance in order to analyze the shear strength of two adopted materials, a series of direct shear tests were additionally conducted on clean sand and pure silt with two different relative densities (70% and 95%) and same initial vertical stress 300 kPa. The direct shear test was also conducted on two sand-silt mixtures with 20% and 50% fines content with the same density of 70%, and the same initial vertical stress.

Figures 4.16a and 4.16b depict the shear response of clean Hostun sand, and pure silt both with high relative density respectively. As can be seen, clean Hostun sand shows dilative behavior at both tested relative densities. In contrast, pure silt at the highest tested density reveals contractive response. It can be observed in Figure 4.17, that the response of the sand-silt mixture with 20% silt content follows the pure sand behavior.

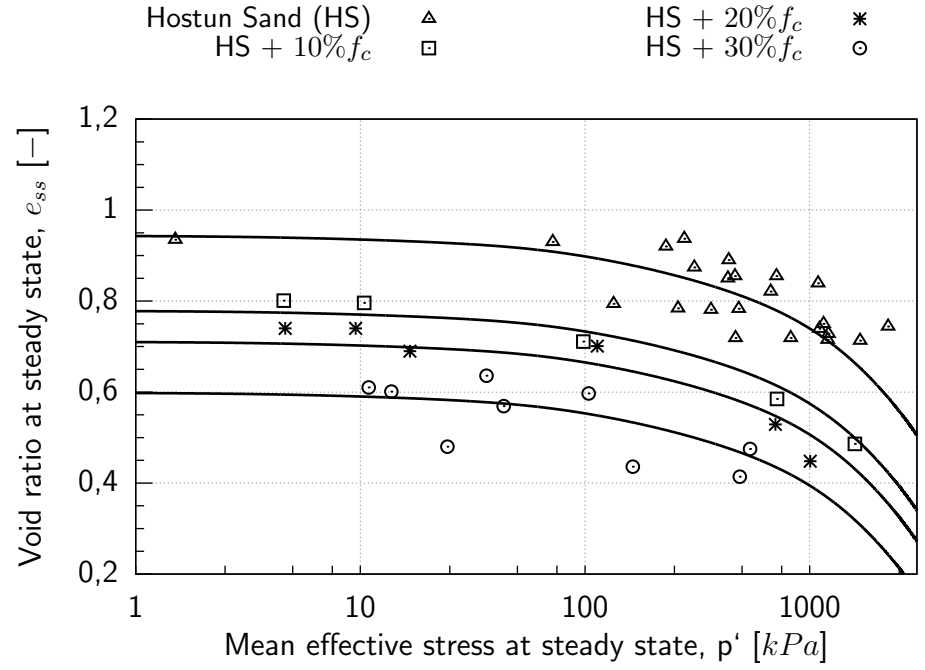

(a)

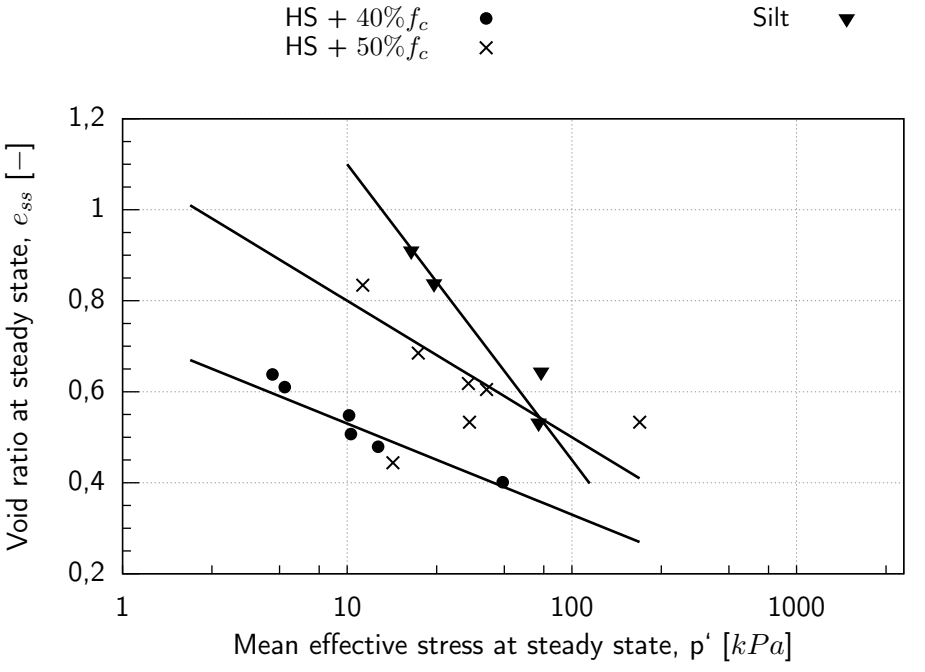

(b)

Figure 4.13.: Steady state lines of Hostun sand-silt mixtures in e-log p' space: (a) fines content less than threshold fines content; (b) fines content larger than threshold fines content

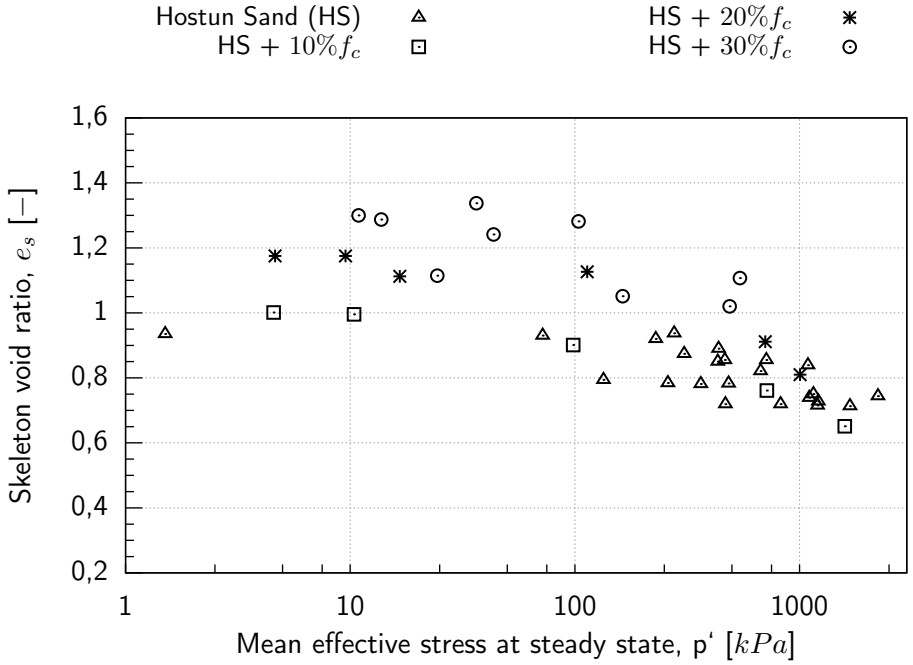

(a)

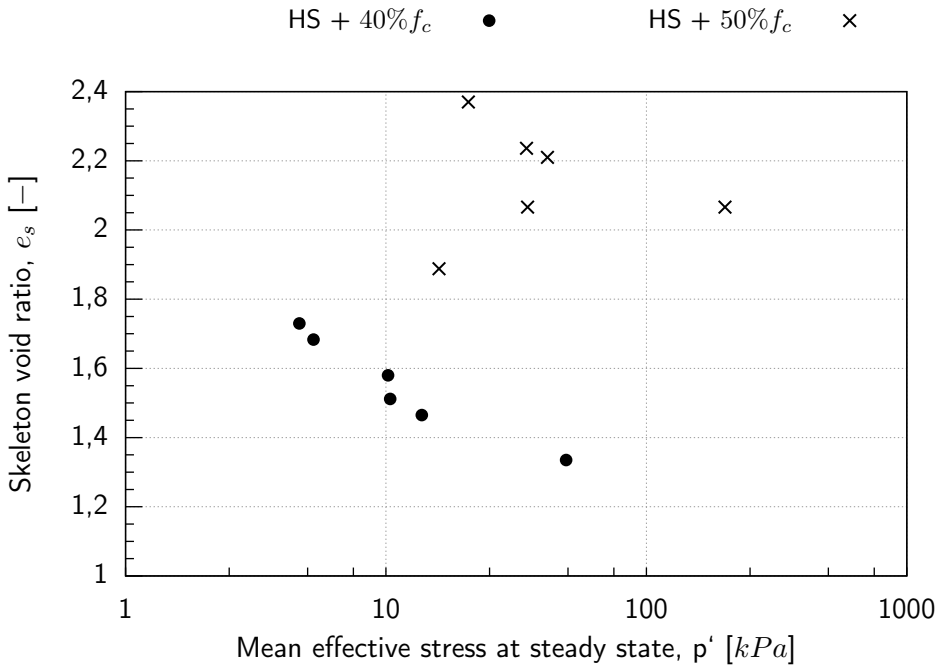

(b)

Figure 4.14.: Steady state lines of Hostun sand-silt mixtures in e_s-log p' plane: (a) fines content less than threshold fines content; (b) fines content larger than threshold fines content

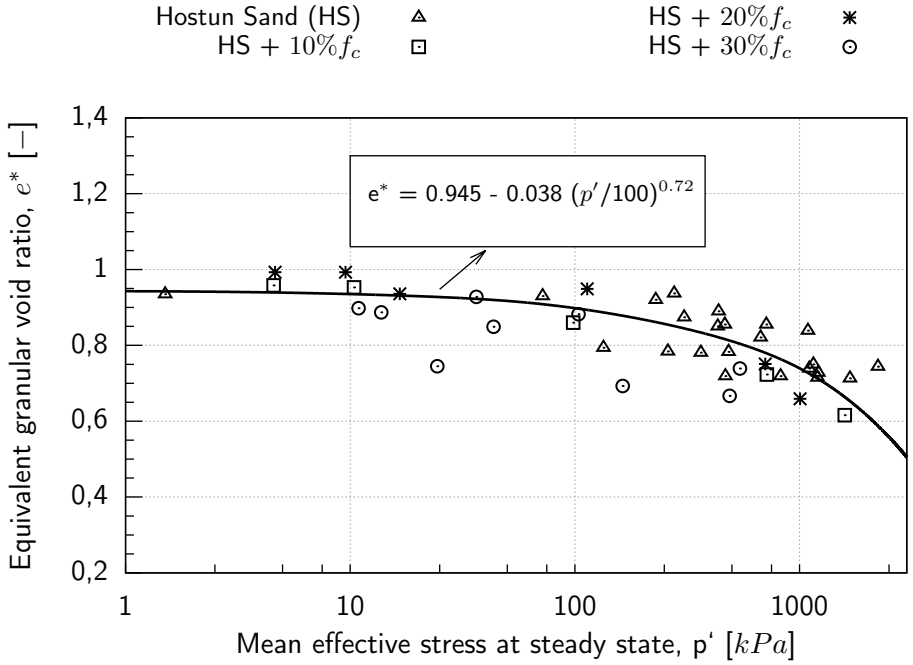

(a)

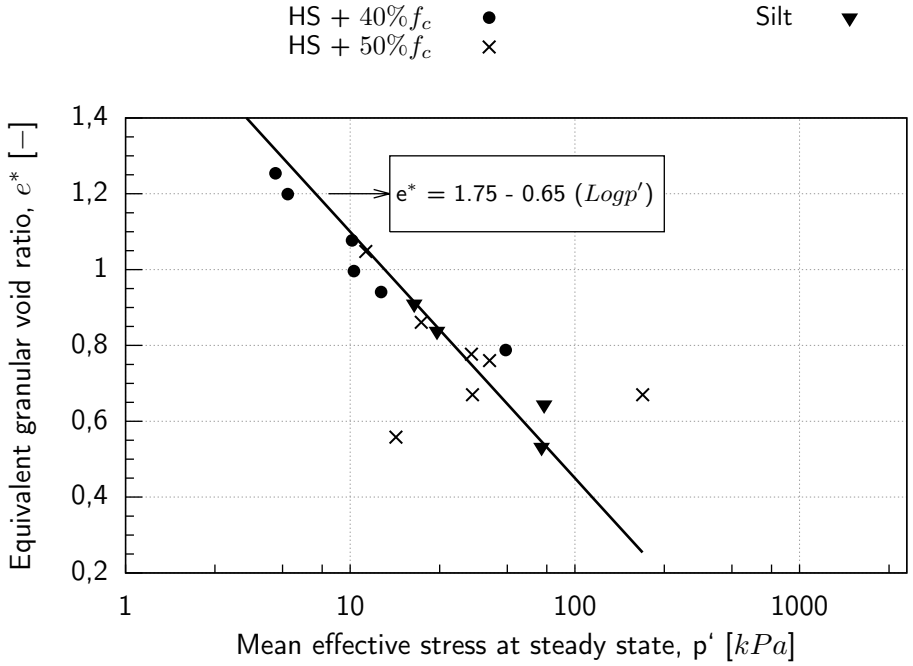

(b)

Figure 4.15.: Equivalent granular steady state lines of Hostun sand-silt mixtures: (a) fines content less than threshold fines content; (b) fines content larger than threshold fines content

However, the response of the sand-silt mixture with 50% silt content looks similar to that of the pure silt.

4.4. Summary

The results of the present study can be summarized as follows:

- Sand-silt mixtures with small amounts of f_c show the same behavior as clean sand samples. A dense initial state leads to a dilative response and a loose one to a contractive behavior.
- Most sand-silt mixtures samples with high f_c showed contractive behavior, even at high relative densities.
- The Hostun sand-silt mixtures with higher fines contents show lower strengths than mixtures with smaller fines content at almost the same relative density. Furthermore, higher excess pore water pressure is generated in sand-silt mixtures with higher fines contents.
- The steady state lines of sand-silt mixtures are located at lower void ratios as the fines content is increased.
- The shape of the steady state line is curved in the e-log p' diagram for fines content below the threshold f_{cth}, while it is linear above.
- Using the equivalent granular void ratio, e^* in lieu of global void ratio, e helps to estimate the behavior of different samples with respect to their fines content and initial state.
- In the current study it is found that the behavior of sand-silt mixtures with $f_c < f_{cth}$ follows the behavior of sand, while the response of sand-silt mixtures with $f_c > f_{cth}$ looks similar to that of silt.
- Based on direct shear test results, the shear response of clean sand and pure silt is completely different at the same relative density. Clean Hostun sand in a dense state indicates dilative behavior, but silt shows contractive behavior under the same initial conditions. It is also observed that the shear response of a sand-silt mixture with fines content 20% ($f_c < f_{cth}$) and a sand-silt mixture with fines content of 50% ($f_c > f_{cth}$) is similar to the shear response of clean sand and pure silt at the same initial state, respectively.

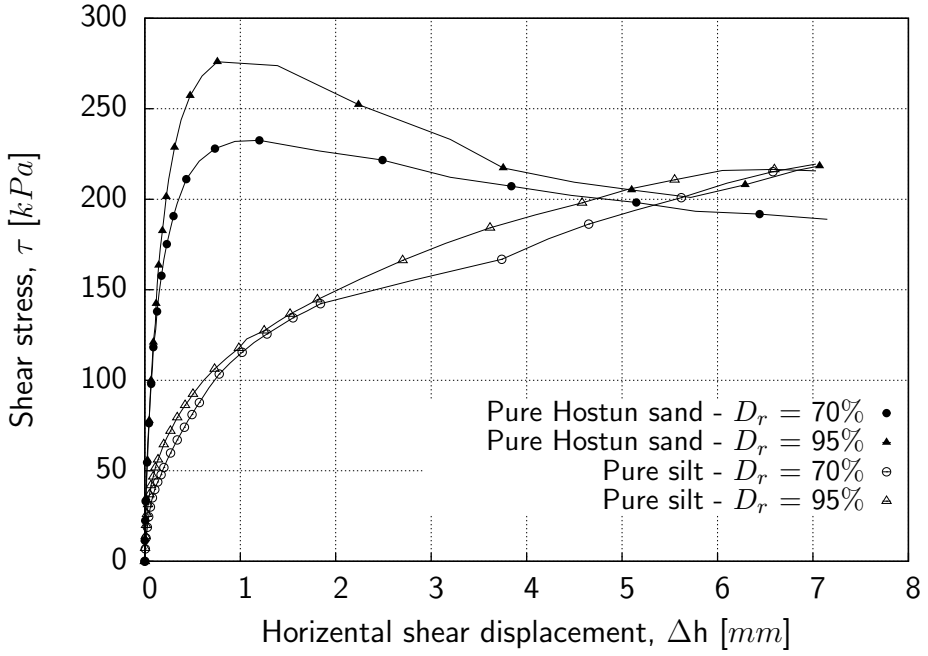

(a)

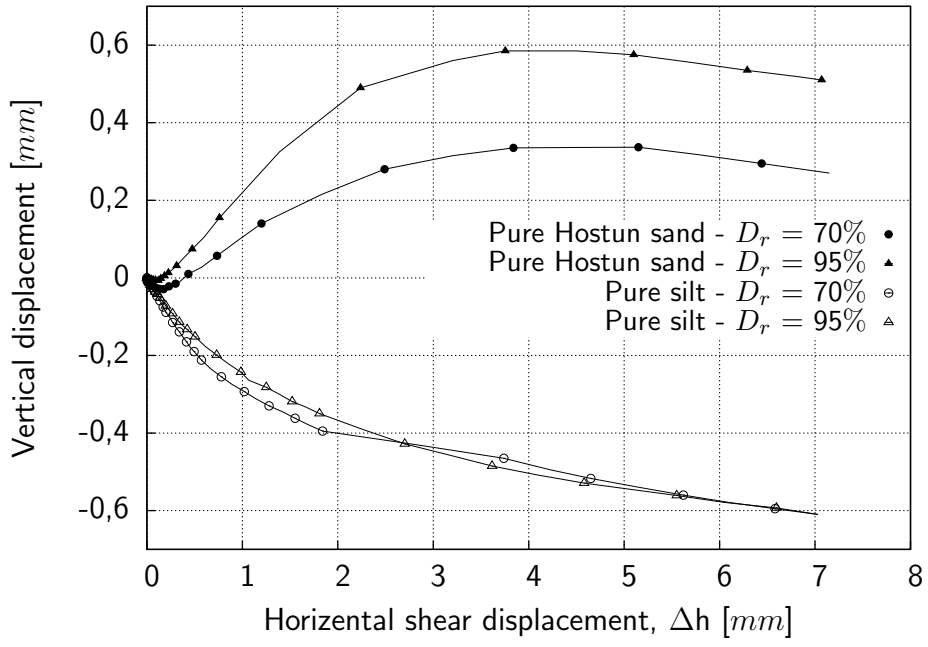

(b)

Figure 4.16.: Response of clean Hostun sand and pure silt in direct shear tests with avertical stress of 300 kPa: (a) shear stress vs. horizontal displacement; (b) vertical displacement vs. horizontal displacement

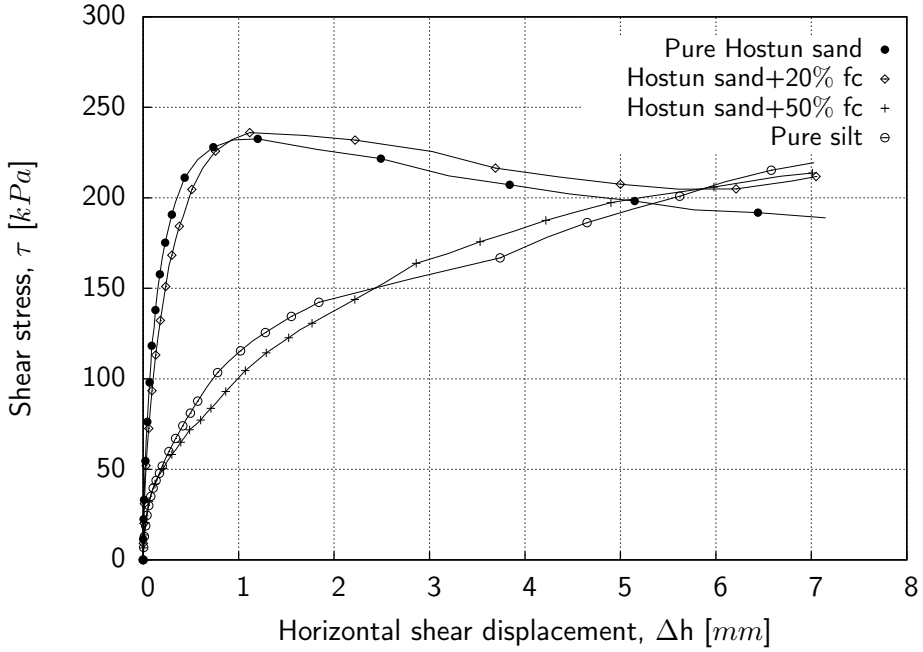

(a)

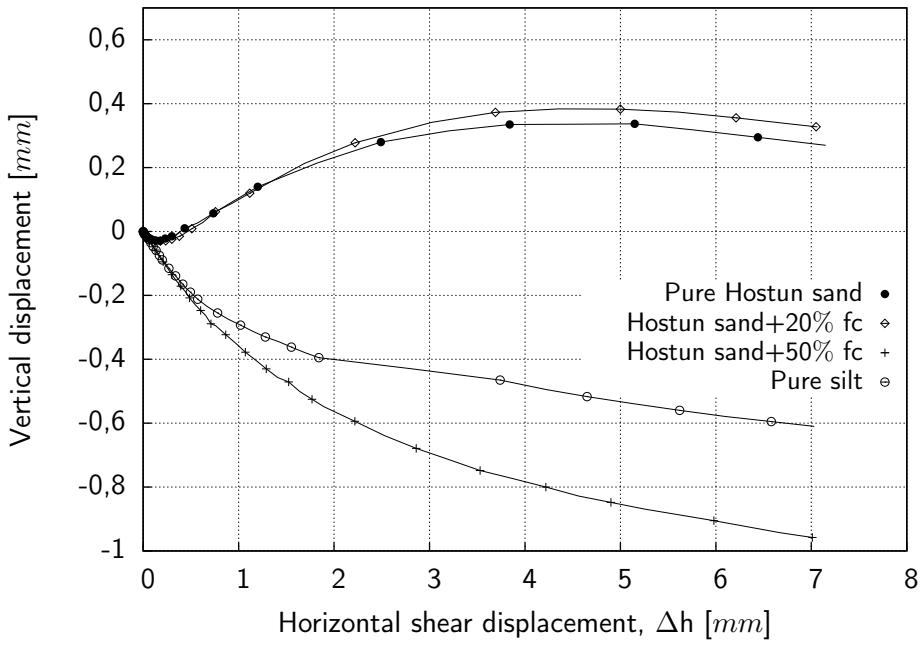

(b)

Figure 4.17.: Response of clean Hostun sand, pure silt and sand-silt mixtures with relative density $D_r = 70\%$ in direct shear tests with a vertical stress of 300 kPa: (a) shear stress vs. horizontal displacement; (b) vertical displacement vs. horizontal displacement

5. Conceptual Approach for Evaluation of Liquefaction Susceptibility In-situ Using Steady State Concept

5.1. General

Numerous liquefaction events have occurred during recent years in the former open-pit mines of the Lusatian (Lausitz) region in Germany. The liquefaction events were not caused by earthquakes, but occurred mostly spontaneously, and partly, the exact trigger of the liquefaction event could not be identified. Generally, the liquefaction phenomena are related to the loose state of the sandy mining dumps as well as to the stop of ground-water lowering measures since the end of active mining and the subsequent groundwater-level rise. The average thickness of the sandy mining dumps is about 50 m. The average groundwater rise is about 1 m/year. The liquefaction induced events were slope failure, large mass movements in horizontal direction (lateral spreading) or ground failure with subsequent vertical ground movement. Figure 5.1 shows photographs of the deposition of sandy soils in the dumps. Considering the importance and the large dimensions of these dumps the static and cyclic behavior of the soils in the dumps as well as their interaction must be well known. Therefore, a part of this project is dedicated to cyclic triaxial tests on samples with the same initial state as in the monotonic triaxial tests, in order to find the linkage between static and cyclic instability zones. Several isotropically and anisotropically consolidated cyclic triaxial tests are performed to estimate the liquefaction resistance of the Lusatian material (Seese sand).

This chapter presents an approach for the evaluation of liquefaction susceptibility of a site using criteria based on critical state soil mechanics, on the instability concept and in-situ properties of the subsoil. First, the procedure of the suggested approach will be presented, followed by the presentation of the triaxial test results for determination of the relevant criteria. Finally, the approach is adopted to a field case using available field

data (CPT, pore water pressure) from a site improved by blasting technique. Different geotechnical investigations were carried out in this area. Beside the in-situ tests triaxial tests have been performed on the material from the site. Figure 5.2 shows some pictures of liquefaction affected areas of the former open pit mines in Lusatia, captured in 2012 or 2015.

(a)

(b)

Figure 5.1.: (a) Sand deposition in mining area (loose state); (b) Hydraulic dump in an opencast pit in the Lusatian area in 1994 (LMBV 2010)

5.2. Procedure of the Suggested Conceptual Approach

The suggested procedure to evaluate the liquefaction potential of the soil samples based on steady state concept consists in the steps described below and summarized in Table 5.1.

1. At first, it is needed to determine the physical properties of the material such as grain size distribution and related parameters like D_{10}, D_{50}, C_u, C_c, fines content and e_{min} and e_{max}. Furthermore, it is also needed to determine the initial stress state of the site for a profile of interest and initial void ratio of soil samples.

2. As the second step it is needed to determine the respective criteria of critical state soil mechanics and instability concept from triaxial tests results. The criteria are:

   a) Steady state line SSL in e-log p' plane.

Figure 5.2.: Liquefaction related phenomena in Lusatian area in year of: (a) 2012 (top); (b) 2015 (below)

b) Steady state line SSL in e-log q plane → based on criteria (a) and (b) and the known initial density and stress state of the sample, the type of failure (cyclic mobility or flow liquefaction) can be predicted.

c) Flow liquefaction surface FLS in p'-q plane → comparison to in-situ stress state.

d) Determination of instability stress ratio η - state parameter ψ relationship.

Table 5.1.: Procedure of application of CSSM for liquefaction assessment

Step 1 In-situ state	Material properties GSD (f_c, D_{50}, D_{10}, d_{50})	Initial state in-situ void ratio e stresses p'_0, q	Loading range static Δq cyclic $\pm q$, N
Step 2 CSSM (Lab)	Susceptibility for liquefaction SSL (e-p')	Instability FLS (p'-q)	Type of liquefaction flow liquefaction cyclic mobility
Step 3 Consideration of fines contents	Transformation of void ratio, $e \rightarrow e^*$ transformed SSL in e^*-log p' f_c, D_{50}, D_{10}, d_{50}, f_{cth}, b, m		
Step 4 Evaluation	Required compaction by transferring the information from Step 1 into the results of Step 2	Allowable pore water pressure	

For determining the relationship between instability stress ratio and state parameter, Yang (2002) proposed the following equation, see Equation 5.1:

$$\eta = A \exp(-B\psi) \tag{5.1}$$

where A and B are fitting parameters. This exponential relationship helps to estimate the behavior of soil elements with a given initial state. It can be realized that having the same initial state parameter results in the same instability stress ratio.

3. This step is taken into account when the sample has fines content. Then the equivalent granular void ratio e^* is used to evaluate the in-situ state with respect to the criteria (SSLs, FLS). The parameters obtained from step one will be used to get e^*.

4. The last but main step is to compare the in-situ state data to the critical state soil mechanics criteria. By this comparison the liquefaction behavior of in-situ state can be estimated, e.g. by displaying in-situ initial void ratio in the e-log p' space. By the location of the in-situ point either above or below the SSL it is known whether the soil is potentially liquefiable (contractive, above SSL) or non-liquefiable (dilative, below SSL).

Figure 5.3 illustrates the initial states of a location in the Lusatian area before and after soil improvement, which are plotted in a e-log p' diagram with the related SSL (obtained from triaxial tests). It can be seen that the initial states are located above the SSL ($\psi > 0$), which means thet the soil is susceptible to liquefaction.

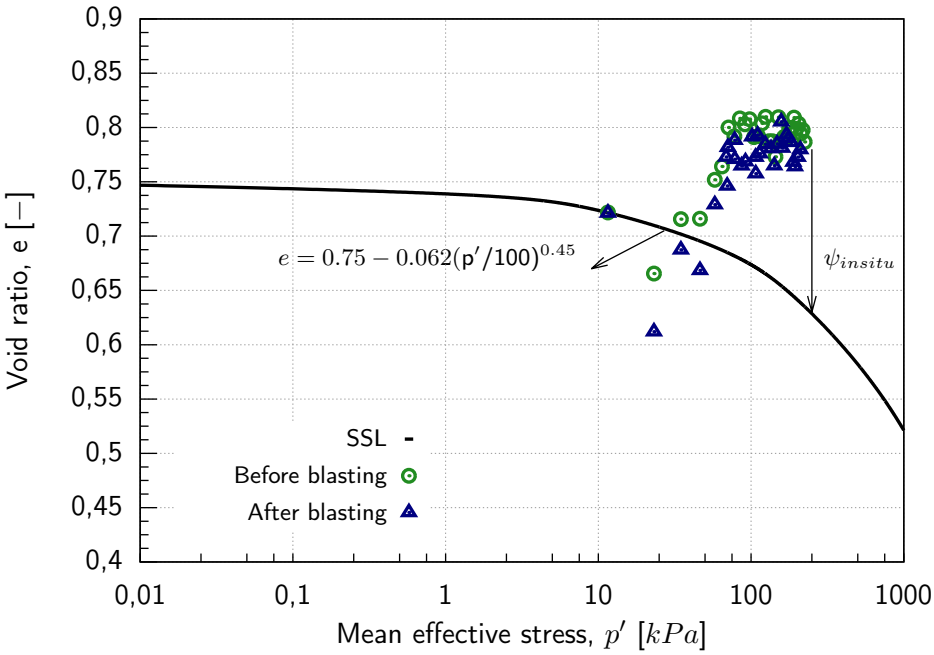

Figure 5.3.: In-situ states of Lusatian material in relation to their steady state line from undrained monotonic triaxial tests

5.3. Overview about Considered Field Case

Experience indicated that the initial density of soil plays an important role in the degree of ground improvement achieved by blasting. The density of loose deposits can typically increase considerably to relative densities in the range of 70 to 80%, whereas soils with

initial relative densities of 60 to 70% can only be densified by a small amount (Keßler & Förster 1992; Gohl et al. 2001; Vega-Posada & Finno 2016).

As a result of blasting the soil is subjected to a dynamic loading. If the soil is saturated, and cannot drain sufficiently, a generation of excess pore water pressure occurs with a simultaneous loss of strength in the soil mass. Liquefaction of the soil is followed by time-dependent dissipation of the excess pore water pressures. A release of large amounts of water at the ground surface is a sign of pore water pressure dissipation.

The blasting induced compaction can be divided into four phases: (1) initial state of the particles as loosely packed grains with initial porosity n_0, (2) destruction of the structure by the dynamic loading leading to a reduction in the grain-to-grain stress, (3) liquid or suspension like state with no stress transfer between the grains and accompanied increase of pore water pressure, and (4) re-deposition of the particles while water drainage (consolidation) leading to a reduced porosity of the redeposited grains and the reduction of the excess pore water pressures (Keßler & Förster 1992).

In order to reduce the liquefaction potential, blast densification technique has been used in Lusatian area to compact the loose, water-saturated sand deposits (Fordham et al. 1991; Keßler & Förster 1992; Gandhi et al. 1999; Gohl et al. 2001; Rollins & Anderson 2008; Narsilio et al. 2009; Vega-Posada & Finno 2016). Within the frame of a cooperation, the Chair of Foundation Engineering, Soil and Rock Mechanics was given access to selected data sets of a realized test blasting campaign (Reinhardt et al. 2014).

The following paragraphs give information about the blasting campaign needed for understanding of Section 5.5, where the in-situ data of the blasting site is used to demonstrate the application of the suggested approach. The test field considred in 12 blasting boreholes named SBL 1 to SBL 12. In each of the boreholes , three blasting passes were installed at certain depths. In three additional boreholes, three pore water pressure sensore were installed at depths of 17 m and 7 m below ground surface (see Figure 5.4). The horizontal distance between each neibouring SBL was 40 m. The location of the boreholes where the pore water pressure sensors P1, P2 and P5 were installed, can be seen from Figure 5.5. The pore water pressure measurements for each blasting borehole (SBL) started about 30 min before each blasting and were stopped about 24 h after the blasting. There were 3 pore water pressure sensors in different locations of the test field to record the pore water pressure variation during the blasting. Sensors P1 and P2 were placed in 17 m depth but at different horizontal distance from the blasting point considered here ($\approx$ 60 to 70 m), while sensor P3 was mounted in 7 m depth and had a horizontal distance of 49 m from the blasting borehole considered here (see Figure 5.6).

The variation of pore water pressure in a given borehole during blasting is displayed in

Figure 5.7. It can be seen in this figure that the excess pore water pressure has a peak value at a certain time after ignition. The in-situ pore water pressure data will be used to plot the stress state over time during a blast event. The location of the obtained in-situ stress path will be compared to the location of the respective FLS valid for the corresponding in-situ ψ, i.e. in-situ void ratio.

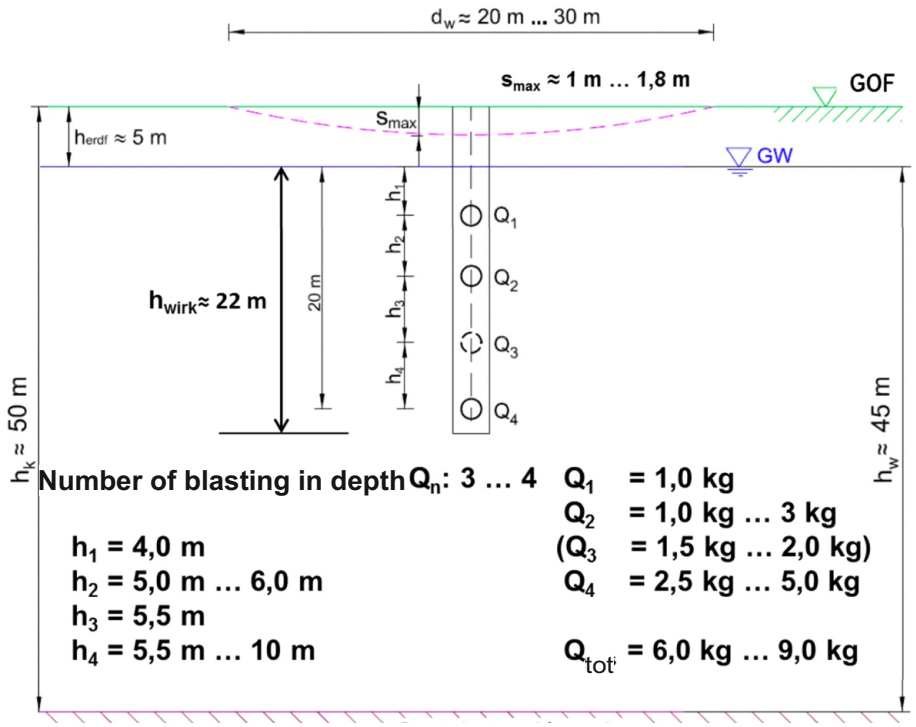

Figure 5.4.: Scheme of blast material distribution in the boreholes for performing soil improvement technique (Reinhardt et al. 2014)

Figure 5.8 illustrates the blast induced settlements as measured by airborne-laser scanning. The maximum settlement in this area was about 2.5 meter (Reinhardt et al. 2014).

Numerous CPT tests have been conducted in the vicinity of the boreholes before and after the explosion. Figure 5.9 shows an example of a CPT test result before and after the blast event. This figure shows that resistance of the soil has been increased due to the blasting.

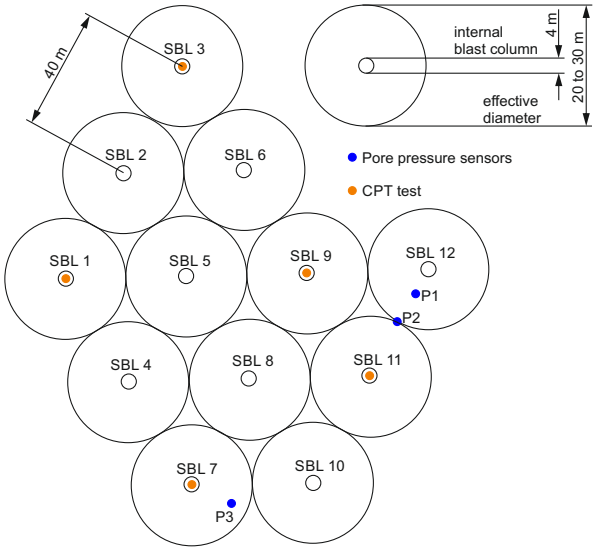

Figure 5.5.: Set up of the boreholes (each borehole known as SBL) and pore water pressure sensors (P1/P2/P3)

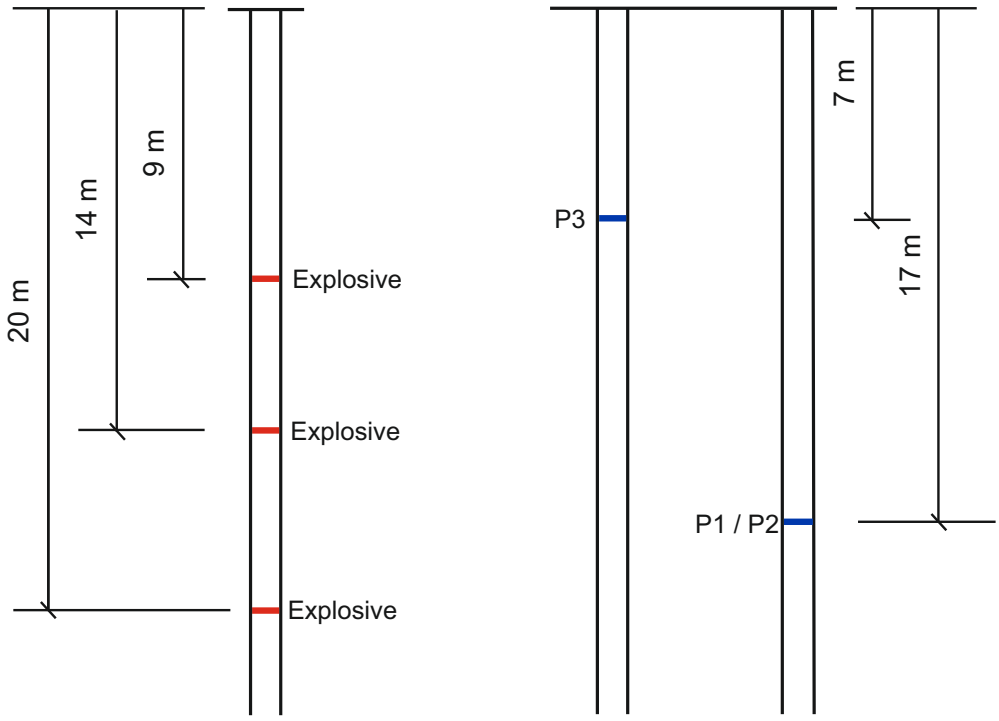

Figure 5.6.: Scheme of the boreholes with explosive (each borehole known as SBL) and pore water pressure sensors (P1/P2/P3)

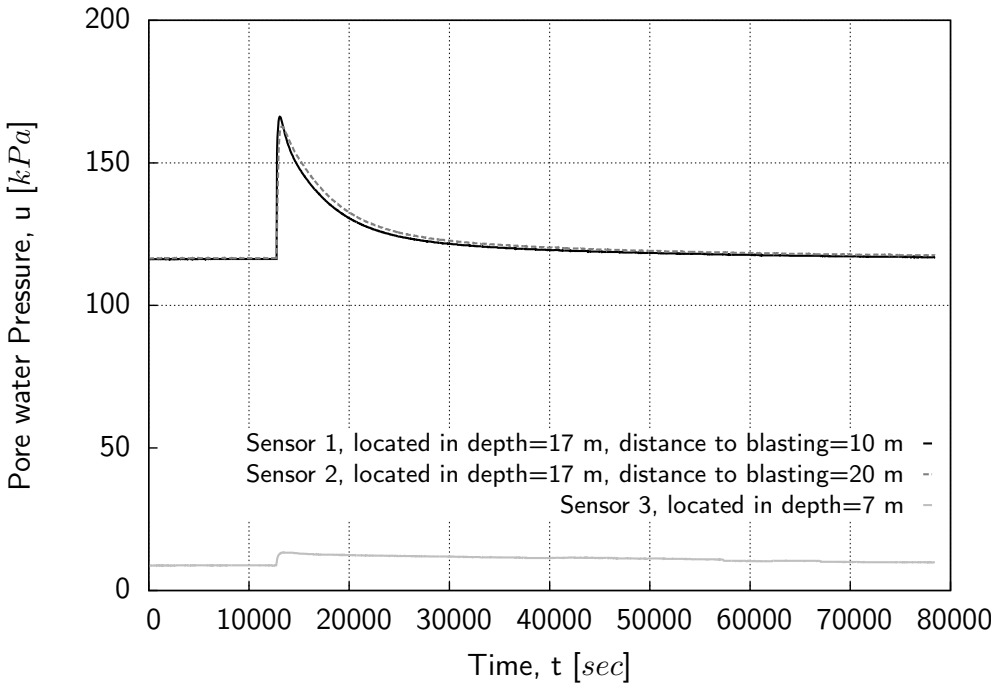

Figure 5.7.: Variation of pore water pressure with time in different distances and depths during blasting

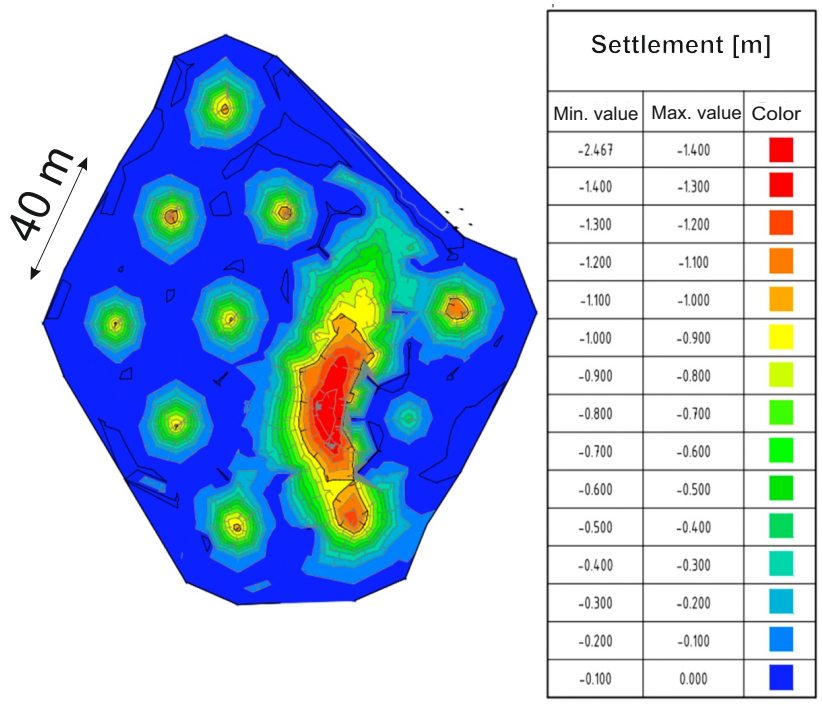

Figure 5.8.: Contour plot of settlement induced by blasting on a test site with 12 boreholes, in which explosive material was placed (Reinhardt et al. 2014)

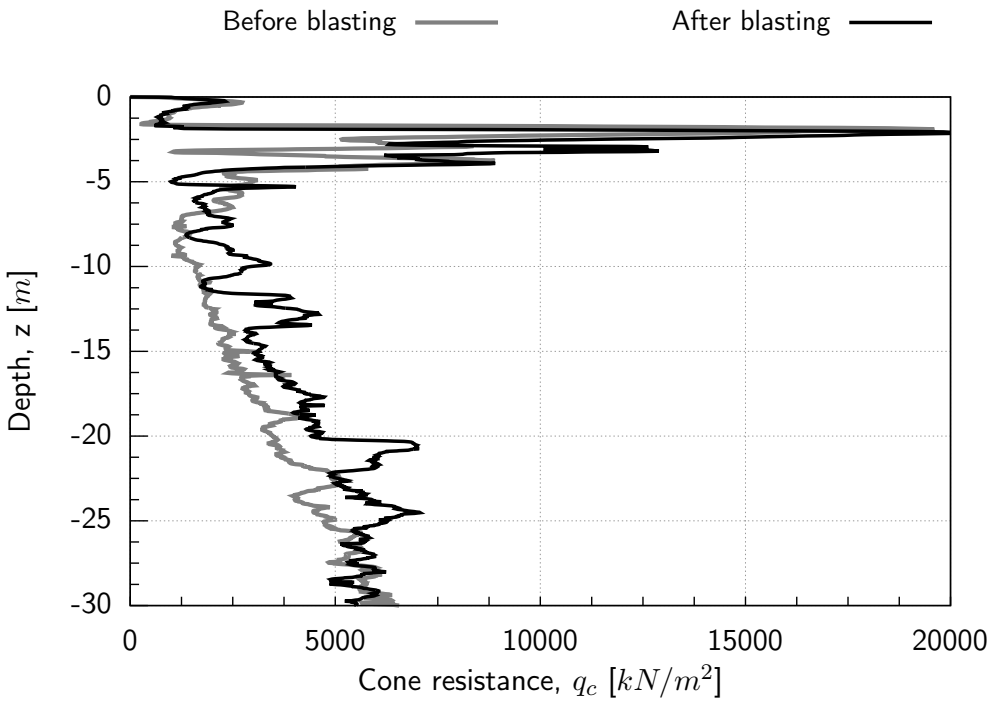

Figure 5.9.: Effect of blasting on cone resistance in CPT test (Reinhardt et al. 2014)

5.4. Determination of the Instability/Steady State Parameters

To determine the steady state and instability state of Lusatian material (Seese sand), a series of monotonic and cyclic triaxial tests under undrained and drained conditions were conducted. The properties of the used material and a table with the test program are presented in Sections 3.2.4 and 3.3.2, respectively.

Based on the triaxial tests results, the steady state data point of each sample was determined, so the Steady State Line (SSL) in the void ratio - mean effective stress space (e-log p') was obtained (the results are presented in following sections). For each sample the Flow Liquefaction Surface (FLS) and the instability stress ratio $\eta_{IS} = q_{max}/\mathrm{p}'_{IS}$ were determined. The instability stress ratio is deduced as a function of state parameter ψ (Been & Jefferies 1985; Lade 1993).

This relationship for Lusatian material is displayed in Figure 5.10. To verify this relationship, all data points are plotted in a normalized diagram in Figure 5.11 which was proposed by Rahman & Lo (2012). In this diagram, the instability stress ratio of the present test series and four studies from the literature are normalized with their respective steady state stress ratio, M and its correlation with equivalent granular state parameter, ψ^* is

examined. Considering the very small amount of fines content ($< 2\%$) of the material tested in the present study, there is negligible difference between the values of equivalent granular void ratio e^* and global void ratio e. Due to this reason the equivalent granular void ratio does not need to be considered here. The same applies to ψ^* ($\psi^* = \psi$). The relationships shown in Figure 5.10 are used to estimate the instability zone (initiation of liquefaction) of given in-situ state and further the cyclic response of the soil.

The laboratory test results (monotonic and cyclic) on Seese sand as well as an investi-

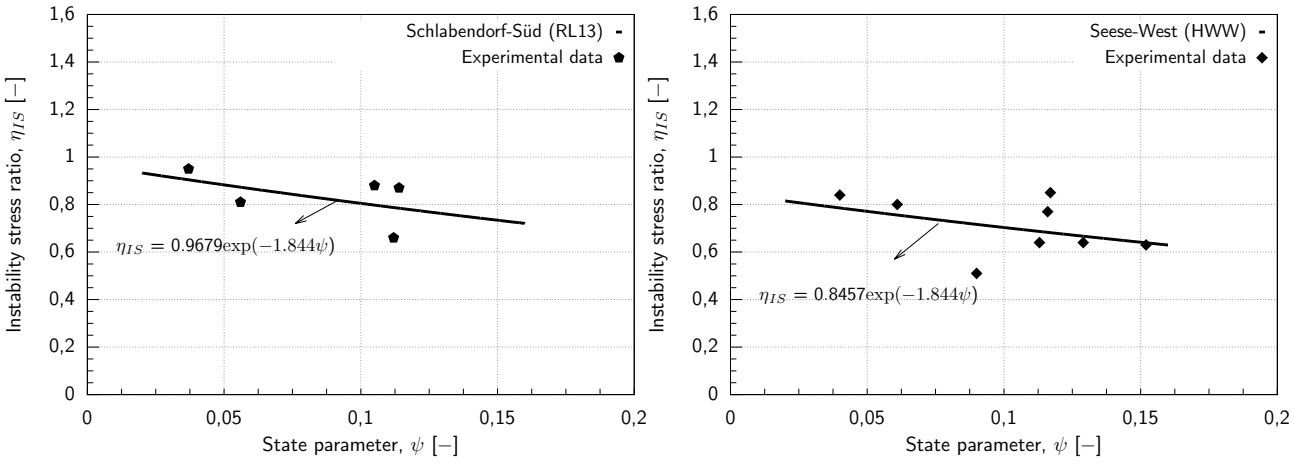

(a) (b)

Figure 5.10.: Relationships between instability stress ratio and state parameter for (a) Schlabendorf-Süd samples; (b) Seese-West samples

gation of liquefaction behavior in the field are presented in oncoming sections.

5.4.1. Presentation of Laboratory Test Results

5.4.1.1. Monotonic Response of Seese Sand

The initial states of the tests are presented in Table 3.7 and Table 3.8 of Chapter 3, Section 3.3.2. All tested samples were prepared with the moist tamping method, with different initial relative density. After preparation, the samples were saturated with water using back pressure method (as it explained in Section 3.4.4). A sufficient degree of saturation was checked by means of Skempton's B-value. All samples achieved B $\geq$ 0.95. Thereafter, all specimens are isotropically consolidated under different initial mean effective stresses and then sheared in a strain-controlled manner with a displacement rate 0.2 mm/min. Specimens were sheared up to an axial strain of about 20 to 25% in order

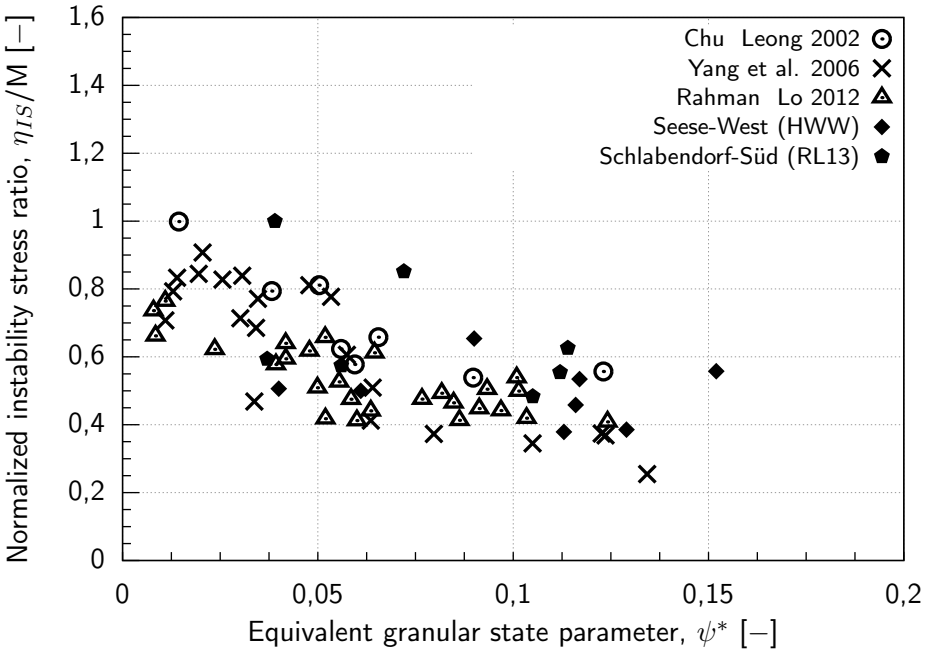

Figure 5.11.: Normalized instability stress ratio versus state parameter for published data and data of current study

to assure that a critical state was reached.
The undrained behavior of the material is presented in Appendix B. Figure 5.12 and Figure 5.13 are selected to demonstrate the typical behavior of Schlabendorf-Süd and Seese-West soils, respectively. The steady state lines are determined by plotting the log mean effective stress at steady state (logarithmic) against the void ratio, e-log p'. The steady state lines of Schlabendorf-Süd and Seese-West are displayed in Figure 5.14a and 5.14b, respectively. The open symbols in these diagrams show the initial states of each sample and the filled symbols represent the steady states of the soil specimens. The related equation of steady state lines are also illustrated.

Figure 5.15 presents the obtained steady states in the p'-q space.

5.4.1.2. Cyclic Response of Seese Sand

A series of cyclic undrained triaxial tests were performed on Seese sandy soils with different initial state. All specimens were prepared using the moist tamping method. After preparing the samples were water-saturated, leading to B values, B $\geq$ 0.95. Some of the specimens were isotropically consolidated, while some other ones were anisotropically

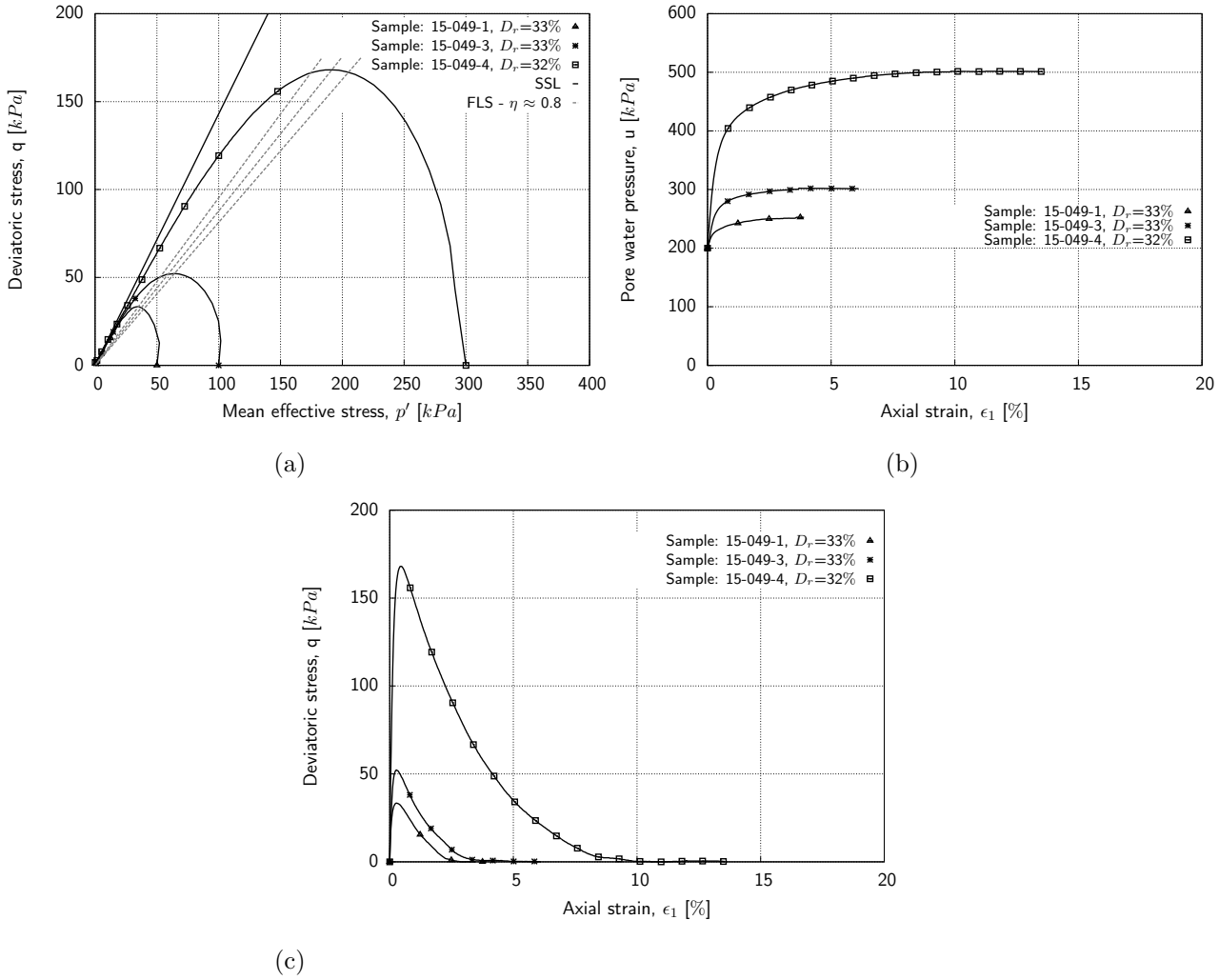

Figure 5.12.: Comparison of undrained monotonic behavior of Schlabendorf-Süd sand samples with the same relative density of about 33% in tests with different initial effective stresses: (a) effective stress path; (b) pore pressure variation vs. axial strain; (c) stress strain behavior

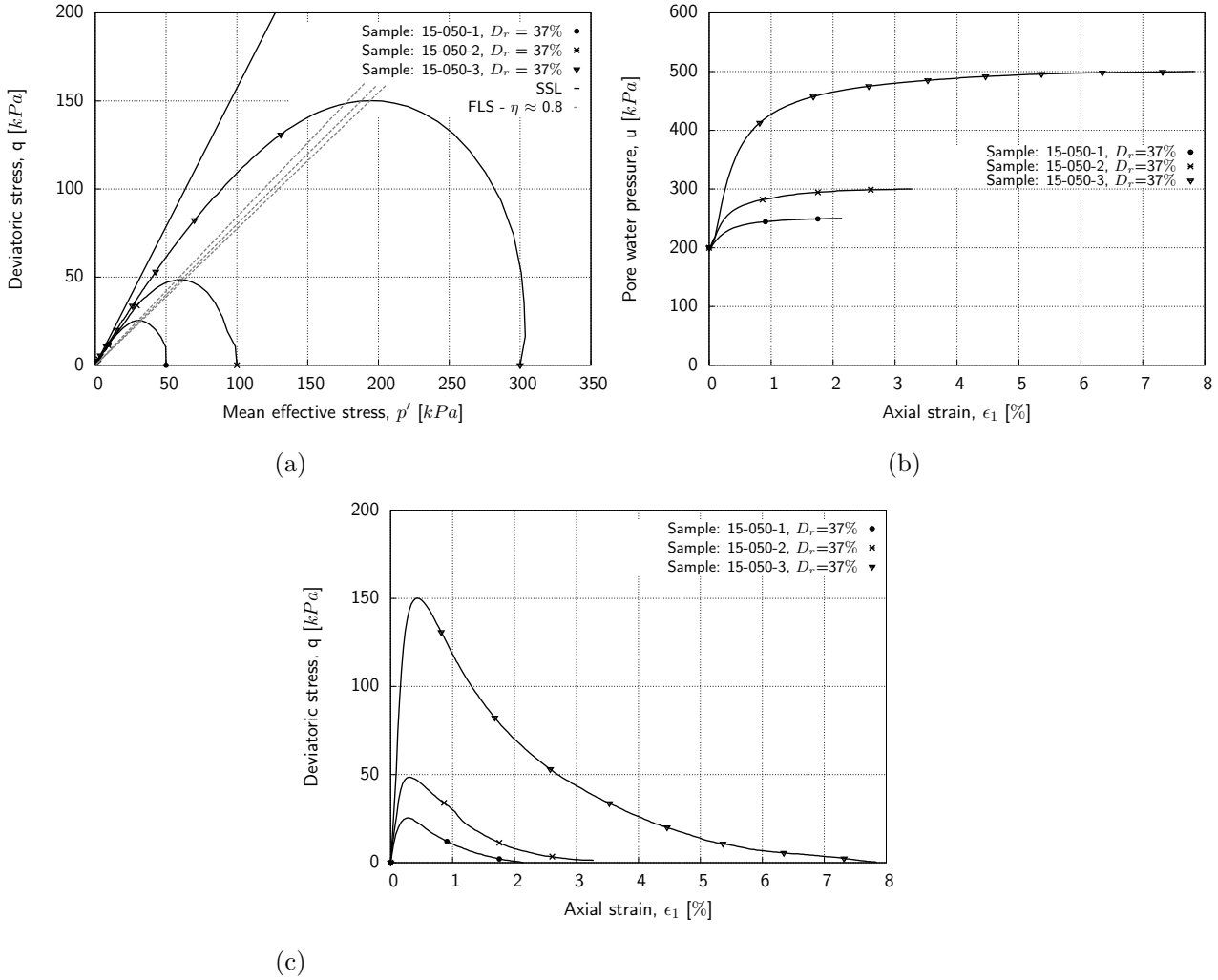

Figure 5.13.: Comparison of undrained monotonic behavior of Seese-West sand samples with the same relative density of 37% in tests with different initial effective stresses: (a) effective stress path; (b) pore pressure variation vs. axial strain; (c) stress strain behavior

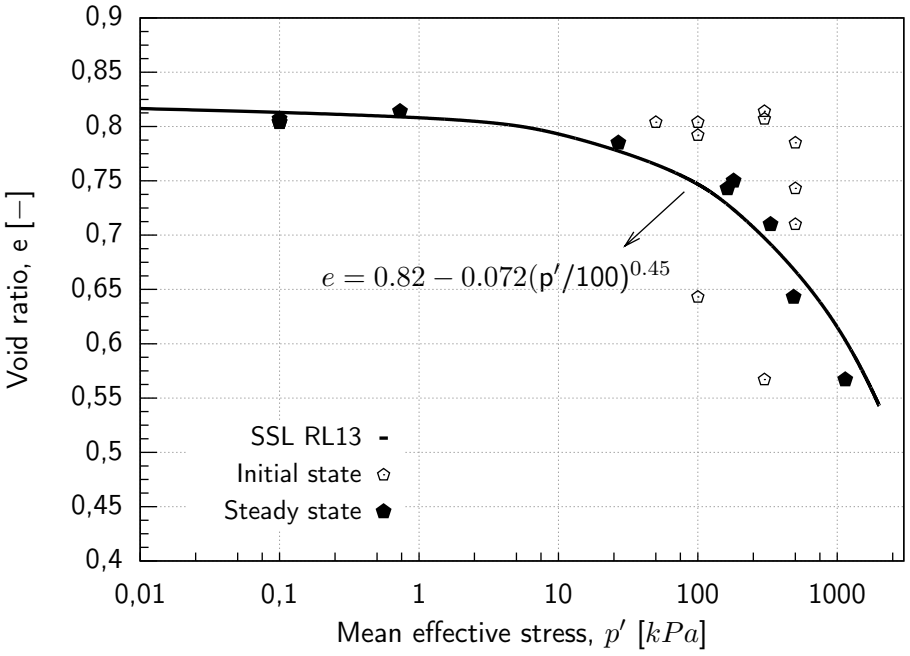

(a)

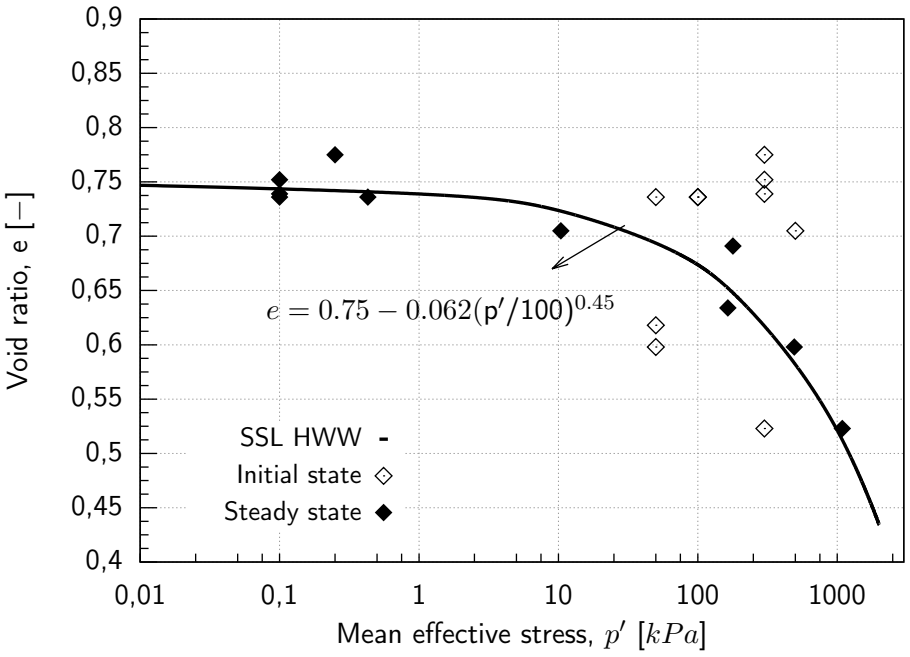

(b)

Figure 5.14.: Steady state line in e-log p' space: (a) Schlabendorf-Süd samples; (b) Seese-West samples

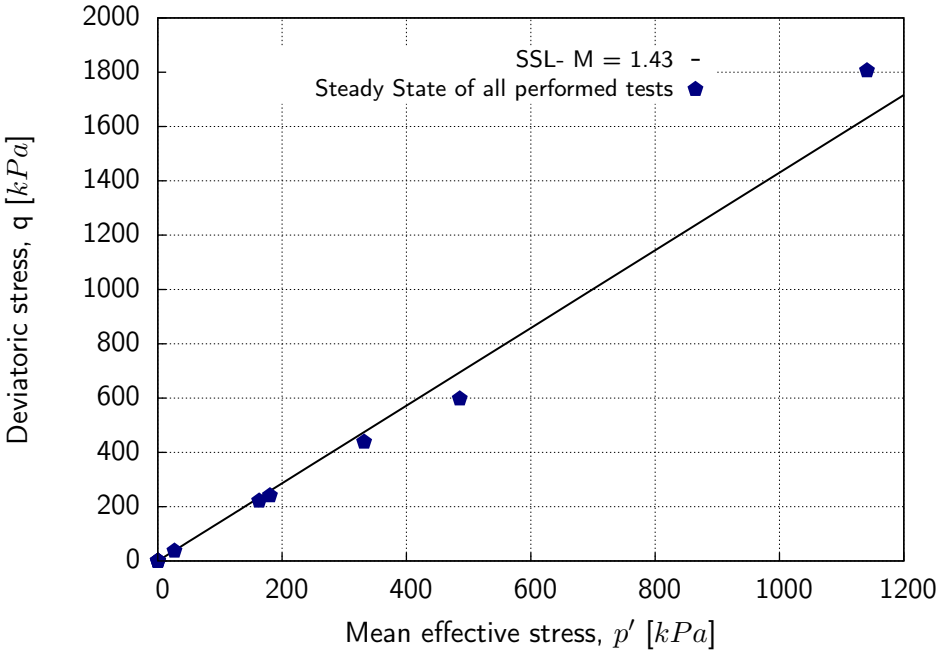

(a)

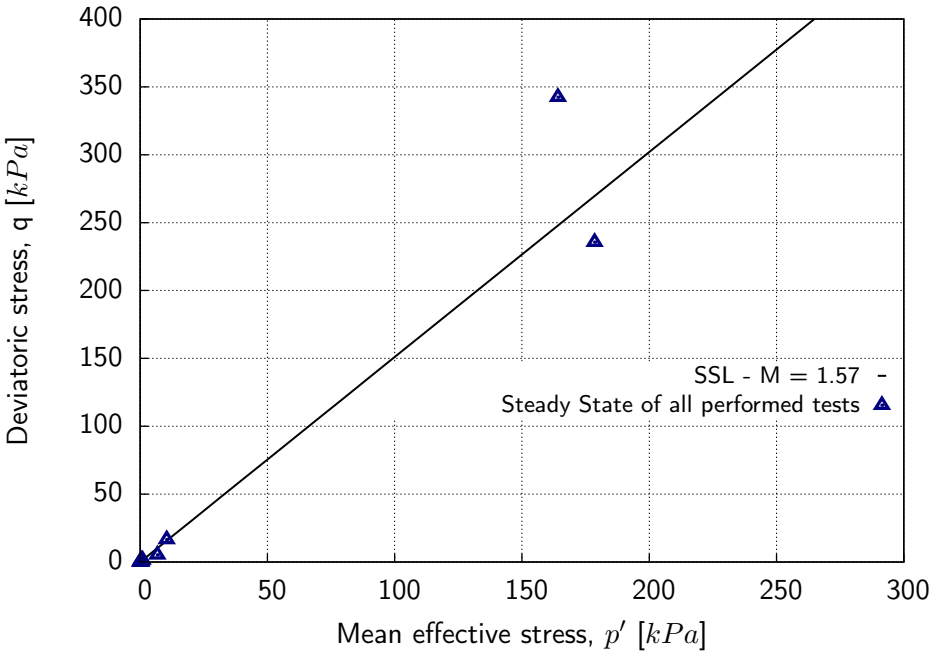

(b)

Figure 5.15.: Steady state line in p'-q space: (a) Schlabendorf-Süd samples; (b) Seese-West samples

consolidated under different ratios $K_0 = \sigma'_3/\sigma'_1$. All tests were performed in a stress-controlled manner at a loading frequency of 0.1 Hz. The initial states of all performed tests are presented in Tables 3.9 and 3.10 for Schlabendorf-Süd material and Tables 3.11 and 3.12 for Seese-West material. More details on the soil samples response will be presented in following sections.

The cyclic loading is applied with a certain amplitude of deviatoric stress q^{ampl} around an average deviatoric stress q^{av}. In the case of the isotropic initial stress condition $q^{av} = 0$ holds. In that case the shear stress is reversed during the cyclic loading (symmetrical loading), while the sign of the shear stress does not change in case of anisotropic loading conditions with $q^{av} > q^{ampl}$. Cyclic stress ratio CSR is defined as the stress amplitude divided by twice the initial mean effective stress, i.e. $CSR = q^{ampl}/(2\ p_0')$. Cyclic liquefaction is defined as reaching a state with zero effective stress ($p' \approx 0$ kPa) which is also called initial liquefaction in the literature. The deformation of the samples under cyclic loading were also visually observed. Figure B.6 in Appendix shows the deformation of different specimens under cyclic loading at the end of the test.

The liquefaction resistance curves were displayed by plotting the cyclic stress ratio (CSR) of a test against the number of cycles needed to reach approximately zero effective stress. To have a better overview of sample response under cyclic loading, the test data for isotropically consolidated and anisotropically consolidated samples were plotted in separate diagrams, see Figure 5.16. The densities of the samples and the number of cycles required to initiate the liquefaction in these tests are summarized in Tables 3.9 and 3.11, in Section 3.3.2. As an example, Figure B.7 to Figure B.9 and Figure B.10 to Figure B.12 demonstrate the cyclic response of Schlabendorf-Süd samples and Seese-West samples, respectively. Comparing these diagrams highlights the effect of cyclic stress ratio on cyclic response of the samples with almost the same initial state.

Furthermore, to resemble the initial stress conditions closer to the field, four anisotropically consolidated triaxial tests have been also conducted on Seese sand. For this purpose, the samples are consolidated at different K_0 values. Figure 5.17 illustrates the effective stress paths measured in the anisotropically consolidated tests in combination with their related flow liquefaction surface. The displayed flow liquefaction surface in these diagrams corresponds to that observed in the monotonic triaxial test on the same material and with the same initial state parameter ψ_0. It can be seen that the initiation of liquefaction under cyclic loading occurred a little bit before the initiation of an instability state of the sample under monotonic loading. Figures 5.17 shows in accordance to Rahman et al. (2012) that the flow liquefaction line as determined from a static test is approximately valid for the initiation of flow liquefaction in a cyclic test on a sample with the same state parameter

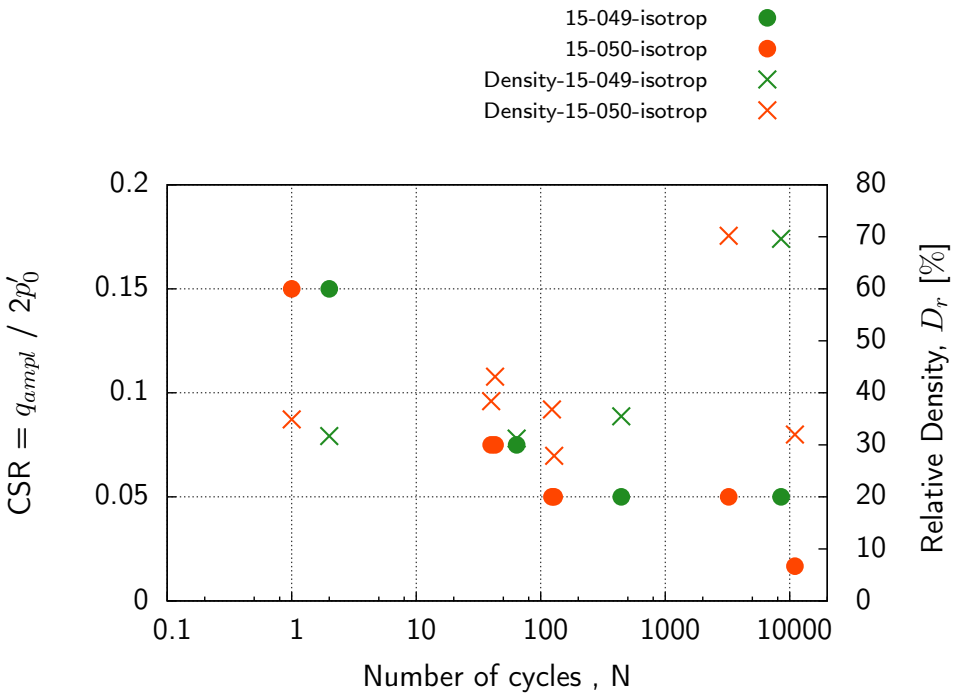

(a)

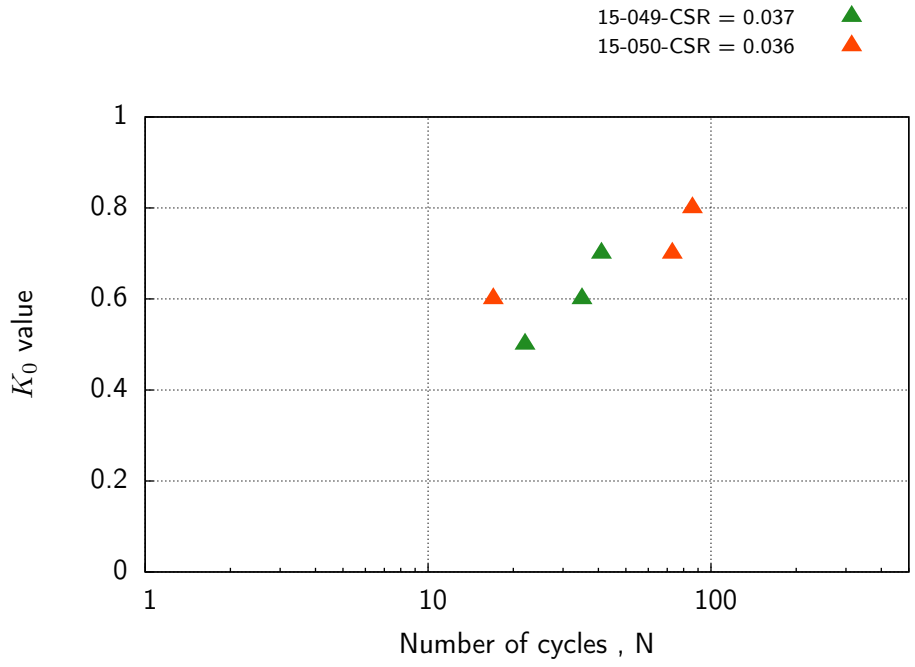

(b)

Figure 5.16.: Number of cycles needed to initiate liquefaction of Seese sand (a) for isotropically consolidated samples versus cyclic stress ratio ; (b) for anisotropically consolidated samples versus K_0 value

ψ. The predicted FLS using the obtained relationship between η and ψ for each soil (see Figure 5.10) is also displayed in Figures 5.17. It can be seen that the predicted FLS is located close to the FLS from the triaxial tests.

5.5. Application of the Proposed Approach Using In-situ Data

5.5.1. Quantification of Possible Compaction Effort

The proposed concept uses the laboratory test results in combination with in-situ test results to estimate the liquefaction susceptibility of the soil in the field. The interpretation of data is based on the location of the initial state of the soil in relation to the SSL in void ratio - depth $e - z$ space. So, when the state of an element of soil (according to in-situ test results) is located on the right side of the SSL in $e - z$ space then soil is susceptible to either flow liquefaction or cyclic liquefaction. If the soil state is located on the left side of SSL, samples are usually not susceptible to flow/cyclic liquefaction but cyclic mobility may happen.
In order to determine the value of in-situ void ratio at different depths following methods have been used: (1) CPT combined with radiometric measurements which directly measures the void ratio in the field, and (2) estimation of void ratio from standard CPT using empirical relationships suggested by Friedrich (2005). Friedrich (2005) proposed an empirical formula based on CPT test results by using different correlations, see Equation 5.2. It should be noted that he calibrated the coefficients of Equation 5.2 based on directly measured porosity in combination with a statistical approach.

$$n = a \cdot \left[(\frac{q_c}{\sigma'_{v0}})^b / (R_f)^c \right]^d \tag{5.2}$$

where: a $\approx$ 0.5 , b $\approx$ 0.3 , c $\approx$ 0.2 , d $\approx$ (-0.1) and R_f is the friction ratio. Note that the values of these coefficients are only applicable for Lusatian material.
The above described procedure was applied to one set of field data as described in Section 5.3. Figure 5.18 displays the void ratio derived from CPT test results together with the SSL of Lusatian soil transferred into $e - z$ plane (see next Section). Since the SSL divides contractive (potential for liquefaction) from dilative soil states (no flow liquefac-

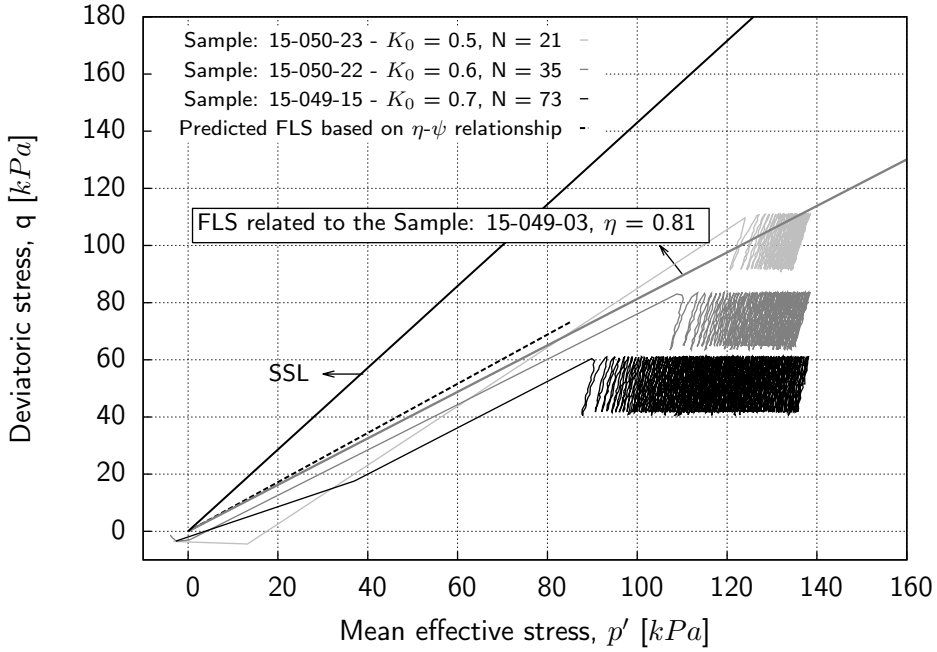

(a)

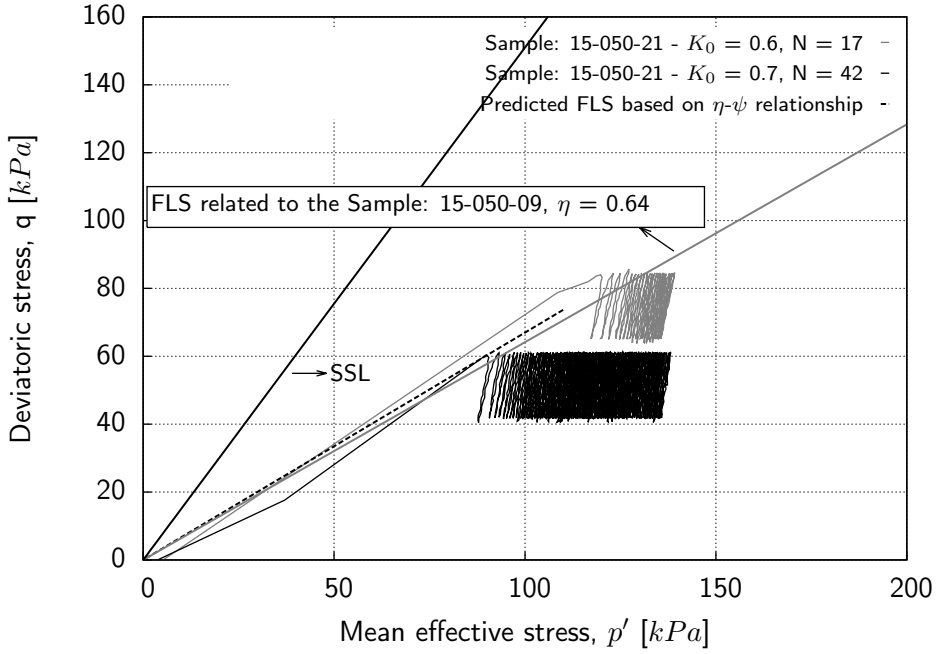

(b)

Figure 5.17.: Cyclic response of (a) Schlabendorf-Süd sand under different anisotropic consolidation states with $\psi \approx 0.056$; (b) Seese-West sand under different anisotropic consolidation states with $\psi \approx 0.139$

tion), the distance between the initial state of a soil element on the contractive side to the SSL defines the compaction effort needed in order to reach a porosity state which is not prone to flow liquefaction. It is to be noted that the specific CPT presented in Figure 5.18 shows a significant reduction in void ratio only in the depth between 5 and about 15 m. However, the void ratio corresponding to steady state was not reached in these depths. The proposed concept for determination of needed compaction effort based on critical state needs further research. One crucial point is the determination of void ratio in-situ based on the CPT results. Based on the limited data presented here, no final recommendation regarding the use of steady state void ratio as compaction criteria can be made. However, it might be possible that future advances in field measurement techniques will allow for more precise measurements of the relevant in-situ state parameters, thus, enabling a better reliability in the predictions using the proposed concept.

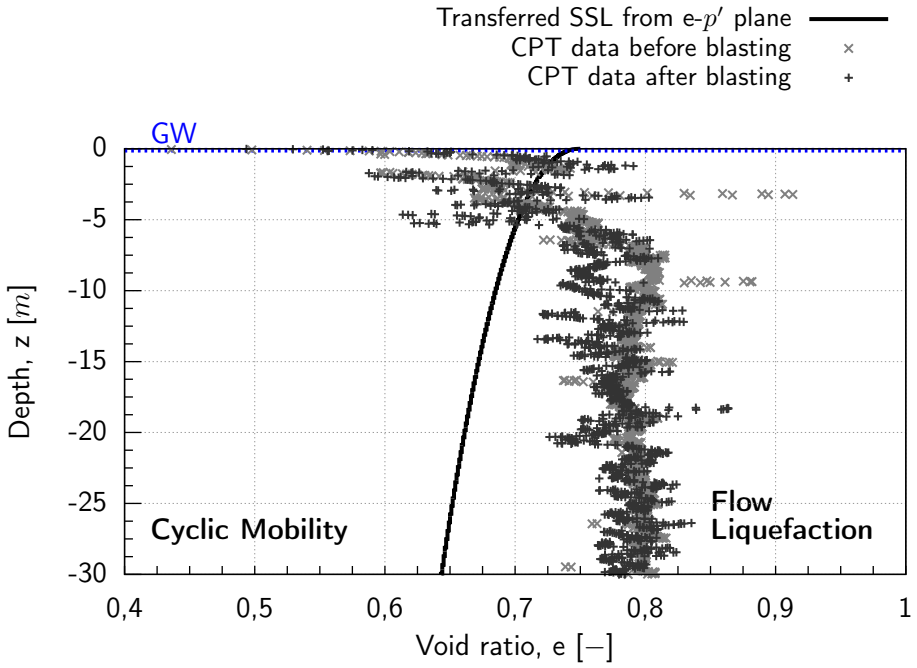

Figure 5.18.: Transferred SSL in $e - z$ space combined with CPT data before and after blasting

5.5.2. Transformation of Steady State Line from e-log p' Plane to $e - z$ Plane

The characteristics of steady state line and flow liquefaction surface have been already explained in Chapter 2. In this Section a new concept will be proposed including a mapping of the steady state line to the void ratio-depth $e - z$ plane in lieu of void ratio-mean effective stress e-log p' plane by using basic equations from soil mechanics (Equation 5.3 to Equation 5.6). It should be noted that in this study the coefficient of earth pressure K_0 is assumed to be constant. Thereafter, the depth will be obtained as a function of initial void ratio e and initial mean effective stress p' by substituting from Equation 5.8 in Equation 5.7. The empirical Equation 5.8 is introduced in previous chapter in Section 2.2.1. So, finally the Equation 5.9 is obtained to use for transferring the SSL into $e - z$ plane. It should be noted that, the analytical transformation of SSL from e-log p' space to $e - z$ space works only when the ground water level is at the ground surface.

$$\sigma_1{}' = \gamma' \cdot z \tag{5.3}$$

$$\sigma_3{}' = K_0 \cdot \gamma' \cdot z \tag{5.4}$$

$$\gamma' = \frac{\gamma_s - \gamma_w}{1 + e} \tag{5.5}$$

$$p' = \frac{\sigma_1' + 2 \cdot \sigma_3'}{3} = \frac{\sigma_z' \cdot (1 + 2 \cdot K_0)}{3} \tag{5.6}$$

$$z = \frac{\sigma_1'}{\gamma'} = \frac{3 \cdot p'}{1 + 2 \cdot K_0} \cdot \frac{1 + e}{\gamma_s - \gamma_w} \tag{5.7}$$

$$p' = p'_{SS} = \left(\frac{-(e - e_{lim})}{\Lambda} \right)^{\frac{1}{\xi}} \cdot p_{atm} \tag{5.8}$$

$$z_{SSL,p'}(e) = \frac{3 \cdot \left(\frac{(e_{lim} - e)}{\Lambda} \right)^{\frac{1}{\xi}} \cdot p_{atm}}{1 + 2 \cdot K_0} \cdot \frac{1 + e}{\gamma_s - \gamma_w} \tag{5.9}$$

where p_{atm} is atmospheric pressure, and e_{lim}, Λ and ξ are empirical parameters. For the studied field case, the ground water level and the related pore water pressures were known from the CPT test results, therefore, the in-situ stress state for a given depth was calculated using assumptions for coefficient of earth pressure at rest, K_0. For any given field location with a certain depth, the corresponding state parameter ψ can be calculated by finding the difference between the steady state void ratio e_{ss} (from laboratory test results) and the in-situ void ratio $e_{in-situ}$. By using this approach, any in-situ state

can be evaluated with respect to the relevant lines SSL in e-log p' and e-log S_{su}. Initial states with potential risk for flow liquefaction ($\psi > 0$) can be distinguished from states with risk for cyclic mobility ($\psi < 0$). Based on the SSL (e-log p') and the SSL($e - z$), a need for compaction can be quantified.

5.5.3. Hydraulic Monitoring

The location of any in-situ stress state expressed as ratio $\eta_{in-situ}$ with respect to the flow liquefaction surface, η_{IS} can be used to quantify a possible pore water pressure reserve Δu (Hydraulic monitoring). In the field case, CPT data as well as in-situ pore water pressure measurements are used to evaluate the state in a given profile of the sandy deposit before, during and after blast densification.

The data of one borehole is selected to show how the laboratory triaxial results can be combined with in-situ test results to estimate the allowable excess pore water pressure during the compaction effort.

The slope of the flow liquefaction surface is predicted by Equation 5.1 for each given initial state of the soil. The allowable excess pore water pressure can be estimated for each element of soil by considering the position of the initial state to the flow liquefaction surface in the p'-q diagram, see Figure 5.19. There are some parameters in this figure which should be introduced e.g. ψ_{min} and ψ_{max} are the state parameter related to the state with larger and smaller relative density, respectively. The point with ψ_{min} is very close to the steady state line and the point with ψ_{max} is far from the steady state line.

In the current study, it is assumed that the coefficient of lateral earth pressure is K_0 = 0.5. Figure 5.19b shows the development of effective stress as calculated based on the estimated initial effective stress and the measured in-situ pore water pressures during blasting. The time t_0 signifies the initial state just before ignition of blasting, time t_1 corresponds to the point of maximum in-situ pore water pressure, and time t_2 signifies the final measured pore water pressure after the end of consolidation.

It can be seen in Figure 5.19b that by blasting the excess pore water pressure generated resulted in a reduction of the initial effective stress (t_0) to some point (t_1) which is in the instability zone (around the corresponding FLS). After the dissipation of the excess pore water pressure the effective stress comes back to its initial state (t_2). However, according to recommendation Senftenberg (1998) to be in a stable condition, the allowable excess pore water pressure amounts around 10% to 40% of the vertical total stress (pore water coefficient r_u = Δu / σ_v between 0.1 and 0.4). The current laboratory test results in

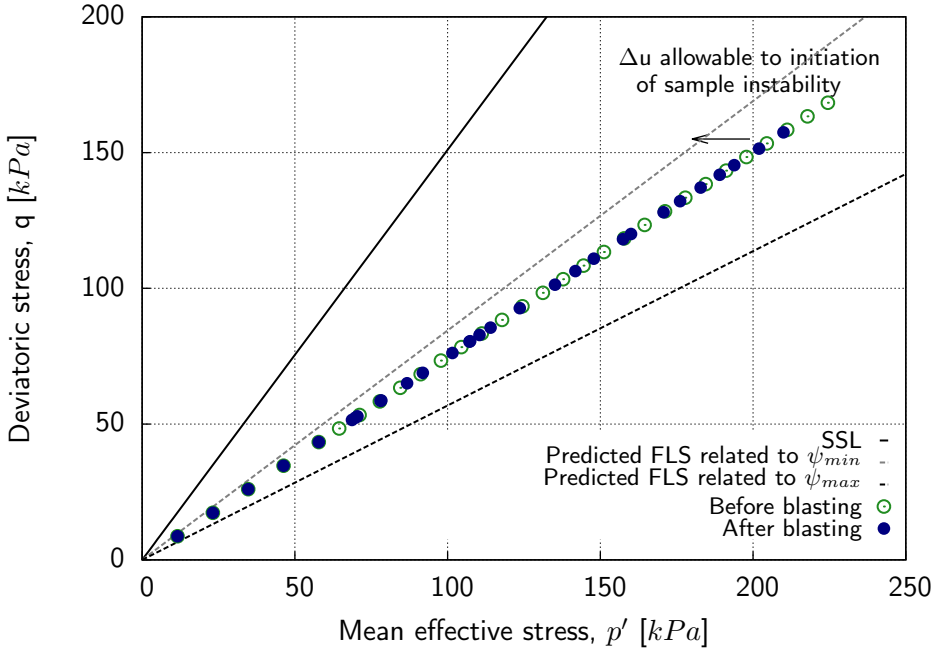

(a)

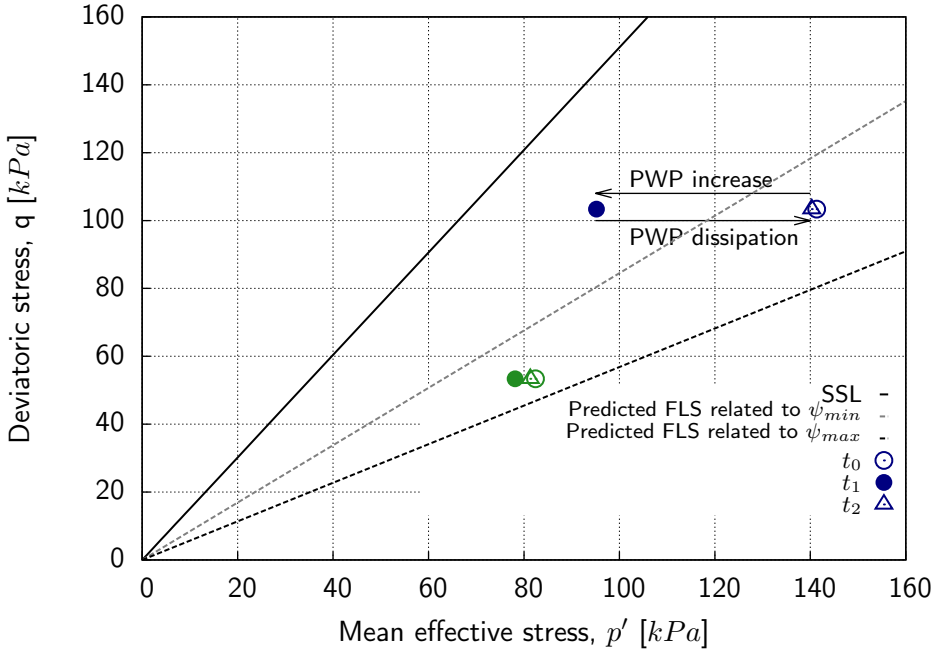

(b)

Figure 5.19.: (a) Position of in-situ initial state of the soil to the FLS; (b) calculated effective stress path from measured variation of pore water pressure in two selected boreholes before, during and after the blasting

combination with empirical relationship show that the initiation of liquefaction can occur before reaching their suggested criteria. Figure 5.20 shows that the stress path calculated based on the in-situ data and an excess pore water pressure = 0.1 σ_v already crosses the FLS (instability zone) obtained from triaxial test results. It means that the suggested range for allowable pore water pressure is not acceptable for all initial states of the soil.

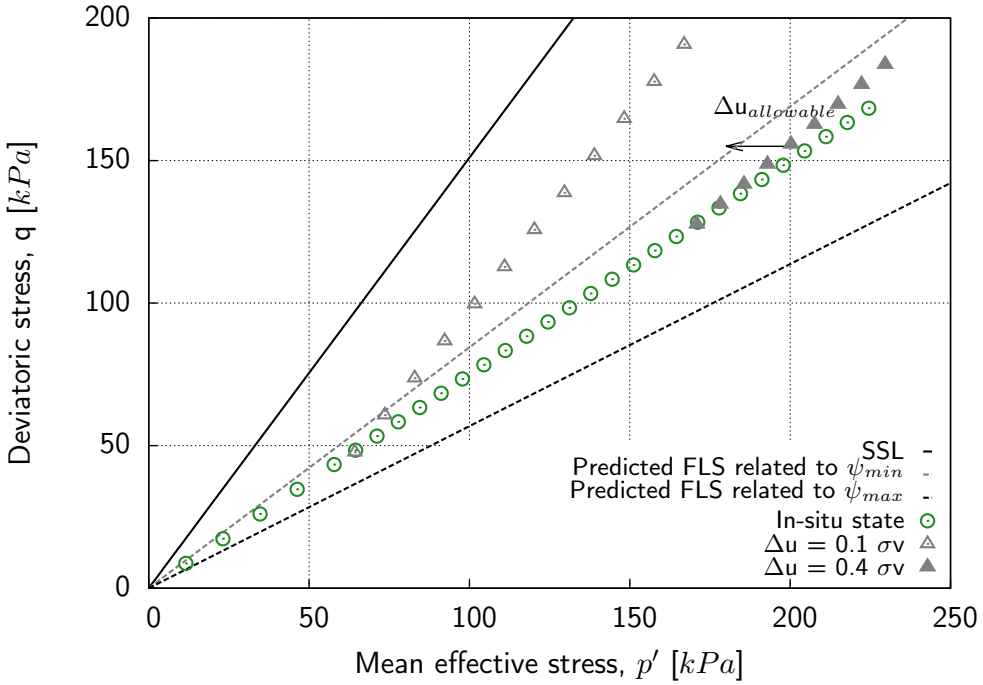

Figure 5.20.: Comparison between criteria suggested by Senftenberg (1998) for allowable excess pore pressure with laboratory results on Seese sand

5.6. Summary

The application of the suggested approach to field data has demonstrated the potential of the approach for an evaluation of the liquefaction susceptibility as well as for the design of monitoring concepts or the design of engineering countermeasures to mitigate the risk of possible liquefaction events. However, further research is needed regarding (1) the uncertainties stemming from the intrinsic heterogeneity of the dumps in terms of state parameters (density, stress state, K_0 value) and material properties (grain size distribution, particle shape, fines content), and (2) the use of correlations for void ratio

calculation based on CPT.
It can be implied from the results of this chapter that the Lusatian sand was recognized as a potentially liquefiable soil at saturated loose state under monotonic and cyclic loading condition. Further outcomes can be summarized as follow:

- Both materials from different locations of the Lusatian area have shown more or less similar behavior under triaxial test conditions.
- Based on the monotonic triaxial test results, the Seese-West soil specimens are liquefied at lower axial strains (earlier) than the Schlabendorf-Süd samples with the same initial conditions.
- For both materials, an increase in sample density resulted in an increase in soil strength and a more dilative response.
- Under static loading conditions isotropically consolidated samples reached their instability state after the excess pore water pressure rose up to approximately 50% of the initial mean effective stress.
- Based on the cyclic triaxial test results, the number of cycles to initiation of liquefaction for Seese-West soil specimens is smaller than for the Schlabendorf-Süd samples with the same initial conditions.
- The initiation of liquefaction for anisotropically consolidated samples under smaller K_0 value (closer to the instability criteria) has occurred at smaller numbers of cycles.

6. Conclusions and recommendations

6.1. Effect of Fines Content

Triaxial compression tests were conducted on Hostun sand to evaluate the influence of initial mean effective stress p', and initial void ratio, e, on the liquefaction behavior of samples. The effect of fines content on position and shape of the steady state lines was investigated with a systematic increase in fines content, f_c up to 50% and by testing the behavior of pure silt corresponding to 100% f_c. The main outcomes of the study are:

- A decrease in shear strength (q_{max}) with an increase in void ratio was observed for clean Hostun sand at the same initial p'. Increasing contractive behavior, this means increasing liquefaction susceptibility was observed for clean Hostun sand with increasing initial effective stress p' at the same density.

- A systematic increase in fines content, f_c up to 50% in triaxial tests shows that q_{max} decreases with an increase in f_c which is consistent with earlier studies for sand with non-plastic fines.

- Based on micro-structural study, it was observed that sand with fines develops two different micro-structures: "fines-in-sand" and "sand-in-fines". For the case "fines-in-sand", fine particles were partially active in the force transformation network and the behavior of the mixture were dominated by the coarse sand fraction. For the case "sand-in-fines", the sand particles were floating within the fines fraction and the behavior of the mixtures were dominated by the fines particle.

- According to the presented results, the shape of steady state line of the mixtures with $f_c < f_{cth}$ follow the shape of clean sand's steady state line (curved shape in this study), and for the mixtures with $f_c > f_{cth}$ follow the pure silt's steady state line (linear shape in this study).
  The global void ratio, e is not an appropriate parameter for a consistent comparison.

The equivalent granular void ratio, e^*, seems to be a consistent state parameter for comparing the behavior of sand dominated mixtures and fines dominated mixtures.

- The steady state lines of the mixtures were located below the steady state line of clean sand moving downwards with increasing fines content up to $f_c = f_{cth}$, beyond this value with the further increasing in the fines content, the shape of the SSLs were found to be linear and the slope of the lines increased with increased fines content.
- Instead of void ratio e, the equivalent granular void ratio e^* have been used as an alternative state variable for anticipating the liquefaction behavior of the sand-silt mixtures under steady state framework. The conversion of e to e^* requires two parameters, b and m parameter. b can be obtained from soil grading properties, and the parameter m was optimized by best fitting the test data.
- Using equivalent granular steady state line (in e^*-log p' space) is suggested to be used for prediction of the steady state lines of sand with particular amount of fines content without the need to conduct triaxial tests on the given mixtures.

These conclusions are derived from the test data for gap graded Hostun sand with non-plastic fines and may not be applicable to the sand with plastic fines.

6.2. Monotonic and Cyclic Response of Seese Sand

A series of monotonic and cyclic triaxial tests were conducted on Seese sand stemming from the dumps in former open pit mines in Lusatian region (Germany). The outcomes of the study are:

- For soil samples at the same initial mean effective stress, as increasing initial relative density resulted in dilative behavior of the samples.
- The state parameter ψ was shown to be the relevant parameter dividing initial states to behave either dilative or contractive during drained and undrained shear loading.
- For all liquefying samples, the inclination η of the flow liquefaction surface as criteria for instability (instability stress ratio) was determined. From all samples with a liquefying stress path, the relationship between the instability ratio η and the state

parameter ψ was quantified. It was shown, that the instability criteria determined from the monotonic tests is also valid for cyclically loaded samples.

- It was shown that the number of cycles N reached before liquefaction depends on both the initial relative density and the cyclic stress ratio CSR. The higher the initial relative density and the lower the cyclic stress ratio, the higher was the number of cycles reached before liquefaction occurred.
- Based on the anisotropically consolidated undrained cyclic tests it was found that, samples with the same initial density, stress state and applied cyclic stress ratio reached a smaller number of cycles with decreasing K_0 or increasing initial static shear stress. The reason is that those initial states are at closer distance to the flow liquefaction surface where flow liquefaction is triggered.

6.3. Application of SSL Concept to the In-situ Data

An approach based critical state soil mechanics and instability concept was suggested to evaluate the liquefaction susceptibilty soil in-situ. The approach was validated using field data of a test field for compaction by blasting. The suggested approach for the field cases has demonstrated the potential of the approach for evaluation of liquefaction susceptibility as well as for the design of monitoring concepts or the design of engineering countermeasures to mitigate the risk of possible liquefaction events.

6.4. Suggested Future Works

Based on the findings of this study further research is suggested as follows:

- Most of the previous studies have been focused on the "fines-in-sand" mixtures. However, the studies on "sand-in-fines" are rare and additional studies are essential to determine the effects of particle characteristics, e.g. size and shape of fine particles, on the steady state line properties of the materials.
- There is no recognized relationship to predict the value of the empirical parameter m for the calculation of equivalent granular void ratio e^* for the sand in fines mixture. Therefore, additional systematic studies on the mixtures containing fines content beyond the threshold fines content f_{cth} must be conducted to determine the empirical

relation between the parameter m and the particle characteristics of fine and coarse particles.

- Regarding the use of the suggested approach for evaluation of liquefaction potential in-situ, the following points need further investigations: (1) quantification of the uncertainties stemming from the intrinsic heterogeneity of the dumps or any site in-situ in terms of state parameters (density, stress state, K_0 value) and material properties (grain size distribution, particle shape, fines content), and (2) search for alternative reliable methods for the precise measurement the void ratio in-situ.

Bibliography

Abedi, M. & Yasrobi, S. (2010), 'Effects of plastic fines on the instability of sand', *Soil Dynamics and Earthquake Engineering* **30, No. 3**, 61–67.

Amat, A. S. (2007), Elastic stiffness moduli of hostun sand, Master's thesis, Department of Civil Engineering, University of Bristol.

Amini, F. & Qi, G. Z. (2000), 'Liquefaction testing of stratified silty sands', *Journal of Geotech and Geoenviron Eng* **126, No. 3**, 208–217.

Athanasopoulos, G. & Xenaki, V. C. (2008), 'Liquefaction resistance of sands containing varying amounts of fines', *Geotechnical Earthquake Engineering and Soil Dynamics* **23**.

Azeiteiro, R. J. N., Coelho, P. A. L. F., Taborda, D. M. G. & Grazina, J. C. D. (2017), 'Critical state-based interpretation of the monotonic behavior of hostun sand', *Journal of Geotechnical and Geoenvironmental Engineering* **143, No. 5**.

Baki, M. A. L. (2011), Cyclic liquefaction behaviour of granular materials with fines, PhD thesis, The University of New South Wales at Australian Defence Force Academy.

Bayat, E. E., Yegian, M. K., Alshawabkeh, A. & Gokyer, S. (2013), 'Liquefation response of partially saturated sands-i: Experimental results', *Journal of Geotechnical and Geoenvironmental Engineering* **139, No. 6**, 863–871.

Baziar, M. & Dobry, R. (1995), 'Residual strength and large deformation potential of loose silty sands', *ASCE J. of Geotechnical Engineering* **121, No. 12**, 896–906.

Baziar, M. H. & Sharafi, H. (2011), 'Assessment of silty sand liquefaction potential using hollow torsional tests-an energy approach', *Soil Dynamics and Earthquake Engineering* **31**, 857–865.

Baziar, M. & Jafarian, Y. (2007), 'Assessment of liquefaction triggering using strain energy concept and ann model: capacity energy', *Soil Dynamics and Earthquake Engineering* **27, No. 12**, 1056–1072.

Been, K. & Jefferies, M. G. (1985), 'A state parameter for sands', *Geotechnique* **35, No. 2**, 99–112.

Been, K., Jefferies, M. G. & Hachey, J. E. (1991), 'The critical state of sands', *Geotechnique* **41, No. 3**, 365–381.

Belkhatir, M., Arab, A., Della, N., Missoum, H. & Schanz, T. (2010a), 'Liquefaction resistance of chlef river silty sand: Effect of low plastic fines and other parameters', *Acta Polytechnica Hungarica* **7, No. 2**, 119–137.

Belkhatir, M., Arab, A., Della, N., Missoum, H. & Schanz, T. (2010b), 'Influence of intergranular void ratio on monotonic and cyclic undrained shear response of sandy soils', *C. R. Mecanique* **338, No. 5**, 290–303.

Belkhatir, M., Schanz, T. & Arab, A. (2013), 'Effect of fines content and void ratio on the saturated hydraulic conductivity and undrained shear strength of sand-silt mixtures', *Journal of Environmental Earth Sciences* **70, No. 6**, 2469–2479.

Belkhatir, M., Schanz, T., Arab, A., Della, N. & Kadri, A. (2014), 'Insight into the effects of gradation on the pore pressure generation of sand-silt mixtures', *Geotechnical Testing Journal* **37, No. 5**.

Bobei, D. C. & Lo, S. R. (2001), 'Static liquefaction of sydney sand mixed with both plastic and non-plastic fines', *In Proceedings of the 14th Southeast Asian Geotechnical Conference, Hong Kong* pp. 485–491.

Bobei, D. C. & Lo, S. R. (2005), 'Reverse behavior and critical state of sand with small amount of fines', *The proceedings of the 161CSMGE, Japan, Millpress Science Publishers, Netherlands* **2**, 475–478.

Bobei, D. C., Lo, S. R., Wanatowski, D., Gnanendran, C. T. & Rahman, M. M. (2009), 'A modified state parameter for characterizing static liquefaction of sand with fines', *Canadian Geotechnical Journal* **46, No. 3**, 281–295.

Bouckovalas, G., Adrianopoulos, K. & Papadimitriou, A. (2003), 'Acritical state interpretation for cyclic liquefaction resistance of silty sands', *Soil and dynamics and earthquake engineering* **23 (2)**, 115–125.

Bowman, E. T., Soga, K. & Drummond, W. (2001), 'Particle shape characterization using fourier descriptor analysis', *Geotechnique* **51, No. 6**, 545–554.

Carraro, J. A. H., Bandini, P. & Salgado, R. (2003), 'Liquefaction resistance of clean and nonplastic silty sands based on cone penetration resistance', *Journal of Geotechnical and Geoenvironmental Engineering, ASCE* **129, No. 11**, 965–976.

Carrera, A., Coopy, M. & Lancellotta, R. (2011), 'Influence of grading on the mechanical behaviour of stava tailings', *Geotechnique* **61, No. 11**, 935–946.

Casagrande, A. (1936), 'Characteristics of cohesionless soils affecting the stability of earth fills', *Journal of Boston Society of Civil Engineers* **23**, 257–276.

Casagrande, A. (1975), Liquefaction and cyclic deformation of sands, Vol. 5, pp. 79–133.

Castro, G. (1969), Liquefaction of sands, PhD thesis, Harvard University; Cambridge, Massachusette.

Castro, G. & Poulos, S. J. (1977), 'Factors affecting liquefaction and cyclic mobility', *Journal of the Geotechnical Engineering* **103, GT6**, 501–516.

Castro, G., Poulos, S. J., W., F. J. & Enos, J. L. (1982), 'Liquefaction induced by cyclic loading', *Report to National Sceience Foundation* .

Castro, G., Seed, R. B., Keller, T. O. & Bolton Seed, H. (1992), 'Steady -state strength analysis of lower san fernando dam slide', *Journal of Geotechnical Engineering, ASCE* **118, No. 3**, 406–427.

Chang, N. Y., Yey, S. T. & Kaufman, L. P. (1982), Liquefaction potential of clean and silty sands, pp. 1018–1032.

Chern, J. C. (1985), Undrained response of saturated sands with emphasis on liquefaction and cyclic mibility, PhD thesis, The University of British Columbia, Vancouver, Canada.

Chien, L. K., Oh, Y. N. & Chang, C. H. (2002), 'Effects of fines content on liquefaction strength and dynamic settlement of reclaimed soil', *Canadian Geotechnical Journal* **39, No. 1**, 254–265.

Chiu, C. F. & Fu, X. J. (2008), 'Interpreting undrained instability of mixed soils by equivalent intergranular state parameter', *Geotechnique* **58, No. 9**, 751–755.

Cho, G. C., Dodds, J. & Santamarina, C. (2006), 'Particle shape effects on packing density, stiffness, and strength:natural and crushed sands', *Journal of Geotechnical and Geoenviromental Engineering* **132**, 591–602.

Chu, J. & Leong, W. (2002), 'Effect of fines on instability behaviour of loose sand', *Geotechnique* **52, No.10**, 751–755.

Chu, J., Lo, S. C. R. & Lee, K. I. (1992), 'Strain softening behavior of granular soil in strainpath testing', *Journal of Geotechnical Engineering, ASCE* **118, No.2**, 119–208.

Chung, E. K. F. (1985), The Effect of Stress Path and Pre-strain History on the Undrained Monotonic and Cyclic Loading Behavior of Saturated Sand, PhD thesis, The University of British Columbia.

Cubrinovski, M. & Ishihara, K. (2000), 'Flow potential of sandy soils with different grain compositions', *Soils and Foundations* **40, No.4**, 103–119.

Das, H. K. & Sitharam, T. G. (2011), 'Undrained monotonic response of sand-silt mixtures: effect of nonplastic fines', *Geomechanics and Geoengineering* **6, No. 1**, 47–58.

De Gennaro, V., Canou, J., Dupla, J. & Benahmed, N. (2004), 'Influence of loading path on the undrained behaviour of a medium loose sand', *Canadian Geotechnical Journal* **41**, 166–180.

Dobry, R., Ladd, R. S., Yokel, F. Y., Chung, R. M. & Powell, D. (1982), 'Prediction of pore pressure buildup and liquefaction of sands during earthquakes by the cyclic strain method', *Building Science Series 138. National Bureau of Standards, U.S. Department of Commerce, Washington, D.C.* .

Fear, C. E. & Robertson, P. K. (1995), 'Estimating the undrained strength of sand: a theoretical framework', *Canadian Geotechnical Journal* **32, No. 5**, 859–870.

Fernlund, J. M. R. (2005), 'Image analysis method for determining 3-d shape of coarse aggregate', *Cement and Concrete Research* **Vol. 35, Issue 8**, 1629–1637.

Finn, W. D. L., Leddbetter, R. H. & Wu, G. (1994), 'Liquefaction in silty soils: design and analysis.', *Ground failures under seismic conditions, geotechnical special publication ASCE* **44**, 51–74.

Fordham, C. J., Mcroberts, E. C., Purcell, B. & Mclaughlin, P. (1991), 'Practical and theoretical problems associated with blast densification of loose sands', *In Proceedings of the 44th Canadian Geotechnical Conference of the Canadian Geotechnical Society, Canadian Geotechnical Society, Richmond, Canada* pp. 92–98.

Fourie, A. B. & Papageorgiou, G. (2001), 'Defining an appropriate steady state line for merriespruit gold tailings', *Canadian Geotechnic* **38, No. 4**, 695–706.

Friedrich, S. (2005), Flaechendeckende Ermittlung bodenphysikalischer Parameter aus Drucksondierergebnissen mittels Korrelationen zu Ergebnissen radiometrischer Sondierungen, PhD thesis, The University of TU Freiberg.

Fuentes, W. & Triantafyllidis, T. (2015), 'A constitutive model for deposited sand', *Deutsche Bodenmechanik Tagung* **10**, 169–187.

Gandhi, S. R., Dey, A. K. & Selvam, S. (1999), 'Densification of pond ash by blasting', *Journal of Geotechnical and Geoenvironmental Engineering* **125, No.10**, 889–899.

Georgiannou, V. N. (2006), 'The undrained response of sands with additions of particles of various shapes and sizes', *Geotechnique* **56, No. 9**, 639–649.

Georgiannou, V. N., Burland, J. B. & Hight, D. W. (1990), 'The undrained behaviour of clayey sands in triaxial compression and extension', *Geotechnique* **41, No. 3**, 383â393.

Ghahremani, M., Ghalandarzadeh, A. & Moradi, M. (2006), 'Effect of plastic fines on the undrained behavior of sands', *Soil and Rock Behavior and Modeling, ASCE* **GSP 150**, 48–54.

Gohl, W. B., Martin, T. E. & Sully, J. (2001), 'Use of controlled detonation of explosives for liquefaction testing', *proceedings, Fourth Int. Conf. On Recent Advances in Geotechnical Earthquake Engineering and Soil Dynamics, San Diego, Calif.* **Paper no. 913**.

Goudarzy, M. (2015), Micro and Macro Mechanical Assessment of Small and Intermediate Strain Properties of Granular Material, PhD thesis, Department of Foundation Engineering, Soil and Rock Mechanics; Ruhr-Universität Bochum.

Goudarzy, M., Rahman, M. M., König, D. & Schanz, T. (2016), 'Influence of non-plastic fines content on maximum shear modulus of granular materials', *Soils and Foundation* .

Grozic, J. L. H., Robertson, P. K. & Morgenstern, N. R. (2000), 'Cyclic liquefaction of loose gassy sand', *Canadian Geotechnics Journal* **37**, 843–856.

Guo, N. & Zhao, J. (2013), 'The signature of shear-induced anisotropy in granular media', *Computers and Geotechnics* **47**, 1–15.

Guzman, A. A., Leonards, G. A. & Chameau, J. L. (1988), 'Undrained monotonic and cyclic strength of sand', *Journal of Geotechnical Engineering, ASCE* **114, No. 10**, 1089–1109.

Hazen, A. (1918), 'A study of the slip in the calaveras dam', *Eng. News* **Rec. 81**, 1158–1164.

Hill, R. (1958), 'A general theory of uniqueness and stability in elastic-plastic solids', *Mechanic of Physics of Solid* **6**, 236–249.

Huang, Y.-T., Huang, A.-B., Kuo, Y.-C. & Tsai, M.-D. (2004), 'A laboratory study on the undrained strength of silty sand from central western taiwan', *Soil Dynamics and Earthquake Engineering* **24**, 733–743.

Ishihara, K. (1993), 'Liquefaction and flow failure during earthquakes', *Geotechnique* **43, No. 3**, 351–415.

Ishihara, K., Tatsuoka, F. & Yasuda, S. (1975), 'Undrained deformation and liquefaction of sand under cyclic stresses', *Soils and Foundations* **15, No. 1**, 29–44.

Kanagalingam, T. & Thevanayagam, S. (2005), 'Discussion: Contribution of fines to the compressive strength of mixed soils', *Geotechnique* **55, No. 8**, 627–628.

Keßler, J. & Förster, W. (1992), Sprengverdichtung zur verbesserung von setzungsfließgefährdeten kippen, Technical report, Bergbau and Geotechnik Bodenmechanik, Freiberger Forschungshefte.

Koester, J. P. (1994), 'The influence of fines type and content on cyclic strength in ground failures under seismic conditions', *GSP* **44**, 17–33.

Konrad, J. M. (1990), 'Minimum undrained strength versus steady -state strength of sand', *Journal of Geotechnical Engineering* **116, No. 6**, 948–963.

Kramer, S. L. (1996), *Geotechnical Earthquake Engineering*, University of Washington Prentice-Hall International Series in Civil Engineering and Engineering Mechanics.

Kuerbis, R. H. (1985), The effect of gradation and fine content on the undrained loading response of sand, PhD thesis, University of British Columbia.

Kuerbis, R. H., Negussey, D. & Vaid, Y. P. (1988), 'Effect of gradation and fines content on the undrained response of sand,', *Hydraulic Fill Structures, ASCE Geotechnical Special Publication* **21**, 330–345.

Kuerbis, R. H. & Vaid, Y. P. (1988), 'Sand sample preparation the slurry deposition method', *Soils and Foundations* **28, No.4**, 107–118.

Lacasse, S. & Nadim, F. (1994), 'Reliability issues and future changes in geotechnical engineering for offshore structures', *NGI publication* **No. 191**.

Ladd, R. S. (1974), 'Specimen preparation and liquefaction of sands', *Journal of the Geotechnical Engineering Division, ASCE* **100,GT10**, 1180–1184.

Ladd, R. S. (1978), 'Preparing test specimens using undercompaction', *American Society for Testing and Materials* **1, No. 1**, 16–23.

Lade, P. V. (1993), 'Initiation of static instability in the submarine nerlerk berm', *Canadian Geotechnical Journal* **30**, 895–904.

Lade, P. V., Liggio, C. D. & Yamamuro, J. A. (1998), 'Effects of non-plastic fines on minimum and maximum void ratios of sand', *Geotechnical Testing Journal* **21, No. 4**, 336–347.

Lade, P. V. & Yamamuro, J. A. (1997), 'Effects of non-plastic fines on static liquefaction of sands', *Canadian Geotechnical Journal* **34**, 905–917.

Lade, P. V. & Yamamuro, J. A. (2011), 'Evaluation of static liquefaction potential of silty sand slopes.', *Canadian Geotechnical Journal* **48, No. 2**, 247–264.

Lade, P. V., Yamamuro, J. A. & Liggio, C. D. (2009), 'Effects of fines content on void ratio, compressibility, and static liquefaction of silty sand', *Geomechanics and Geoengineering* **1, No. 1**, 1–15.

Lambe, T. W. (1951), *Soil Testing for Engineers*, The Massachusetts Institute of Tchnology, John Wiley and Sons, Inc., New York.

Lashkari, A. (2014), 'Recommendations for extension and re-calibration of an existing sand constitutive model taking in to account varying non-plastic fines content', *Soil Dynamicsand Earthquake Engineering* **61**, 212â238.

Lashkari, A. (2015), 'Prediction of flow liquefaction instability of clean and silty sands', *Acta Geotechnica* **11, No. 5**, 987â1014.

Lee, K. L. & Albaisa, A. (1974), 'Earthquake induced settlements in saturated sands', *Journal of Geotechnical Engineering Division* **GT4**, 387–406.

Lee, K. L. & Fitton, J. A. (1968), 'Factors affecting the cyclic loading strength of soil', *Vibration Effects of Earthquakes on Soils and Foundations, ASTM STP 450, American Society for Testing and Materials* pp. 71–95.

Li, X. & Ming, H. Y. (2000), 'Unifieded modeling of flow liquefaction and cyclic mobility', *Soil Dynamics and Earthquake Engineering* **19**, 363–369.

Lins, Y. (2009), Hydro-Mechanical Properties of Partially Saturated Sand, PhD thesis, RUB.

Liu, J., Gang, L., Zhen, Y., Dano, C., Hicher, P., Xia, X. & Wang, J. (2013), 'Influence of grading on the undrained behavior of granular materials', *Comptes Rendus MÃ©canique, Elsevier Masson* **342, No. 2**, 85–95.

Lo, S. R., Rahman, M. M. & Bobei, D. (2010), 'Limited flow behaviour of sand with fines under monotonic and cyclic loading', *Geomechanics and Geoengineering* **5, No. 1**, 15–25.

McGeary, R. K. (1961), 'Mechanical packing of spherical particles', *Journal of the American Ceramic Society* **44, No.10**, 513–522.

Mitchell, J. K. (1976), *Fundamental of soil behavior*, Taylor and Francis, London, UK.

Mitchell, J. K. & Soga, K. (2005), *Fundamental of soil behavior*, John Willey and sons.

Moayerian, S., Reipas, L. K., Cascante, G. & Newson, T. (2011), Equipment effects on dynamic properties of soils in resonant column testing, *in* 'Geotechnical conference'.

Mohamad, R. & Dobry, R. (1986), 'Undrained monotonic and cyclic triaxial strength of sand', *Journal of Geotechnical Engineering - ASCE* **112, No. 10**, 941–958.

Monkul, M. M. & Yamamuro, J. A. (2011), 'Influence of silt size and content on liquefaction behavior of sands', *Canadian Geotechnical Journal* **48**, 931–942.

Mulilis, J. P., Chan, C. K. & Seed, H. B. (1975), Effects of method of sample preparation on the cyclic stress-strain behavior of sands, Technical report, Report No. EERC 75-18, Earthquake Engineering Research Center, University of California, Berkeley, July.

Mulilis, J. P., Townsend, F. C. & Horz, R. C. (1978), 'Triaxial testing techniquesand sand liquefaction', *Dynamic Geotechnical Testing, ASTM STP 654, American Society for Testing and Materials* pp. 265–279.

Murthy, T. G., Loukidis, D., Carraro, J. A. H., Prezzi, M. & Salgado, R. (2007), 'Undrained monotonic response of clean and silty sands', *Geotechnique* **57**, No. 3.

Naeini, S. A. & Baziar, M. H. (2004), 'Effect of fines content on steady-state strength of mixed and layered samples of a sand', *Soil Dynamics and Earthquake Engineering* **24**, 181–187.

Narsilio, G. A., C., S. J., Hebeler, T. & Bachus, R. (2009), 'Blast densification: multi-instrumented case history', *Journal of Geotechnical and Geoenvironmental Engineering* **135, No. 6**, 723–734.

Ni, Q., Tan, T. S., Dasari, G. R. & Hight, D. W. (2004), 'Contribution of fines to the compressive strength of mixed soils', *Canadian Geotechnical Journal* **54, No. 9**, 561–569.

Olson, S. M. (2001), Liquefaction analysis of level and sloping ground using field case histories and penetration resistance, PhD thesis, Department of Civil Engineering, University of Illinois at Urbana Champaign.

Papadopoulou, A. & Tika, T. (2008), 'The effect of fines on critical state and liquefaction resistance characteristics of non-plastic silty sands', *Soils and Foundation* **48, No. 5**, 713–725.

Pitman, T. D., Robertson, P. K. & Sego, D. C. (1994), 'Influence of fines on the collapse of loose sands', *Canadian Geotechnical Journal* **31**, 728–739.

Polito, C. P. (1999), The Effects Of Non-Plastic and Plastic Fines On The Liquefaction Of Sandy Soils, PhD thesis, Faculty of the Virginia Polytechnic Institute and State University.

Polito, C. P. & Martin, J. R. (2001), 'Effects of nonplastic fines on the liquefaction resistance of sands', *J. Geotech. Geoenviron. Eng.,* **127, No. 5**, 408â415.

Porcino, D., Cicciu, G. & Ghionna, V. N. (2004), 'Laboratory investigation of the undrained cyclic behaviour of a natural coarse sand from undisturbed and reconstituted samples', *In Triantafyllidis (ed.) Cyclic Behaviour of Soils and Liquefaction Phenomena, Proc. of CBS04, Bochum* pp. 187–192.

Poulos, S. J. (1981), 'The steady state of deformation', *J. Geotech. Eng. Div., ASCE 107* **5**, 553– 562.

Poulos, S. J., Castro, G. & France, J. W. (1985), 'Liquefaction evaluation procedure', *Journal of Geotechnical Engineering , ASCE* **11, No. 6**, 772– 792.

Powers, M. C. (1953), 'A new roundness scale for sedimentary particles', *Journal of Sedimentary Research* **23 (2)**, 117– 119.

Rahman, M. (2009), Modelling the influence of fines on liquefaction behaviour, PhD thesis, The University of New South Wales at Australian Defence Force Academy.

Rahman, M., Lo, S. & Baki, M. A. L. (2011), 'Equivalent granular state parameter and undrained behaviour of sandâfines mixtures', *Journal of Acta Geotechnica* **6**, 183–194.

Rahman, M., Lo, S. & Baki, M. A. L. (2014), 'Undrained behavior of sand-fines mixtures and their state parameter', *Journal of Geotechnical and Geoenvironmental Engineering* **140, No. 7**, 04014036.

Rahman, M., Lo, S. & Gnanendran, C. T. (2008), 'On equivalent granular void ratio and steady state behaviour of loose sand with fines', *Canadian Geotechnical Journal* **45**, 1439–1456.

Rahman, M. M., Baki, M. A. L., Lo, S. R. & Gnanendran, C. T. (2012), 'Linkage between static and cyclic liquefaction of loose sand with a range of fines contents', *Canadian Geotechnical Journal* **49**, 891–906.

Rahman, M. M., Cubrinovski, M. & Cameron, D. (2012), 'Undrained behaviour of sand with fines', *Geomechanics and Geoengineering: An international Journal* **7**, 219–226.

Rahman, M. M. & Lo, S. R. (2008), 'The prediction of equivalent granular steady state line of loose sand with fines', *Geomechanics and Geoengineering: An International Journal* .

Rahman, M. M. & Lo, S. R. (2012), 'Predicting of the onset of static liquefaction of loose sand with fines', *Journal of Geotechnical and Geoenvironmental Engineering* **138, No. 8**, 1037–1041.

Rahman, M. M., Lo, S. R. & Cubrinovski, M. (2010), Equivalent granular void ratio and behaviour of loose sand with fines, *in* 'Fifth international conference on recent advances geotechnical earthquake engineering and soil dynamics'.

Rees, S. D. (2010), Effects of Fines on the Undrained Behaviour of Christchurch Sandy Soils, PhD thesis, University of Canterbury, Christchurch, New Zealand.

Reinhardt, K., Kessler, J., Sommer, B. & Erler, R. (2014), Schonende sprengverdichtung auf innenkippen- für den sanierungsbergbau der lausitz der richtige weg? ein erfahrungs-

und ergebnisbericht, *in* 'Beiträge zum 2. Kolloquium Bodenverflüssigung bei Kippen des Lausitzer Braunkohleberghaus'.

Robertson, P. K. (1992), 'Suggested terminology for liquefaction', *Proc. 47th Canadian Geotechnical Conference* **29**, 686–695.

Robertson, P. K. (2015), 'Comparing cpt and vs liquefaction triggering methods', *Journal of the Geotechnical and Geoenvironmental Engineering, ASCE* **141, Issue 9**, 1–10.

Robertson, P. K., Woeller, D. J. & Finn, W. D. L. (1994), 'Seismic cone penetration test for liquefaction potential under cyclic loading', *Canadian Geotechnical Engineering* **29**, 277–286.

Rodriguez, J. M., Edeskaer, T. & Knutsson, S. (2013), 'Particle shape quantities and measurement techniques - a review', *Electronic Journal of Geotechnical Engineering* **18A**, 169198–37.

Rollins, K. M. & Anderson, J. K. S. (2008), 'Cone penetration resistance variation with time after blast liquefaction testing.', *In Proceedings of Geotechnical Earthquake Engineering and Soil Dynamics IV. ASCE, Reston, VA, USA* **GSP 181**, 10.

Roscoe, K. H., Schofield, A. N. & Wroth, C. P. (1958), 'On the yielding of soils', *Geotechnique 8* **1**, 22– 52.

Sadek, S. & Saleh, M. (2007), 'The effect of carbonaceous fines on cyclic resistance of poorly graded sands', *Journal of Geotechnical and Geological Engineering* **25**, 257–264.

Sadek, T., Lings, M., Dihoru, L. & Wood, D. M. (2006), 'Wave transmission in hostun sand: multiaxial experiments', *Rivista Italiana Di Geotechnica* **2**, 69–84.

Salgado, R., Bandini, P. & Karim, A. (2000), 'Shear strength and stiffness of silty sand', *Journal of Geotechnical and Geoenviromental Engineering* **126, No.5**, 451–462.

Schanz, T. & Vermeer, P. A. (1996), 'Angles of friction and dilatancy of sand', *Geotechnique* **46, No. 1**, 145–151.

Schofield, A. N. & Wroth, C. P. (1968), *Critical State Soil Mechanics*, McGraw-Hill, London.

Seed, H. B. (1979), 'Soil liquefaction and cyclic mobility evaluation for level ground during earthquakes', *Journal of the Geotechnical Division, ASCE* **105, GT2**, 201–255.

Seed, H. B. & Idriss, I. M. (1971), 'Simplified procedure for evaluating soil liquefaction potential', *Journal of the Geotechnical Division, ASCE* **97, Nr. 9**, 1249–1273.

Seed, H. B. & Lee, K. L. (1966), 'Liquefaction of saturated sands during cyclic loading', *Journal ofSoil Mechanics and Foundations Division, ASCE* **92, SM6**, 105–134.

Senftenberg (1998), Assessment of the slide flow potential and protection of embankments against sloughing (in german), Technical report, LMBV.

Shen, C. K., Vrymoed, J. L. & Uyeno, C. K. (1977), 'The effects of fines on liquefaction of sands', *In: Proceedings 9th international conference soil mechanics and foundation engineering. Tokyo* **2**, 381–385.

Silver, M., Chan, C., Ladd, R., Lee, K., Tiedmann, D., Townsend, F., Valera, J. & Wilson, J. (1976), 'Cyclic strength of standard test sand', *Journal of the Geotechnical Engineering Division, ASCE* **102(5)**, 511–523.

Sladen, J. A., D' Hollander, R. D. & Krahn, J. (1985), 'The liquefaction of sands, a collapse surface approach', *Can. Geotech. 1. 22* **4**, 564– 578.

Sladen, J. A. & Handford, G. (1987), 'A potential systematic error in laboratory testing of very loose sands', *Canadian Geotechnical Journal* **24**, 462–466.

Stamatopoulos, C. A. (2010), 'An experimental study of the liquefaction strength of silty sands in terms of the state parameter', *Soil Dynamicsand Earthquake Engineering* **30, No. 8**, 662–678.

Stark, T. D. & Olson, S. M. (1995), 'Liquefaction resistance using cpt and field case histories', *Journal of Geotechnical Engineering - ASCE* **121**, 856–869.

Sze, H. Y. & Yang, J. (2014), 'Failure modes of sand in undrained cyclic loading: Impact of sample preparation', *Journal of American Society of Civil Engineers* **140, No. 1**, 152–169.

Tao, M., Figueroa, J. L. & Saada, A. S. (2004), 'Influence of nonplastic fines content on the liquefaction resistance of soil in terms of the unit energy', *Proc., Cyclic Behaviour of Soils and Liquefaction Phenemena, A.A. Balkema Publishers Bochum, Germany* pp. 223–231.

Terzaghi, K. (1956), 'Varieties of submarine slope failures', *Proceedings, 8th Conference of Soil Mechanics and Foundations, Division, Texas* **Article 3**.

Terzaghi, K. & Peck, R. (1948), *Soil Mechanics in Engineering Practice, 1st Edition*, John Wiley and Sons, Newyork.

Thevanayagam, S. (1998), 'Effect of fines and confining stress on undrained shear strength of silty sands', *Journal of Geotechnical and Geoenviromental Engineering* **124, No.6**, 479–491.

Thevanayagam, S. (2000), Liquifaction potential and undrained fragility of silty soils, *in* '12th World Conference on Earthquake Engineering, Auckland, New Zealand'.

Thevanayagam, S. & Martin, G. R. (2002), 'Liquefaction in silty soils - screening and remediation issues', *Soil Dynamics and Earthquake Engineering* **22**, 1035–1042.

Thevanayagam, S. & Mohan, S. (2000), 'Intergranular state variables and stressâstrain behaviour of silty sands', *Geotechnique* **50, No. 1**, 1â23.

Thevanayagam, S., Shenthan, T. & Mohan, S.and Liang, J. (2002), 'Undrained fragility of clean sands, silty sands, and sandy silts', *Journal of Geotechnical and Geoenvironmental Engineering* **128, No. 10**, 849–859.

Troncoso, J. H. (1986), 'Critical state of tailing silty sands for earthquake loadings', *SDEE* **5, No. 3**, 248â252.

Troncoso, J. H. & Verdugo, R. (1985), 'Silt content and dynamic behaviour of tailing sands', *Proceedings 11th International Conference on Soil Mechanics and Foundation Engineering* **3**, 1311–1314.

Vaid, Y. P. (1994), 'Liquefaction of silty soils', *Proc., Ground failures under seismic conditions, Geotech. Spec. Publ., ASCE* **44**, 1–16.

Vaid, Y. P. & Chern, J. C. (1985), 'Cyclic and monotonic undrained response of saturated sands. in advances in the art of testing soils under cyclic conditions', *American Society of Civil Engineering* pp. 120–147.

Vaid, Y. P. & Sivathayalan, S. (2007), 'Fundamental factors affecting liquefaction susceptibility of sands', *Canadian Geotechnical Journal* **37, No. 3**, 592–606.

Vega-Posada, C. A. & Finno, R. J. (2016), 'Ground surface settlements of sands densified with explosives', *Proceedings of the Institution of Civil Engineers* **169, No. 2**, 90–97.

Verdugo, R. (1992), Characterization of sandy soil behavior under large deformation, PhD thesis, University of Tokyo, Tokyo.

Verdugo, R. & Ishihara, K. (1996), 'The steady state of sandy soils', *Soil and Foundation* **36, No. 3**, 81–91.

Wadell, H. (1933), 'Sphericity and roundness of rock particles', *Journal of Geology* **41, No. 33**, 310–331.

Wang, Z. L., Dafalias, Y. F., Li, X. S. & Makdisi, F. I. (2002), 'State pressure index for modeling sand behavior', *Geotechnic and Geoenvironmental engineering* **6 No. 511**, 511–519.

Wei, L. M. & Yang, J. (2014), 'On the role of grain shape in static liquefaction of sandâsilt mixtures', *Geotechnique* **64, No. 9**, 740–745.

Wichtmann, T. (2005), Explicit accumulation model for non-cohesive soils under cyclic loading, PhD thesis, Ruhr-Universität Bochum.

Wichtmann, T. (2015), 'New findings regarding the behaviour of soils under cyclic loading', *Deutsche Bodenmechanik Tagung* **3**, 47–67.

Xenaki, V. C. & Athanasopoulos, G. (2003), 'Liquefaction resistance of sandâsilt mixtures: an experimental investigation of the effect of fines', *Soil Dynamics and Earthquake Engineering* **23**, 183–194.

Yamamuro, A. & Covert, K. M. a. (2001), 'Monotonic and cyclic liquifaction of very loose sands with high silt content', *Journal of Geotechnical an Geoenviromental Engineering* **127, No.4**, 314–324.

Yamamuro, J. A. & Lade, P. V. (1997), 'Static liquefaction of very loose sands', *Canadian Geotechnical Journal* **34**, 905–917.

Yamamuro, J. A. & Lade, P. V. (1998), 'Seady state concepts and static liquefaction of silty sands', *Mech. of Cohesive-Frictional Mat.* **124, No. 9**, 868–877.

Yamamuro, J. A. & Lade, P. V. (1999), 'Experiments and modeling of silty sands susceptible to static liquefaction', *Journal of Geotechnical and Geoenvironmental Engineering* **4, No. 6**, 545–877.

Yamamuro, J. A., Wood, F. M. & Lade, P. V. (2008), 'Effect of depositional method on the microstructure of silty sand', *Canadian Geotechnical Journal* **45**, 1538–1555.

Yang, J. (2002), 'Non-uniqueness of flow liquefaction line for loose sand', *Geotechnique* **52, No. 10**, 257–760.

Yang, J. & Sze, H. (2010), 'Failure of saturated sand in non-symmetrical cyclic loading', *5th International Conference on Recent Advances in Geotechnical Earthquake Engineering and Soil Dynamics, San Diego, California* **May 24-29**.

Yang, S. L. (2004), Characterization of the properties of sand-silt mixtures, PhD thesis, Norwegian University of Science and Technology, Norway.

Yang, S. L., Sandven, R. & Grande, L. (2006a), 'Steady-state lines of sand-silt mixtures', *Canadian Geotechnical Journal* **43**, 1213–1219.

Yang, S. L., Sandven, R. & Grande, L. (2006b), 'Instability of sand-silt mixtures', *Soil Dynamics and Earthquake Engineering* **26**, 183–190.

Yang, S., Lacasse, S. & Rolf Sandven, R. (2005), 'Determination of the transitional fines content of mixtures of sand and non-plastic fines', *Geotechnical Testing Journal* **Vol. 29**, No. 2.

Youd, T. L. & Idriss, I. M. (2001), 'Liquefaction resistance of soils: Summary report from the 1996 nceer and 1998 nceer/nsf workshops on evaluation of liquefaction resistance of soils', *Journal of Geotechnical and Geoenvironmental Engineering, ASCE* **Vol. 127, No. 4**, 297–313.

Zhang, H. (1997), Steady state behavior of sands and limitations of the triaxial test, PhD thesis, University of Ottawa, Ontario Canada.

Zlatovic, S. & Ishihara, K. (1995), 'On the influence of nonplastic fines on residul strength', *The First International Conference on Earthquake Geotechnical Engineering/Tokyo* **1**, 239–244.

Zuo, L. & Baudet, A. (2015), 'Determination of the transitional fines content of sand-nonplastic fines mixtures', *Soils and Foundations* **55,No. 1**, 213–219.

A. Triaxial Test Results on Hostun Sand-Silt Mixtures

Appendix A

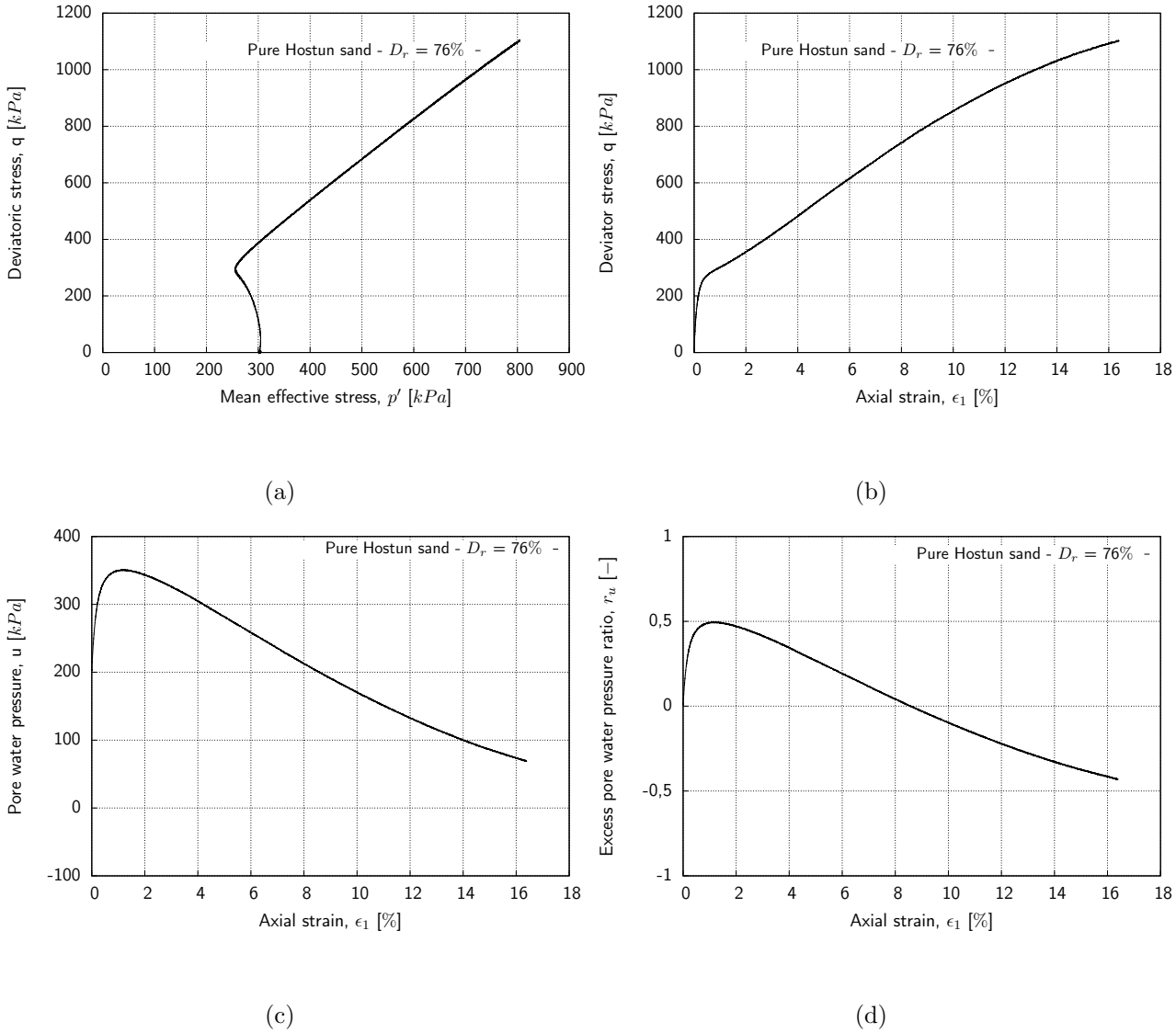

Figure A.1.: Undrained behavior of pure Hostun sand, Sample CU01-00-300: (a) stress path; (b) stress strain behavior; (c) pore pressure variation vs. axial strain; (d) excess pore water pressure ratio vs. axial strain

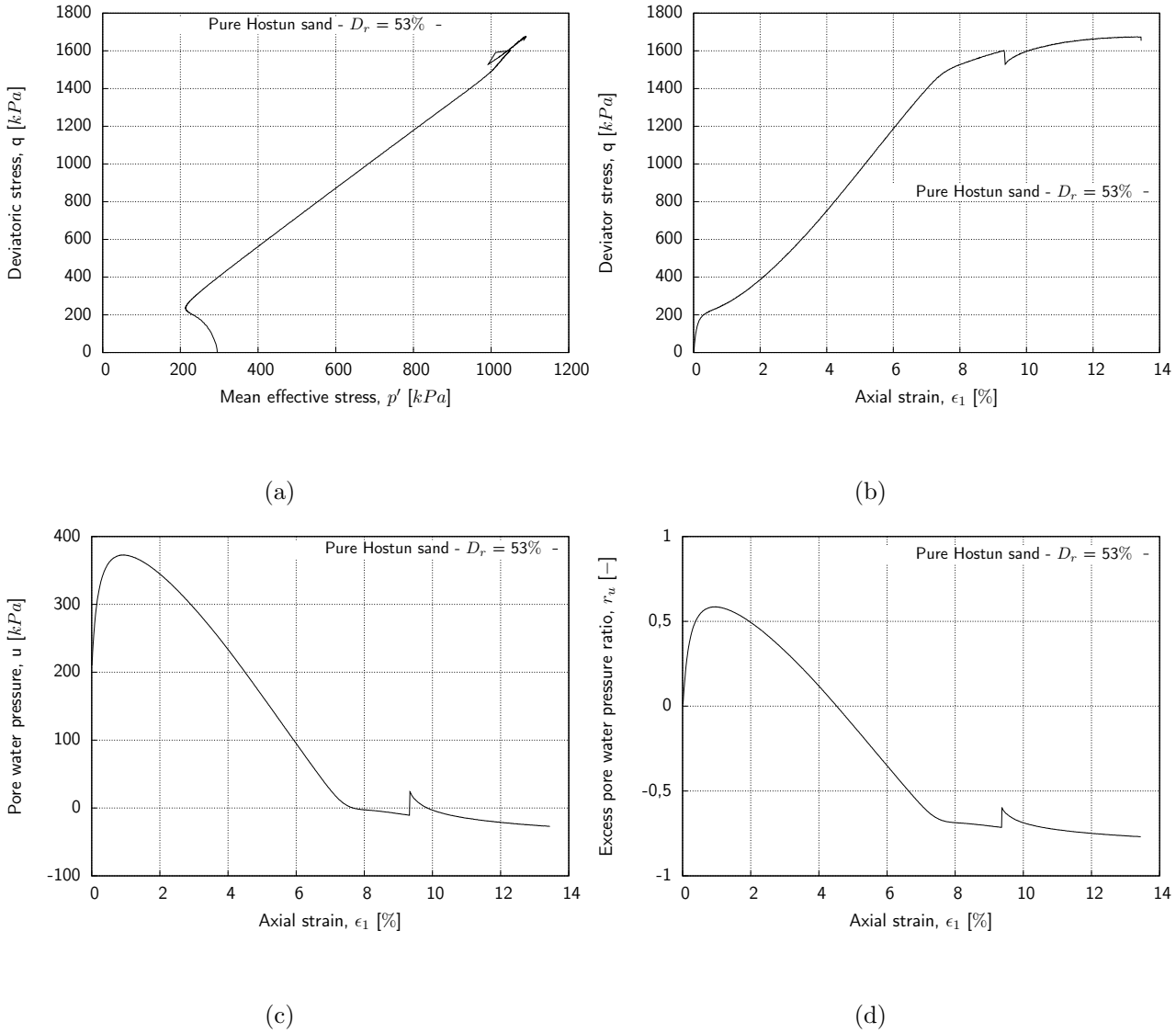

Figure A.2.: Undrained behavior of pure Hostun sand, Sample CU02-00-300: (a) stress path; (b) stress strain behavior; (c) pore pressure variation vs. axial strain; (d) excess pore water pressure ratio vs. axial strain

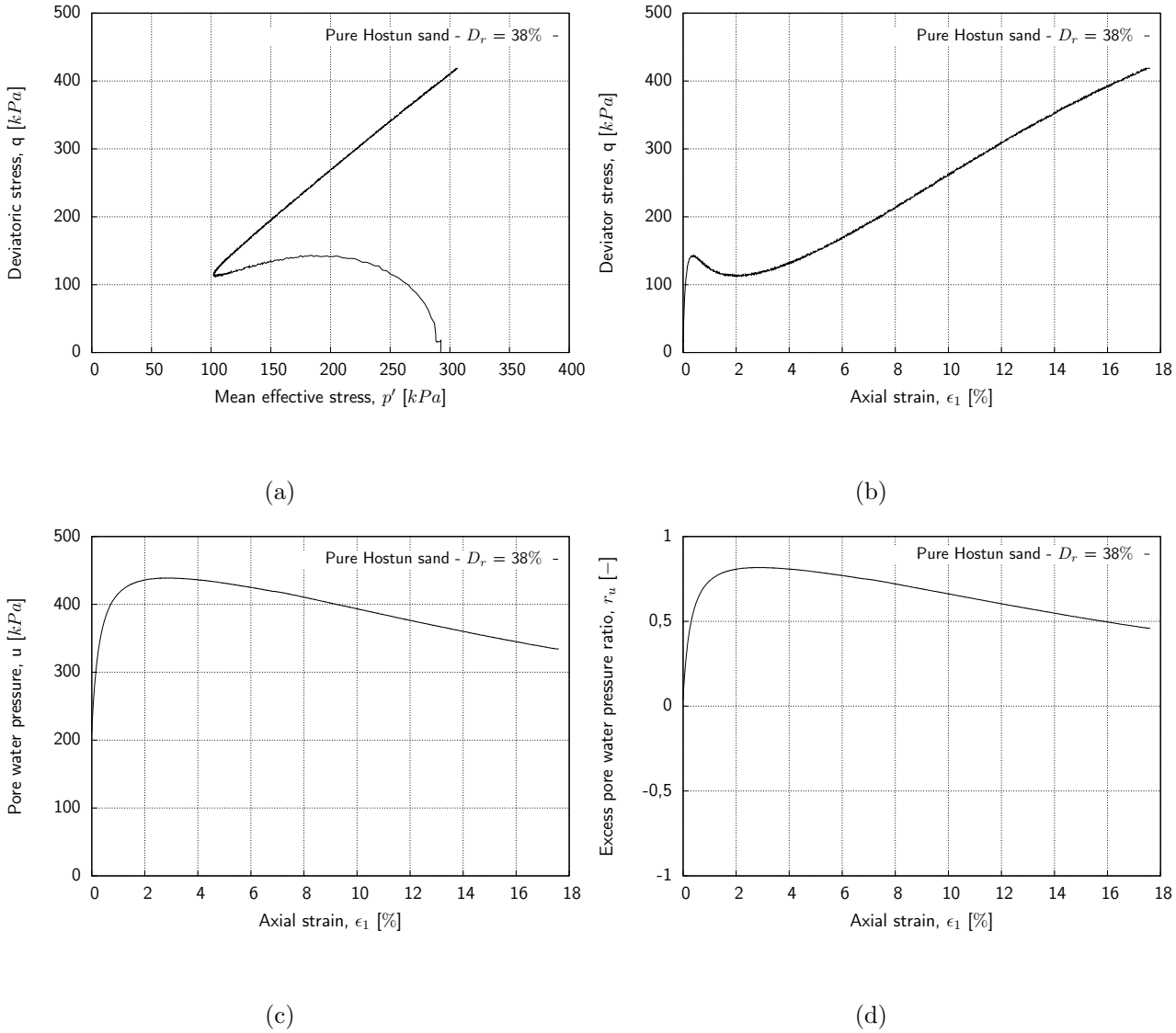

Figure A.3.: Undrained behavior of pure Hostun sand, Sample CU08-00-300: (a) stress path; (b) stress strain behavior; (c) pore pressure variation vs. axial strain; (d) excess pore water pressure ratio vs. axial strain

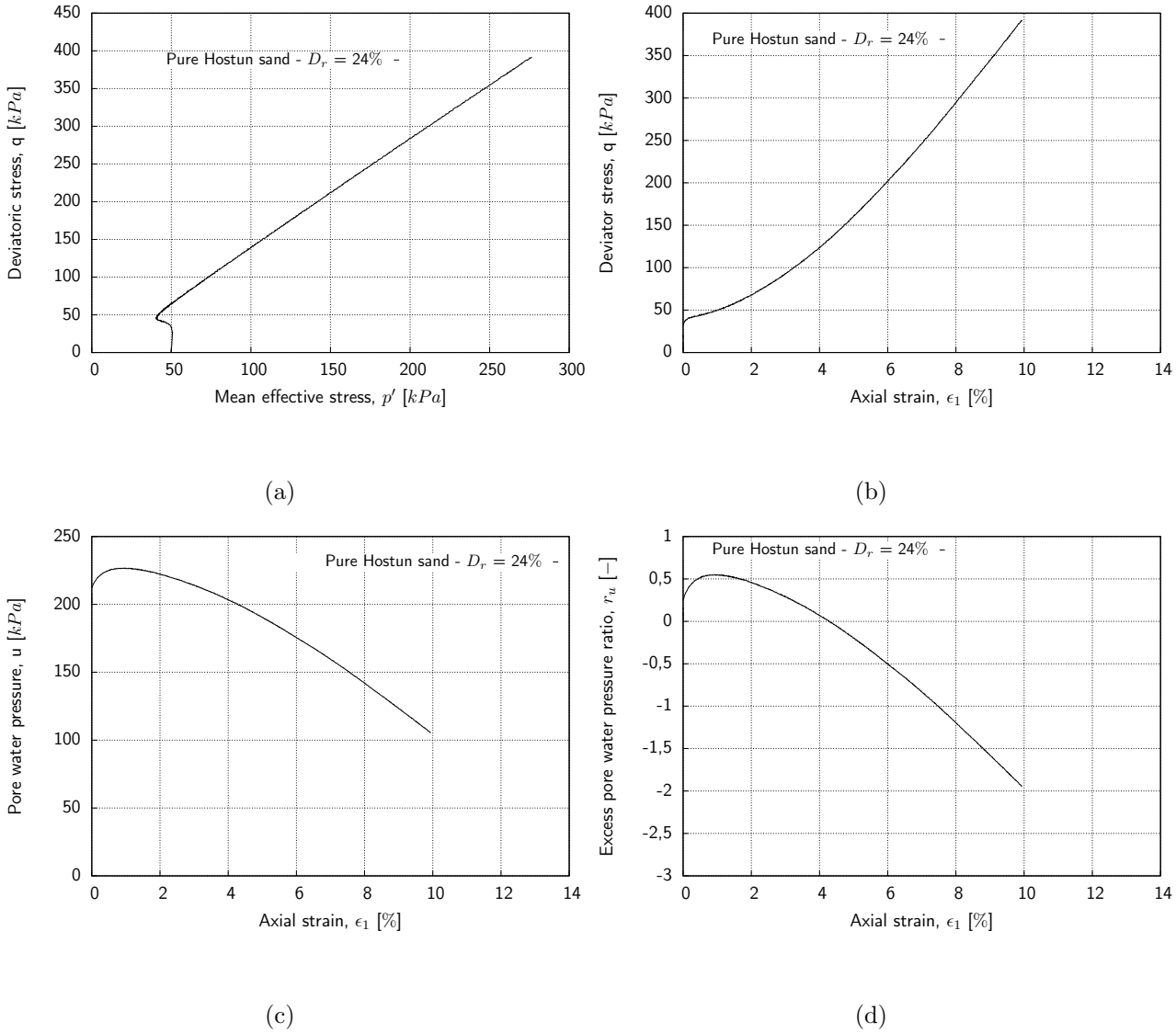

Figure A.4.: Undrained behavior of pure Hostun sand, Sample CU09-00-50: (a) stress path; (b) stress strain behavior; (c) pore pressure variation vs. axial strain; (d) excess pore water pressure ratio vs. axial strain

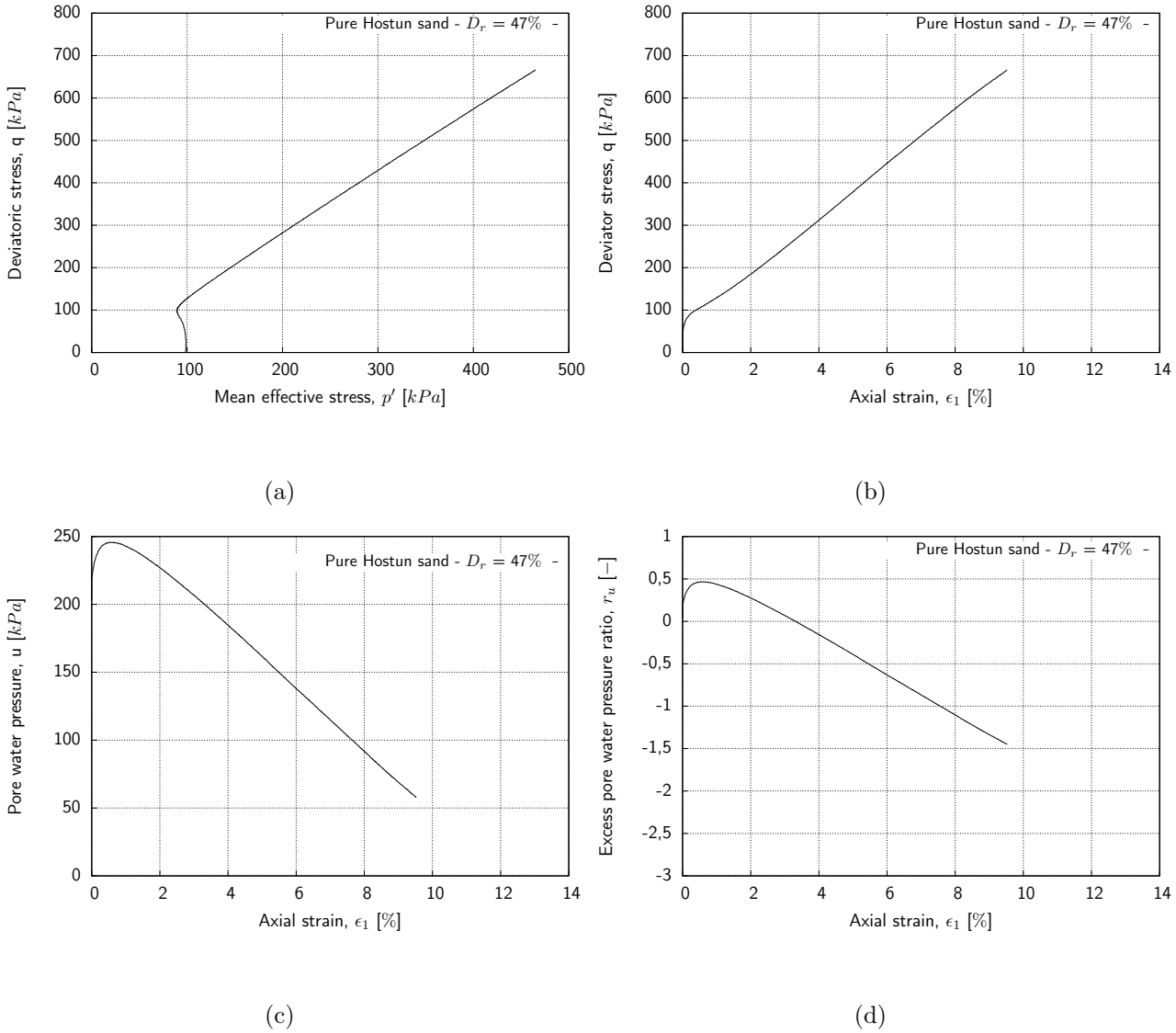

Figure A.5.: Undrained behavior of pure Hostun sand, Sample CU10-00-100: (a) stress path; (b) stress strain behavior; (c) pore pressure variation vs. axial strain; (d) excess pore water pressure ratio vs. axial strain

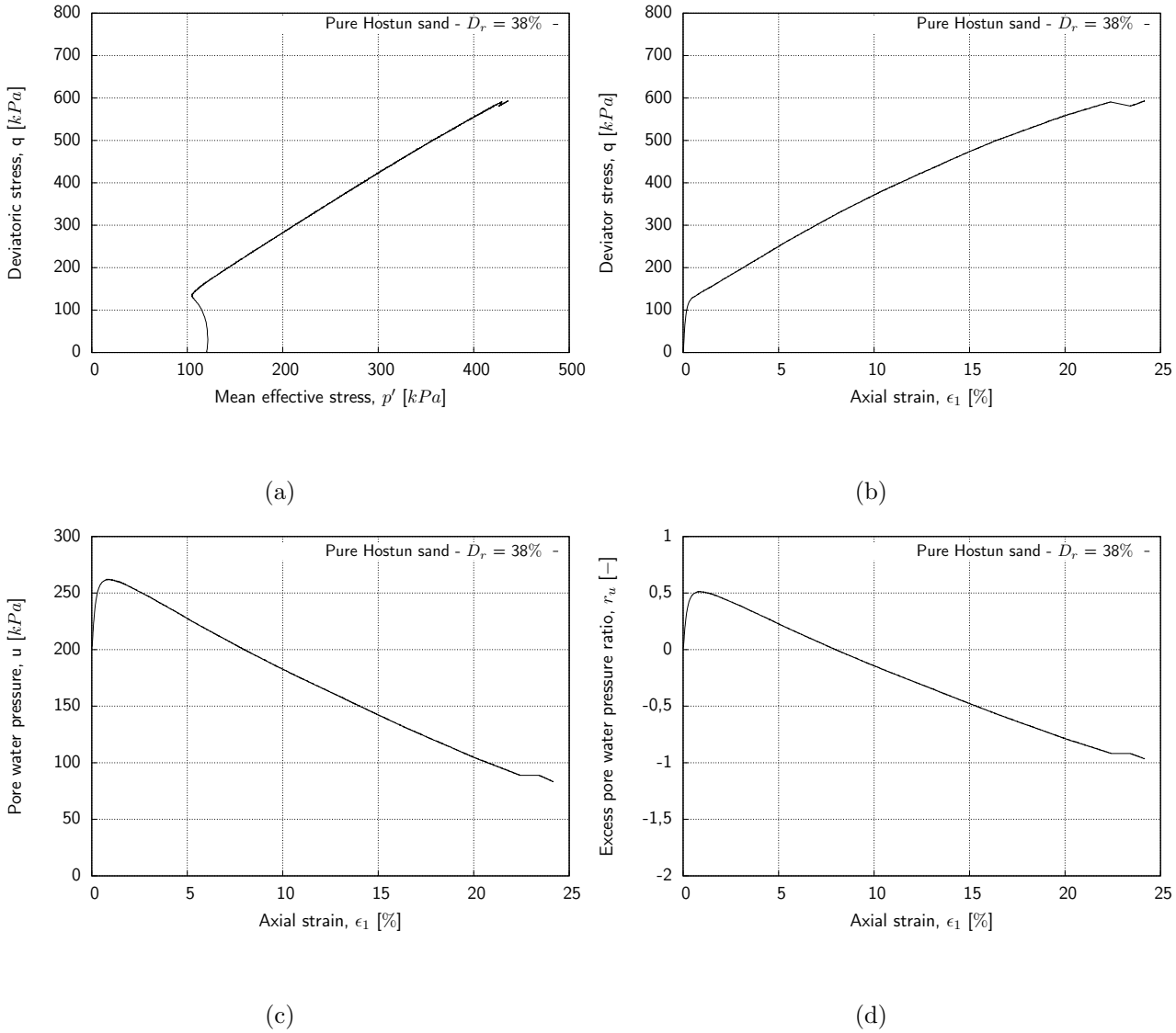

Figure A.6.: Undrained behavior of pure Hostun sand, Sample CU11-00-120: (a) stress path; (b) stress strain behavior; (c) pore pressure variation vs. axial strain; (d) excess pore water pressure ratio vs. axial strain

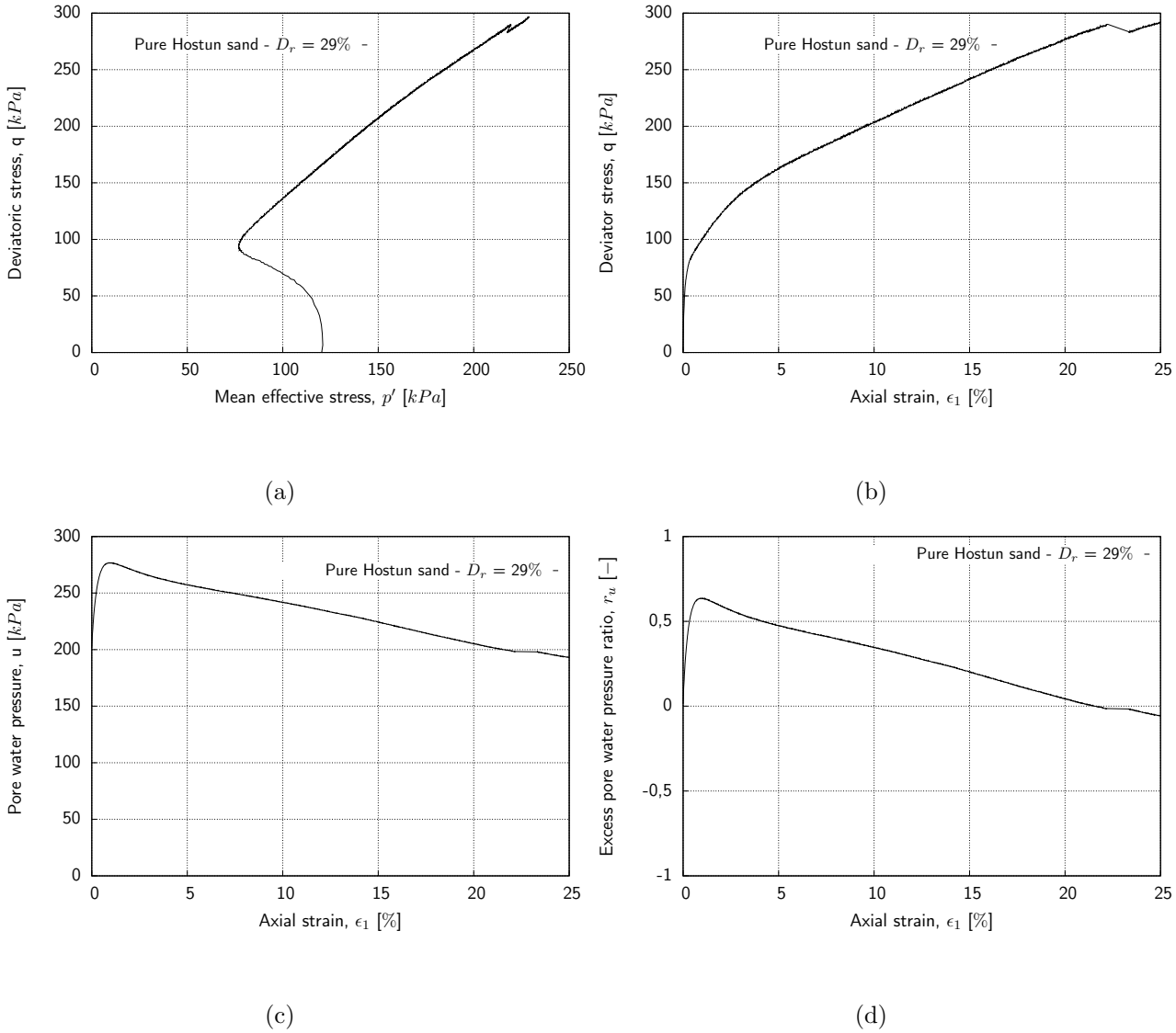

Figure A.7.: Undrained behavior of pure Hostun sand, Sample CU12-00-120: (a) stress path; (b) stress strain behavior; (c) pore pressure variation vs. axial strain; (d) excess pore water pressure ratio vs. axial strain

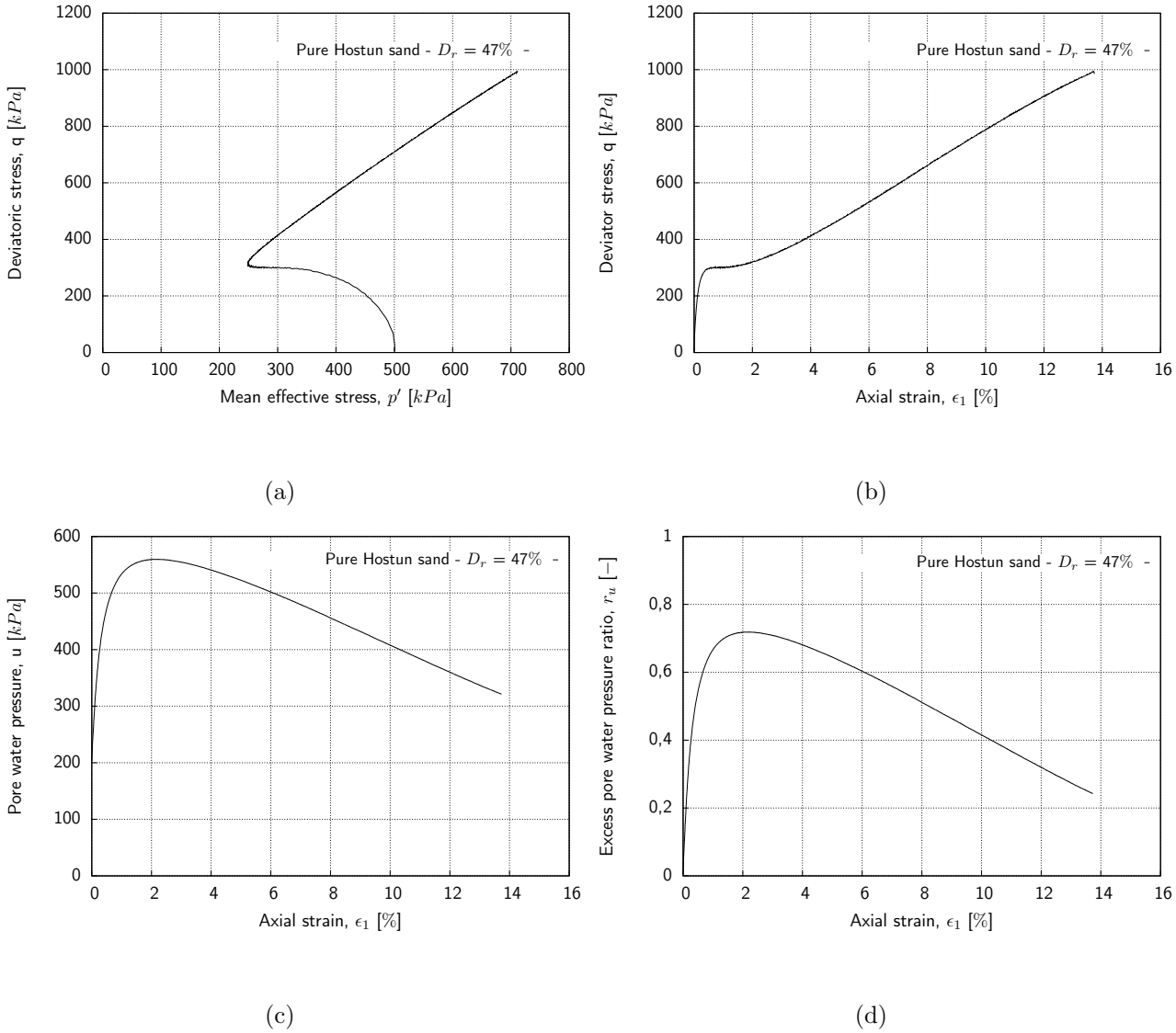

(a) (b)

(c) (d)

Figure A.8.: Undrained behavior of pure Hostun sand, Sample CU15-00-500: (a) stress path; (b) stress strain behavior; (c) pore pressure variation vs. axial strain; (d) excess pore water pressure ratio vs. axial strain

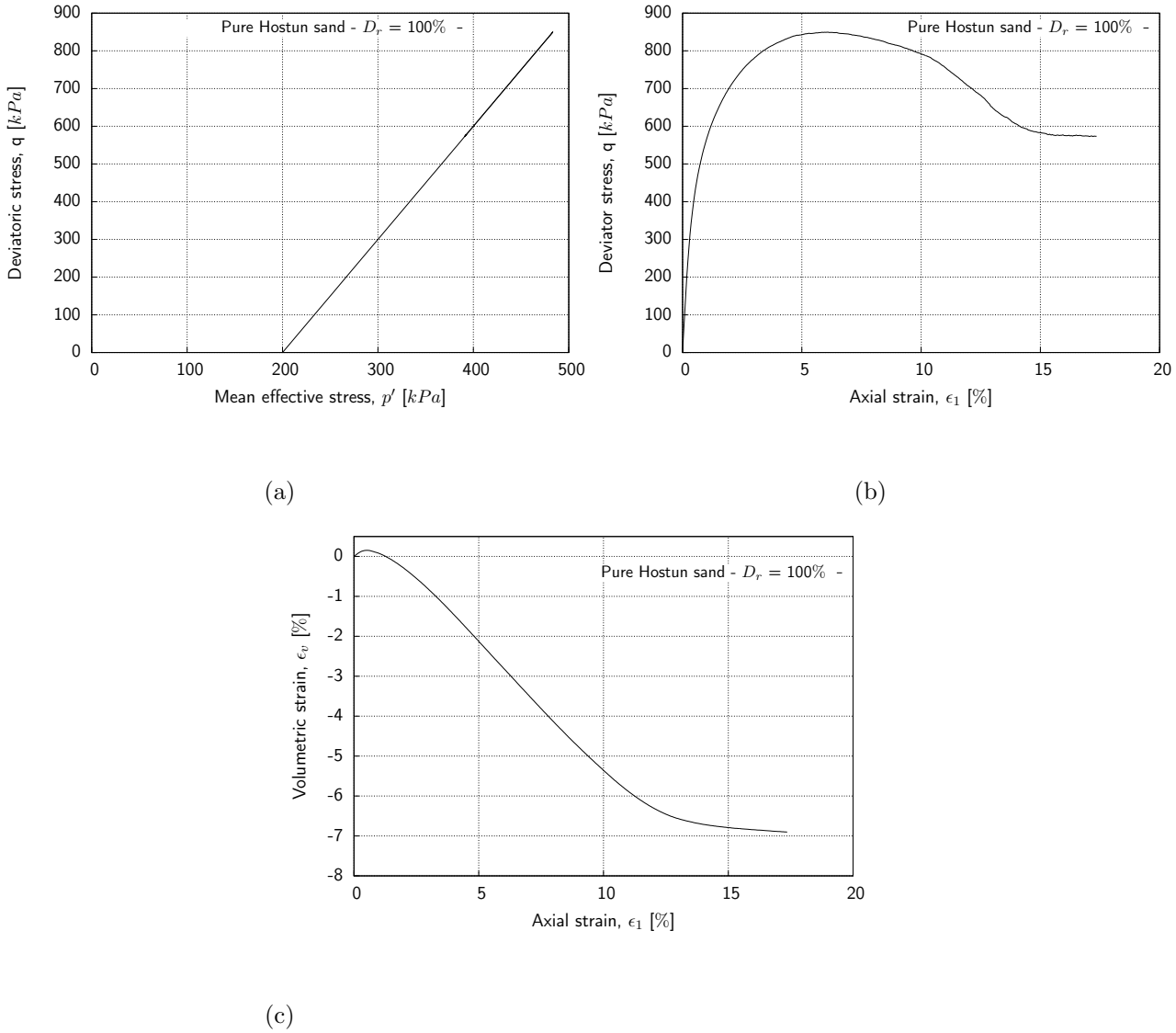

Figure A.9.: Drained behavior of pure Hostun sand, Sample CD19-00-200: (a) stress path; (b) stress strain behavior; (c) volumetric strain vs. axial strain

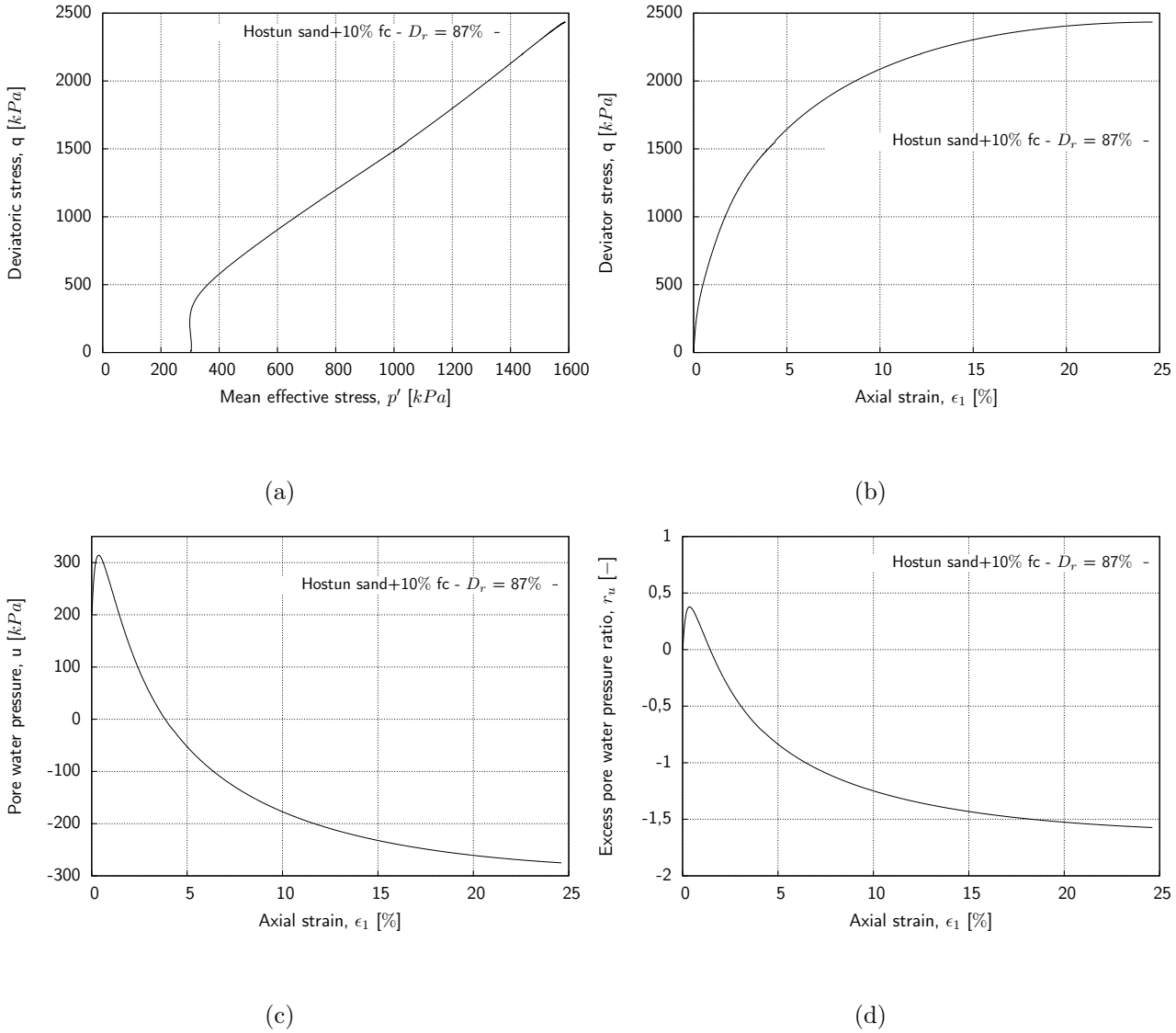

Figure A.10.: Undrained behavior of Hostun sand with 10% silt, Sample CU23-10-300: (a) stress path; (b) stress strain behavior; (c) pore pressure variation vs. axial strain; (d) excess pore water pressure ratio vs. axial strain

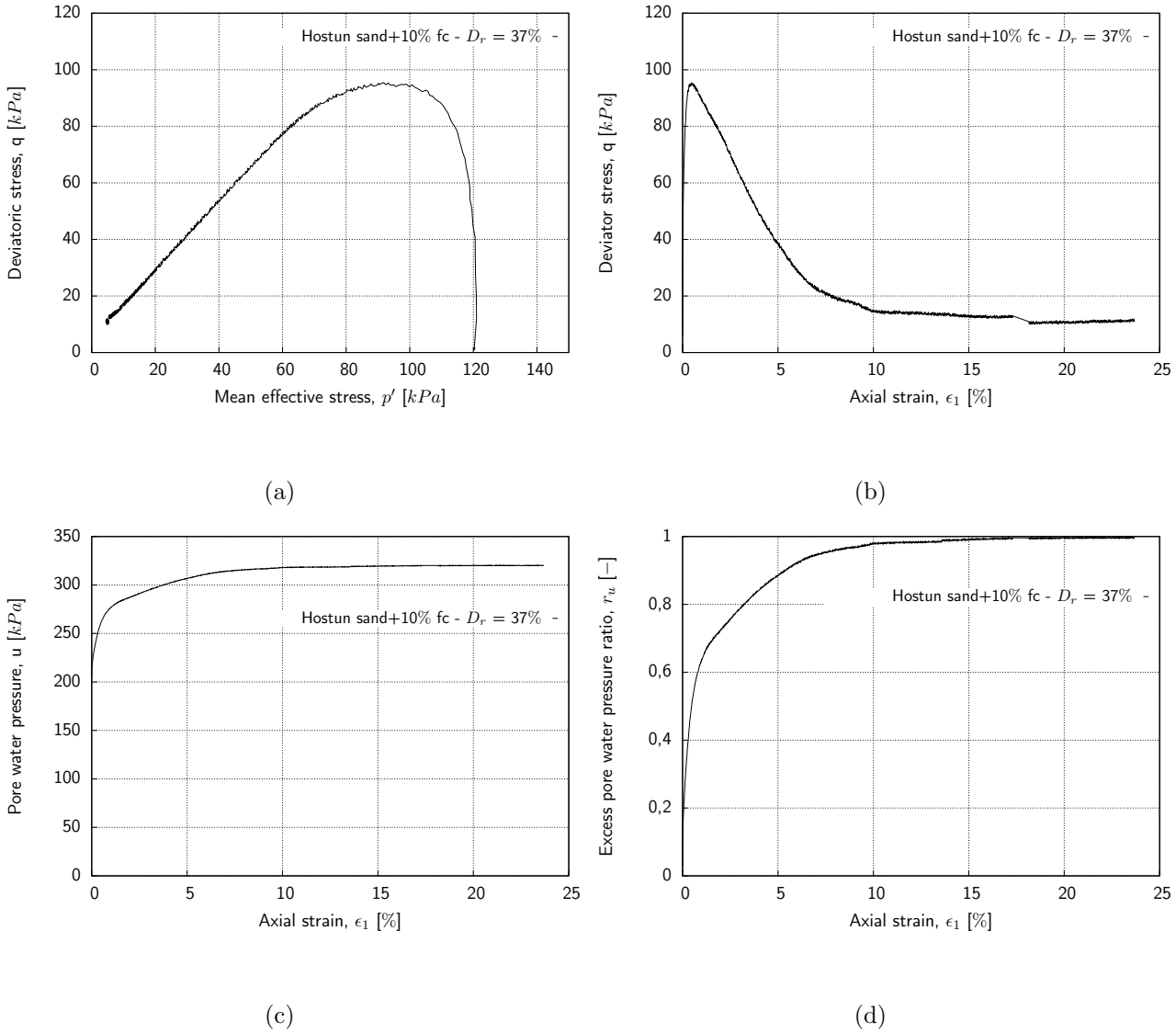

Figure A.11.: Undrained behavior of Hostun sand with 10% silt, Sample CU26-10-120: (a) stress path; (b) stress strain behavior; (c) pore pressure variation vs. axial strain; (d) excess pore water pressure ratio vs. axial strain

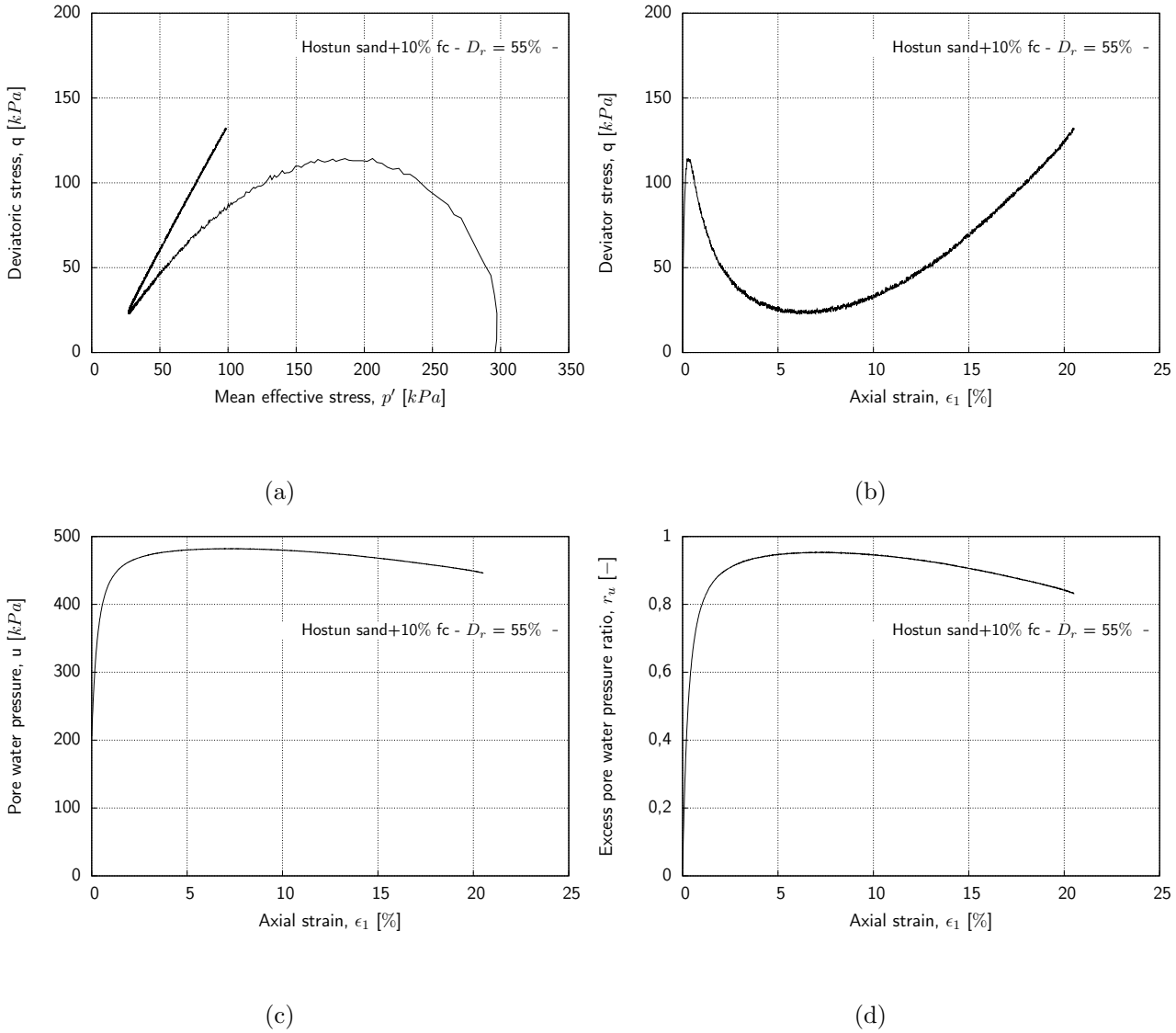

(a) (b)

(c) (d)

Figure A.12.: Undrained behavior of Hostun sand with 10% silt, Sample CU27-10-300: (a) stress path; (b) stress strain behavior; (c) pore pressure variation vs. axial strain; (d) excess pore water pressure ratio vs. axial strain

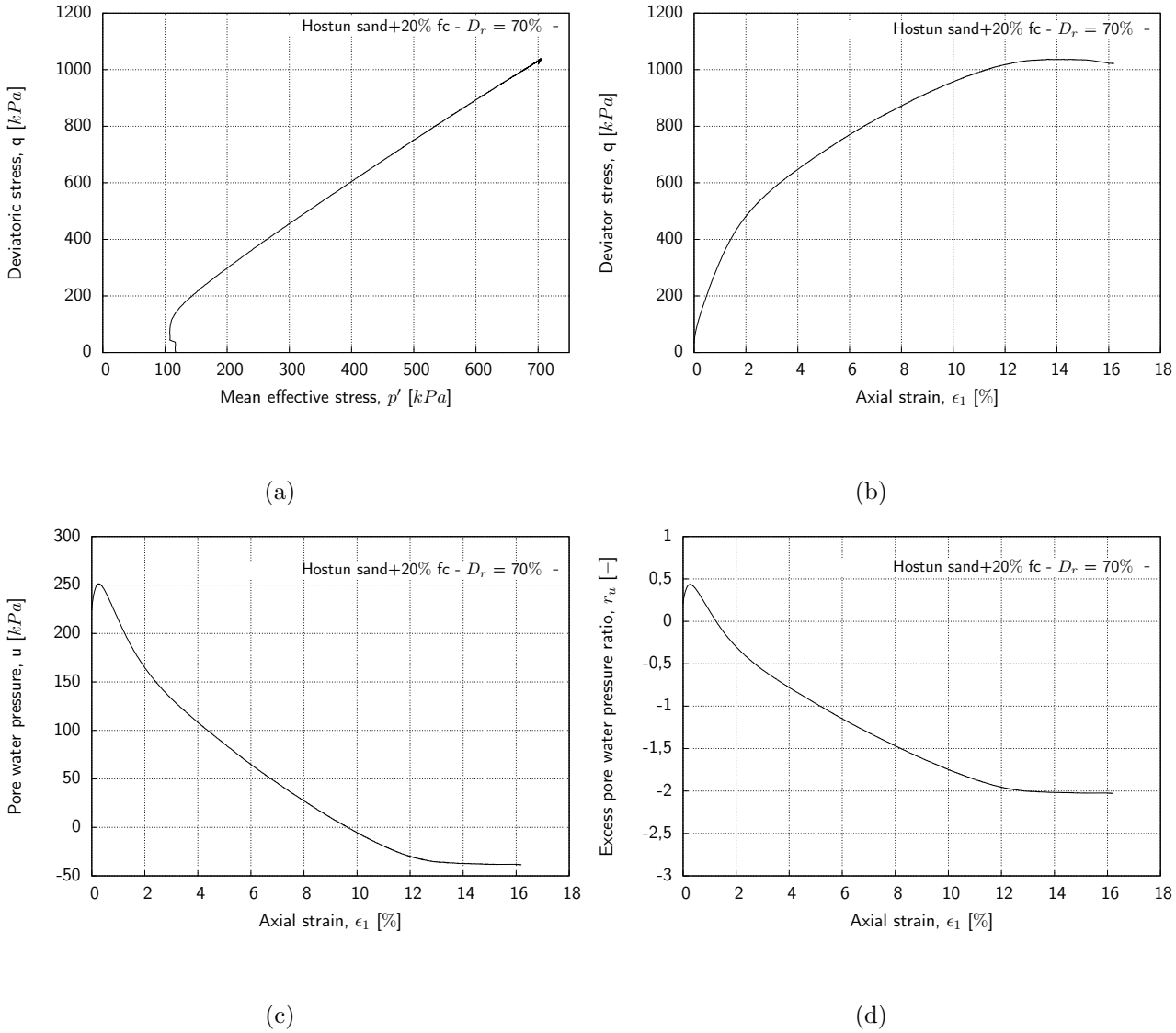

Figure A.13.: Undrained behavior of Hostun sand with 20% silt, Sample CU29-20-120: (a) stress path; (b) stress strain behavior; (c) pore pressure variation vs. axial strain; (d) excess pore water pressure ratio vs. axial strain

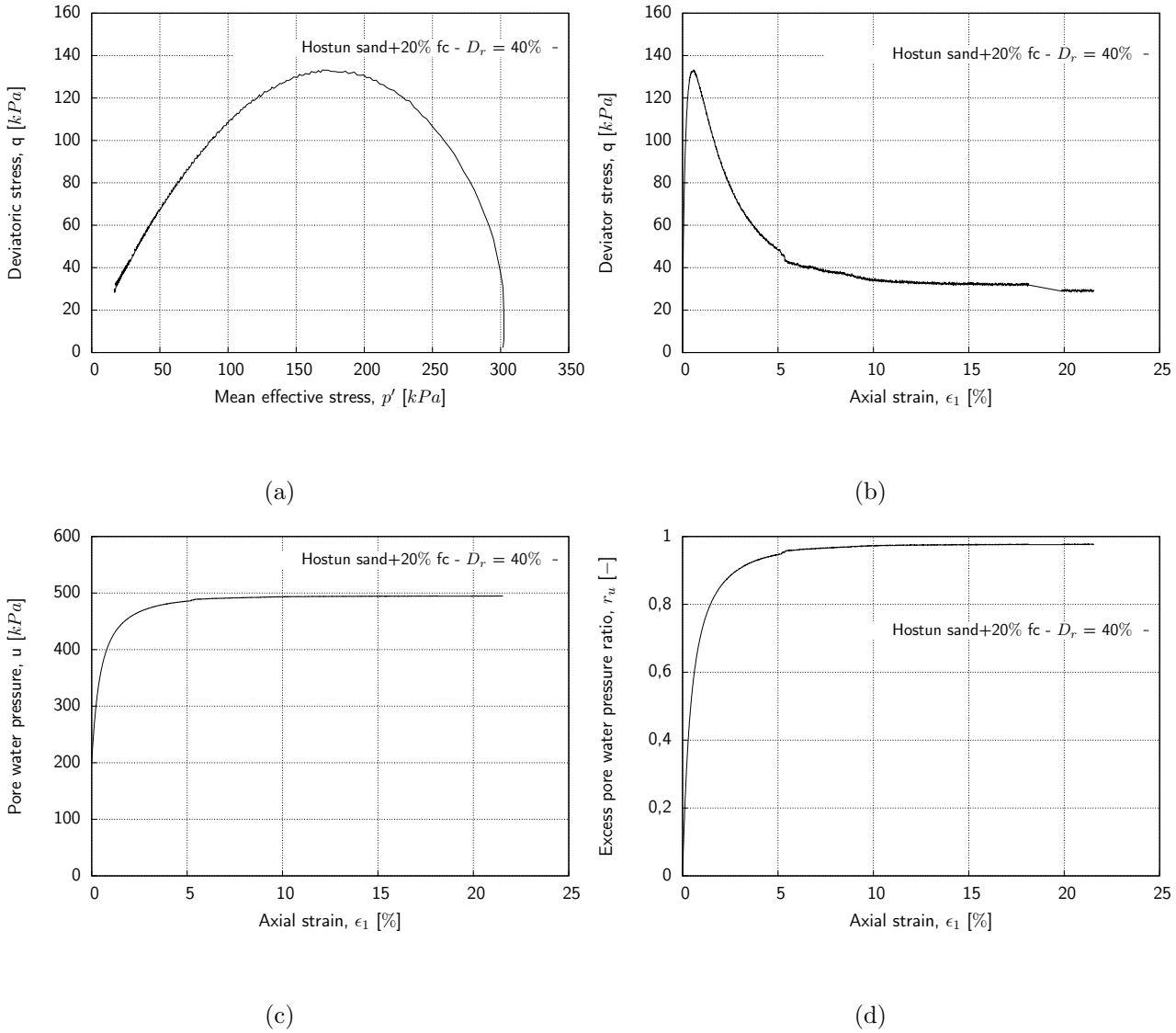

(a) (b)

(c) (d)

Figure A.14.: Undrained behavior of Hostun sand with 20% silt, Sample CU31-20-300: (a) stress path; (b) stress strain behavior; (c) pore pressure variation vs. axial strain; (d) excess pore water pressure ratio vs. axial strain

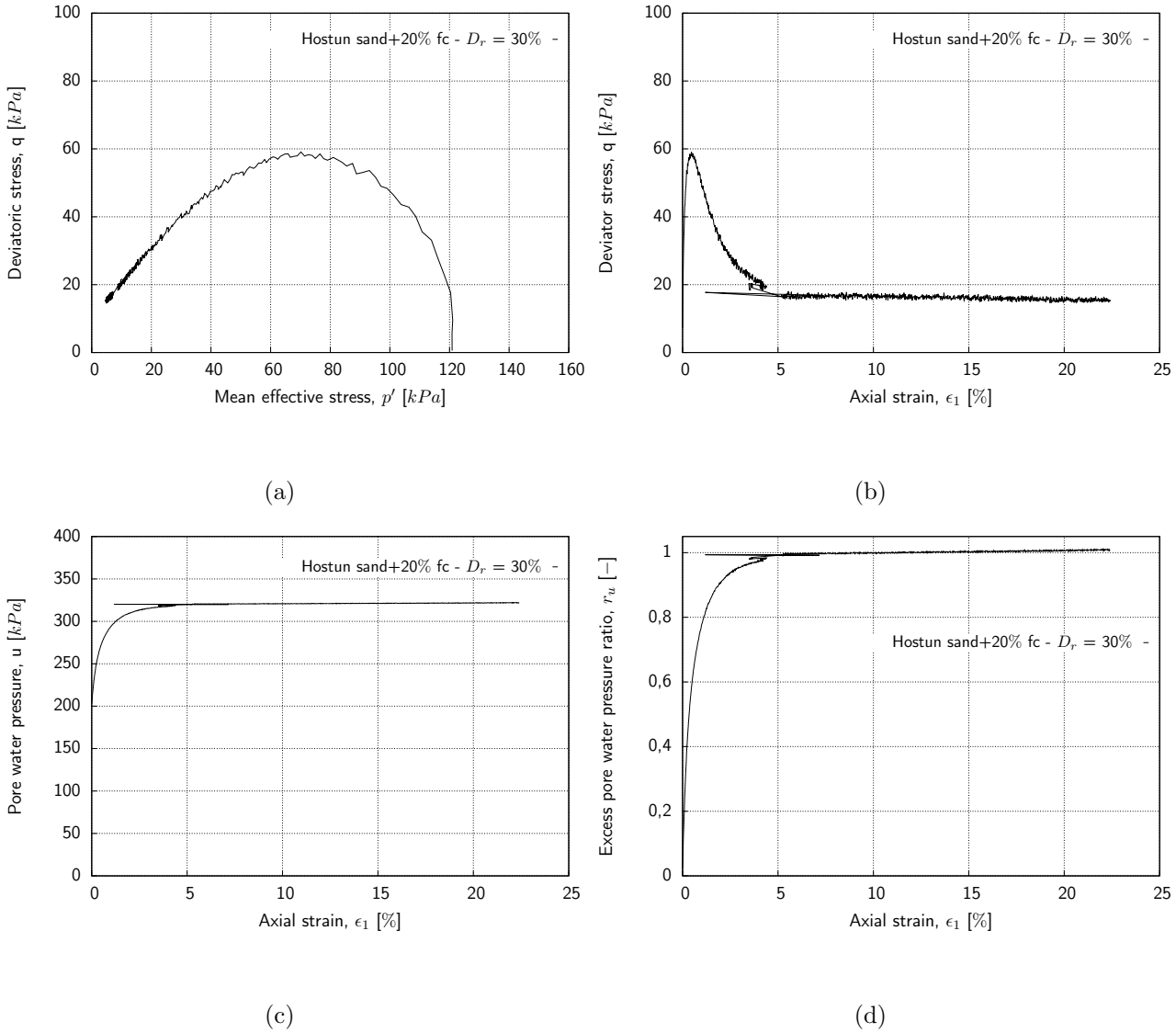

Figure A.15.: Undrained behavior of Hostun sand with 20% silt, Sample CU32-20-120: (a) stress path; (b) stress strain behavior; (c) pore pressure variation vs. axial strain; (d) excess pore water pressure ratio vs. axial strain

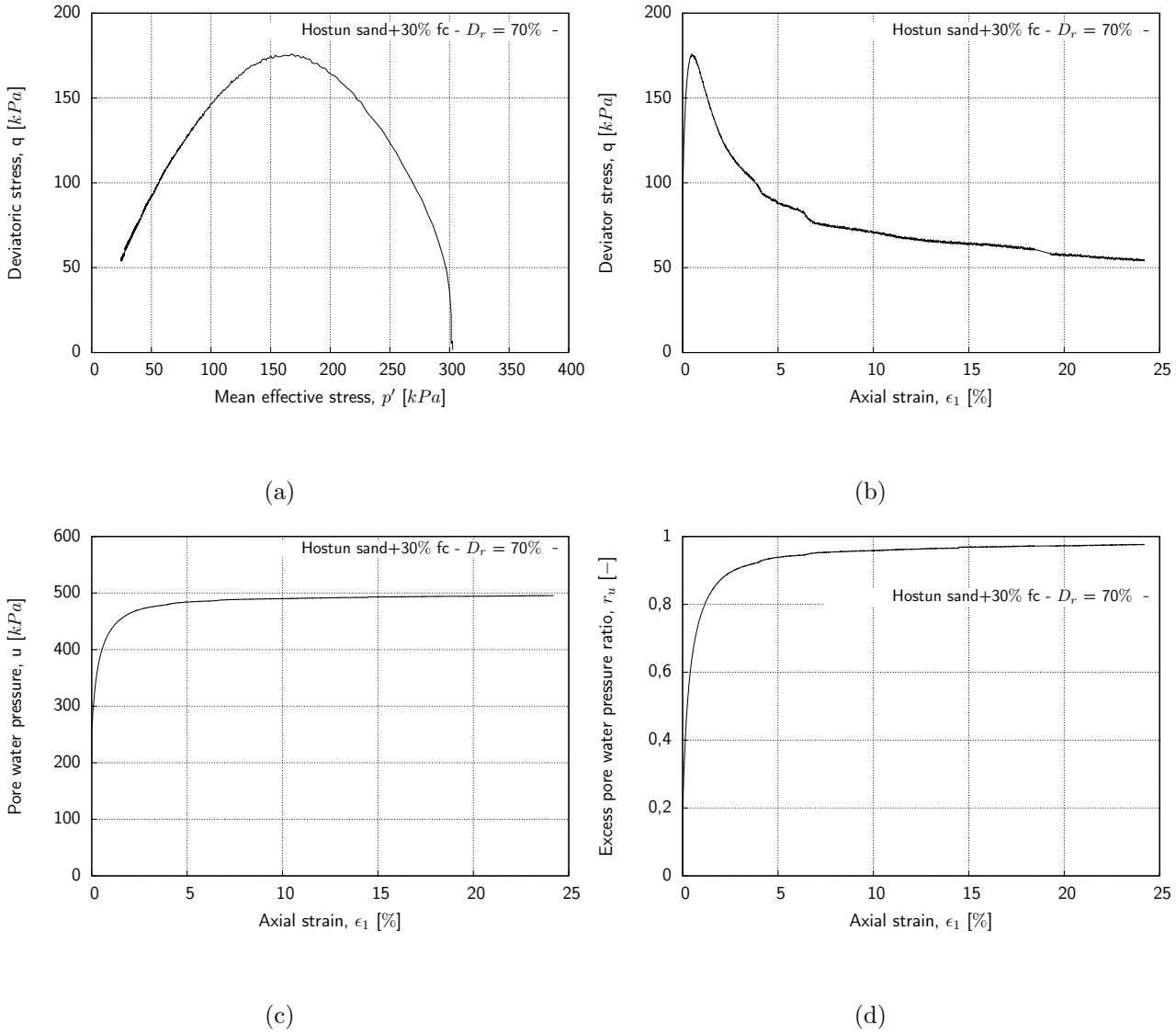

Figure A.16.: Undrained behavior of Hostun sand with 30% silt, Sample CU35-30-300: (a) stress path; (b) stress strain behavior; (c) pore pressure variation vs. axial strain; (d) excess pore water pressure ratio vs. axial strain

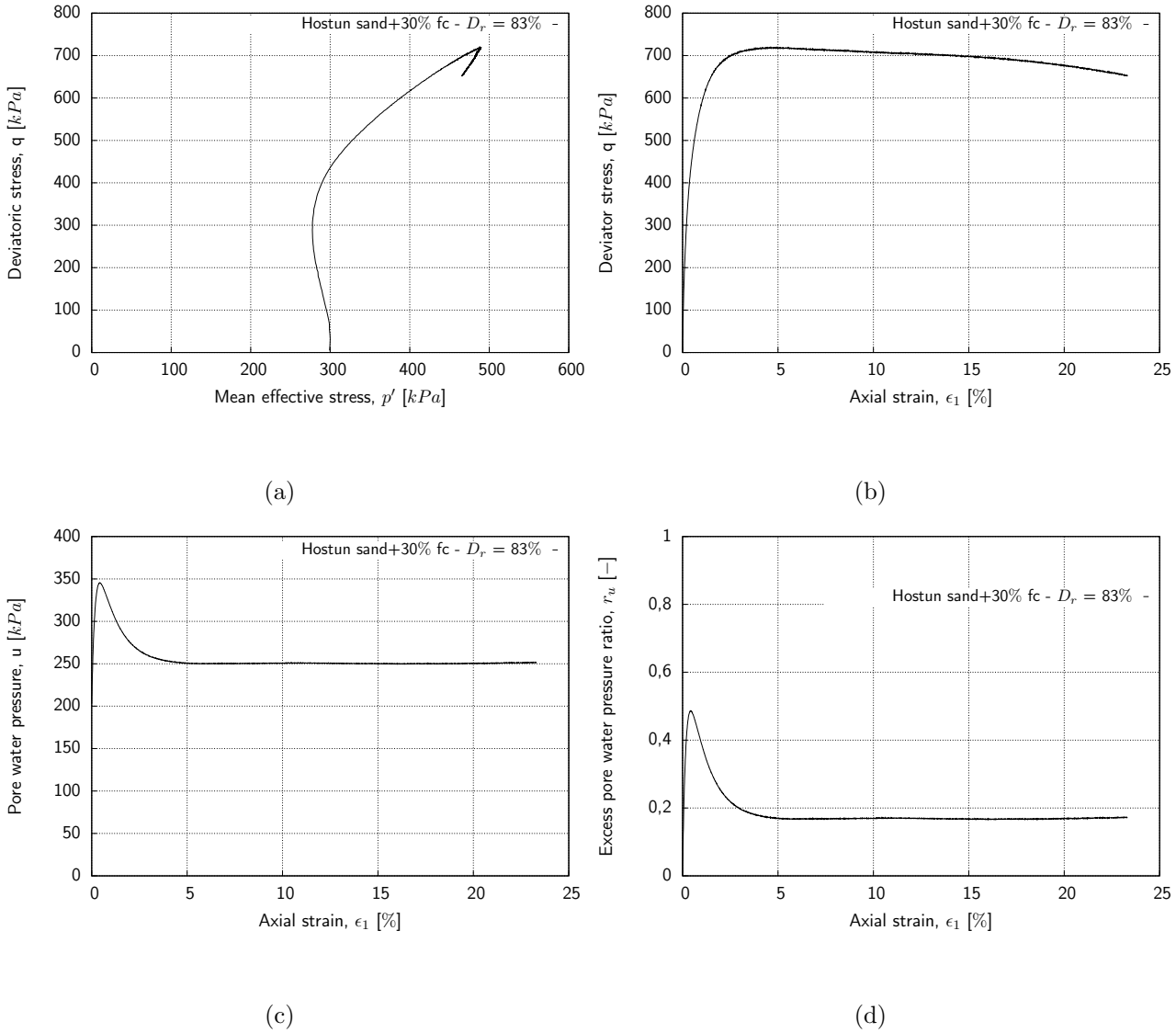

(a) (b)

(c) (d)

Figure A.17.: Undrained behavior of Hostun sand with 30% silt, Sample CU37-30-300: (a) stress path; (b) stress strain behavior; (c) pore pressure variation vs. axial strain; (d) excess pore water pressure ratio vs. axial strain

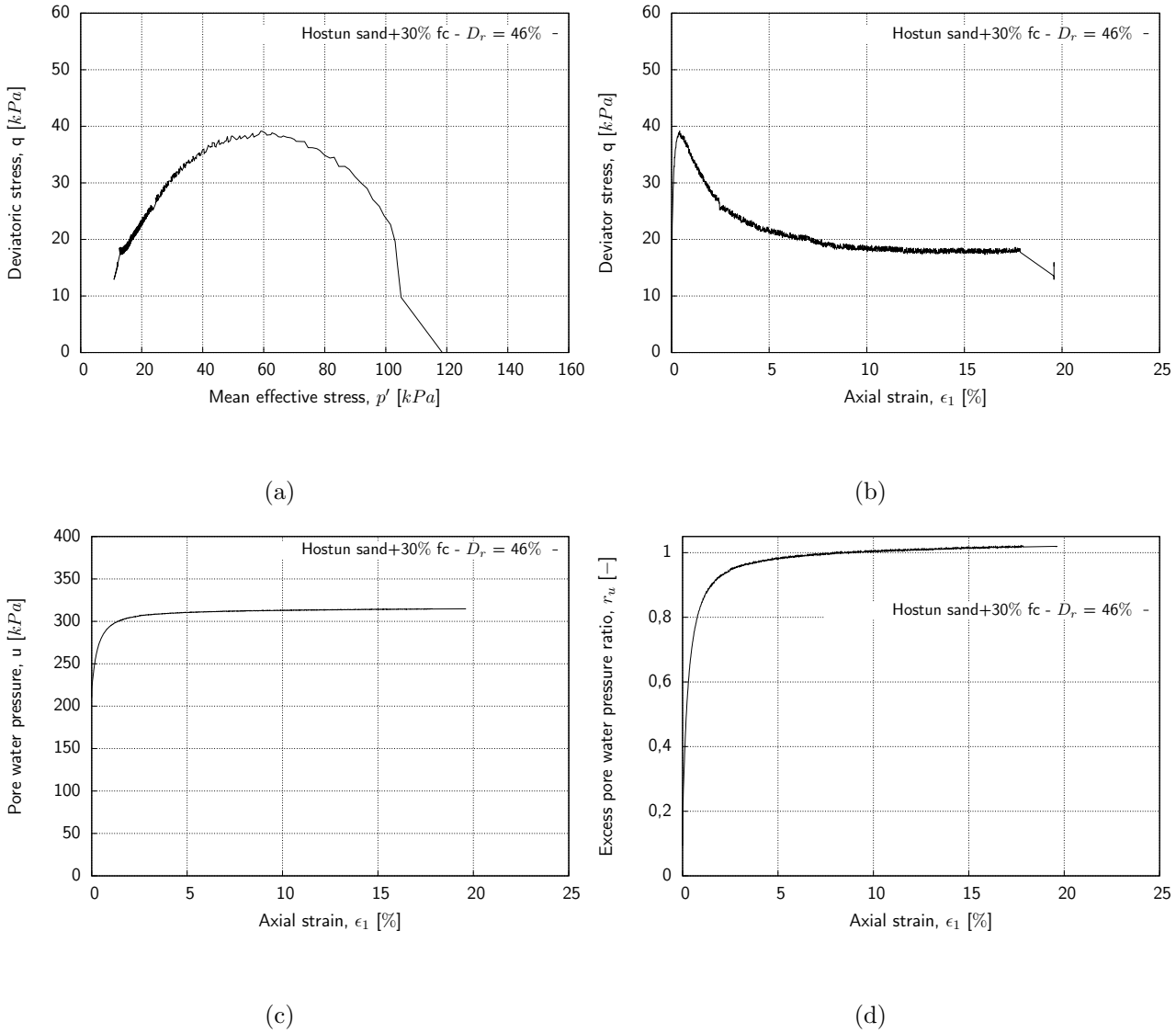

Figure A.18.: Undrained behavior of Hostun sand with 30% silt, Sample CU38-30-120: (a) stress path; (b) stress strain behavior; (c) pore pressure variation vs. axial strain; (d) excess pore water pressure ratio vs. axial strain

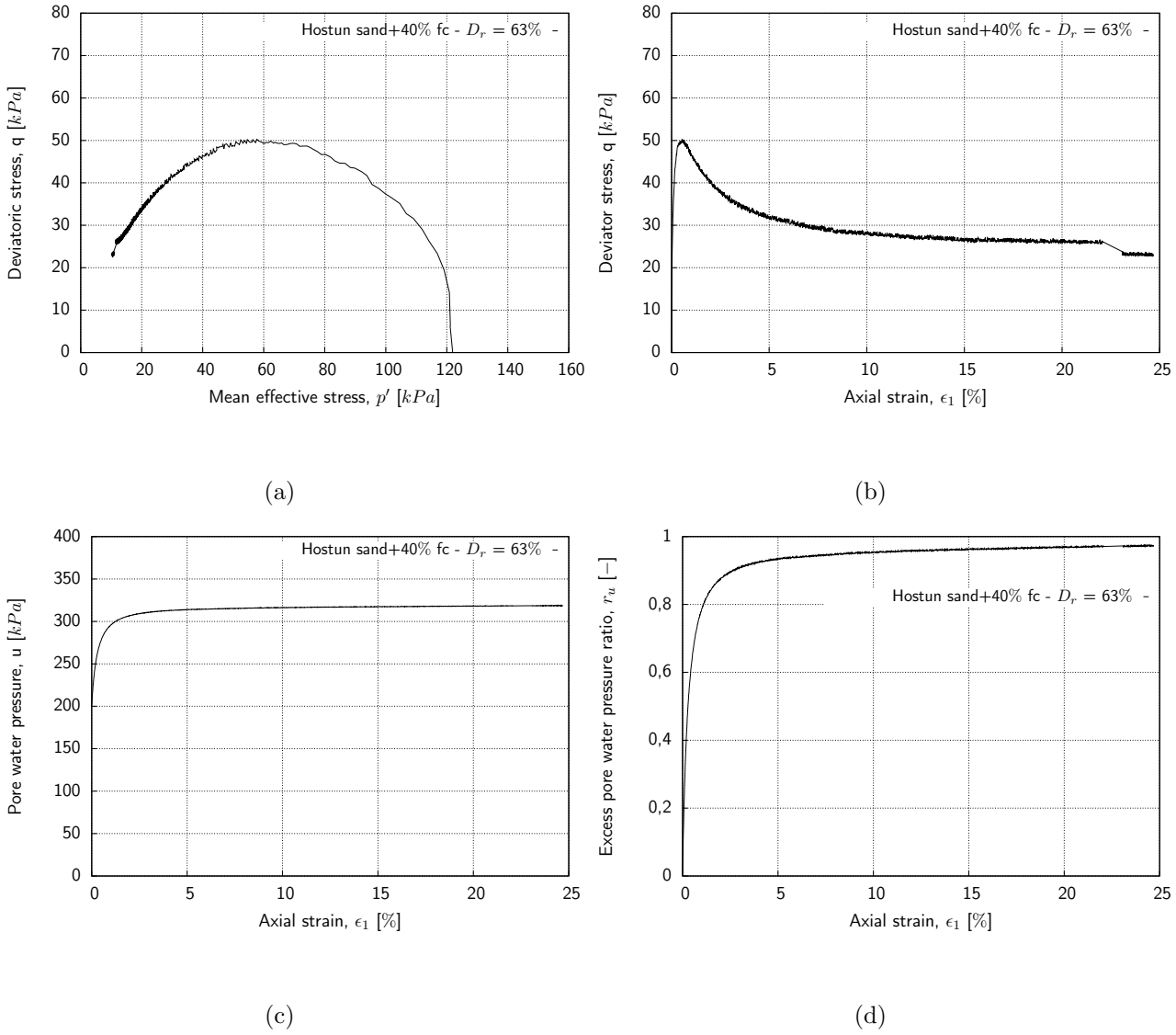

Figure A.19.: Undrained behavior of Hostun sand with 40% silt, Sample CU43-40-120: (a) stress path; (b) stress strain behavior; (c) pore pressure variation vs. axial strain; (d) excess pore water pressure ratio vs. axial strain

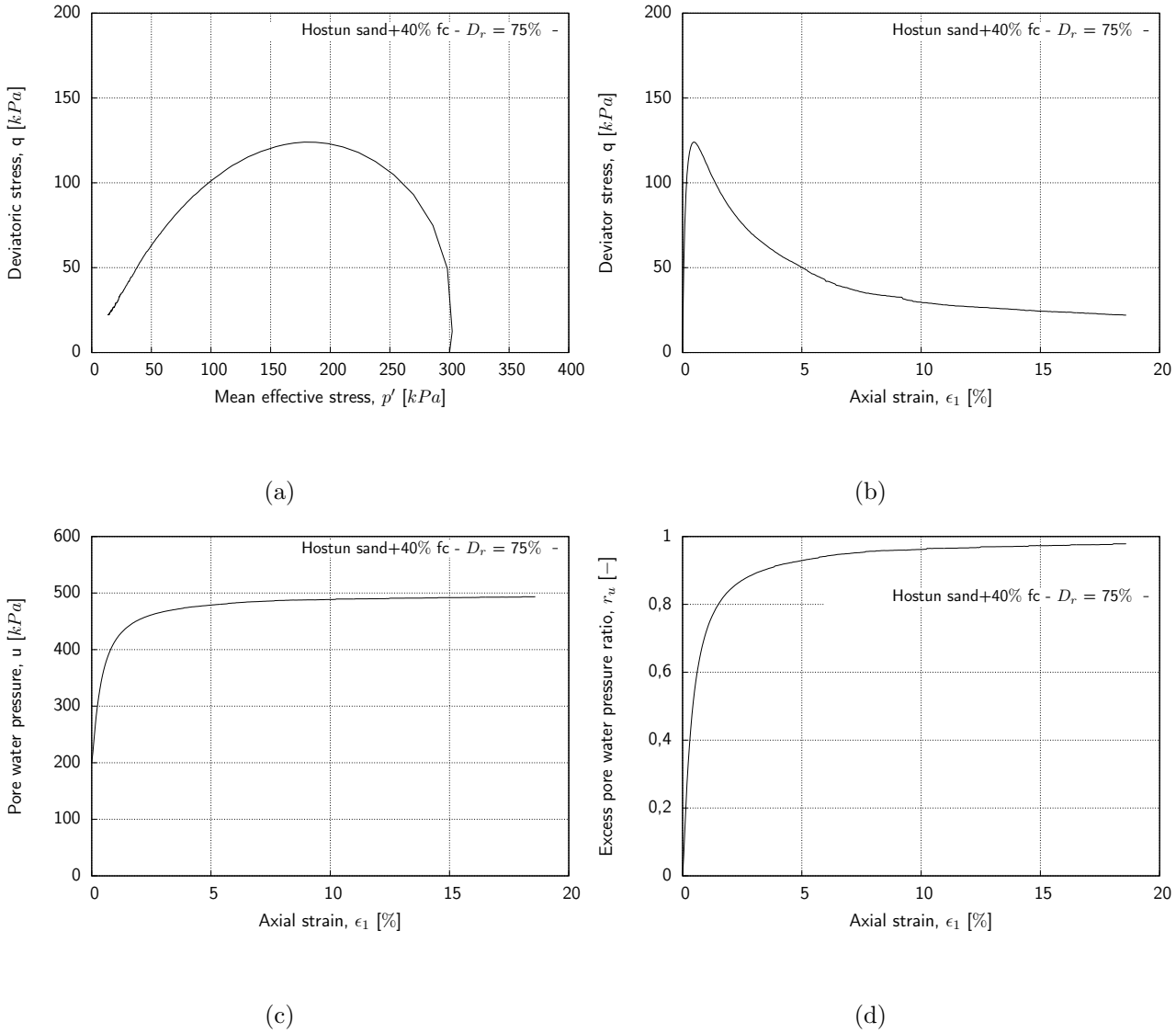

(a) (b)

(c) (d)

Figure A.20.: Undrained behavior of Hostun sand with 40% silt, Sample CU46-40-300: (a) stress path; (b) stress strain behavior; (c) pore pressure variation vs. axial strain; (d) excess pore water pressure ratio vs. axial strain

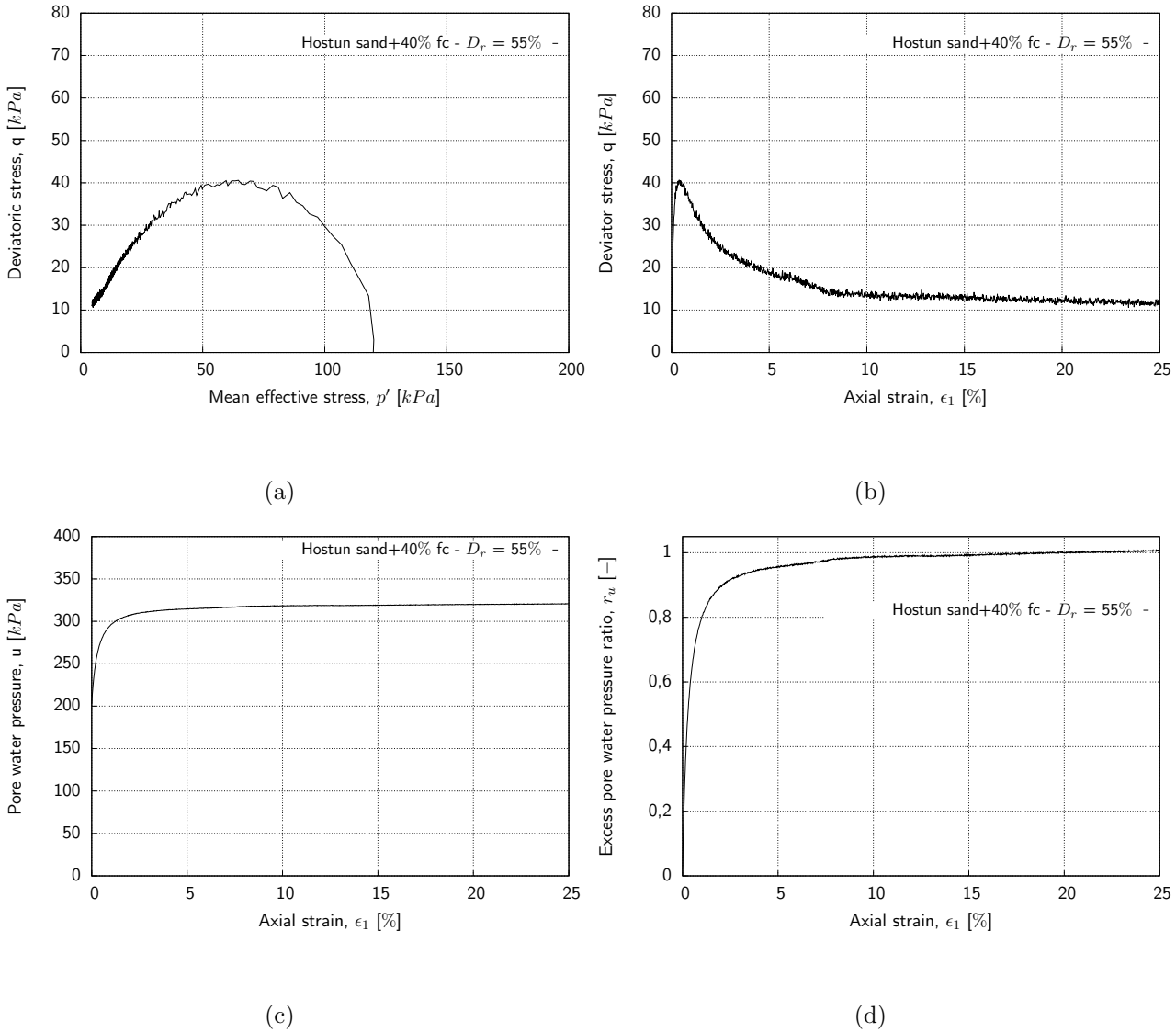

Figure A.21.: Undrained behavior of Hostun sand with 40% silt, Sample CU48-40-120: (a) stress path; (b) stress strain behavior; (c) pore pressure variation vs. axial strain; (d) excess pore water pressure ratio vs. axial strain

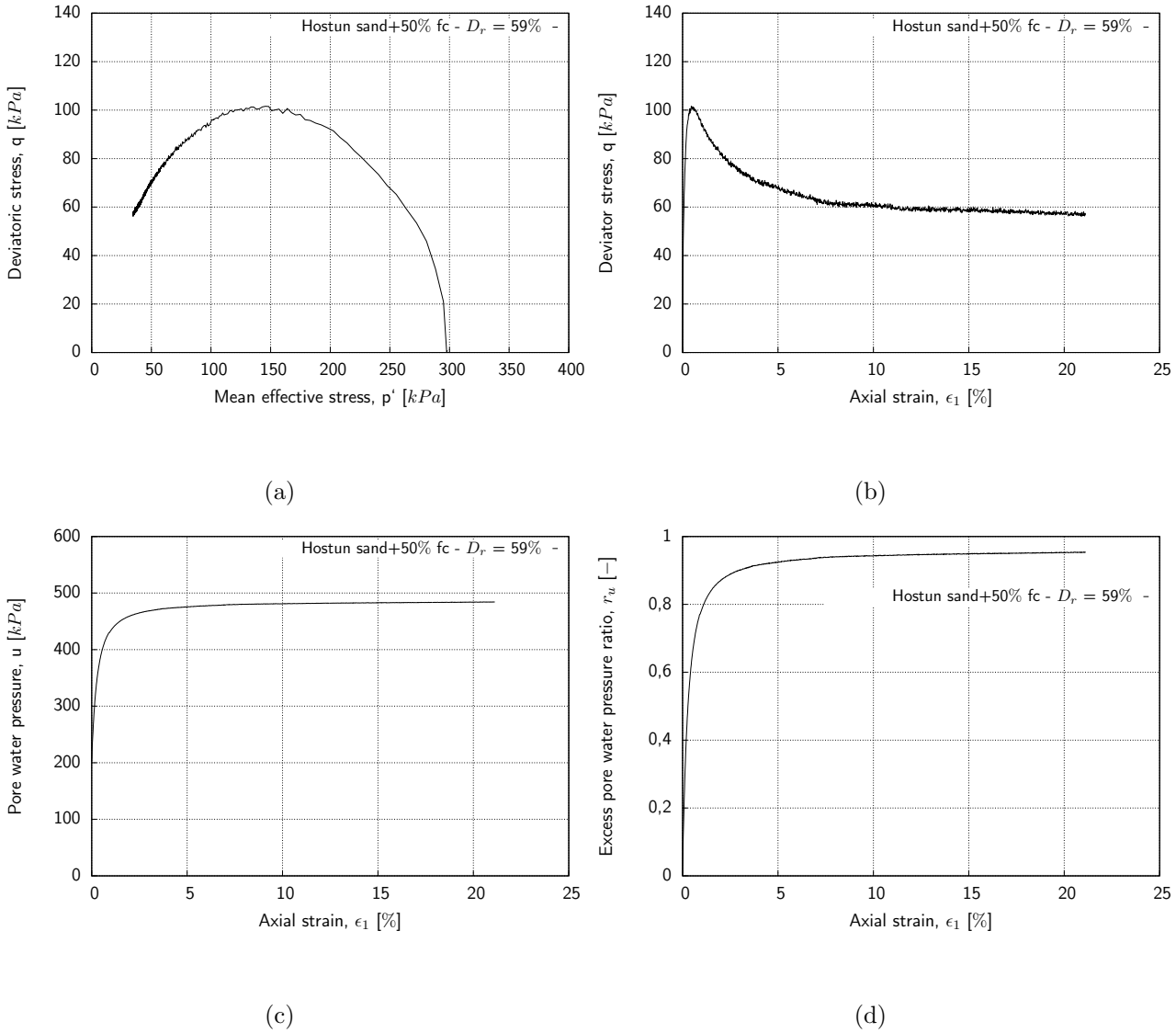

(a) (b)

(c) (d)

Figure A.22.: Undrained behavior of Hostun sand with 50% silt, Sample CU51-50-300: (a) stress path; (b) stress strain behavior; (c) pore pressure variation vs. axial strain; (d) excess pore water pressure ratio vs. axial strain

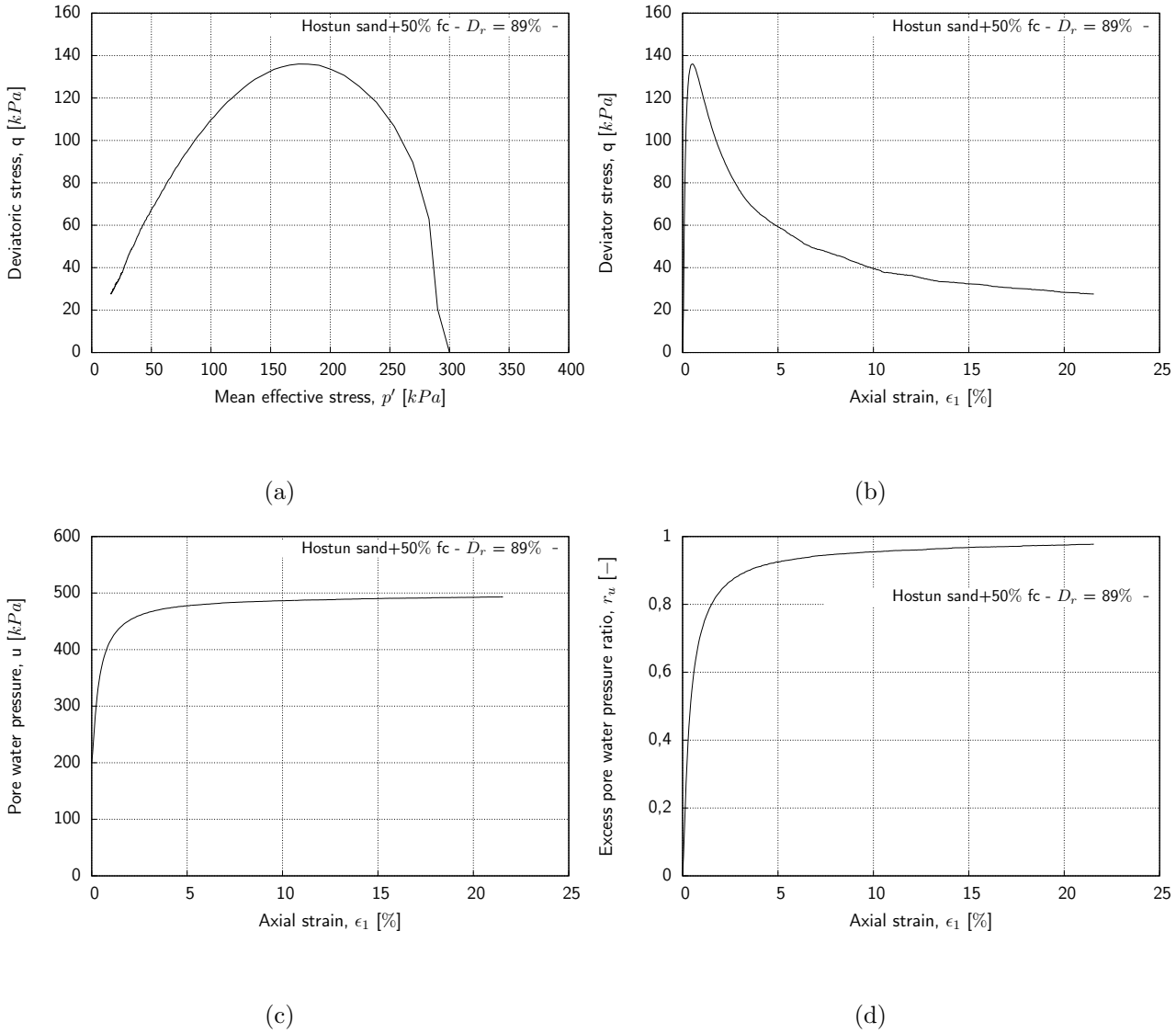

(a) (b)

(c) (d)

Figure A.23.: Undrained behavior of Hostun sand with 50% silt, Sample CU53-50-300: (a) stress path; (b) stress strain behavior; (c) pore pressure variation vs. axial strain; (d) excess pore water pressure ratio vs. axial strain

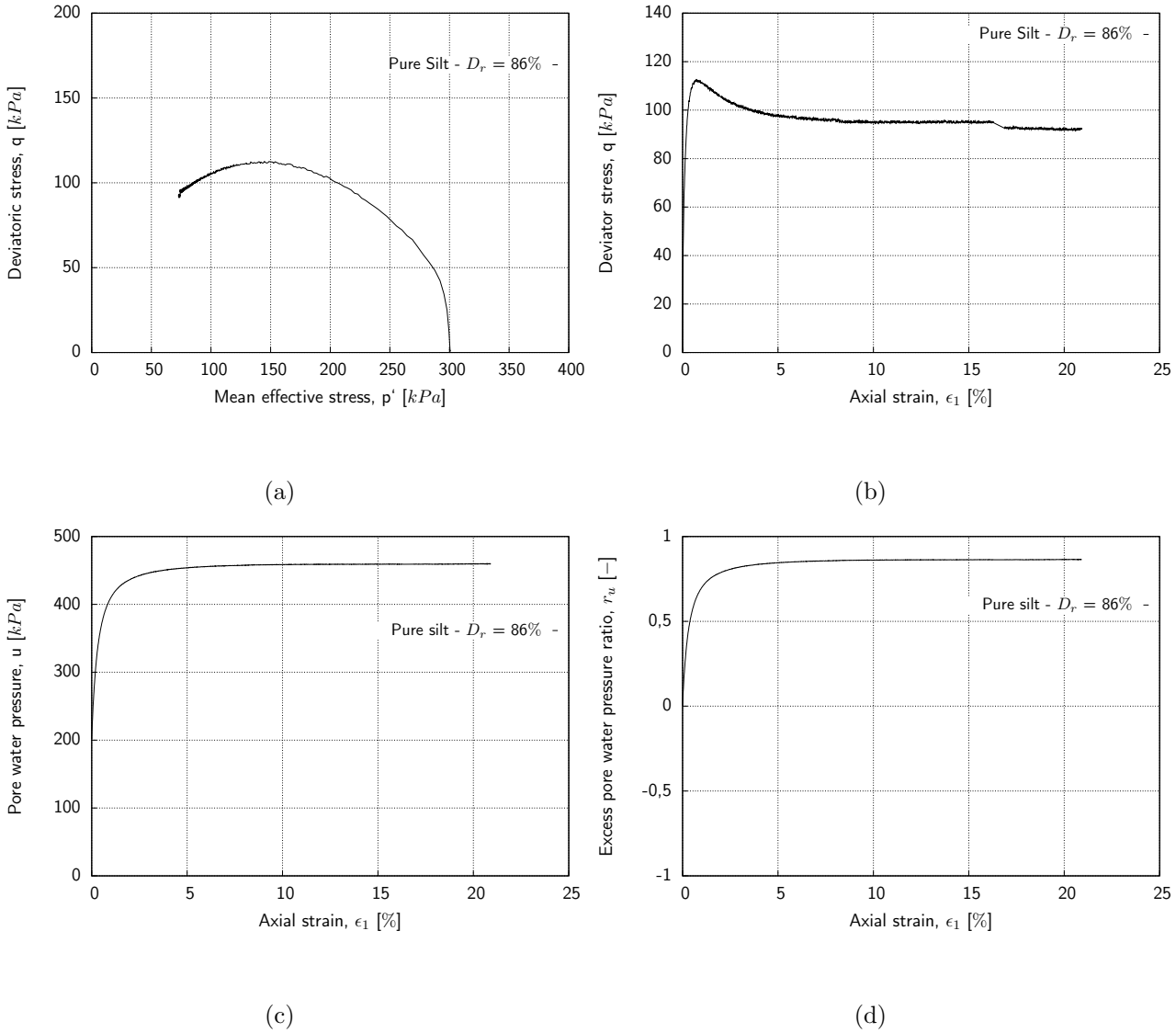

Figure A.24.: Undrained behavior of pure silt, Sample CU58-100-300: (a) stress path; (b) stress strain behavior; (c) pore pressure variation vs. axial strain; (d) excess pore water pressure ratio vs. axial strain

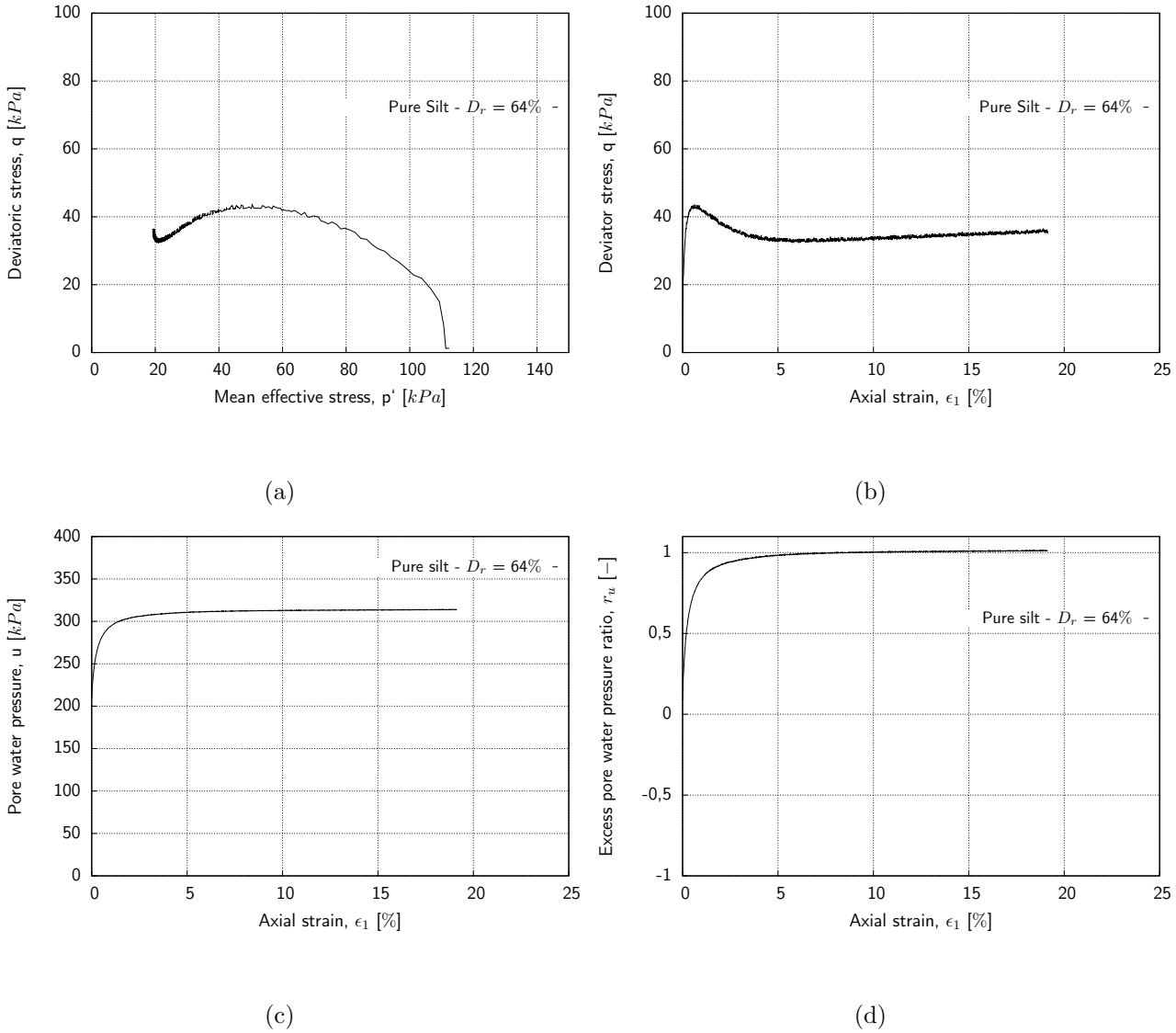

Figure A.25.: Undrained behavior of pure silt, Sample CU60-100-120: (a) stress path; (b) stress strain behavior; (c) pore pressure variation vs. axial strain; (d) excess pore water pressure ratio vs. axial strain

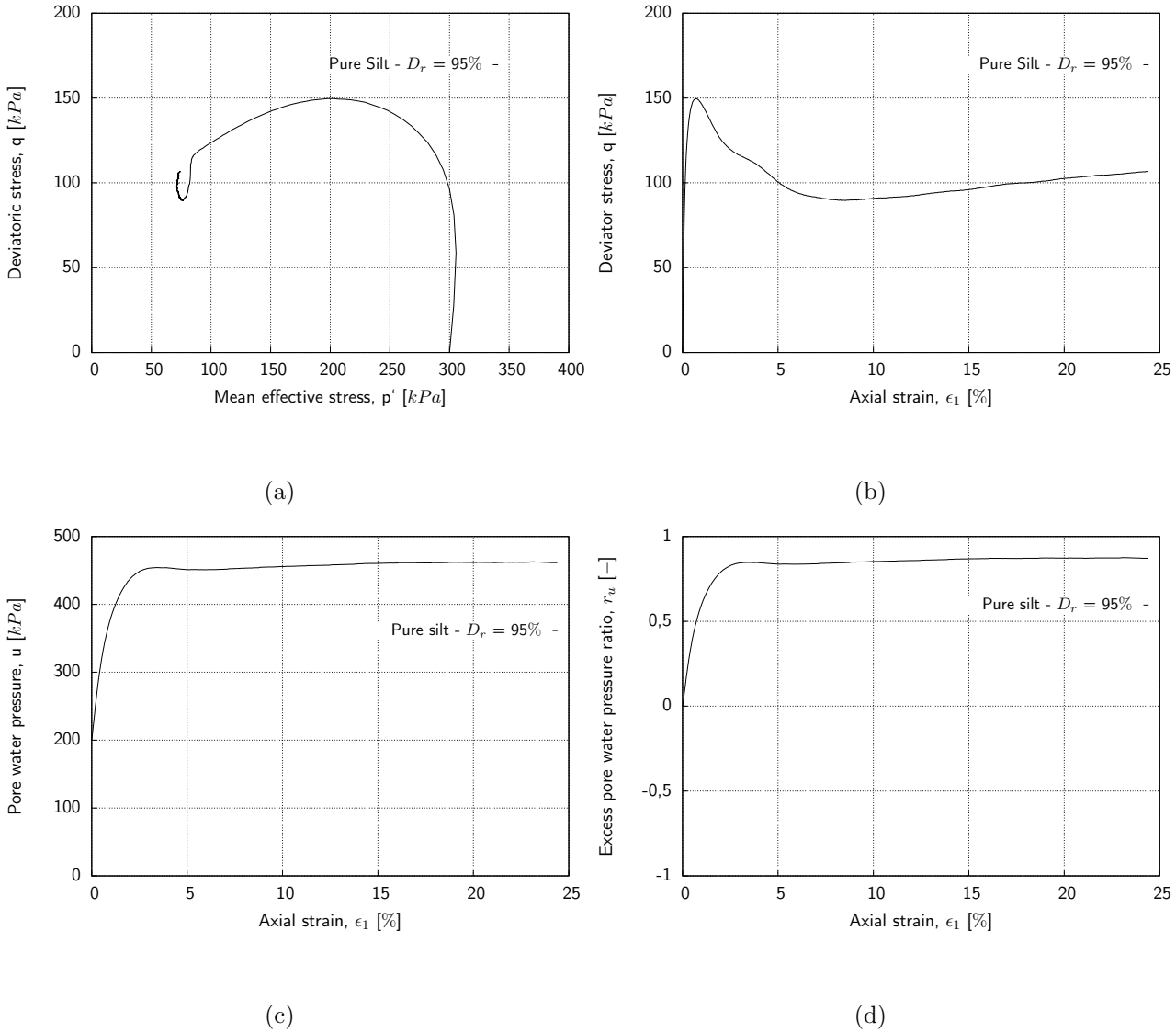

Figure A.26.: Undrained behavior of pure silt, Sample CU61-100-300: (a) stress path; (b) stress strain behavior; (c) pore pressure variation vs. axial strain; (d) excess pore water pressure ratio vs. axial strain

B. Triaxial Test Results on Seese Sand

Appendix B

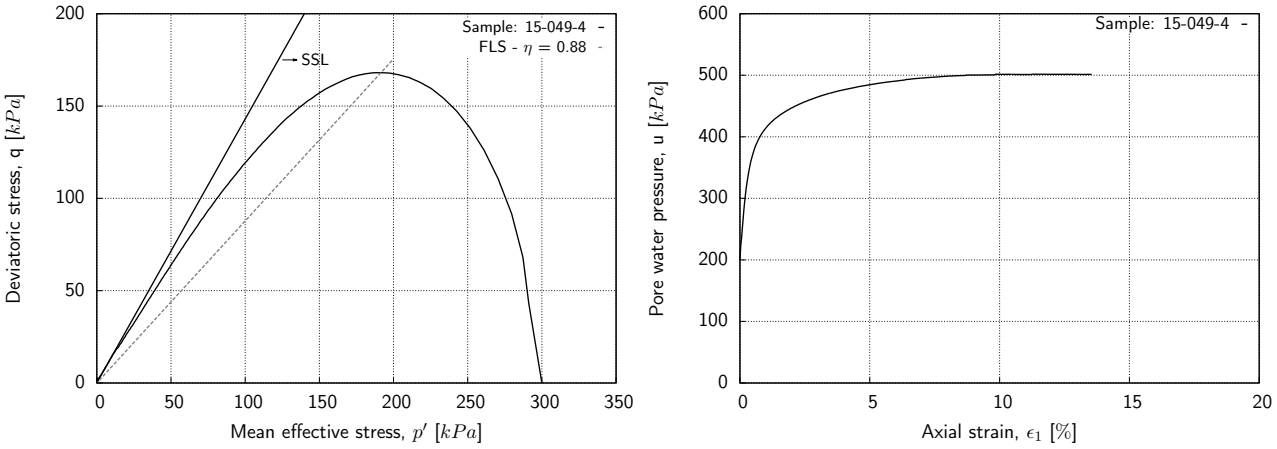

(a)

(b)

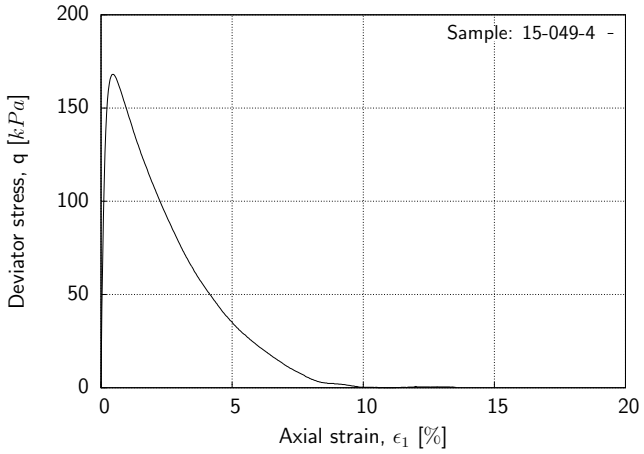

(c)

Figure B.1.: Undrained behavior of Schlabendorf-Süd sand $D_r = 32\%$: (a) stress path; (b) excess pore pressure variation vs. axial strain; (c) stress strain behavior

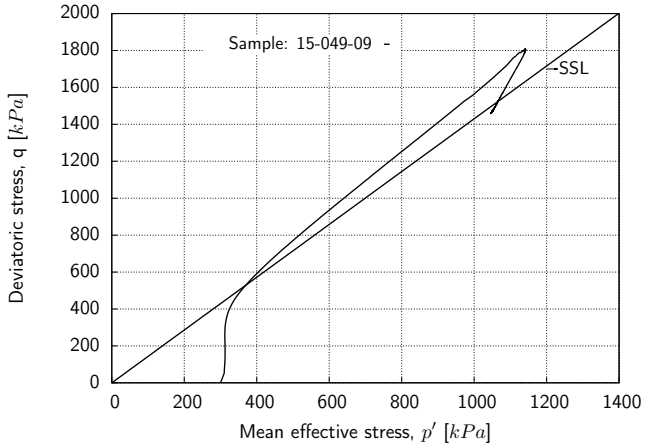

(a)

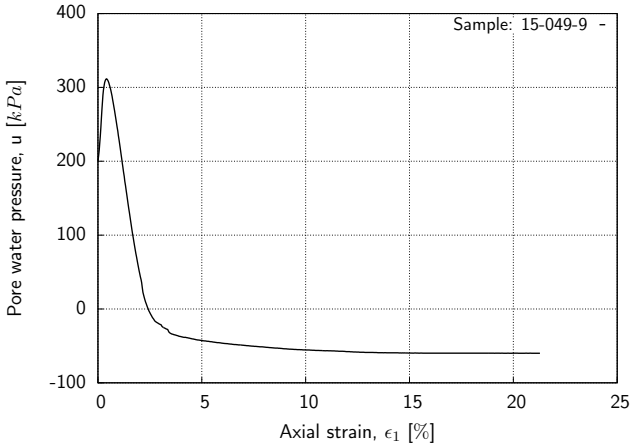

(b)

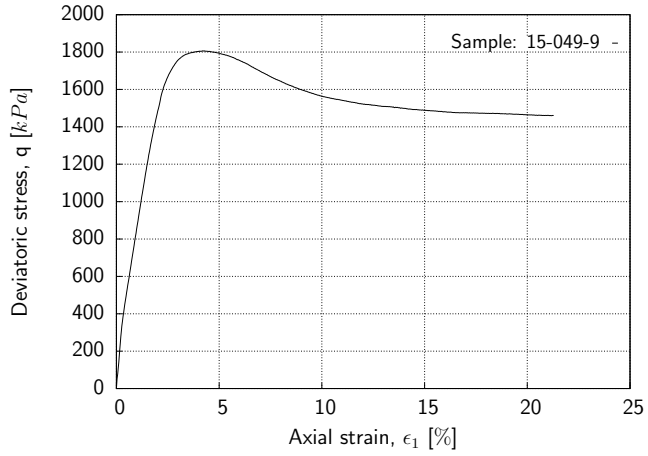

(c)

Figure B.2.: Undrained behavior of Schlabendorf-Süd sand $D_r = 87\%$: (a) stress path; (b) excess pore pressure variation vs. axial strain; (c) stress strain behavior

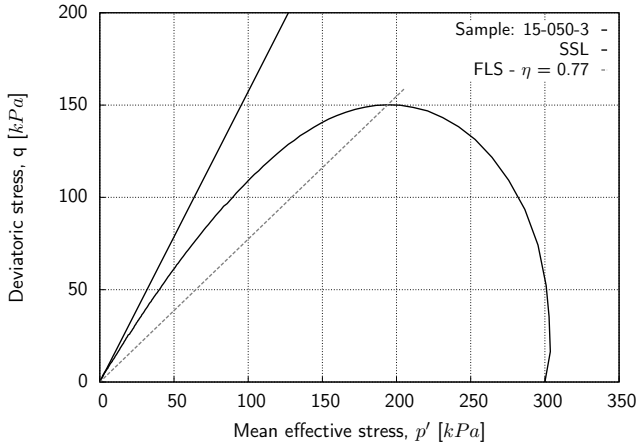

(a)

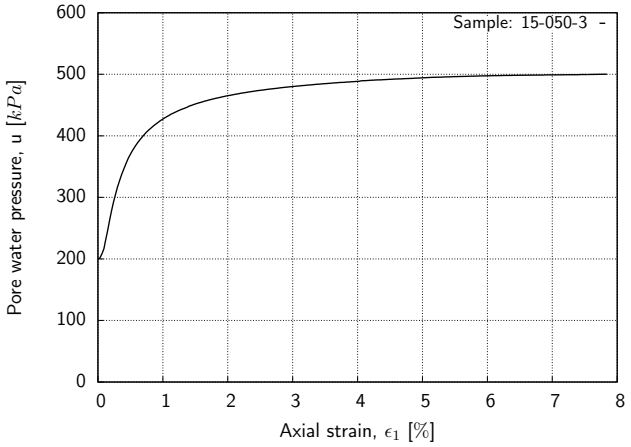

(b)

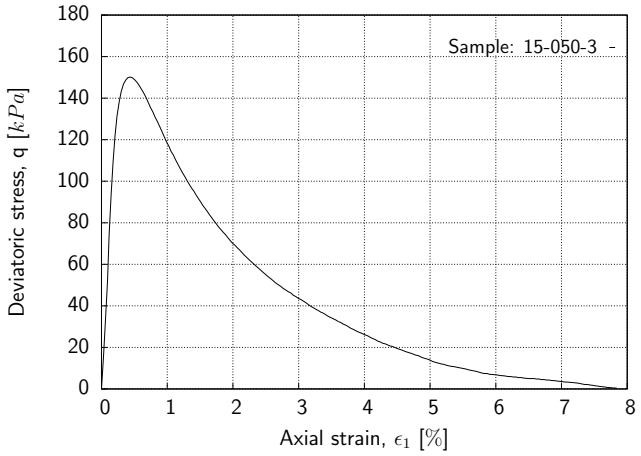

(c)

Figure B.3.: Undrained behavior of Seese-West (HWW) sand $D_r = 37\%$: (a) stress path; (b) excess pore pressure variation vs. axial strain; (c) stress strain behavior

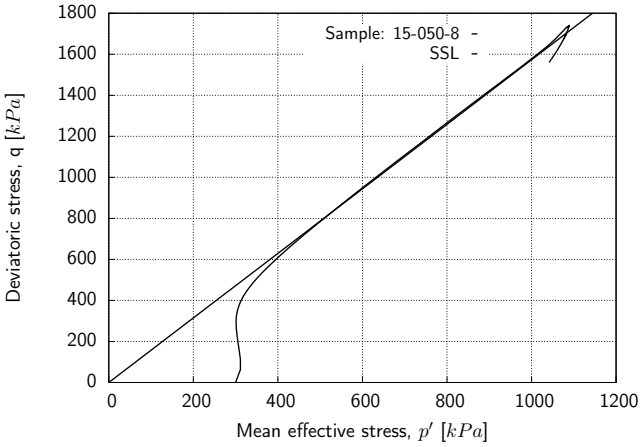

(a)

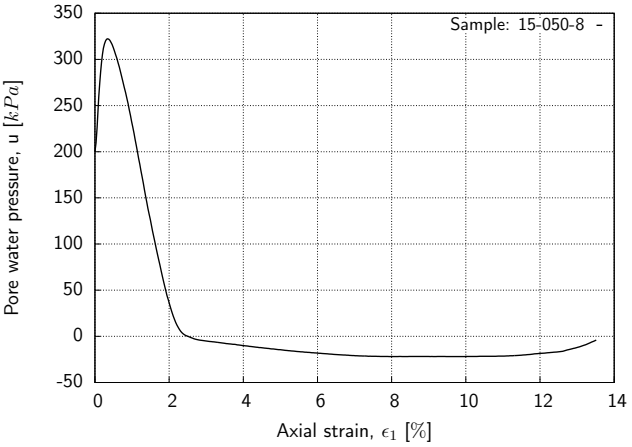

(b)

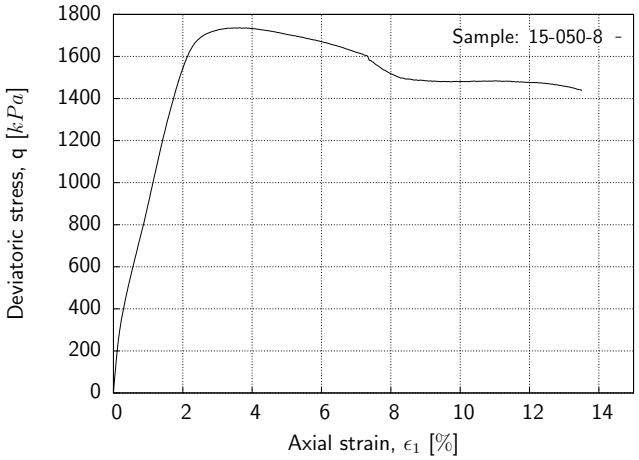

(c)

Figure B.4.: Undrained behavior of Seese-West (HWW) sand $D_r = 86\%$: (a) stress path; (b) excess pore pressure variation vs. axial strain; (c) stress strain behavior

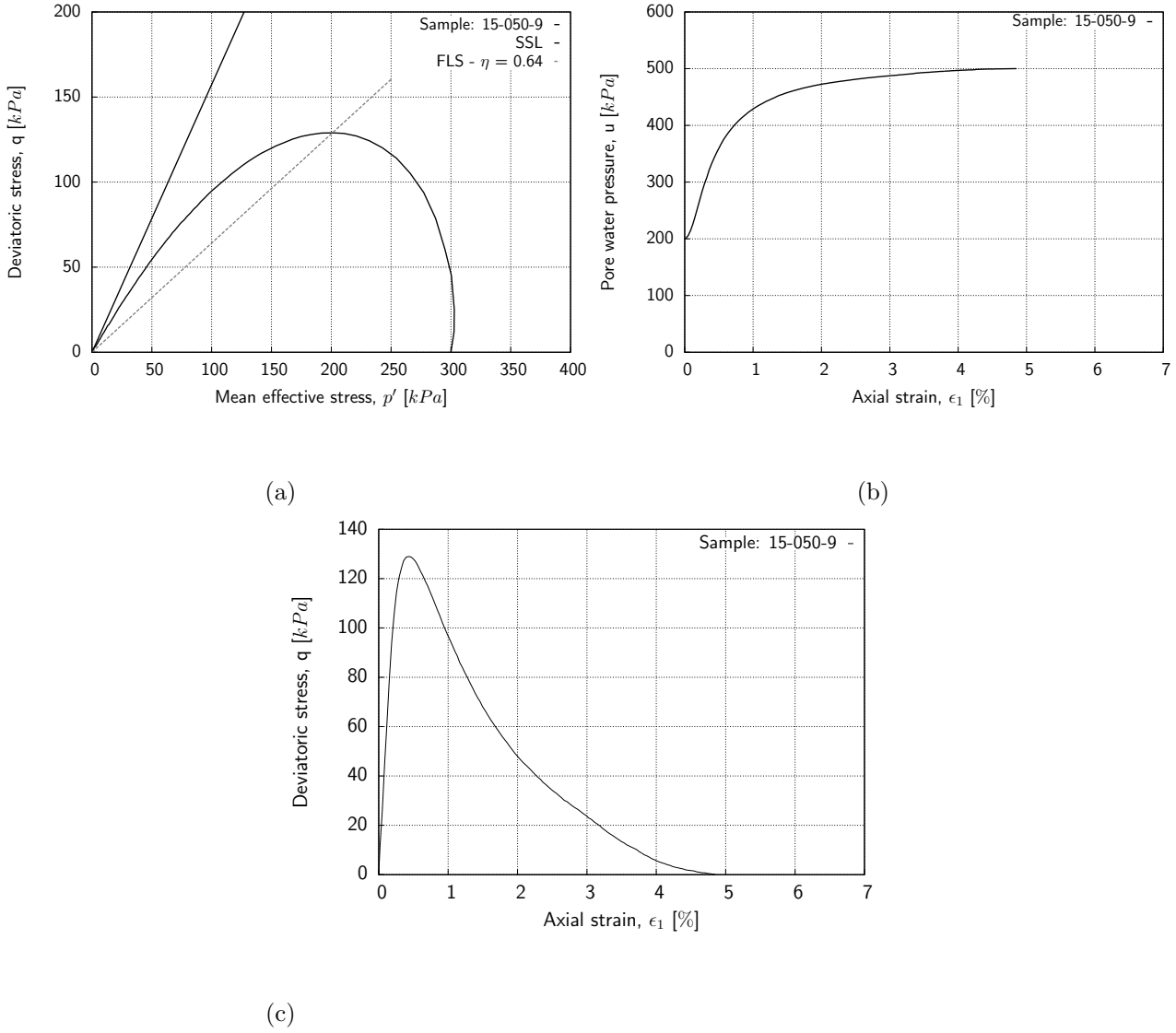

Figure B.5.: Undrained behavior of Seese-West (HWW) sand $D_r = 33\%$: (a) stress path; (b) excess pore pressure variation vs. axial strain; (c) stress strain behavior

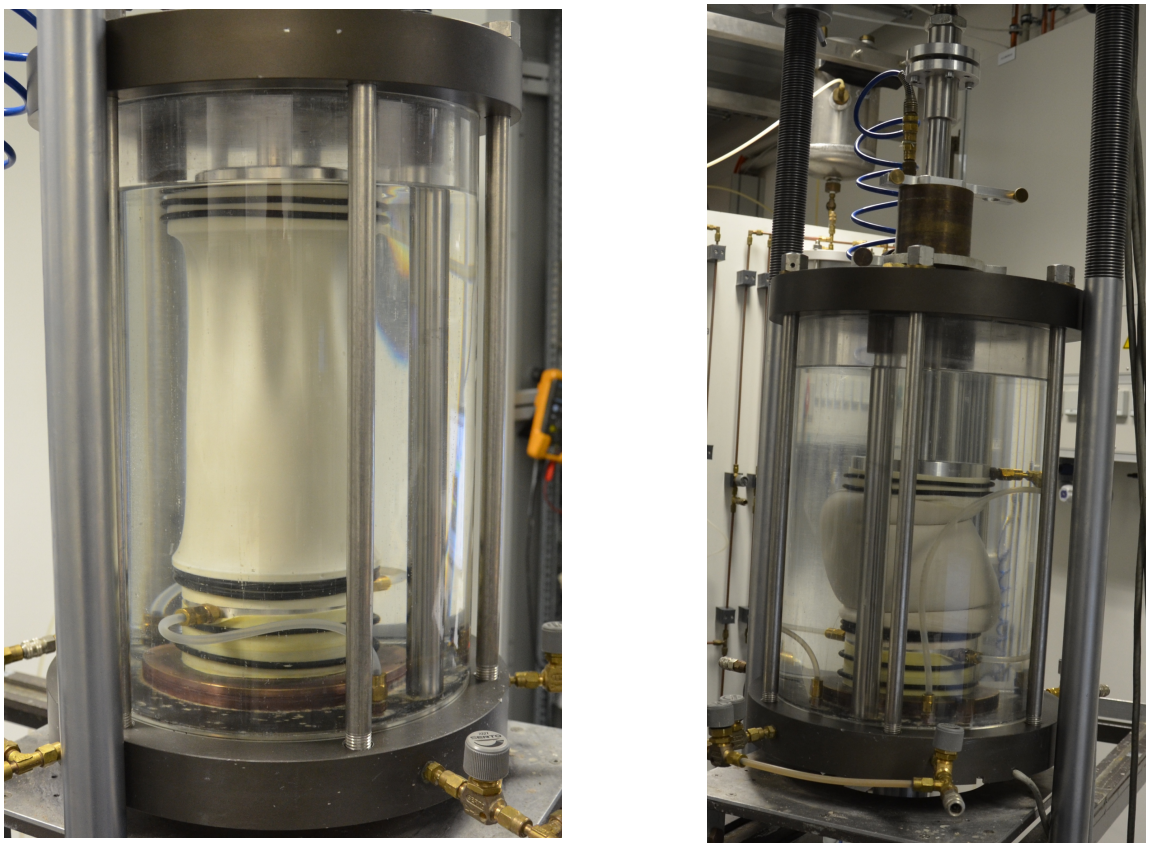

(a) (b)

Figure B.6.: Deformation of the samples under cyclic triaxial test

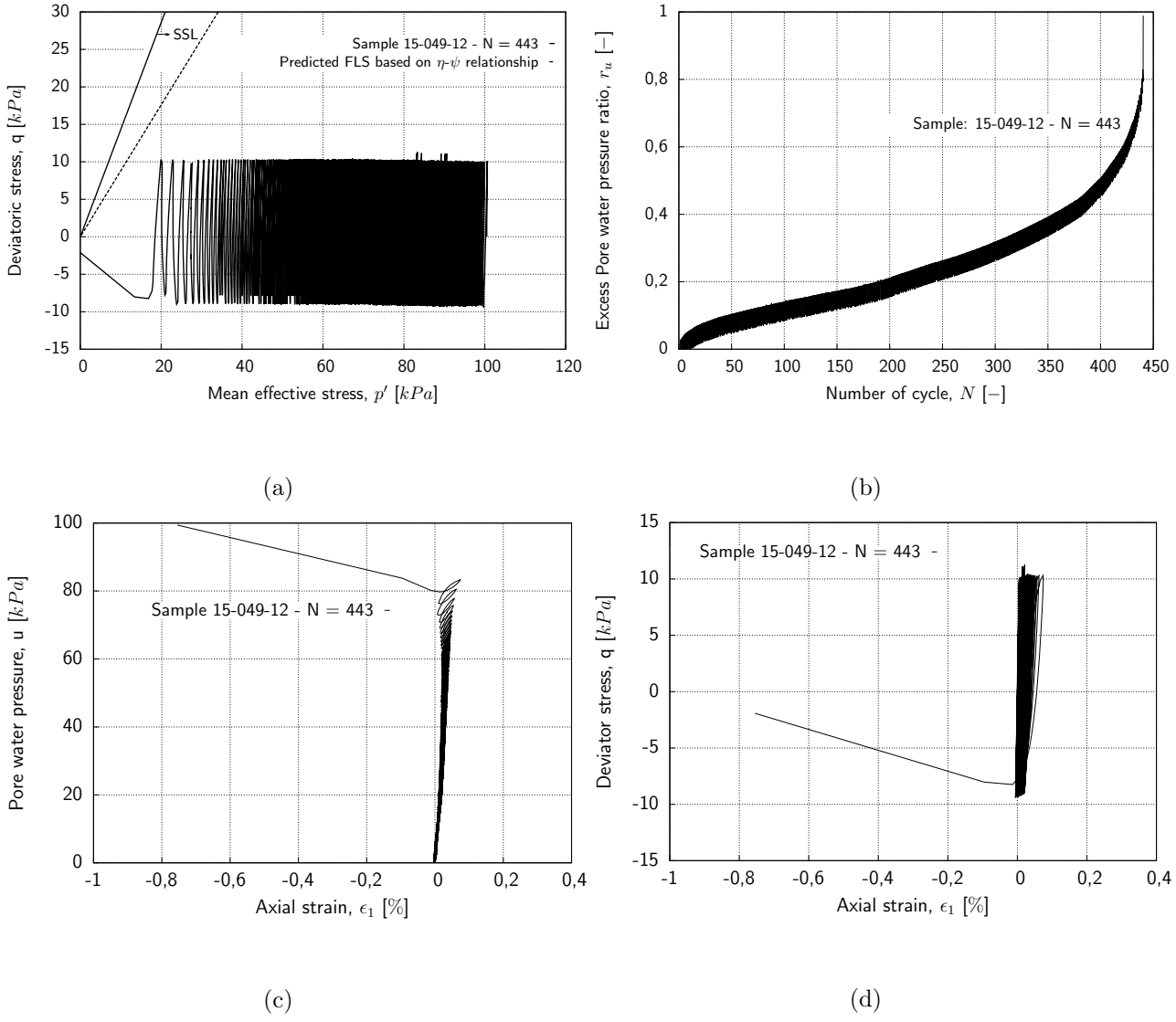

Figure B.7.: Cyclic response of Schlabendorf-Süd sand $D_r = 35\%$, CSR = 0.05: (a) stress path - predicted $\eta = 0.88$; (b) excess pore water pressure ratio vs. number of cycles to liquefaction; (c) excess pore pressure variation vs. axial strain; (d) stress strain behavior

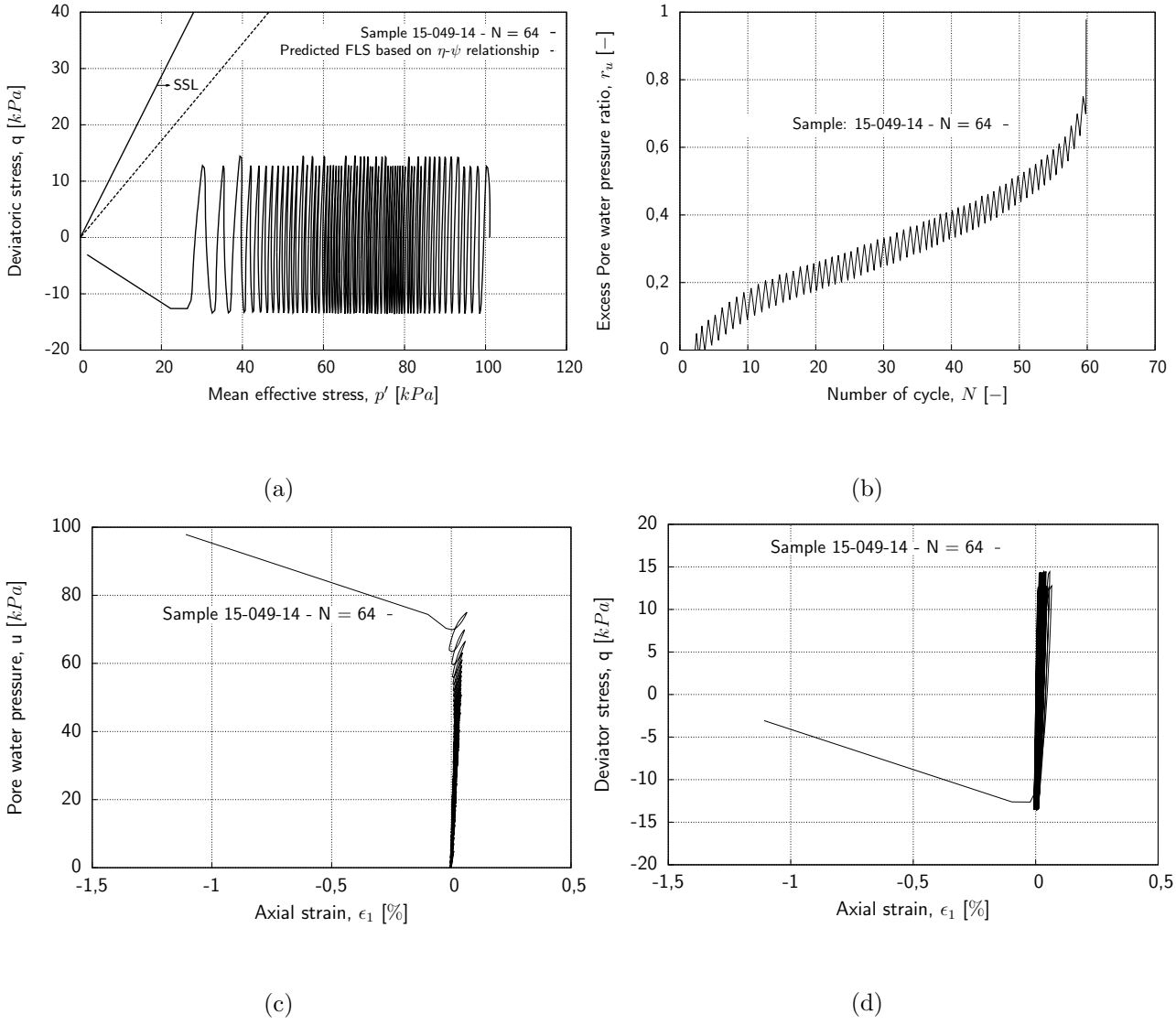

Figure B.8.: Cyclic response of Schlabendorf-Süd sand $D_r = 31\%$, CSR = 0.075: (a) stress path - predicted $\eta = 0.86$; (b) excess pore water pressure ratio vs. number of cycles to liquefaction; (c) excess pore pressure variation vs. axial strain; (d) stress strain behavior

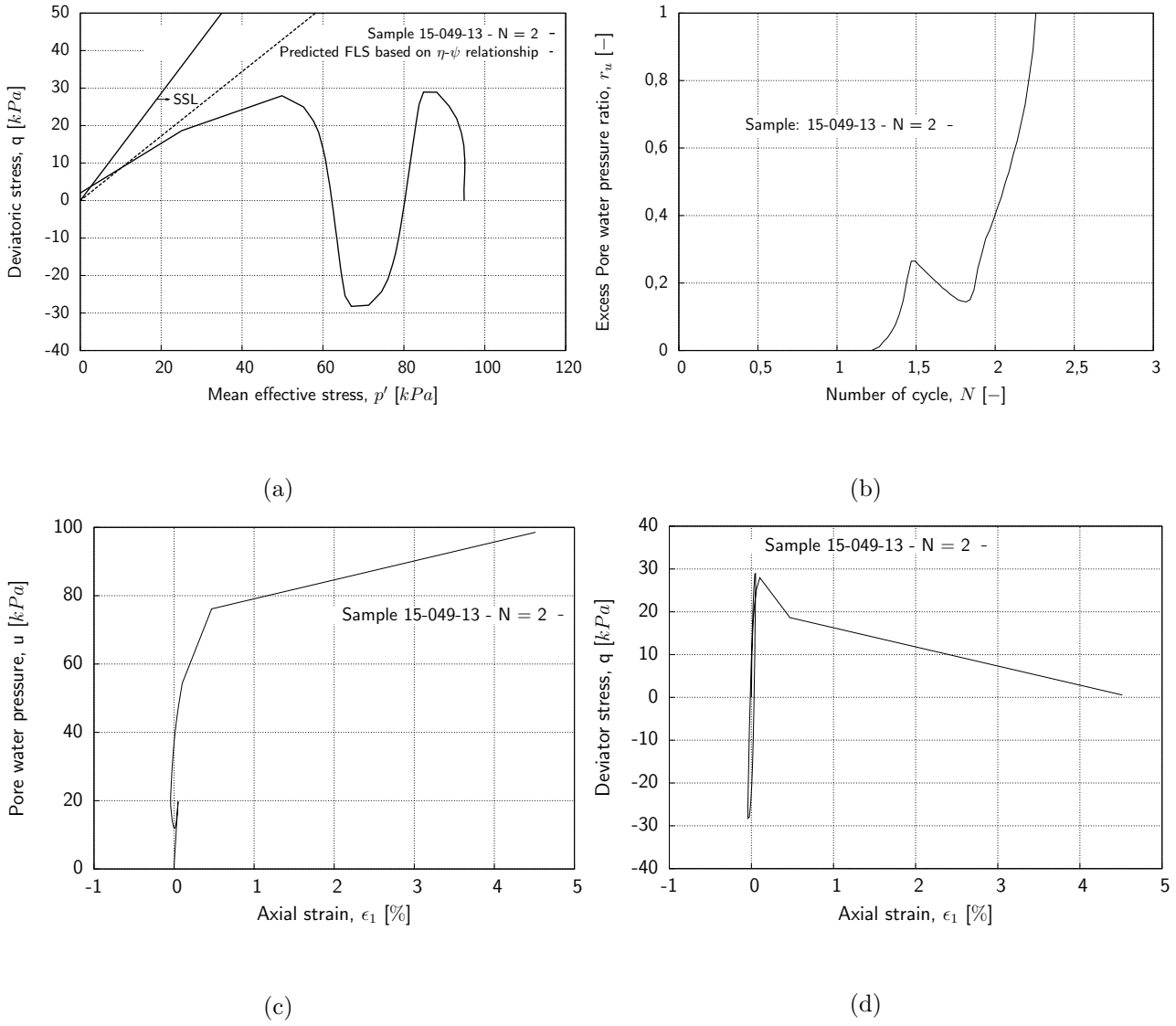

Figure B.9.: Cyclic response of Schlabendorf-Süd sand $D_r = 31\%$, CSR = 0.15: (a) stress path - predicted $\eta = 0.86$; (b) excess pore water pressure ratio vs. number of cycles to liquefaction; (c) excess pore pressure variation vs. axial strain; (d) stress strain behavior

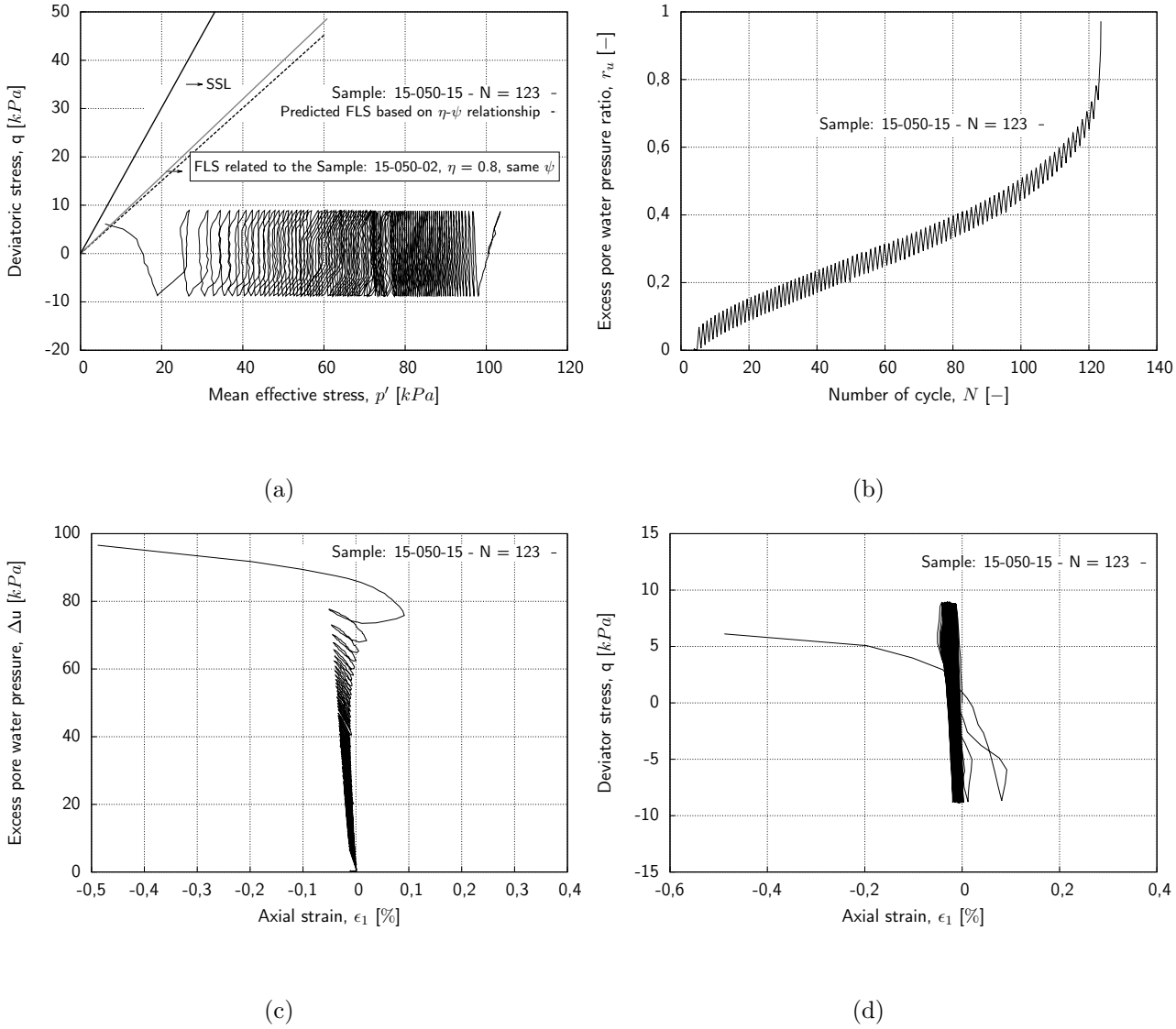

Figure B.10.: Cyclic response of Seese-West sand $D_r = 37\%$, CSR = 0.05: (a) stress path - predicted $\eta = 0.75$; (b) excess pore water pressure ratio vs. number of cycles to liquefaction; (c) excess pore pressure variation vs. axial strain; (d) stress strain behavior

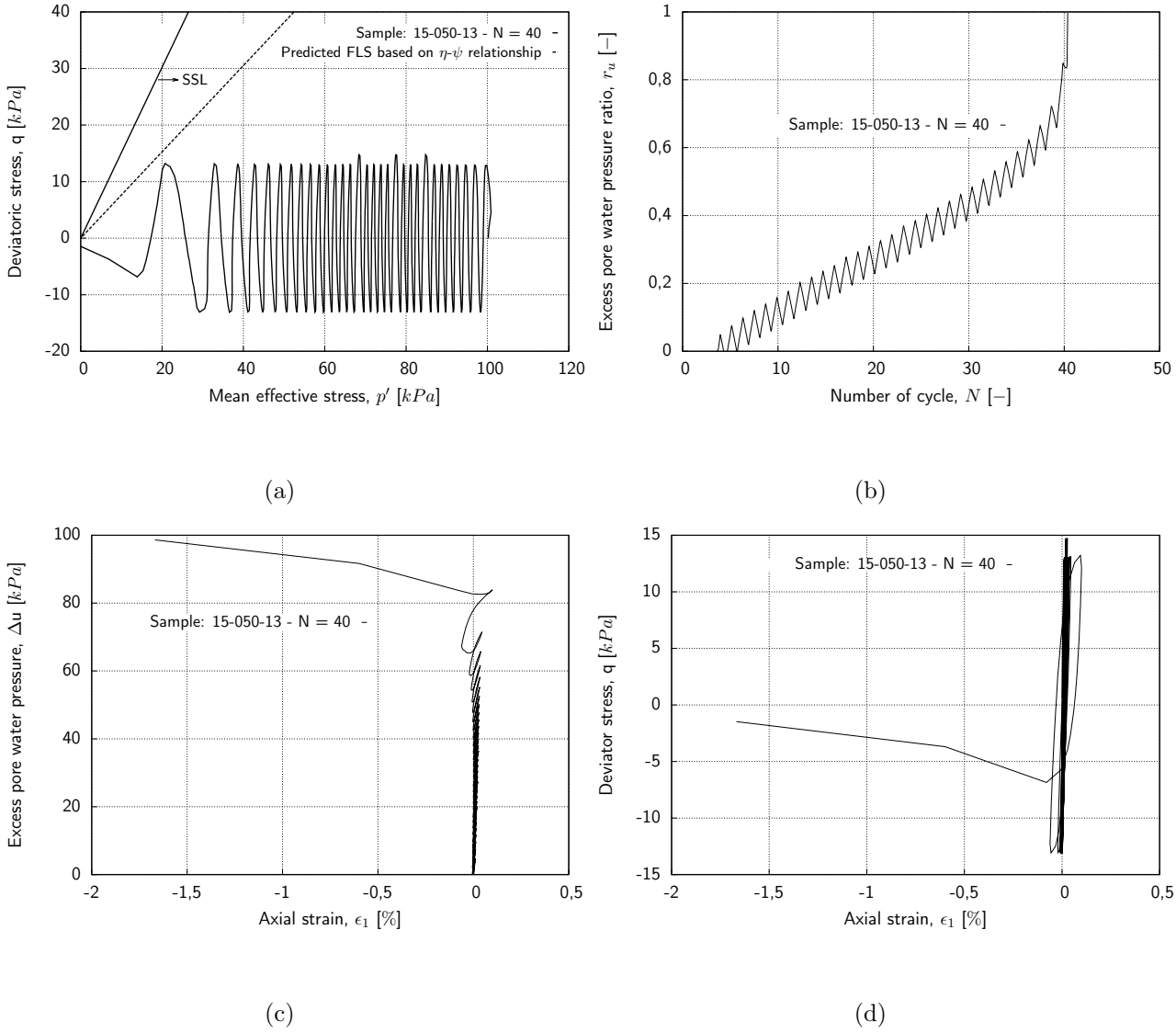

Figure B.11.: Cyclic response of Seese-West sand $D_r = 38\%$, CSR = 0.075: (a) stress path - predicted $\eta = 0.76$; (b) excess pore water pressure ratio vs. number of cycles to liquefaction; (c) excesspore pressure variation vs. axial strain; (d) stress strain behavior

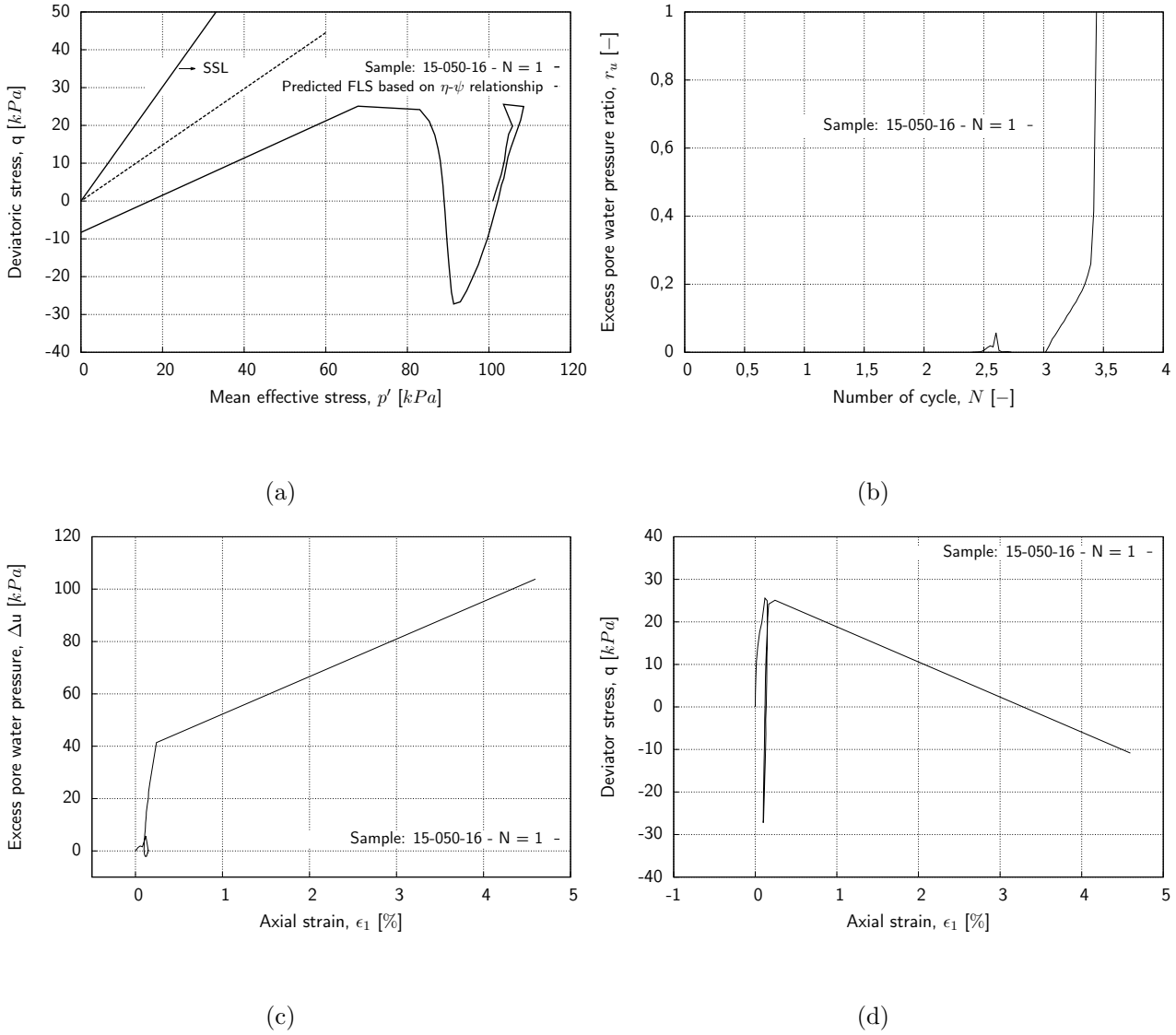

Figure B.12.: Cyclic response of Seese-West sand $D_r = 34\%$, CSR = 0.15: (a) stress path - predicted $\eta = 0.74$; (b) excess pore water pressure ratio vs. number of cycles to liquefaction; (c)excess pore pressure variation vs. axial strain; (d) stress strain behavior

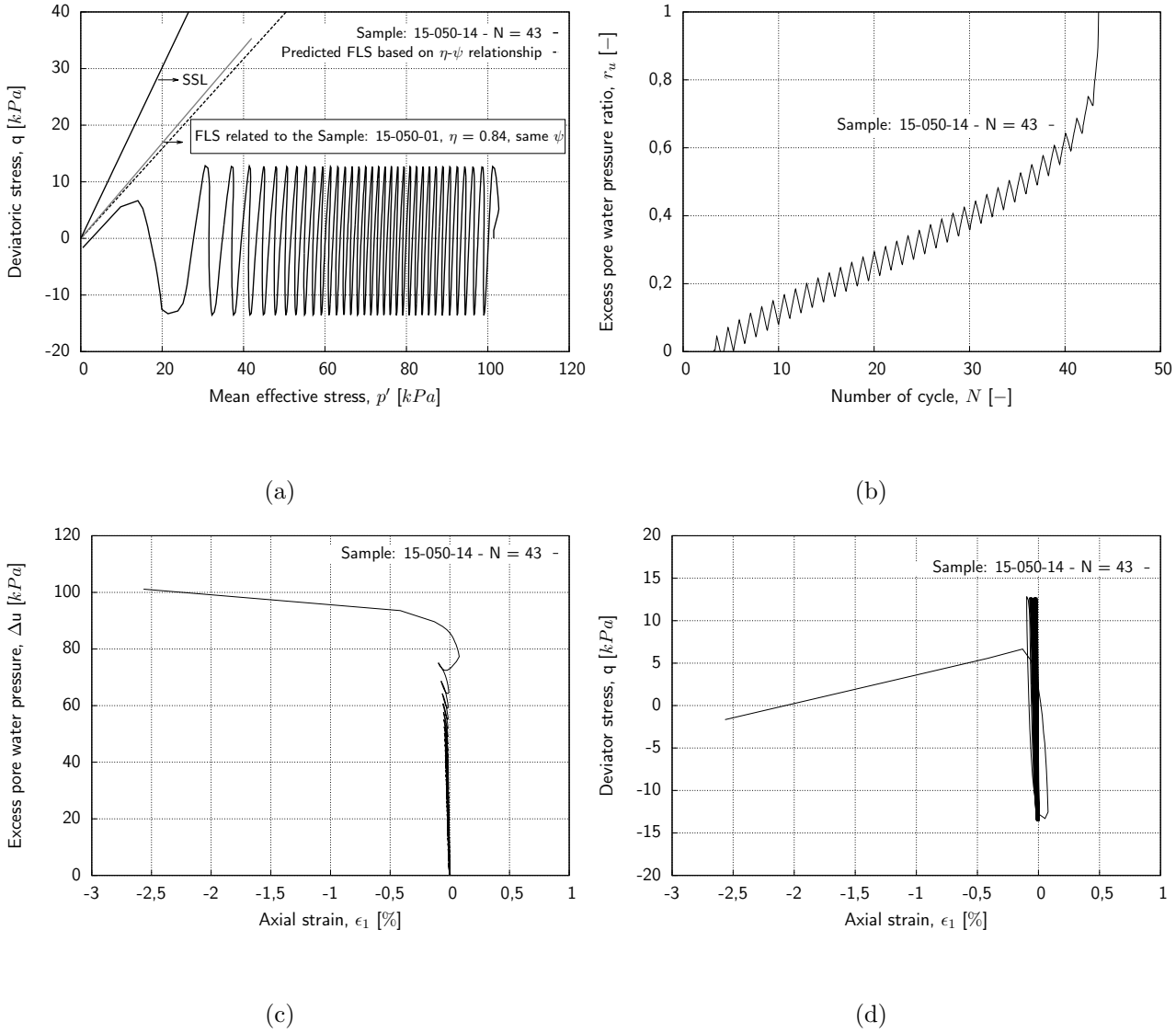

(a) (b)

(c) (d)

Figure B.13.: Cyclic response of Seese-West sand $D_r = 37\%$, CSR = 0.075: (a) stress path - predicted $\eta = 0.79$; (b) excess pore water pressure ratio vs. number of cycles to liquefaction; (c) excess pore pressure variation vs. axial strain; (d) stress strain behavior

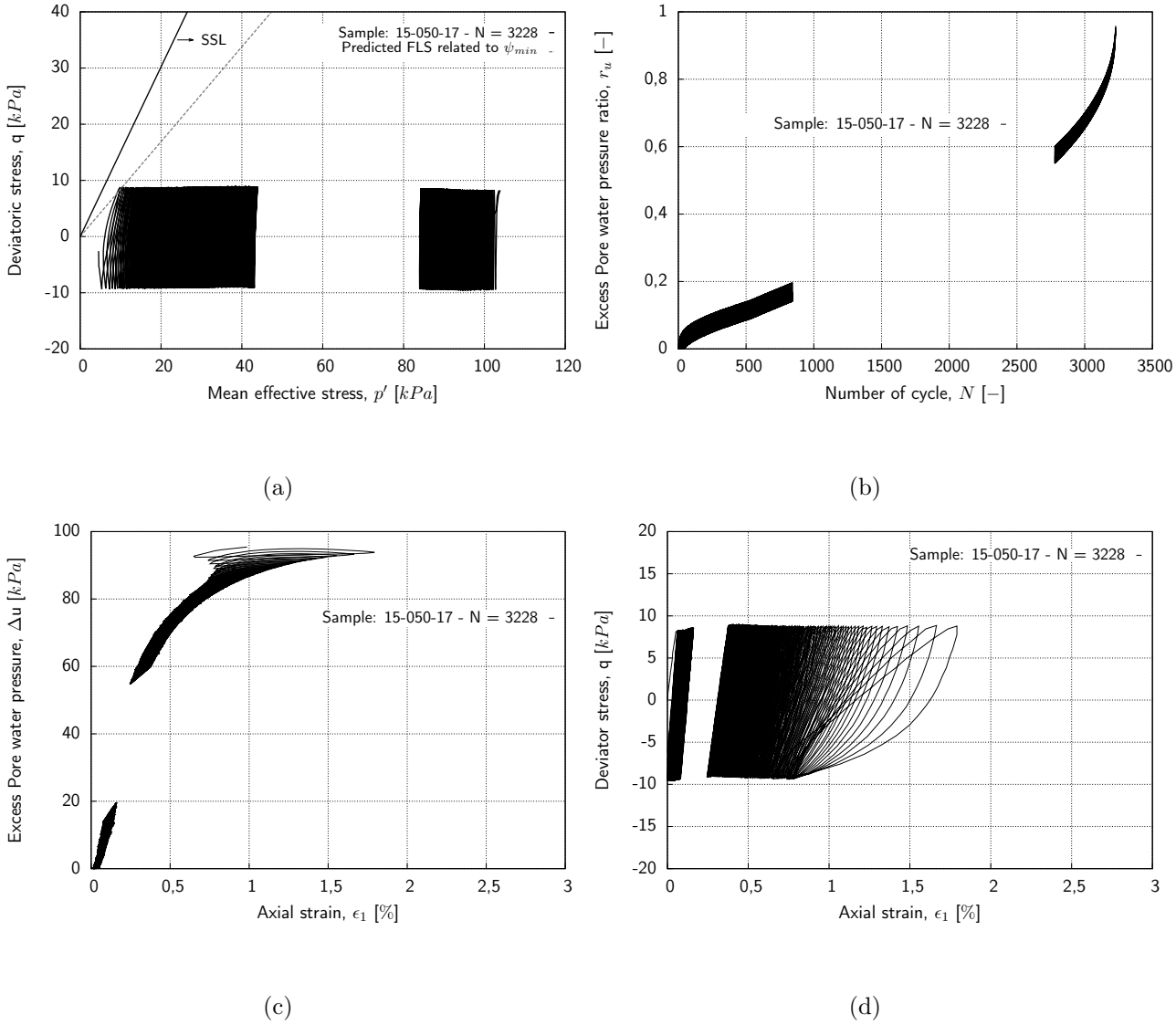

Figure B.14.: Cyclic response of Seese-West sand $D_r = 70\%$, CSR = 0.05: (a) stress path - predicted $\eta = 0.98$; (b) excess pore water pressure ratio vs. number of cycles to liquefaction; (c) excess pore pressure variation vs. axial strain; (d) stress strain behavior

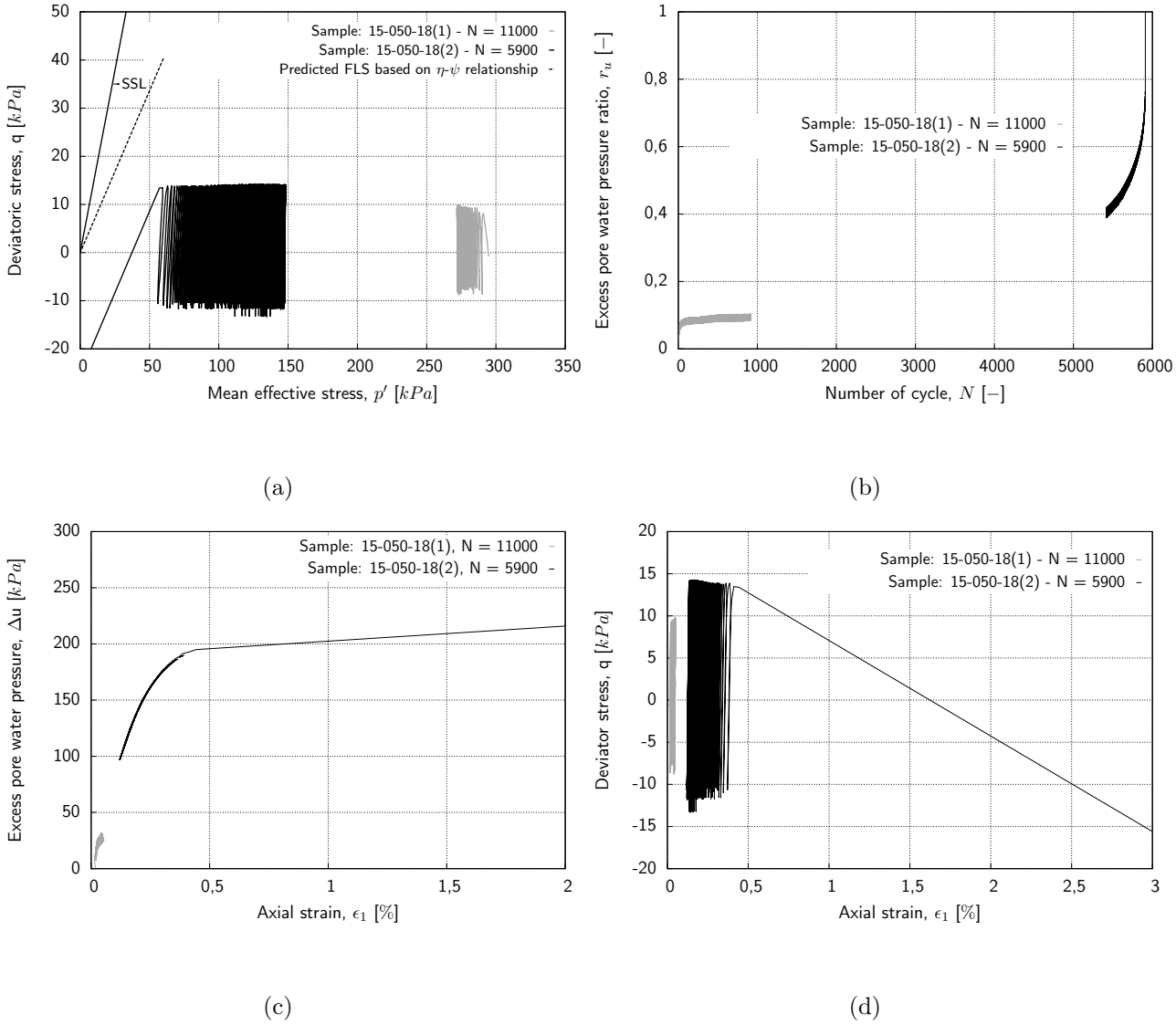

Figure B.15.: Cyclic response of Seese-West sand $D_r = 32\%$, CSR = 0.017: (a) stress path - predicted $\eta = 0.65$; (b) excess pore water pressure ratio vs. number of cycles to liquefaction; (c) excess pore pressure variation vs. axial strain; (d) stress strain behavior

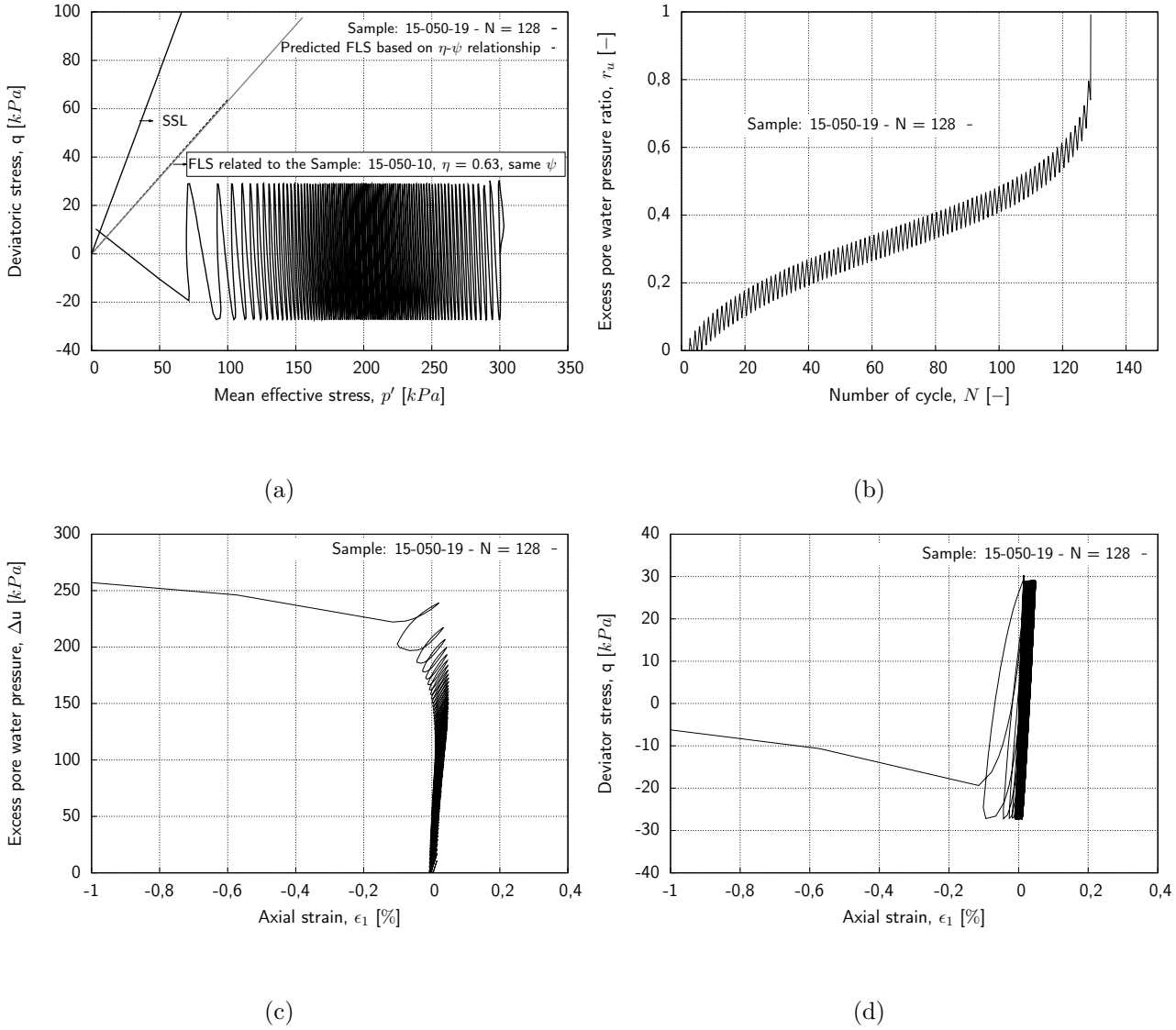

Figure B.16.: Cyclic response of Seese-West sand D_r = 27%, CSR = 0.05: (a) stress path - predicted η = 0.63; (b) excess pore water pressure ratio vs. number of cycles to liquefaction; (c) excess pore pressure variation vs. axial strain; (d) stress strain behavior

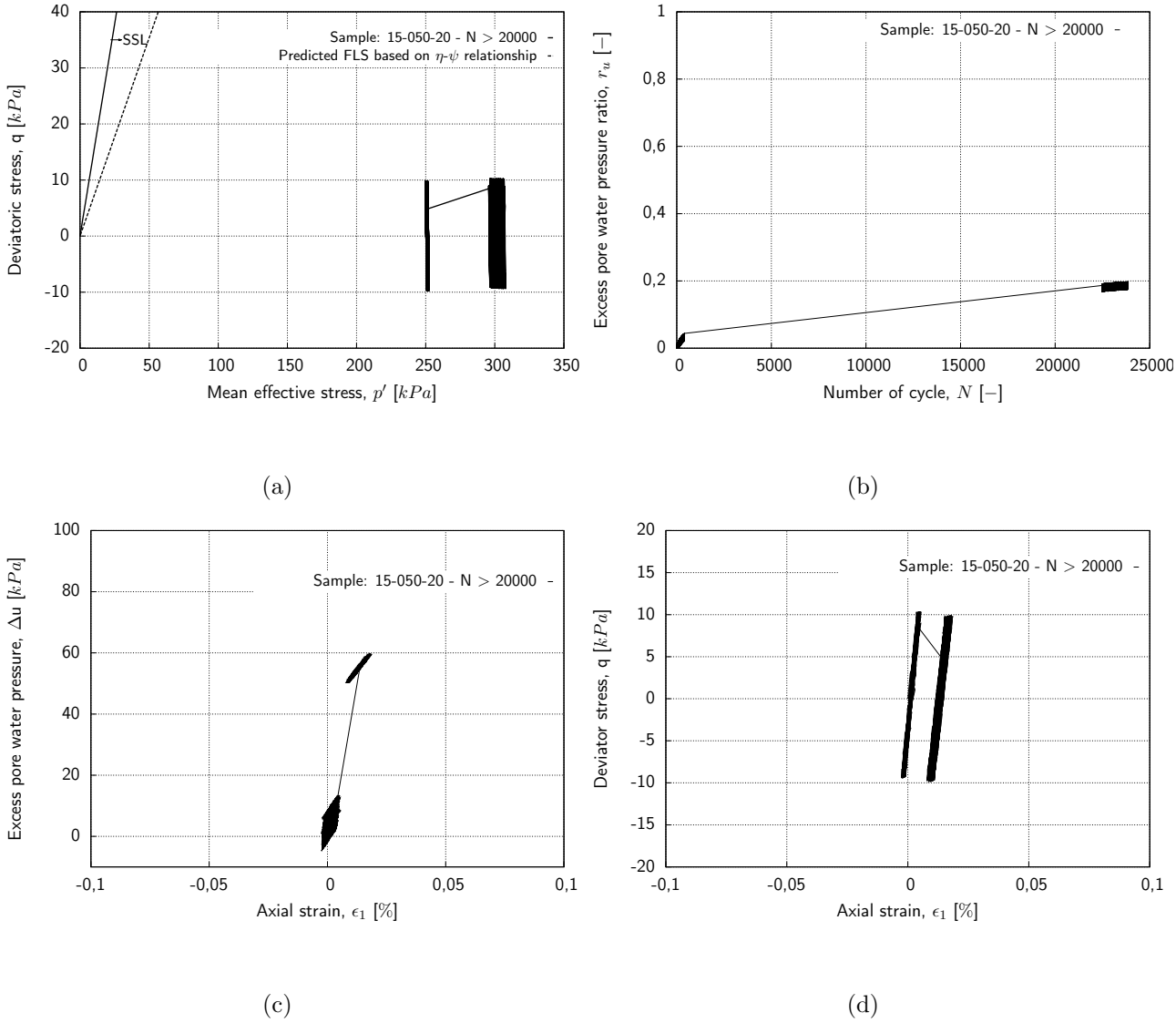

Figure B.17.: Cyclic response of Seese-West sand $D_r = 41\%$, CSR = 0.017: (a) stress path - predicted $\eta = 0.70$; (b) excess pore water pressure ratio vs. number of cycles to liquefaction; (c) excess pore pressure variation vs. axial strain; (d) stress strain behavior

Schriftenreihe des Lehrstuhls für Grundbau, Boden- und Felsmechanik der Ruhr-Universität Bochum

Herausgeber: H.L. Jessberger

1 (1979) **Hans Ludwig Jessberger**
Grundbau und Bodenmechanik an der Ruhr-Universität Bochum

2 (1978) **Joachim Klein**
Nichtlineares Kriechen von künstlich gefrorenem Emschermergel

3 (1979) **Heinz-Joachim Gödecke**
Die Dynamische Intensivverdichtung wenig wasserdurchlässiger Böden

4 (1979) **Poul V. Lade**
Three Dimensional Stress-Strain Behaviour and Modeling of Soils

5 (1979) **Roland Pusch**
Creep of soils

6 (1979) **Norbert Diekmann**
Zeitabhängiges, nichtlineares Spannungs-Verformungsverhalten von gefrorenem Schluff unter triaxialer Belastung

7 (1979) **Rudolf Dörr**
Zeitabhängiges Setzungsverhalten von Gründungen in Schnee, Firn und Eis der Antarktis am Beispiel der deutschen Georg-von-Neumayer- und Filchner-Station

8 (1984) **Ulrich Güttler**
Beurteilung des Steifigkeits- und Nachverdichtungsverhaltens von ungebundenen Mineralstoffen

9 (1986) **Peter Jordan**
Einfluss der Belastungsfrequenz und der partiellen Entwässerungs-möglichkeiten auf die Verflüssigung von Feinsand

10 (1986) **Eugen Makowski**
Modellierung der künstlichen Bodenvereisung im grundwasserdurchströmten Untergrund mit der Methode der finiten Elemente

11 (1986) **Reinhard A. Beine**
Verdichtungswirkung der Fallmasse auf Lastausbreitung in nichtbindigem Boden bei der Dynamischen Intensivverdichtung

12 (1986) **Wolfgang Ebel**
Einfluss des Spannungspfades auf das Spannungs-Verformungsverhalten von gefrorenem Schluff im Hinblick auf die Berechnung von Gefrierschächten

13 (1987) **Uwe Stoffers**
Berechnungen und Zentrifugen-Modellversuche zur Verformungsabhängigkeit der Ausbaubeanspruchung von Tunnelausbauten in Lockergestein

14 (1988) **Gerhard Thiel**
Steifigkeit und Dämpfung von wassergesättigtem Feinsand unter Erdbebenbelastung

15 (1991) **Mahmud Thaher**
Tragverhalten von Pfahl-Platten-Gründungen im bindigen Baugrund,
Berechnungsmodelle und Zentrifugen-Modellversuche

16 (1992) **Rainer Scherbeck**
Geotechnisches Verhalten mineralischer Deponieabdichtungsschichten
bei ungleichförmiger Verformungswirkung

17 (1992) **Martin M. Bizialiele**
Torsional Cyclic Loading Response of a Single Pile in Sand

18 (1993) **Michael Kotthaus**
Zum Tragverhalten von horizontal belasteten Pfahlreihen aus langen Pfählen in Sand

19 (1993) **Ulrich Mann**
Stofftransport durch mineralische Deponieabdichtungen:
Versuchsmethodik und Berechnungsverfahren

20 (1992) **Festschrift anlässlich des 60. Geburtstages von**
Prof. Dr.-Ing. H. L. Jessberger
20 Jahre Grundbau und Bodenmechanik an der Ruhr-Universität Bochum

21 (1993) **Stephan Demmert**
Analyse des Emissionsverhaltens einer Kombinationsabdichtung im Rahmen der
Risikobetrachtung von Abfalldeponien

22 (1994) **Diethard König**
Beanspruchung von Tunnel- und Schachtausbauten in kohäsionslosem Lockergestein
unter Berücksichtigung der Verformung im Boden

23 (1995) **Thomas Neteler**
Bewertungsmodell für die nutzungsbezogene Auswahl von Verfahren zur Altlastensanierung

24 (1995) **Ralph Kockel**
Scherfestigkeit von Mischabfall im Hinblick auf die Standsicherheit von Deponien

25 (1996) **Jan Laue**
Zur Setzung von Flachfundamenten auf Sand unter wiederholten Lastereignissen

26 (1996) **Gunnar Heibrock**
Zur Rissbildung durch Austrocknung in mineralischen Abdichtungsschichten
an der Basis von Deponien

27 (1996) **Thomas Siemer**
Zentrifugen-Modellversuche zur dynamischen Wechselwirkung zwischen Bauwerken
und Baugrund infolge stoßartiger Belastung

28 (1996) **Viswanadham V. S. Bhamidipati**
Geosynthetic Reinforced Mineral Sealing Layers of Landfills

29 (1997) **Frank Trappmann**
Abschätzung von technischem Risiko und Energiebedarf bei Sanierungsmaßnahmen
für Altlasten

30 (1997) **André Schürmann**
Zum Erddruck auf unverankerte flexible Verbauwände

31 (1997) **Jessberger, H. L. (Herausgeber)**
Environment Geotechnics, Report of ISSMGE Technical Committee TC 5
on Environmental Geotechnics

Herausgeber: Th. Triantafyllidis

32 (2000) **Triantafyllidis, Th. (Herausgeber)**
Boden unter fast zyklischer Belastung: Erfahrung und Forschungsergebnisse (Workshop)

33 (2002) **Christof Gehle**
Bruch- und Scherverhalten von Gesteinstrennflächen mit dazwischenliegenden Materialbrücken

34 (2003) **Andrzej Niemunis**
Extended hypoplastic models for soils

35 (2004) **Christiane Hof**
Über das Verpressankertragverhalten unter kalklösendem Kohlensäureangriff

36 (2004) **René Schäfer**
Einfluss der Herstellungsmethode auf das Verformungsverhalten von Schlitzwänden in weichen bindigen Böden

37 (2005) **Henning Wolf**
Zur Scherfugenbänderung granularer Materialien unter Extensionsbeanspruchung

38 (2005) **Torsten Wichtmann**
Explicit accumulation model for non-cohesive soils under cyclic loading

39 (2008) **Christoph M. Loreck**
Die Entwicklung des Frischbetondruckes bei der Herstellung von Schlitzwänden

40 (2008) **Igor Arsic**
Über die Bettung von Rohrleitungen in Flüssigböden

41 (2009) **Anna Arwanitaki**
Über das Kontaktverhalten zwischen einer Zweiphasenschlitzwand und nichtbindigen Böden

Herausgeber: T. Schanz

42 (2009) **Yvonne Lins**
Hydro-Mechanical Properties of Partially Saturated Sand

43 (2010) **Tom Schanz (Herausgeber)**
Geotechnische Herausforderungen beim Umbau des Emscher-Systems
Beiträge zum RuhrGeo Tag 2010

44 (2010) **Jamal Alabdullah**
Testing Unsaturated Soil for Plane Strain Conditions: A New Double-Wall Biaxial Device

45 (2011) **Lars Röchter**
Systeme paralleler Scherbänder unter Extension im ebenen Verformungszustand

46 (2011) **Yasir Al-Badran**
Volumetric Yielding Behavior of Unsaturated Fine-Grained Soils

47 (2011) **Usque ad finem**
Selected research papers

48 (2012) **Muhammad Ibrar Khan**
Hydraulic Conductivity of Moderate and Highly Dense Expansive Clays

49 (2014) **Long Nguyen-Tuan**
Coupled Thermo-Hydro-Mechanical Analysis: Experimental and Back Analysis

50 (2014) **Tom Schanz (Herausgeber)**
Ende des Steinkohlenbergbaus im Ruhrrevier: Realitäa und Perspektiven für die Geotechnik Beiträge zum RuhrGeo Tag 2014

51 (2014) **Usque ad finem**
Selected research papers

52 (2014) **Houman Soleimani Fard**
Study on the Hydro-Mechanical Behaviour of Fiber Reinforced Fine Grained Soils with Application to the Preservation of Historical Monuments

53 (2014) **Wiebke Baille**
Hydro-Mechanical Behavior of Clays - Significance of Mineralogy

54 (2014) **Qasim Abdulkarem Jassim Al-Obaidi**
Hydro-Mechanical Behavior of Collapsible Soils

55 (2015) **Veselin Zarev**
Model Identification for the Adaption of Numerical Simulation Models - Application to Mechanized Shield Tunneling

56 (2015) **Meisam Goudarzy**
Micro and Macro Mechanical Assessment of Small and Intermediate Strain Properties of Granular Material

57 (2016) **Oliver Detert**
Analyse einer selbstregulierenden interaktiven Membrangründung für Schüttkörper auf geringtragfähigen Böden

58 (2016) **Yang Yang**
Analyses of Heat Transfer and Temperature-induced Behaviour in Geotechnics

59 (2016) **Alborz Pourzargar**
Comparison of Measured and Predicted Suction Stress in Partially Saturated Compacted Soils

60 (2017) **Hanna Haase**
Multiscale Analysis of Clay-Polymer Composites for Geoenvironmental Applications

61 (2017) **Kavan Khaledi**
Constitutive Modeling of Rock Salt with Application to Energy Storage Caverns

62 (2017) **Nina Silvia Müthing**
On the consolidation behavior of fine-grained soils under cyclic loading

63 (2017) **Elham Mahmoudi**
Probabilistic analysis of a rock salt cavern with application to energy storage systems

64 (2017) **Negar Rahemi**
Evaluation of liquefaction behavior of sandy soils using critical state soil mechanics and instability concept